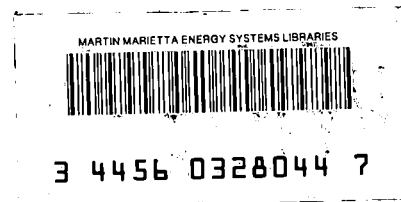


# ornl



**OAK RIDGE  
NATIONAL  
LABORATORY**

**MARTIN MARIETTA**

## The Development, Characterization, and Performance Evaluation of a New Combination Type Personnel Neutron Dosimeter

J. (Chwei-jeng) C. Liu  
C. S. Sims  
J. W. Poston

OAK RIDGE NATIONAL LABORATORY  
CENTRAL RESEARCH LIBRARY  
CIRCULATION SECTION  
4500N ROOM 1-5  
**LIBRARY LOAN COPY**  
DO NOT TRANSFER TO ANOTHER PERSON  
If you wish someone else to see this  
report, send in name with report and  
the library will arrange a loan.

UCN 1963 4 9 77

OPERATED BY  
MARTIN MARIETTA ENERGY SYSTEMS, INC.  
FOR THE UNITED STATES  
DEPARTMENT OF ENERGY

This report has been reproduced directly from the best available copy.

Available to DOE and DOE contractors from the Office of Scientific and Technical Information, P.O. Box 62, Oak Ridge, TN 37831; prices available from (615) 576-8401, FTS 626-8401.

Available to the public from the National Technical Information Service, U.S. Department of Commerce, 5285 Port Royal Rd., Springfield, VA 22161.  
NTIS price codes—Printed Copy: A10 Microfiche A01

This report was prepared as an account of work sponsored by an agency of the United States Government. Neither the United States Government nor any agency thereof, nor any of their employees, makes any warranty, express or implied, or assumes any legal liability or responsibility for the accuracy, completeness, or usefulness of any information, apparatus, product, or process disclosed, or represents that its use would not infringe privately owned rights. Reference herein to any specific commercial product, process, or service by trade name, trademark, manufacturer, or otherwise, does not necessarily constitute or imply its endorsement, recommendation, or favoring by the United States Government or any agency thereof. The views and opinions of authors expressed herein do not necessarily state or reflect those of the United States Government or any agency thereof.

ORNL-6593

THE DEVELOPMENT, CHARACTERIZATION, AND PERFORMANCE  
EVALUATION OF A NEW COMBINATION TYPE  
PERSONNEL NEUTRON DOSIMETER

James (Chwei-jeng) C. Liu  
C. S. Sims  
John W. Poston\*

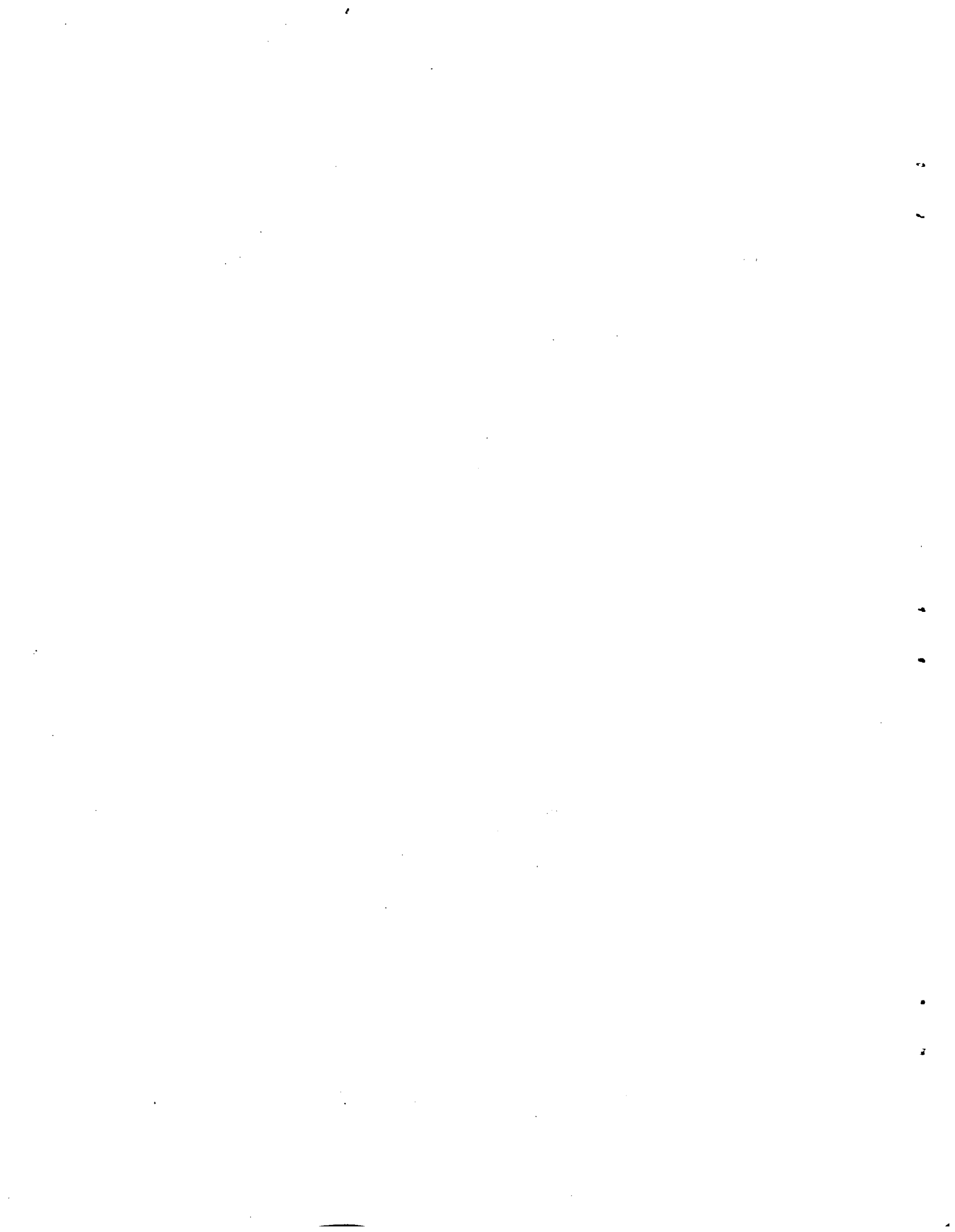
Date Published - October 1989

Prepared by the  
Oak Ridge National Laboratory  
Oak Ridge, TN 37831  
operated by  
MARTIN MARIETTA ENERGY SYSTEMS, INC.  
for the  
U. S. DEPARTMENT OF ENERGY  
under contract DE-AC05-84OR21400

\*Texas A & M University, Department of Nuclear Engineering, College Station, Texas 77843



3 4456 0328044 7



**ABSTRACT**

The Development, Characterization, and Performance Evaluation of a New  
Combination Type Personnel Neutron Dosimeter. (December 1989)

Chwei-jeng Liu, B.S., National Tsing-Hua University;

M.S., National Tsing-Hua University

Co-Chairs of Advisory Committee: Dr. John W. Poston

Dr. C. S. Sims

A new combination type personnel neutron dosimeter has been designed and developed at the Oak Ridge National Laboratory (ORNL). The combination personnel neutron dosimeter (CPND) consists of a Harshaw albedo neutron thermoluminescent dosimeter (two pairs of TLD-600/TLD-700) and two bubble detectors (one BD-100R and one BDS-1500 from Bubble Technology Industries, Canada). The CPND was developed with the aim of having crude neutron spectrometric capability, universal applicability, better angular response, and an improved lower limit of detection (LLD). The CPND has been well characterized in the following areas: reusability, linearity, lower limit of detection (LLD), detection capability in mixed neutron-gamma fields, angular dependence, and neutron energy dependence. The characterization was accomplished with irradiations using a  $^{238}\text{Pu}$ -Be source, a  $^{252}\text{Cf}(\text{D}_2\text{O})$  source, a  $^{252}\text{Cf}$  source, a  $^{252}\text{Cf}(\text{PE})$  source, monoenergetic neutrons from accelerator and reactor filtered beams,  $^{137}\text{Cs}$ , and X-rays. Optimum signal readout procedures, signal processing techniques, routine operational usage, and neutron dose equivalent evaluation algorithms for the CPND were developed with the goals of having the best precision and accuracy as well as being convenient to use.

Various reference spectra were developed to evaluate the performance (mainly the spectrometric and the dose equivalent measurement capabilities) of the CPND. The performance of the CPND was evaluated by *in-situ* tests in radiation fields existing in the working environment at ORNL. The spectra in these areas were measured previously with a calibrated Bonner multisphere spectrometer. The CPND also was tested with laboratory radioisotopic sources in single-source and multi-source exposure situations. Finally, the CPND was tested by participating in the fourteenth Personnel Dosimetry Intercomparison Study. The results of the tests mentioned above demonstrated that the CPND meets the ambitious design purposes. Because of its 4-interval spectrometric capability and high sensitivity, the CPND can be used, without prior knowledge of the spectrum or calibration in the field, to provide accurate dose equivalent estimates. The results of the detailed characterization and performance tests showed that the new CPND is an excellent personnel neutron dosimeter.

## ACKNOWLEDGEMENTS

I would like first to thank my two dissertation advisors, Dr. C. S. Sims of Oak Ridge National Laboratory and Professor John W. Poston of Texas A&M University, for their endless supervision, guidance, and support in both my Ph.D. study and my personal living.

Special thanks go to Dr. W. H. Casson of Oak Ridge National Laboratory (ORNL), Dr. Ferenc Hajnal of Environmental Measurements Laboratory, Dr. Leon West of University of Arkansas, and Dr. R. B. Schwartz of National Institute of Standards and Technology, for their collaboration and essential assistance in some of the experiments.

The research was supported by the Environmental and Health Protection Division of ORNL. Special thanks are extended to Dr. James S. Bogard and Mr. T. A. Rhea for their continuous support for this research.

I would also like to thank Dr. M. E. McLain and Dr. G. A. Schlapper of the Nuclear Engineering Department, and Dr. E. A. Schweikert of the Chemistry Department for serving as my committee members, and Dr. D. L. Clark for serving as my graduate council representative. Their helpful reviews are greatly appreciated.

I also owe many persons a debt of gratitude for their kind help and valuable discussions. Particular thanks are expressed to Dr. H. Ing of Bubble Technology Industries, Dr. Y.-C. Lo of Massachusetts General Hospital, Dr. R. E. Apfel of Apfel Enterprises, Mr. D. E. Hankins of Lawrence Livermore National Laboratory, and Dr. N. Ipe of Stanford University.

Many thanks also are expressed to Dr. A. B. Ahmed, Mr. M. Buckner, Ms. K. McMahan, Mr. D. Colwell, and Mr. Paul Smith for their assistance and discussions on

the Harshaw TLD system. The administrative help of Mrs. L. R. Pyles and Ms. Phyllis Shaver also is appreciated.

The gratitude I feel toward my friends is immense, particularly Dr. C. F. Wu, Mr. G. Akabani, and Dr. E. Hui. All of them have helped me in every way they could.

I am indebted to my mother, brothers, and sisters for their continuous encouragement and spiritual support throughout my life. The steadfast support, understanding, help, care, and love of my wife, Tsai-O Liu, throughout the years has been a most essential contribution for which I will always be grateful. This dissertation is dedicated to my family.

## TABLE OF CONTENTS

	Page
ABSTRACT . . . . .	iii
ACKNOWLEDGEMENTS . . . . .	v
TABLE OF CONTENTS . . . . .	vii
LIST OF TABLES . . . . .	x
LIST OF FIGURES . . . . .	xii
 CHAPTER	
I INTRODUCTION AND OBJECTIVES . . . . .	1
1.1 Origins . . . . .	1
1.2 Characteristics of Personnel Neutron Dosimetry . . . . .	3
1.3 Combination Dosimeter Concept . . . . .	5
1.4 Overview of Personnel Neutron Dosimeters . . . . .	6
1.5 Research Outline . . . . .	14
II DOSIMETRIC THEORY OF THE CPND . . . . .	16
2.1 Albedo TLD . . . . .	16
2.2 Bubble Detectors . . . . .	26
III CHARACTERIZATION OF THE CPND . . . . .	34
3.1 Introduction . . . . .	34
3.2 Reusability and Optimized Readout Procedure . . . . .	36
3.3 Linearity of Response . . . . .	57
3.4 Lower Limit of Detection . . . . .	64
3.5 Detection Capability in Mixed Neutron-Gamma Fields . . . . .	66
3.6 Angular Dependence . . . . .	74
3.7 Neutron Energy Dependence . . . . .	89

IV	DOSE EQUIVALENT EVALUATION ALGORITHM FOR THE CPND AND ITS OPERATIONAL USAGE . . . . .	101
4.1	Dose Equivalent Evaluation Algorithm . . . . .	101
4.2	Operational Usage . . . . .	108
V	REFERENCE NEUTRON SPECTRA AND DOSIMETRY . . . . .	110
5.1	Spectrometer System . . . . .	110
5.2	Reference Spectra and Dosimetry at TRU . . . . .	119
5.3	Reference Spectra and Dosimetry at RADCAL . . . . .	131
VI	PERFORMANCE EVALUATION OF THE CPND . . . . .	141
6.1	TRU Field Tests . . . . .	141
6.2	RADCAL Radioisotopic Source Tests . . . . .	156
VII	SUMMARY AND CONCLUSIONS . . . . .	171
7.1	Summary . . . . .	171
7.2	Conclusions Based on This Research . . . . .	174
	REFERENCES . . . . .	176
	APPENDIX	
1.	A printout of the reader calibration factor report from the Harshaw 8800 reader . . . . .	187
2.	A printout of the readout procedure in the data acquisition report from the Harshaw 8800 reader . . . . .	188
3.	Data for the photon linearity tests of the Harshaw albedo TLD to the <sup>137</sup> Cs source . . . . .	189
4.	Data for the neutron linearity tests of the Harshaw albedo TLD . . . . .	190
5.	Data for the neutron angular dependence of the Harshaw albedo TLD . . . . .	191

6. Data for the effect of photon angular dependence on the response of the Harshaw albedo TLD* . . . . .	192
7. TRU field survey data . . . . .	193
8. Relative detector response of the multisphere spectrometer for the neutron fields at the ORNL TRU facility . . . . .	194
9. Data for the 26-energy-group flux spectrum evaluated with the multisphere spectrometer . . . . .	195
10. Relative detector response of the multisphere spectrometer for the neutron spectra at the ORNL RADCAL facility . . . . .	196
VITA . . . . .	197

## LIST OF TABLES

		Page
Table 1.4.1	Comparison of personnel neutron dosimeter characteristics . . . . .	8
Table 3.1.1	Radiation source characteristics at RADCAL . . . . .	35
Table 3.2.1	Stability of TLD-700 exposed to gamma radiation (1 mSv) and heated with time-temperature-profile 1 (nC) . . . . .	41
Table 3.2.2	Stability of TLD-600 exposed to $^{238}\text{Pu}$ -Be neutron radiation (1 mSv) and heated with time-temperature-profile 1 (nC) . . . . .	42
Table 3.2.3	TLD stability for different time-temperature-profiles . . . . .	43
Table 3.5.1	Precision of neutron and gamma dose responses in mixed neutron-gamma fields . . . . .	68
Table 3.5.2	Bias of neutron and gamma dose responses in mixed neutron-gamma fields . . . . .	69
Table 3.5.3	Accuracy of neutron and gamma dose responses in mixed neutron-gamma fields . . . . .	70
Table 3.7.1	Characteristics of the monoenergetic neutron fields from the Van de Graaff accelerator at PNL <sup>a</sup> . . . . .	90
Table 3.7.2	Characteristics of the reactor filtered beams at NIST . . . . .	93
Table 3.7.3	Energy responses per unit fluence of the albedo TLD and the bubble detectors (BD-100R and BDS-1500), and the 9"-to-3" sphere response ratio for the ISO reference neutron radiations . . . . .	95
Table 4.1.1	The fit response function for the albedo TLD and the equations for the ICRP Publication 21 fluence-to-dose equivalent conversion factors over the energy intervals . . . . .	103

Table 4.1.2	The average sensitivities of the albedo TLD and the bubble detectors and the average fluence-to-dose equivalent conversion factors over the four neutron energy intervals . . . . .	105
Table 5.2.1	Reference neutron spectra measured with the Bonner multisphere spectrometer at TRU . . . . .	130
Table 5.3.1	Reference neutron spectra at RADCAL . . . . .	136
Table 5.3.2	Estimates of scattered neutron components for the neutron sources at RADCAL for the PDIS 14 . . . . .	140
Table 6.1.1	Data from the CPND measurements in the TRU neutron fields . . . . .	143
Table 6.1.2	Spectrum results obtained with the CPND at TRU . . . . .	144
Table 6.1.3	Comparison of the dose equivalent rates measured with different detector systems in the TRU fields ( $\mu\text{Sv h}^{-1}$ ) . . . . .	153
Table 6.2.1	Data from the CPND measurements for the neutron sources at RADCAL . . . . .	157
Table 6.2.2	Comparison of the dose equivalent rates measured with different detector systems for the neutron sources at RADCAL ( $\text{mSv h}^{-1}$ ) . . . . .	165
Table 6.2.3	Performance results of the CPND in the PDIS 14 . . . . .	168

## LIST OF FIGURES

	Page
Figure 2.1.1 The Harshaw albedo neutron TL dosimeter design . . . . .	17
Figure 2.2.1 Illustration of the bubble detector . . . . .	29
Figure 3.2.1 The digitized glow curve output of LiF-TLD in the Harshaw 8800 reader, the CGCD (computerized glow curve deconvolution) program options, and five TL light signals (integral light, ROI, peaks 3+4+5, peaks 4+5, and peak 5) . . . . .	38
Figure 3.2.2 Reusability of BDS-1500. Recompressed on the second day with the personal recompression device (5 MPa - 0.5 h) . . . . .	49
Figure 3.2.3 Reusability of BDS-1500. Recompressed on the second day (2.8 MPa - 1 h) . . . . .	51
Figure 3.2.4 Reusability of BDS-1500. Recompressed weekly (2.8 MPa - 1 h) . . . . .	52
Figure 3.2.5 Reusability of BDS-1500. Recompressed biweekly (2.8 MPa - 2 h) . . . . .	53
Figure 3.2.6 Reusability of BD-100R. Recompressed on the second day (2.8 MPa - 1 h) . . . . .	54
Figure 3.2.7 Reusability of BD-100R with sensitivity in normal production range and recompressed on the second day . . . . .	56
Figure 3.3.1 Linearity of the four elements in the albedo neutron TLD exposed to a $^{137}\text{Cs}$ source free in air . . . . .	58
Figure 3.3.2 Linearity of the albedo neutron TLD exposed to the $^{252}\text{Cf(PE)}$ neutron source . . . . .	60

Figure 3.3.3	Linearity of the albedo neutron TLD exposed to the $^{238}\text{Pu}$ -Be source . . . . .	61
Figure 3.3.4	Linearity of the bubble detectors exposed to the $^{238}\text{Pu}$ -Be source . . . . .	63
Figure 3.6.1	Irradiation set-up for the angular response study . . . . .	75
Figure 3.6.2	Angular response of the albedo TLD to the bare $^{252}\text{Cf}$ source . . . . .	78
Figure 3.6.3	Angular response of the albedo TLD to the $^{252}\text{Cf}(\text{D}_2\text{O})$ source . . . . .	79
Figure 3.6.4	The effect of $^{137}\text{Cs}$ photon angular dependence on the response of the albedo TLD . . . . .	85
Figure 3.6.5	The effect of M150 X-ray photon angular dependence on the response of the albedo TLD . . . . .	86
Figure 3.7.1	Neutron energy response per unit fluence of the CPND . . . . .	97
Figure 3.7.2	Neutron energy response per unit dose equivalent of the CPND . . . . .	98
Figure 3.7.3	The relationship between the calibration factor of the albedo TLD (Cd-covered TLD-600) and the 9"/3" response ratio . . . . .	99
Figure 5.1.1	Response functions of the Bonner multisphere spectrometer ( $^{10}\text{BF}_3$ gas spherical counter) . . . . .	114
Figure 5.1.2	Comparison of the reference spectrum and the unfolded spectrum from the Bonner multisphere spectrometer for the $^{252}\text{Cf}$ source . . . . .	118

Figure 5.2.1	Locations in the Transuranium Processing Plant (TRU) in which spectra were characterized with the Bonner multisphere spectrometer . . . . .	120
Figure 5.2.2	Relative detector response of the Bonner multisphere spectrometer for the neutron fields at the Transuranium Processing Plant, ORNL . . . . .	123
Figure 5.2.3	Neutron spectrum at the glove box, TRU, measured with the Bonner multisphere spectrometer . . . . .	125
Figure 5.2.4	Neutron spectrum in the cave area A, TRU, measured with the Bonner multisphere spectrometer . . . . .	126
Figure 5.2.5	Neutron spectrum in the control room, TRU, measured with the Bonner multisphere spectrometer . . . . .	127
Figure 5.2.6	Neutron spectrum in the waste transfer area, TRU, measured with the Bonner multisphere spectrometer . . . . .	128
Figure 5.2.7	Neutron spectrum in the analytical laboratory, TRU, measured with the Bonner multisphere spectrometer . . . . .	129
Figure 5.3.1	Neutron irradiation room at the RADCAL facility and positions characterized with the multisphere spectrometer . . . . .	132
Figure 5.3.2	Relative detector response of the Bonner multisphere spectrometer for the neutron spectra of the RADCAL $^{252}\text{Cf}(\text{PE})$ source . . . . .	134
Figure 5.3.3	Neutron spectrum of the RADCAL $^{252}\text{Cf}(\text{PE})$ source measured with the Bonner multisphere spectrometer . . . . .	135

Figure 6.1.1	Comparison of the spectrum and dose equivalent evaluated with the CPND and the multisphere spectrometer at the glove box, TRU . . . . .	145
Figure 6.1.2	Comparison of the spectrum and dose equivalent evaluated with the CPND and the multisphere spectrometer in the cave area A, TRU . . . . .	146
Figure 6.1.3	Comparison of the spectrum and dose equivalent evaluated with the CPND and the multisphere spectrometer in the control room, TRU . . . . .	147
Figure 6.1.4	Comparison of the spectrum and dose equivalent evaluated with the CPND and the multisphere spectrometer in the waste transfer area, TRU . . . . .	148
Figure 6.1.5	Comparison of the spectrum and dose equivalent evaluated with the CPND and the multisphere spectrometer in the analytical laboratory, TRU . . . . .	149
Figure 6.2.1	Comparison of the spectrum and dose equivalent evaluated with the CPND and the multisphere spectrometer for the $^{252}\text{Cf}(\text{PE})$ source at RADCAL . . . . .	158
Figure 6.2.2	Comparison of the spectrum and dose equivalent evaluated with the CPND and the reference value for the $^{238}\text{Pu}\text{-Be}$ source at RADCAL . . . . .	159
Figure 6.2.3	Comparison of the spectrum and dose equivalent evaluated with the CPND and the reference value for the $^{252}\text{Cf}(\text{D}_2\text{O})$ source at RADCAL . . . . .	160

Figure 6.2.4	Comparison of the spectrum and dose equivalent evaluated with the CPND and the reference values for a mixture of two sources at RADCAL . . . . .	161
Figure 6.2.5	Comparison of the spectrum and dose equivalent evaluated with the CPND and the reference values for a mixture of three sources at RADCAL . . . . .	162

## CHAPTER I

### INTRODUCTION AND OBJECTIVES

The problems of current personnel neutron dosimetry are discussed and a solution using a combination personnel neutron dosimeter is proposed. A review of current neutron dosimeters and the dissertation research outline are presented.

#### 1.1 ORIGINS

Due to the growth of the nuclear power industry, wide use of accelerators, neutron radiodiagnosis and radiotherapy, and research associated with fusion technology, more people are being exposed to neutron radiation. It was estimated that over 100,000 persons in the United States (Brackenbush et al. 1980) and over 40,000 persons in the United Kingdom (Harvey 1985) may have neutron exposures. This is a small, but increasing proportion (3-4%) of the radiation-monitored workers in these two countries.

Today, radiation workers are more aware of and concerned about their exposure to radiation and its potential effects. More stringent regulations and increasing compensation litigation concerning radiation safety also emphasize the need for more accurate and reliable personnel monitoring dosimetry. This demand is partially reflected by the fact that the U.S. Nuclear Regulatory Commission (NRC) requires by law, effective in February 1988, that licensees use dosimeter processors who have been certified by the National Voluntary Laboratory Accreditation Program (NVLAP) (USNRC 1988). The U.S. Department of Energy (DOE) has a similar accreditation

-----  
The style and format of the Health Physics Journal were followed in the dissertation.

program (DOELAP), effective in December 1989, required for departmental and contractor external dosimetry programs (USDOE 1987).

In contrast to the dosimetry for photon, the current status of personnel neutron dosimetry is still unsatisfactory. Neutron dosimeter field performance studies at nuclear power plants (Endres 1981; Schwartz et al. 1982) and DOE facilities (Brackenbush et al. 1980) showed the necessity for improvement in neutron dosimetry. Results of the Personnel Dosimetry Intercomparison Studies held periodically by the Oak Ridge National Laboratory's (ORNL) Dosimetry Applications Research (DOSAR) facility also has revealed a number of problems (Swaja and Sims 1988).

An increase of neutron quality factors by a factor of two has been recommended by several organizations, e.g., the International Commission on Radiological Protection (ICRP 1985), the International Commission on Radiation Units and Measurements (ICRU 1986), and the National Council on Radiation Protection and Measurements (NCRP 1987). The implementation of this increase would further urge the need for improvement, especially in dosimeter sensitivity.

Recognizing the problems, various research efforts have been initiated in the United States. The Personnel Neutron Dosimeter Evaluation and Upgrade Project was initiated by DOE at the Pacific Northwest Laboratories (PNL) in 1980. This project is a continuing effort with a primary aim to improve personnel neutron dosimetry. The complete performance assessment of current personnel neutron dosimeters (Brackenbush et al. 1980; McDonald and Hadley 1985) and the development of the DOELAP (USDOE 1986) are major accomplishments of this project. The DOE neutron dosimetry workshop, held periodically since 1969, also has provided a place for expert communication and organizational collaboration on solving the problems. A new combination dosimeter of TLD and CR-39 TED (thermoluminescent dosimeter / CR-39

track etch detector) was proposed as the interim neutron dosimeter at DOE facilities (PNL 1989). In the past, research on personnel neutron dosimetry has been somewhat fragmentary. Each user has developed his own dosimeter system specifically tailored to meet his own needs. Many new ideas about neutron dosimetry which may well solve the problems in the future have been suggested and studied. However, the important work now is to identify the state-of-the-art dosimeter to meet the immediate need.

The first objective of this research was to assess current dosimetry techniques and identify the best types of dosimeters that are more universally applicable. The other main goal of this research was to develop a dosimeter that has a spectrometric capability and is very sensitive to all neutrons over the energy range of interest in personnel monitoring. A dosimeter with such unique capability would be able to solve the most serious problems that current dosimeters have.

## 1.2 CHARACTERISTICS OF PERSONNEL NEUTRON DOSIMETRY

The main characteristics of neutron fields, which also make personnel neutron monitoring difficult, are the following. First, the wide neutron energy range covers 9 decades (from 0.025 eV to 10 MeV), and there are different and varying interaction cross sections in this range. Second, significantly different neutron spectra with regard to energy and direction exist due to the neutron scattering and moderation in both the source and shielding. Third, the variation of fluence-to-dose equivalent conversion factors or quality factors over the energy range of interest is large (a factor of ~ 40 and 10, respectively). Last, neutrons always are accompanied by gamma radiation which requires the capability for mixed field dosimetry.

Traditionally in neutron dosimetry, the fluence spectrum (the basic quantity) has to be multiplied by the fluence-to-dose equivalent conversion factors to obtain the dose equivalent quantity. Whenever the conversion factors are revised, problems entail for the dosimeters that are calibrated to read the dose equivalent quantity directly. Moreover, several sets of fluence-to-dose equivalent conversion factors exist currently (Sims et al. 1987). People using different sets of conversion factors for the same spectrum would obtain different dose equivalent values. In current practice, an ideal neutron dosimeter is the one that has a fluence energy response (i.e., response per unit fluence) which follows closely the fluence-to-dose equivalent conversion factor curve (ICRP 1973). In addition, the dosimeter should have an isotropic response. Unfortunately, such a dosimeter does not exist.

Much of the error in personnel neutron dosimetry is due to the strong dependence of the response with neutron energy and direction in currently available dosimeters. Low accuracy in the low dose equivalent range ( $< 0.5$  mSv) is another problem. Therefore, information concerning the energy and directional characteristics of the neutron field, even crude, is very crucial to accurate personnel neutron dosimetry. The common neutron spectra at many different facilities have been measured and such results may be helpful for rough personnel dose interpretation in some static-field exposure cases (Portal et al. 1985). However, the neutron spectra to which workers are exposed are usually time- and position- dependent. Therefore, a dosimeter with a spectrometric capability to measure the basic quantity (i.e., fluence spectrum) is highly desirable. Such capability is one of the design purposes for the new combination type personnel neutron dosimeter (CPND) in this research. Once the spectrum is measured, the dose equivalent can be obtained by multiplying the spectrum by appropriate fluence-to-dose equivalent conversion factors. The fluence-to-dose

equivalent conversion factors used in this research are the ones in the ICRP Publication 21 (ICRP 1973).

### 1.3 COMBINATION DOSIMETER CONCEPT

Currently, no single detector can meet all the personnel neutron dosimetry requirements for energy response, sensitivity, linear response range, angular response, photon insensitivity, operational and environmental factors, etc. in all neutron environments or situations. Consequently, combination type dosimeters whose components can complement each other should be more universally applicable. The use of such combination type neutron dosimeters to cope with the problem of neutron monitoring has been suggested by many authors (Brackenbush et al. 1980; Griffith and McMahon 1982; Piesch et al. 1984; Piesch and Burgkhardt 1985; PNL 1989; Griffith 1988a).

ORNL has just procured a Harshaw automatic TLD system. The system is comprised of a Harshaw 8800 Workstation and four types of dosimeter assemblies. The personnel neutron dosimeter is an albedo type neutron TLD. The albedo type TLD has given the most accurate results in the performance tests. Therefore, it was selected for personnel neutron monitoring at ORNL. However, this albedo TLD has some disadvantages and limitations. Every kind of albedo TLD has severe energy dependence. The sensitivity is high for energies less than 10 keV, but low for fast neutrons (Piesch and Burgkhardt 1985). To solve the problems of the serious energy dependence and the low sensitivity for fast neutrons, a new combination dosimeter (CPND), a Harshaw albedo TLD and additional detectors, was designed and developed. Not only will the error associated with the energy-dependence be reduced by the new CPND, but also rough spectral information can be derived through the use

of an appropriate algorithm with the new CPND. Therefore, the development, characterization, and performance evaluation of the CPND are the main objectives of this dissertation research.

The key considerations in selecting the detectors to combine with the albedo TLD were :

1. Respond to fast neutrons, preferably with a flat fluence response and a low energy threshold ( $\sim 10$  keV) to complement the albedo TLD response;
2. High sensitivity with a lower limit of detection (LLD) below  $100 \mu\text{Sv}$  (10 mrem);
3. Stability and reproducibility;
4. Wide and linear response range;
5. Insensitive to other radiations;
6. Resistant to environmental factors, e.g., temperature, humidity, pressure, light, etc.;
7. Operational factors, e.g., ease of processing, low cost, no interference with or hazard to the wearer, etc.; and
8. Currently feasible and does not require years of developmental research.

#### 1.4 OVERVIEW OF PERSONNEL NEUTRON DOSIMETERS

There are many excellent review papers on personnel neutron dosimeters (Griffith et al. 1979; Brackenbush et al. 1980; Ing and Piesch 1985; Sims et al. 1987; Griffith 1988b; Gibson 1988). Some personnel neutron dosimeters are not suitable for consideration as the complementary detector for the albedo TLD. The oldest dosimeter, NTA film, relies on counting of the proton recoil tracks from neutrons scattering with hydrogen nuclei in a thin photographic emulsion. The main disadvantages that make NTA film unsuitable as the candidate are its high energy threshold ( $\sim 0.7$  MeV), high

LLD (~ 0.5 mSv), and strong angular dependence. The fission track etch dosimeter relies on detection of fission fragment tracks in a polycarbonate sheet. The fission fragments originate from a fissile radiator ( $^{237}\text{Np}$  or  $^{232}\text{Th}$ ) placed in close proximity to the polycarbonate sheet. The main reasons that disqualify it from being the candidate are that regulatory and administrative problems forbid the use of radioactive material in personnel dosimeters. The exposure from the fissile material also poses some problems. Activation detectors are usually of low sensitivity and do not have thresholds around the desired range of 10-500 keV. Therefore, activation detectors are not suitable for routine monitoring, but can be useful in criticality accident dosimetry. Some neutron detectors are still in the developmental stage for use as a neutron dosimeter. These detectors include solid-state devices, electrets, thermally stimulated exoelectron emission detectors, and lyoluminescent chemicals.

According to the selection criteria, five potential detectors were considered to complement the Harshaw albedo TLD. These were the bubble detector (BD), superheated drop detector (SDD\*), CR-39 track etch detector (TED), miniature tissue equivalent proportional counter (MTEPC), and deep trap TLD (also called high temperature peaks TLD).

Characteristics of these dosimeters, together with the albedo TLD's, are compared and summarized in Table 1.4.1. The SDD is not listed in Table 1.4.1 because it has characteristics similar to the BD, except in the readout method and in reusability. These five candidates were thoroughly reviewed to determine which was to

---

\* SDD is a trademark of Apfel Enterprises, Inc., 25 Science Park, New Haven, CT 06511

Table 1.4.1. Comparison of personnel neutron dosimeter characteristics.

Characteristic	Albedo <sup>a</sup> TLD	Bubble <sup>b</sup> Detector	CR-39 <sup>c</sup> TED	MTEPC <sup>d</sup>	Deep Trap <sup>e</sup> TLD
LLD ( $\mu\text{Sv}$ )	100	<10	100	1	100
Energy Dependence	Strong	Fair	Fair	No	Unknown
Lower Threshold	No	10 keV	50 keV	100 keV	No
Linearity Range	$10^4$	$10^2$	$10^2$	$10^4$	$10^2$
Reusability	Yes	Yes	No	Yes	Yes
Reproducibility ( $1\sigma$ )	5%	20%	15%	Good	Unknown
Angular Dependence	Cosine	Isotropic	Cosine	Isotropic	Cosine
Photon Interference	Low	No	No	Medium	Strong
Readout Time	30 s	Instant	>6 h	Instant	60 s
Spectrometry	No	Yes	Yes	Yes	Unknown
Environmental Factors	Light	Temperature	Light	No	Light
Size (mm)	10x40x60	16x80	1x40x40	46x72x203	-
Cost (\$) Each	21	40-90	10	2000	-
Automation	Yes	Yes	No	Yes	Yes

a. Harshaw albedo neutron TLD.

b. From Bubble Technology Industries.

c. Reference: Hankins et al. 1988.

d. Reference: Brackenbush et al. 1985.

e. Reference: Shachar and Horowitz 1988.

be used in the new combination dosimeter. A brief summary of the review is given below.

#### Bubble Detector and Superheated Drop Detector

The BD and SDD detect neutrons based on the same principle: charged particle recoils from neutron interactions with superheated liquid drops cause the drops to vaporize into visible bubbles (Apfel 1979). The superheated liquid detection technique has many prominent advantages (Apfel and Lo 1989). The energy threshold is selectable (depends on the liquid material) and can be as low as 10 keV (Lo 1987; Ing and Tremblay 1988). The SDD based on freon-12 liquid has a neutron fluence energy response which largely follows the ICRP Publication 21 fluence-to-dose equivalent conversion factor curve, especially for neutrons greater than 0.5 MeV (Roy et al. 1987). A small personnel spectrometer consisting of bubble detectors with different energy thresholds is possible. The ultra-high sensitivity of the detector (LLD < 0.01 mSv) is also adjustable, depending on the number of liquid drops in the detector. Other advantages include isotropic angular dependence, photon and beta insensitivity (Ipe and Busick 1987), and instant readout. The main disadvantage is that the sensitivity is temperature dependent.

The difference between Apfel's SDD and Ing's BD is in the readout method. Apfel mixed the sensitive liquid with gel to form the SDD. Since the gel cannot hold the bubbles, a piezoelectric transducer is used to detect instantaneously the acoustic pulses from the vaporization events (Lo 1987). Associated electronics also are needed to register the signal pulses. Consequently, a pocket size readout device has to be used and the price is high (\$1600 while the liquid detector itself is only \$13.50). A bubble volume measurement technique, to estimate the dose equivalent, also has been tried.

However, successful results have not been reported yet. Furthermore, the SDD is not reusable. A nonlinear response correction is required when the amount of drops are consumed to a certain extent. The linear response range of the SDD seems wider than that of the BD.

Ing of Bubble Technology Industries (BTI), Canada, has successfully incorporated the liquid drops in polymer and, consequently, optical bubble counting is feasible even long after exposure (Ing and Birnboim 1984). The bubbles can be recompressed into liquid drops making the BD reusable. The reusability greatly reduces the cost. The common size of a cylindrical BD tube is 1.6 cm in diameter and 8 cm in length.

#### CR-39 Track Etch Detector

The CR-39 (Columbia Resin - 39) TED is basically a small organic plastic insulator sheet in which recoil protons from either the radiator or the CR-39 itself can produce damaging tracks. To facilitate track counting, the tracks are enlarged by an electrochemical etching (ECE) process. Therefore, the properties of the CR-39 TED (e.g., the neutron energy dependence and the LLD) greatly depend on the CR-39 material, the radiator, and the ECE process. For personnel neutron dosimetry purposes, Hankins' CR-39 TED system may be the best of those available (Hankins et al. 1987; Hankins et al. 1988). It consists of a dosimetry grade CR-39 foil from American Acrylics and is processed by a special ECE procedure (Tommasino et al. 1984; Hankins et al. 1987).

The energy response per unit dose equivalent of the CR-39 TED with the ECE process is flat over the range of 150 keV to 4 MeV and is low outside this range. It is sensitive having a LLD around 0.1 mSv (10 mrem). It does not respond to photons

and betas. The linear response range is about two orders of magnitude (up to 4.5 mSv with a sensitivity of 800 tracks  $\text{cm}^{-2}$  per mSv). It is inexpensive, but not reusable. A reproducible ECE process, and good packaging and storage are needed to produce consistent results (Hankins et al. 1988). A boron-loaded radiator is being tried to increase the response to low energy neutrons (PNL 1989).

Rough neutron spectrometry is possible when several CR-39 TED's are etched under different conditions, because of the different response functions produced (Hankins et al. 1987; Griffith 1988a). Polycarbonate and LR-115 (cellulose nitrate) TED's have energy thresholds around 1.5 MeV and 4 MeV, respectively, and are useful in conjunction with CR-39 to give additional and more accurate information on fast neutron spectra (Griffith and McMahon 1982). CR-39 coupled with different radiators also has been used to improve spectrometric analysis (Matiullah and Durrani 1986; Dajko and Somogyi 1986). Automatic track counting equipment (Majborn 1986) greatly elevates the potential of the CR-39 TED as a personnel fast neutron dosimeter. Some investigators are still working on methods of deriving spectral information from track size distribution (Hankins et al. 1987) or track shape analysis (Turner et al. 1984) with the assistance of automatic track counting.

The main disadvantages of the CR-39 TED are the quality of the CR-39 material, strong directional dependence due to its planar shape, and the time-consuming ECE process (> 6 h). The sensitivity of CR-39 would be marginal if an increase of quality factor is implemented. The flat energy response range, especially in the lower energy end, also needs to be extended.

### Miniature Tissue Equivalent Proportional Counter

The main components of a MTEPC-based detector are the proportional counter, analogue-to-digital converter (ADC), and a microprocessor. The MTEPC consists of Shonka A-150 tissue equivalent plastic wall surrounding a small cavity with low pressure tissue equivalent gas inside to simulate a small tissue volume about 1-2  $\mu\text{m}$  in diameter (Brackenbush et al. 1985). Since cavity theory requirements are met in the MTEPC, absolute measurement of the absorbed dose in tissue can be made. The MTEPC can measure the dose distribution as a function of the lineal energy ( $y$ ) in tissue through which the dose distribution as a function of linear energy transfer (LET) can also be derived. With the ADC and an appropriate preprogrammed algorithm in the microprocessor, the quality factor and the dose equivalent can be obtained from the measured absorbed dose spectrum,  $D(y)$  or  $D(\text{LET})$  (Brackenbush et al. 1985).

The most attractive features of the MTEPC are its tissue-equivalence over the neutron energy of interest and its spherical or cylindrical shape. These features greatly reduce energy and directional dependence problems. The MTEPC is very sensitive (the LLD is 1  $\mu\text{Sv}$  for  $^{252}\text{Cf}$ ). With advances in microelectronics, compact MTEPC detectors with great capability and flexibility could become personnel monitors.

The main problems which forbid the use of the MTEPC for mass personnel monitoring now are its high cost (\$ 2000), large volume, and heavy weight. Low energy neutrons (less than 100 keV) also are indiscernible from the photons due to their similar pulse height signals. Minor problems include gain shifts with temperature, saturation in high dose rate fields, and the batteries need to be recharged frequently. Details of the MTEPC can be found in the literature (Brackenbush et al. 1985; Vasilik et al. 1985; Menzel et al. 1988).

### Deep Trap TLD

LiF:Mg,Ti and CaF<sub>2</sub>:Tm materials have high temperature peaks, i.e., deep traps, that are more sensitive to high LET radiations than are the low temperature peaks. The possibility of using differential glow peak responses in mixed field neutron-gamma dosimetry has been studied (Shachar and Horowitz 1988; Uray 1986; Pradhan and Rassow 1987; Pradhan et al. 1986; Lakshmanan 1982). An albedo TLD for slow neutrons and a deep trap TLD for fast neutrons may be the least-costly and most easily-implemented combination neutron dosimeter. The LiF deep trap TLD is advantageous in that no extra TLD's are required. However, CaF<sub>2</sub>:Tm is superior to LiF in the deep trap TLD technique due to the higher sensitivity and wider linear response range of CaF<sub>2</sub>:Tm (Lakshmanan 1982; Shachar and Horowitz 1988).

Based on the assumption of first order TL kinetics, a computerized glow curve deconvolution (CGCD) program in the Harshaw 8800 reader system can be used to separate the composite glow curve into individual glow peaks (Horowitz et al. 1986). The CGCD can be used to identify each peak area more clearly and improve the measurement precision at low doses. Therefore, the deep trap TLD with CGCD can become more feasible for personnel neutron dosimetry (Shachar and Horowitz 1988).

Some disadvantages and additional work required for the deep trap TLD are as follows: the energy response needs to be examined more thoroughly; the sensitivity is still low; photons, especially low energy X-rays, would affect the neutron dose estimates using deep trap TLD; and the deep trap characteristics of CaF<sub>2</sub>:Tm seems to be heating-rate and batch dependent.

## 1.5 RESEARCH OUTLINE

After extensive review of relevant literature and critical consideration based on the criteria, two bubble detectors (one BD-100R and one BDS-1500 from BTI) were chosen to be combined with a Harshaw albedo neutron TLD to form the CPND. The BD's were chosen because of their spectrometric capability, ultra-high sensitivity to fast neutrons, low energy threshold, isotropic response, instant readout capability, convenient use, and reasonable cost. Besides being more universally applicable, the CPND was designed to be superior to present neutron dosimeters in that it will have crude neutron spectrometric capability, better angular response, improved LLD, and higher neutron sensitivity.

A detailed review of the Harshaw albedo TLD and the BD's of BTI is given in Chapter 2. A computer-aided TLD signal processing technique for better precision and accuracy also is described in Chapter 2.

The CPND has been well characterized in the following areas: reusability, linearity of response, LLD, mixed field neutron-gamma dosimetry capability, angular dependence, and neutron energy dependence. The characterization was accomplished with the irradiations of  $^{238}\text{Pu-Be}$ ,  $^{252}\text{Cf}$  (bare,  $\text{D}_2\text{O}$ -moderated, and polyethylene-moderated), monoenergetic neutrons from accelerator and reactor filtered beams,  $^{137}\text{Cs}$  photons, and X-rays. The characterization procedures and results are presented in Chapter 3.

The neutron spectral stripping and dose equivalent evaluation algorithms, optimum signal readout procedures, signal processing techniques, and routine operational usage for the CPND were developed and suggested with the goals of having the best precision, accuracy, and convenient usage. These are described in Chapter 4.

The CPND performance (mainly the unique capabilities for spectrometry and low dose equivalent measurement) was evaluated in three tests: 1). *in-situ* tests in radiation fields within the ORNL working environment, 2). laboratory tests of single-source and multi-source exposures with the radioisotopic sources at DOSAR, and 3). participation in the fourteenth Personnel Dosimetry Intercomparison Study (14th PDIS). Reference spectra and dose equivalent rates for the radiation fields and the radioisotopic sources were either measured with a well-calibrated Bonner multisphere spectrometer or calculated (Chapter 5). Compared with the reference spectra and dose equivalents, the CPND performance was evaluated. A performance comparison between the CPND and other detector systems also was made in these three tests. The CPND performance evaluation results are presented in Chapter 6. The summary and conclusions of this dissertation research are presented in Chapter 7.

## CHAPTER II

### DOSIMETRIC THEORY OF THE CPND

The CPND consists of a Harshaw albedo TLD and two bubble detectors. The detailed dosimetric theory of each detector component is presented in this chapter.

#### 2.1 ALBEDO TLD

The Harshaw albedo neutron TLD design is shown in Fig. 2.1.1. The aluminum card (43x31x1 mm) has four holes to contain two TLD-600\* (elements 1 and 4) and two TLD-700\* (elements 2 and 3) chips (3.2x3.2x0.9 mm) which are encapsulated between two thin sheets of Teflon. The ABS (acrylonitrile butadiene styrene) plastic holder (62x41x6 mm) is made to be both light- and water- tight. One pair of TLD-600 and TLD-700 (elements 1 and 2) is shielded in front by a cadmium sheet in the holder. The cadmium sheet (28x13x0.46 mm) absorbs 99.5% of incident thermal neutrons. A special opener has to be used to open the holder.

The TLD-600 element is LiF-TLD enriched with ~ 95.62%  ${}^6\text{Li}$ , and the TLD-700 element is LiF-TLD enriched with ~ 99.93%  ${}^7\text{Li}$ . The TLD-600 and TLD-700 elements have similar photon sensitivities due to their similar masses and atomic numbers. However, due to the large thermal neutron absorption cross section of the  ${}^6\text{Li}(n,\alpha){}^3\text{H}$  reaction (940 b), the TLD-600 has a higher thermal neutron sensitivity (about 3 orders of magnitude) than the TLD-700. Because of the  $1/v$  characteristic of the neutron absorption cross section, the fast neutron response is much smaller than the

---

\* TLD-600 and TLD-700 are trademarks of Harshaw/Filtrol Partnership (currently Englehard), 6801 Cochran Road, Solon, OH 44139.

ORNL-DWG 89M-10601

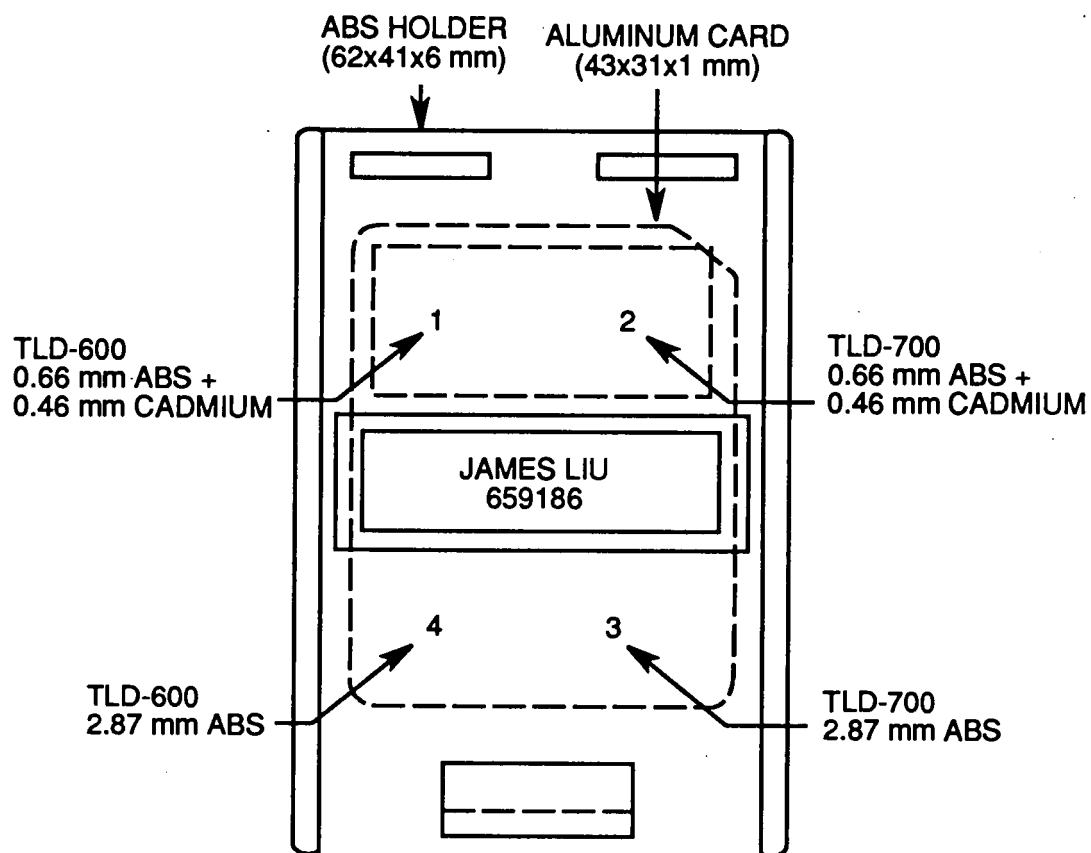


Fig. 2.1.1. The Harshaw albedo neutron TL dosimeter design.

thermal neutron response in LiF-TLD materials. Therefore, the TLD-700 elements are used to estimate the photon signals of their paired TLD-600 elements.

The Cd-covered TLD-600 (i.e., element 1) detects only albedo thermal neutrons and the other TLD-600 (i.e., element 4) detects both incident thermal neutrons and albedo thermal neutrons. The dose detection principle of the albedo TLD is based on the fact that incident neutrons are moderated and scattered inside the body, and the reflected thermal neutrons (albedo neutrons) will be detected by the TLD-600 worn on the surface of the body. Therefore, the incident fast neutron fluence can be measured indirectly with the Cd-covered TLD-600 element in a much higher efficiency, and the incident thermal neutron fluence also can be estimated with the response difference of the two TLD-600 elements. The response of the Harshaw albedo TLD here refers to the neutron response of the Cd-covered TLD-600 element.

#### Properties of the Albedo TLD

The albedo TLD has an advantage over other types of personnel neutron dosimeters in that it has a reasonable sensitivity over a wide energy range (thermal - 20 MeV). It is reusable, low cost, and can be easily automated. It has been available commercially and has become the most popular personnel neutron dosimeter.

The main disadvantage of an albedo TLD is the strong energy-dependent response, which inevitably results from the detection mechanism. The number of albedo neutrons which emerge from the body depends on both the incident fluence and the incident neutron energy. The albedo factor, defined as the ratio of reflected neutron fluence to the incident fluence, is 0.8 for thermal neutrons and decreases to 0.1 for 1 MeV neutrons (Alsmiller and Barish 1974). In addition to the above, the fluence-to-dose equivalent conversion factor for fast neutrons is about a factor of 40 higher than

that for thermal neutrons (ICRP 1973). These two factors cause the response of the albedo TLD to be highly energy dependent. The albedo response is high and flat at low energies, but the response starts falling off rapidly above 10 keV. The response changes by a factor of 10 over the energy range 0.1-2 MeV. This response is opposite to the ideal dosimeter response. Because most neutron fields encountered in radiation protection have energies in the region that the response of an albedo TLD varies most, accurate dose equivalent determination using the albedo TLD requires proper energy dependence correction.

It can be seen also that proper wearing of an albedo TLD is important to its accuracy. The albedo TLD should be worn tightly against the body and properly oriented, i.e., face toward the source. The cosine shape angular dependence of the albedo TLD is another minor problem. However, it is acceptable, if the directional dose equivalent quantity is adopted to be the quantity to be measured in personnel monitoring (see Section 3.6 for details).

#### Energy Dependence Correction

The severe energy dependence of the albedo TLD can be tackled with several appropriate calibration methods. First, the albedo TLD can be calibrated in the laboratory with a neutron spectrum similar to that in the working environment. One example is to calibrate the albedo TLD used in nuclear power plants with the source of  $^{252}\text{Cf}$  moderated by a 15 cm  $\text{D}_2\text{O}$  sphere. This source has a spectrum close to that inside the reactor containment (Schwartz et al. 1982). This calibration method is the simplest method, but it can be used correctly only in environments with small variations in spectra.

The second method is to use an analyzer type albedo TLD which has two or more TLD-600 elements (Piesch and Burgkhardt 1985; Nash et al. 1985; Piesch and Burgkhardt 1978). For example, a calibration factor based on the neutron response ratio of the TLD-600 element and the Cd-covered TLD-600 element in the Harshaw albedo TLD (this ratio is called the energy index, EI) can be used to correct the spectral difference. Low energy neutrons will induce higher response ratios than high energy neutrons. This correction method is useful in cases when field survey information is not available. However, the albedo TLD must be calibrated in various neutron fields to obtain the relationship between the EI values and the energy-dependent calibration factors. This method also suffers in that the thermal neutron component variation that results from moderation or scattering can alter the response ratio, especially the response of the uncovered TLD-600 element.

The third method is the most time-consuming, but the most accurate. The procedure is to calibrate the albedo TLD directly in every working field which has been characterized by the spectrometer technique (Bonner multisphere is the one most commonly used). These elaborate neutron spectrum measurements and the *in-situ* TLD calibration provide accurate field-specific calibration factors for the albedo TLD. However, successful use of this sophisticated technique requires skill and experience.

The most popular calibration method is to make a field survey by using two types of instruments: one reference instrument which can measure the field's dose equivalent and another which has a response similar to the albedo TLD. The Eberline bare  $^{10}\text{BF}_3$  tube inside a 22.9 cm diameter polyethylene sphere (called 9" sphere) or a 7.6 cm diameter polyethylene sphere covered with a 0.025 cm layer of cadmium (called 3" sphere) can be such instruments (Piesch and Burgkhardt 1985). The response ratio of the 9" to 3" spheres (called the 9"/3" ratio) can be related to the albedo TLD's

calibration factor, which is simply the ratio of the neutron dose equivalent measured by the 9" sphere to the albedo TLD response. The relationship between the 9"/3" ratio and the calibration factor is always linear and needs to be determined experimentally only once. Periodic checks of the 9"/3" ratios in radiation fields are easier than spectrum measurements and can be used readily to detect field spectrum changes.

The disadvantages of the 9"/3" ratio correction method are that the 9" sphere overestimates the dose equivalent for neutrons below 100 keV and the 3" sphere response does not match the albedo TLD response accurately, especially for thermal neutrons. The response ratio of the 9" sphere to the bare BF<sub>3</sub> tube (called the 9"/bare ratio) has been used, together with the 9"/3" ratio, to overcome the above disadvantage (Nash et al. 1985).

Whenever field calibration techniques are used, the albedo TLD has to be fixed on a suitable phantom over a period of time for the dose equivalent measurements. Field characteristics such as spatial non-uniformity, multidirectionality, time-dependent spectrum, and time-dependent intensity should be noted. Radiation fields in the work environment are always multidirectional, due to the room scattering. Since the reference instruments (Bonner multisphere and 9" sphere) generally have isotropic response, they measure the maximum dose equivalent quantity. The response of the albedo TLD is angular-dependent. Therefore, it may be difficult to interpret the calibration factor of the albedo TLD in a multidirectional field. In the calibration, one should also be aware of that the albedo TLD is sensitive to variations in the thermal neutron component. While variations in the thermal neutron component may only slightly change the total dose equivalent, it may greatly change the response of the albedo TLD and result in error in the calibration factor.

One important, but not widely addressed, issue related to the albedo TLD is the measurement capability when exposed to more than one neutron spectrum in different times (multi-source exposure). The above calibration methods deal with TLD calibration in only one spectrum. Generally, in multi-source exposures, information about the exposure time for each source has to be estimated or assumed from the individual's work record. The TLD signal fraction for each source is estimated from the survey data. An appropriate calibration factor is applied to the corresponding fraction of the TLD signal from every source, and the total dose equivalent is derived. An easier way is to use a mean calibration factor for all sources, if all calibration factors are similar. Either way, it can be expected that such a dose estimation technique results in large errors. As will be shown later, the CPND with a spectrometric capability is definitely superior to the albedo TLD or any other dosimeter in this aspect.

#### Evaluation Technique for the Harshaw Albedo TLD

Individual TLD element sensitivity correction, by using the element correction coefficient (ECC) concept, can improve greatly the precision of TLD dosimetry (Zeman and Snyder 1979; Burgkhardt and Piesch 1982). A detailed procedure to produce the ECC's for a large number of TLD's (Plato and Miklos 1985) has been followed in this study to produce the ECC's for the Harshaw albedo TLD's. The ECC production procedure is described briefly below.

Ten albedo TLD's were chosen randomly out of the TLD pool as the calibration TLD's. The rest were called field cards and were used for experiments. The panoramic  $^{137}\text{Cs}$  source at the ORNL Radiation Calibration Laboratory (RADCAL) was used to irradiate the ten calibration TLD cards to the same exposure. Uniform

irradiation of all TLD's and readout at nearly the same time after irradiation are necessary. The ECC's for the ten calibration cards then were derived as:

$$ECC_{ij} = R_i / R_{ij}, \quad (2.1.1)$$

where  $ECC_{ij}$  = the ECC for element  $i$  of card  $j$ ,  $i = 1-4$ ,  $j = 1-10$ ;

$R_i$  = the mean TL signal of element  $i$  of the ten cards (nC); and

$R_{ij}$  = the TL signal of element  $i$  of card  $j$  (nC).

Then, the field cards and the calibration cards were irradiated together again to the same exposure. The mean reading of element  $i$  ( $R_i$ ) for the ten calibration cards can be derived using the following equation:

$$R_i = \sum_j (R_{ij} ECC_{ij}) / 10, \quad j = 1-10. \quad (2.1.2)$$

The  $R_{ij}$  and  $ECC_{ij}$  in equation 2.1.2 refer to the calibration card  $j$ . Then, the ECC's for the field cards can be derived from equation 2.1.1 with the  $R_i$  from the calibration cards, the  $R_{ij}$  from field card  $j$ , and the  $ECC_{ij}$  for field card  $j$ .

The ECC values are used to correct the individual photon sensitivity variation of the TLD chips in the same element position  $i$  for all cards. It is recognized that, because the photon sensitivity depends on the TLD chip mass and the thermal neutron sensitivity depends on the amount of  ${}^6\text{Li}$  of the TLD chip, the neutron ECC may not be the same as the photon ECC for an individual chip. However, due to the experimental difficulty in generating the neutron ECC, the neutron ECC was assumed to be the same as the photon ECC, based on the reasonable assumption that the  ${}^6\text{Li}$  concentration in all TLD-600 chips is the same (Burgkhardt and Piesch 1982; Plato and Miklos 1985).

The ECC represents only the sensitivity variation correction for those TLD chips in the same element position. It depends on the TLD chip itself, not on the reader, since the chips in the same position are read by the same heating and light detection channel. The ECC value should not change for a long time after it is determined (Burgkhardt and Piesch 1982):

Basically, the Harshaw 8800 TLD Workstation has an automatic TLD card reader and the TLD Radiation Evaluation and Management System, which includes a personal computer and relevant software programs. The reader uses hot nitrogen gas for non-contact linear heating and the four TLD elements of a card can be heated simultaneously. The TL light is detected with the photomultiplier tube (PMT). A detailed description of the Harshaw/Filtrol model 8800 TLD Workstation can be found in their training manuals\*.

The reader stability, i. e., the four chip heating and TL light detection channels for the four TLD elements, must be checked periodically. The stability relies mainly on variations of the PMT's and less on changes in the heating. The reference light readouts are good only for the stability check of the light detection system. To ensure constancy of the whole reader, the following reader calibration factor (RCF) method was used.

The ten calibration cards were irradiated to a fixed and highly reproducible  $^{137}\text{Cs}$  exposure at RADCAL and were read just before reading the exposed field cards.

---

\* Harshaw/Filtrol Partnership (currently Englehard). TLD system 8800 Workstation user's manual and TLD Radiation Evaluation and Management System (TLDREMS) training manual. 6801 Cochran Road, Solon, OH 44139, 1989.

Then,

$$RCF_i = R_i / X, \quad (2.1.3)$$

where  $RCF_i$  = the reader calibration factor of the reader channel  $i$  which readouts the TLD element  $i$  ( $nC\ mR^{-1}$ );

$R_i$  = the mean ECC-corrected response of the element  $i$  for the ten calibration cards ( $nC$ ); and

$X$  = reproducible  $^{137}Cs$  exposure at RADCAL ( $mR$ ).

The four RCF's are used to trace the stability of the four reader channels. Unlike the ECC, the RCF is changed to compensate for the instability of the corresponding reader channel. Reader calibration is undertaken prior to reading the experimental field cards. Therefore, all the experimental TLD data obtained in this research can be normalized to a constant  $^{137}Cs$  exposure at RADCAL. The constant  $^{137}Cs$  exposure is used for the TLD response stability normalization and refers specifically to the panoramic  $^{137}Cs$  source output at RADCAL. Therefore, the more common unit ( $mR$ ) is used for the TLD response, instead of the SI unit ( $\mu C\ kg^{-1}$ ). A computer printout of the reader calibration factor report is shown in Appendix 1.

After the field cards are evaluated, the two neutron responses of the Harshaw albedo TLD card  $j$  can be evaluated by:

$$A_j = R_{1j} ECC_{1j} / RCF_1 - R_{2j} ECC_{2j} / RCF_2, \quad (2.1.4)$$

$$T_j = R_{4j} ECC_{4j} / RCF_4 - R_{3j} ECC_{3j} / RCF_3, \quad (2.1.5)$$

where  $A_j$  and  $T_j$  = the neutron responses of the Cd-covered TLD-600 and the other TLD-600 for field card  $j$ , respectively (mR );

$R_{ij}$  = the reading of element  $i$  for field card  $j$  (nC);

$ECC_{ij}$  = the ECC of element  $i$  for field card  $j$ ; and

$RCF_i$  = same as that in equation 2.1.3.

The subtraction process in equation 2.1.4 or 2.1.5 eliminates the photon signal. Responses  $A$  and  $T$  are called the albedo and the total responses of the Harshaw albedo TLD, respectively. The energy index (EI) value in the energy dependence calibration method is equal to the ratio of  $T$  to  $A$ , i.e.,  $EI = T / A$ . In the following text, except for the reusability study results, the neutron response is expressed in units of mR, i.e., the RADCAL panoramic  $^{137}\text{Cs}$  exposure which would give the same TL response.

The above comprehensive albedo TLD signal evaluation technique is expedited by the use of a personal computer on-line with the Harshaw 8800 reader. The program in the computer can be used to store all applicable correction factors (ECC's for all albedo TLD's and the four RCF's for the reader) and process the raw TL signals. Greater precision and accuracy, and improved reproducibility and stability of the TLD dosimetry have been attained through this good quality control procedure.

## 2.2 BUBBLE DETECTORS

In a conventional bubble chamber, a track of visible bubbles is formed along the path of the charged particle traversing the superheated liquid. The charge and momentum of the particle can be studied by applying a magnetic field. Reuse of the bubble chamber is possible only after repressurizing it. As mentioned before, Apfel

and Ing have developed two different fast neutron detectors, although they are based on the same superheated liquid detection principle (Apfel 1979; Ing and Birnboim 1984).

#### Apfel's Superheated Drop Detector

Apfel first dispersed thousands of superheated liquid drops (~ 150  $\mu\text{m}$  diameter) in gel (Apfel 1979; Apfel and Roy 1984). Each drop acts like a miniature bubble chamber in that a charged particle from a neutron interaction passing through the drop can cause the drop to vaporize and form a small gas bubble. Although using the gel to hold the superheated liquid in its metastable state is easier and more economical, the gel does not hold the gas bubbles long enough. Instantaneous recording of the vaporization events by using a piezoelectric transducer to pick up the pressure pulses from the vaporization events is necessary (Apfel and Roy 1984). The registered counts can be related to the dose equivalent. A pocket size electronics readout device is, however, necessary for such a recording function (Lo 1987). This type of superheated drop detector can be used as an alarm dosimeter or an area monitor. The price and the size, however, limit its suitability as a personnel dosimeter for routine situations.

Another way of using the SDD to measure the dose equivalent is to collect and measure the volume of the vapor after the superheated liquid drops evaporate. A pen-like SDD is being developed by Apfel based on this volume-measurement technique. The pen SDD is designed for routine personnel monitoring\*. The pen SDD was included in the 14th PDIS, but the test results are not yet available. The pen SDD is not

---

\* Apfel, R. E. Personal communication. Apfel Enterprises, Inc. 25 Science Park. New Haven, CT 06511, 1989.

available commercially. Apfel's SDD is more sensitive than Ing's bubble detector, but the SDD is not reusable after the drops are consumed.

### Ing's Bubble Detector

In the Ing design, the superheated liquid drops (mixture of two brands of fully fluorinated hydrocarbon) are suspended in the polymer (polypropenamide,  $C_2H_5CONH_2$ ) medium. The elastic polymer holds not only the liquid drops ( $\sim 25 \mu m$  diameter), but also the visible gas bubbles (1-2 mm diameter) formed by interactions of the radiation. Interference between the drops will not occur. Simple visual counting of the bubbles is feasible and the bubble number can be related to the neutron dose equivalent. A schematic diagram of the bubble detector is shown in Fig. 2.2.1. Due to the intimate contact between the drops and the polymer and the elastic properties of the polymer, the bubbles are recompressible. The BD is made reusable through the use of hydraulic pressure to recompress the bubbles back into drops. The useful lifetime of the BD depends on the degree of deterioration of the polymer.

The BD-100R (100 is the nominal threshold energy in keV and R stands for reusable) bubble detector is the latest BTI product designed for personnel monitoring. BTI also has developed a spectrometer set which consists of six bubble detectors having six different neutron threshold energies (Ing and Tremblay 1988). These are BDS-10, BDS-100, BDS-600, BDS-1500, BDS-2500, and BDS-10000 (number is the threshold in keV and S stands for spectrometer set). The spectrometer set is said to be less reusable than the BD-100R. The reusability feature greatly reduces the cost of the bubble detector. A reasonable price (\$43 for one BD-100R and \$92 for each BD in the spectrometry set), the small size, and the operational convenience contribute to the great potential of bubble detector as a personnel dosimeter.

ORNL-DWG 89M-9621

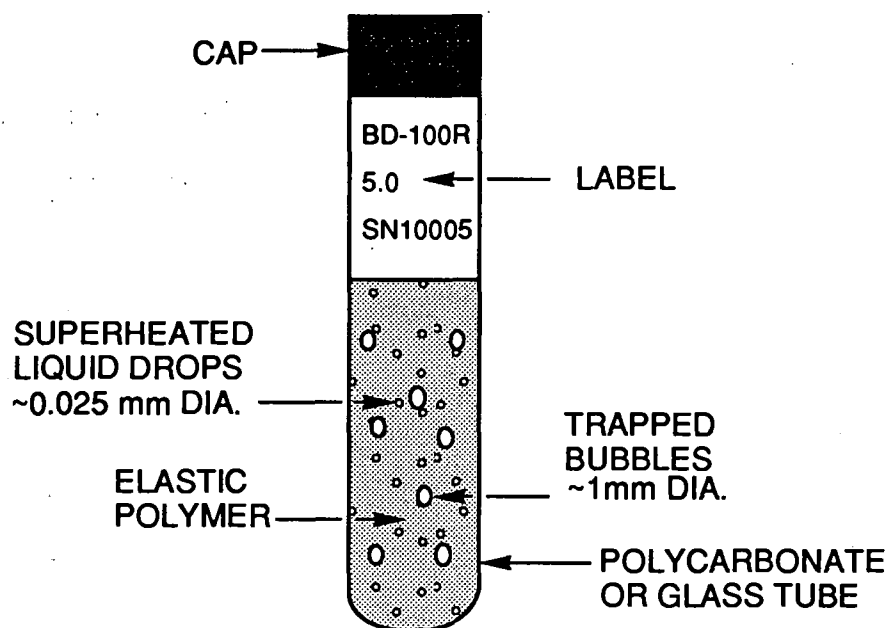


Fig. 2.2.1. Illustration of the bubble detector. The microscopic droplets are uniformly distributed in the polymer. The cylindrical tube (1.6 cm dia.; 8 cm height) holds the nearly transparent mixture. When a neutron hits the drop, the drop vaporizes to become a visible bubble.

Considering the stability of the BD materials, the variation of the fluence-to-dose equivalent conversion factors as a function of neutron energy, and practicality, one BD-100R and one BDS-1500 bubble detector were chosen to be combined with a Harshaw albedo TLD to form the new combination personnel neutron dosimeter.

The production procedure of the BD is similar to that of the SDD, except in the polymerization stage for the BD. First, the detector liquid is put on the top of the monomer solution in a vial under low temperature (the SDD is produced under pressure). The liquid is drained into the monomer with a vortex machine and emulsified by mechanical agitation until the dispersion is appropriate in terms of drop number, drop size, and uniformity of drop density inside the vial. Then, the detector vial is put in a 24 °C water bath for polymerization so that the drops are immobilized. An overlay of the same detector liquid is added on top of the detector medium at low temperature, and the cap is sealed. The vapor pressure exerted by the overlay liquid will keep the BD insensitive. Simple unscrewing of the cap at room temperature makes the liquid drops superheated and the BD is sensitized and ready to use.

The sensitivity of BD depends on the number of superheated liquid drops inside the polymer. Both the vortexing and polymerization steps affect the sensitivity. The normal sensitivity range produced is 0.1-1 bubbles per  $\mu\text{Sv}$  for the BD-100R and 0.1-0.5 bubbles per  $\mu\text{Sv}$  for the BDS-1500. One of the main reasons for choosing the BD as the counterpart of the albedo TLD for the CPND is this high sensitivity to fast neutrons. The direct readout capability of the BD-100R also provides instant and rough measurement of fast neutron dose equivalent (which usually accounts for a large fraction of the neutron dose equivalent). This additional advantage of being an "alarm" dosimeter is similar to the function of  $^{10}\text{B}$ -lined ionization chamber for thermal neutrons and the quartz-fiber electroscope for photons.

In the past two years, the BD may be the one dosimeter, among the neutron dosimeters, that has been most rapidly and widely developed. Like other personnel dosimeters, the BD suffered from many problems in the developmental stage, e.g., bubble fading (Ing and Birnboim 1984), sensitivity drop after sensitization (Ing and Birnboim 1985), sensitivity loss after storage (Perks et al. 1988), and non-uniform drop distribution (Ipe et al. 1988). However, all the above problems now have been solved. Today the bubble detector, with its many novel advantages, is already very promising for personnel fast neutron dosimetry applications.

#### Detection Principle

A liquid can be made into a metastable state with temperature higher than its boiling point and still not vaporize. This superheated state of the liquid can be triggered to boiling by the absorption of energy or the presence of heterogeneous nucleation sites such as solid impurity or air bubbles. By mixing the superheated liquid drops with the perfectly smooth medium (polymer or gel), heterogeneous nucleation sites are reduced and only the mechanism of energy absorption from radiation interaction, temperature increases, or mechanical shock may cause nucleation of the drop.

Detailed descriptions of the neutron detection principle based on the superheated liquid theory have been published (Apfel et al. 1985; Lo 1987). The thermal spike model can best explain the phenomenon of radiation induced nucleation. The model states that a minimum energy is required to be absorbed by the drop for it to form a microscopic embryo bubble. If the embryo bubble reaches a critical radius, the bubble becomes thermodynamically unstable and grows to observable size through the evaporation of the superheated liquid. The critical radius,  $R_c$ , is dependent on the

surface tension and the degree of superheat of the liquid. These relationships are given by the following equation:

$$R_c = 2 \gamma(T) / \Delta P, \quad (2.2.1)$$

where  $\gamma(T)$  = surface tension of the liquid at temperature T; and

$\Delta P$  = pressure difference between the liquid's vapor pressure and the external pressure.

The above equation implies that as  $\Delta P$  increases (the degree of superheat increases), the critical radius decreases and, hence, less energy is required to trigger a nucleation. At constant temperature and pressure, the lower the boiling point of the superheated liquid, the higher the vapor pressure and, therefore, the lower energy threshold would be. This forms the basis of the spectrometric capability for a set of BD's consisting of different superheated liquids which have different boiling points.

However, as shown in equation 2.2.1, when the temperature increases (the surface tension decreases), the threshold energy will be lowered, depending on the degree of the superheat. For a superheated liquid, there is an inhibition temperature below which no neutron can cause nucleation and a limiting temperature above which self-nucleation would occur. Between these two extreme temperatures, an increase in the temperature of the BD will increase its sensitivity. For example, a 1 °C change in a BD-100R causes about 5% change in response. The magnitude of the response change due to the temperature change is also dependent on the neutron spectrum to which the BD is exposed. This is the main disadvantage of the BD for its routine use in personnel monitoring.

Fortunately, this temperature dependent problem can be solved in several ways. One method is to compensate for the decrease of the degree of superheat due to the temperature increase. Ing used an overlay of a suitable superheated liquid which exerts an increasing pressure with temperature in such a way that the effective degree of superheat of the BD remains unchanged (Ing 1986). This technique is being developed at BTI, but it currently has the disadvantage of high cost due to the small quantity of devices produced\*. Response correction by using knowledge of the temperature dependence of the bubble detector is another rough solution. The BD has little temperature dependence in temperature-controlled environments. A BD holder which provides short-term temperature insulation also can be used in case of the short-period exposure in extreme temperature situations.

Fast neutrons transfer energy to recoil ions through elastic scattering when they hit the liquid drops. The recoil ions have short ranges ( $\sim \mu\text{m}$  order) and can deposit energy locally in a form of heat. The ion which has the highest stopping power in the liquid medium plays the major role in bubble nucleation. If the stopping power of the relevant ions in the liquid is known, the threshold neutron energy required to trigger a given state of superheated liquid can be estimated (Lo 1987). With information on the threshold energy and the scattering cross section, the sensitivity of the BD can be calculated (Lo 1987). The BD is insensitive to photons less than 6 MeV or betas due to their insufficient energy deposition. The contribution of the recoil ions from the polymer medium to nucleation also is small due to the short range of ion.

---

\* Ing, H. Personal communication. Bubble Technology Industries. Highway 17, Chalk River, Ontario, K0J0J1, Canada, 1989.

## CHAPTER III

### CHARACTERIZATION OF THE CPND

The CPND consists of one Harshaw albedo neutron TLD and two bubble detectors (one BD-100R and one BDS-1500). Both parts had to be characterized extensively so that the capabilities and limitations of the CPND could be known. This chapter presents the experimental methods and results of the characteristic investigation for the albedo TLD and the BD's.

#### 3.1 INTRODUCTION

The characteristics studied were reusability and optimized readout procedure, linearity of response, LLD, detection capability in mixed neutron-gamma fields, angular dependence, and neutron energy dependence.

All irradiations, unless otherwise specified, were conducted at ORNL's new Radiation Calibration Laboratory (RADCAL). RADCAL is a part of the DOSAR facility and its capabilities have been documented (Casson and Sims 1988). Five radiation sources at RADCAL, which are traceable to the National Institute of Standards and Technology (NIST), were used for the studies. The source characteristics are shown in Table 3.1.1. The  $^{252}\text{Cf}$  neutron source moderated by a 15 cm radius polyethylene sphere or by a 15 cm radius  $\text{D}_2\text{O}$  sphere covered with a cadmium shell is called  $^{252}\text{Cf}(\text{PE})$  and  $^{252}\text{Cf}(\text{D}_2\text{O})$ , respectively. All irradiations, unless otherwise specified, were performed by irradiating the TLD's and BD's perpendicularly on a standard 40x40x15 cm Lucite slab phantom for either neutron or photon radiations. The irradiation times were all at least 100 times longer than the source on-off time and, therefore, no correction for source on-off error was made.

ORNL WSM-9191

Table 3.1.1. Radiation source characteristics at RADCAL.

Source <sup>a</sup>	Mean Energy (MeV)	Nominal Dose Equivalent Rate (mSv h <sup>-1</sup> ) <sup>b</sup>	Operating Mode	Source On-off Time (s)
<sup>137</sup> Cs	0.662	15.57 at 0.5 m	Pneumatic	< 1
<sup>137</sup> Cs	0.662	36.73 at 1 m	Magnetic	< 2
<sup>238</sup> Pu-Be	4.0	0.24 at 1 m	Manual	< 3
<sup>252</sup> Cf (PE) <sup>c</sup>	0.65	0.602 at 2 m	Manual	< 4
<sup>252</sup> Cf (D <sub>2</sub> O) <sup>c</sup>	0.55	11.38 at 1 m	Manual	< 4

- a. All sources are traceable directly or indirectly to NIST (National Institute of Standards and Technology).
- b. ICRP 21 dose equivalent rate in January 1989.
- c. The bare <sup>252</sup>Cf source can be moderated by a 15 cm radius polyethylene sphere or D<sub>2</sub>O sphere covered with a Cd-shell. The moderated sources are called <sup>252</sup>Cf (PE) and <sup>252</sup>Cf (D<sub>2</sub>O).

### 3.2 REUSABILITY AND OPTIMIZED READOUT PROCEDURE

The dosimeter should be reusable and have a reproducible response over a long time and many reuses, considering economic factors. The reuse and signal readout procedures should be simple and operationally convenient.

#### Albedo TLD\*

The response stability of a TLD system can be influenced by the TLD sensitivity variation, the heating system, and the TL light detection system (mainly the PMT). The sensitivity of LiF-TLD is affected by many factors, the primary one being the thermal procedures involved in the use of the TLD. Recommended pre-irradiation oven anneal procedures for LiF-TLD are: 400 °C - 1 h, followed by 80 °C - 24 h or 100 °C - 10 min (Horowitz 1984). The reusability of the oven anneal LiF-TLD's has been demonstrated (Horowitz 1984). However, for the highly automatic Harshaw TLD reader and the Teflon encapsulated TLD card, the conventional high temperature and time-consuming oven anneal method is impractical. Therefore, a reader anneal method has to be adopted. A few authors have shown that the reader anneal TLD system may have higher instability as a function of reuse than the oven anneal TLD system (Julius and De Planque 1984; Driscoll and Richards 1987; Ogunleye et al. 1987; Lakshmanan and Tuyn 1987).

The Harshaw Company has proved the good reusability of the 8800 TLD system (Moscovitch et al. 1987). However, to 1). verify the vendor's claim, 2).

---

\* A detailed version for these results was published in an ORNL report (ORNL-TM-11137, May 1989) and in Radiat. Prot. Manag. 6:55-70; 1989, titled "Optimization of the readout procedures for the Harshaw 8800 automatic TL dosimetry system".

include neutron radiation and a fading time variable in the test, and 3). optimize the readout procedure, the reusability of this new reader anneal automatic TLD system was studied. Factors such as the stability, glow curve reproducibility, and the speed of the readout process were considered in the reusability and optimization studies.

The studies were conducted by exposing 6 groups of TLD-700 free in air to  $^{137}\text{Cs}$ , and 6 groups of TLD-600 on a phantom to  $^{238}\text{Pu-Be}$  (4 Harshaw beta-gamma TLD's per group, 3 groups to 1 mSv, 3 groups to 15 mSv). The exposed TLD groups were read with three different heating profiles after varying fading times (1-37 days). There was no oven anneal between readouts. The above process was repeated 8-10 times.

The readout procedure discussed here refer to both the time-temperature-profile (TTP) heating method and the TL signal processing method. The stability of five types of TL signal for TLD-600 and TLD-700 heated with the Harshaw suggested time-temperature-profile as a function of reuse were compared. A comparison of the stability of TLD's heated with three different time-temperature-profiles also was made.

Two linear heating cycles were used. These two cycles (TTP's) had the same preheat temperature (50 °C), no preheat time, a linear heating rate (25 °C s<sup>-1</sup>), and a maximum temperature (300 °C). The hold time at the maximum temperature was 3.33 s for TTP1 and 6.67 s for TTP 2. The TL light acquisition time was 13.33 s for TTP1 and 16.67 s for TTP 2. The TTP1 heating cycle is shown in Fig. 3.2.1a. TTP1 and TTP2 are the time-temperature-profiles suggested in the Harshaw manual for reading TLD chips that are exposed to low LET and high LET radiations, respectively. The maximum temperature was set at 300 °C to prevent melting the Teflon sheets.

Since the maximum temperature of 300 °C and the hold time at 300 °C did not completely empty the high temperature traps, there were some residual signals,

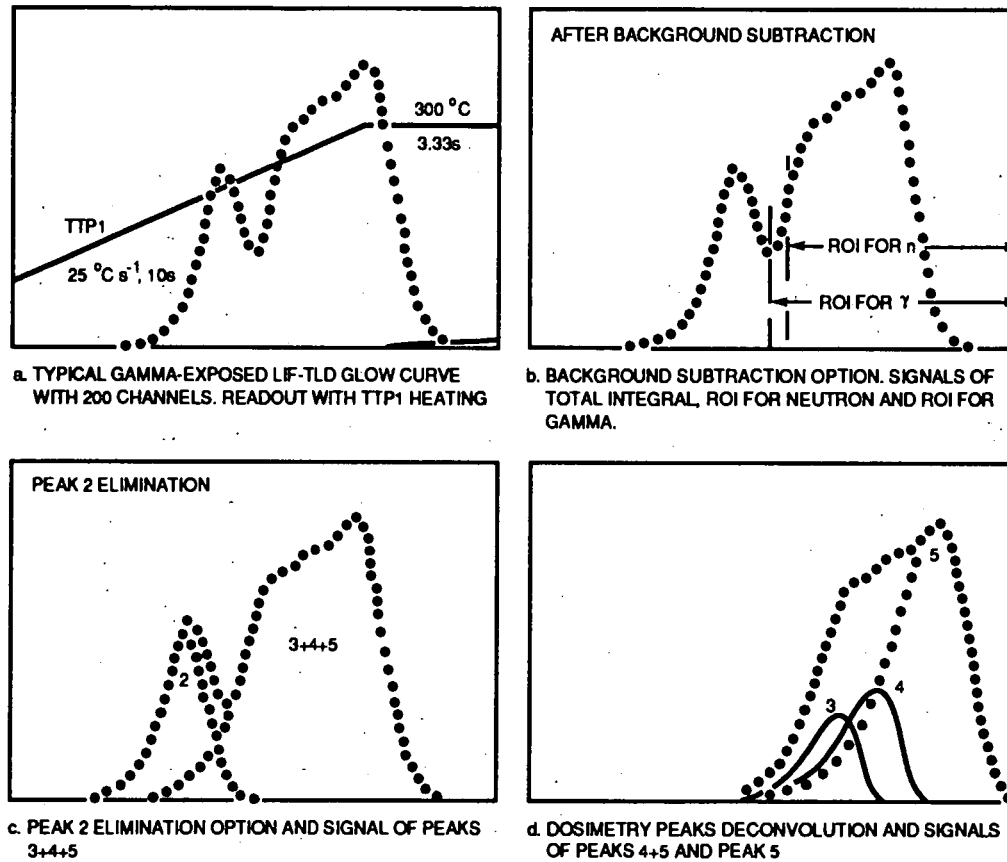


Fig. 3.2.1. The digitized glow curve output of LiF-TLD in the Harshaw 8800 reader, the CGCD (computerized glow curve deconvolution) program options, and five TL light signals (integral light, ROI, peaks 3+4+5, peaks 4+5, and peak 5).

especially for neutron exposures. To study the residual signals, an additional time-temperature-profile 3 (TTP3) was used. TTP3 is set to read the TLD twice with the same TTP1 heating cycle. The time interval between the two TTP1 readouts was about one hour, which was long enough for the TLD's to cool down. The second reading was compared to the first reading to estimate the magnitude of the residual signal.

In practical TLD dosimetry, it is necessary that the fading effect of the low temperature peaks (peak 2 in LiF) be eliminated without significantly affecting the response of the dosimetric peaks (peaks 3, 4, and 5 in LiF). Because no preheat was applied to remove peak 2 in the heating cycle (to save the processing time), TL signal from a carefully chosen region of interest (ROI, which covers only peaks 3, 4, and 5) or the computerized glow curve deconvolution program was used to cope with the fading problem.

The five TL signals used for the stability comparison are shown in Fig. 3.2.1. Figure 3.2.1a shows a typical 200-channel digitized gamma-exposed LiF glow curve obtained with the reader. Figure 3.2.1b shows the integral TL signal and the two ROI signals for neutron and gamma radiation. The integral TL signal includes peak 2 and should have the worst stability. The ROI signal for TLD-700 in gamma exposure was from channel 101 (the saddle point between peaks 2 and 3 for TTP1 heating) to channel 200. The ROI signal for TLD-600 in neutron exposure was also between channels 101 and 200 for first few runs. However, a new ROI from channel 116 (about the middle of the rising part of peak 3) to channel 200 later was found more appropriate due to the more severe fading in peak 3 for TLD-600 in neutron exposure.

Figure 3.2.1c shows the peaks 3+4+5 TL signal after eliminating peak 2 using the CGCD program. The use of ROI and peaks 3+4+5 signals should solve the fading problem to some extent. Figure 3.2.1d shows the deconvolution of the composite

peaks 3+4+5 into individual peaks 3, 4, and 5. Theoretically, the signals of peaks 4+5 and peak 5 should give the best stability over reuse since there is no fading effect.

Tables 3.2.1 and 3.2.2 show the stability comparison of the five TL signals for the TLD-700 and the TLD-600 heated with time-temperature-profile 1, respectively. The stability comparison of TLD's heated with TTP1, TTP2, and TTP3 is shown in Table 3.2.3.

The reference light (RL) signals of the four PMT's were monitored after every ten card readouts. The TLD-700 and TLD-600 were read by PMT's 1 and 4, respectively. The RL measurements served to check both the short-term variation and long-term stability of the TL light detection system and also to estimate its contribution to the TLD stability as a function of reuse (see column 3 in Tables 3.2.1 and 3.2.2).

The storage time before irradiation ( $t_1$ ) and the fading time after irradiation ( $t_2$ ) are shown in column 2 of Tables 3.2.1 - 3.2.3. Those runs with  $t_2$  longer than 2 days can be regarded as having long fading times. Peak 2 has faded and cannot be identified in the glow curves of the long fading runs. Peak 3 of some glow curves in the last run were also not distinct due to its 37-day fading.

The signal of peaks 3+4+5 in the tables was derived in two CGCD options. For the runs with short fading times, peak 2 and peaks 6+7 (TLD-600 in neutron exposure) were removed by the peak 2 elimination option in the CGCD program and peaks 3+4+5 was derived (see Fig. 3.2.1c). However, for the runs with long fading times, the peak 2 elimination option did not work well due to unclear peak 2 identification. Therefore, for the long-fading runs, the background subtraction option in the CGCD program was used to derive peaks 3+4+5 (see Fig. 3.2.1b). The signals of peaks 4+5 and peak 5 were derived by the peak separation option in the CGCD program (see Fig. 3.2.1d).

ORNL WSM-9192

Table 3.2.1. Stability of TLD-700 exposed to gamma radiation (1 mSv) and heated with time-temperature-profile 1 (nC).

Run No.	Day (t1, t2) <sup>a</sup>	RL <sup>b</sup>	IL <sup>c</sup>	ROI <sup>d</sup>	Peaks 3+4+5	Peaks 4+5	Peak 5
1	(1,2)	228	46.0	44.6	45.3	35.9	24.8
2	(3,1)	228	47.3	45.9	44.9	36.9	27.3
3	(3,10)	228	44.1	44.5	42.8	37.5	26.8
4	(1,< 1)	223	52.1	44.9	44.5	35.8	24.6
5	(1,< 1)	224	51.4	44.0	43.5	34.8	25.2
6	(< 1,< 1)	226	50.4	42.1	42.3	34.0	24.5
7	(1,< 1)	226	49.5	43.4	42.6	34.8	25.0
8	(1,7)	232	43.6	43.2	42.3	33.3	25.4
9	(4,37)	238	41.5	43.4	41.7	38.7	30.1
Mean		228	47.3	44.0	43.3	35.7	26.0
1 $\sigma$ of Mean		2.3%	8.0%	2.5%	3.0%	4.8%	7.0%
Max. Variat.		4.0%	-12.0%	4.0%	5.0%	8.0%	16.0%

a. t1 is storage time before exposure, t2 is fading time after exposure.

b. RL is the reference light standard in the Harshaw reader.

c. Integral light (IL): channels 1 - 200.

d. Region of interest (ROI): channels 101 - 200.

ORNL WSM-9193

Table 3.2.2. Stability of TLD-600 exposed to  $^{238}\text{Pu}$ -Be neutron radiation (1 mSv) and heated with time-temperature-profile 1 (nC).

Run No.	Day (t1, t2) <sup>a</sup>	RL <sup>b</sup>	IL <sup>c</sup>	ROI <sup>d</sup>	Peaks 3+4+5	Peaks 4+5	Peak 5
1	(1,2)	245	30.8	30.3	29.6	18.9	14.6
2	(3,1)	245	32.2	30.8	26.5	18.1	14.4
3	(1,12)	248	25.8	26.1	23.9	19.0	16.5
4	(< 1,< 1)	243	31.9	29.1	27.3	21.6	14.6
5	(< 1,< 1)	244	33.5	29.1	26.2	16.1	12.5
6	(< 1,< 1)	244	34.1	26.2 <sup>d</sup>	28.0	17.6	13.0
7	(< 1,< 1)	243	34.0	25.6	25.3	19.4	13.0
8	(< 1,< 1)	243	32.5	25.2	25.6	16.4	12.2
9	(1,7)	245	27.4	24.4	22.2	16.7	13.9
10	(4,37)	246	22.3	23.1	20.5	16.7	14.5
Mean		245	30.5	24.9	25.5	18.1	13.9
1 $\sigma$ of Mean		0.7%	13%	4.8%	11%	9.5%	9.2%
Max. Variat.		1.0%	-27%	-7%	-20%	19%	19%

a. t1 is storage time before exposure, t2 is fading time after exposure.

b. RL is the reference light standard in the Harshaw reader.

c. Integral light (IL) : channels 1-200.

d. Region of interest (ROI) changed from channels 101 -200 to channels 116 -200 after run no. 5.

ORNL WSM-9194

Table 3.2.3. TLD stability for different time-temperature-profiles.

Run No.	Day (t1, t2) <sup>a</sup>	TLD-700 (15 mSv H <sub>γ</sub> )		TLD-600 (15 mSv H <sub>n</sub> )		
		TTP1	TTP3	TTP1	TTP2	TTP3
1	(1,2)	653	----	396	480	434
2	(3,1)	653	632	375	487	432
3	(3,10)	603	588	314	417	394
4	(1,< 1)	631	614	360	491	455
5	(1,< 1)	627	604	378	499	462
6	(< 1,< 1)	615	597	366	481	444
7	(1, < 7)	600	585	344	---	419
8	(4, 37)	574	566	255	355	343
Mean		620	598	349	459	423
1 σ of Mean		4.4%	3.6%	13%	12%	9%
Max. Variat.		-7.4%	5.7%	-27%	-23%	-19%

1. TL signal is peaks 3+4+5 in nC.

a. t1 is storage time before exposure, t2 is fading time after exposure.

The indices for the TL signal stability are one standard deviation ( $1\sigma$ ) and the maximum variation of the TL signal as a function of reuse. The maximum variation in the last row of Tables 3.2.1-3.2.3 refers to the maximum deviation (in %) from the mean signal for all TL signals in the same column.

Some observations and conclusions from the results in Tables 3.2.1 - 3.2.3 are as follows:

1. For TLD-700 using TTP1 heating, no residual signal for low gamma exposures and a residual signal of  $\sim 0.4\%$  for high gamma exposure were found. For TLD-600, neutrons induce higher peaks 6+7 and lower peaks 3+4 than photons. The second to first reading ratios in TTP3 heating for TLD-600 in both low and high neutron exposures were  $\sim 0.02$ .
2. The glow curves were very reproducible for TLD-600 and TLD-700 for all TTP's used. This proved the stability of the TLD heating process and agreed with Harshaw's results (Moscovitch et al. 1987).
3. The reader PMT stability (expressed in  $1\sigma$  and maximum variation, respectively) was  $\sim 2.3\%$  and  $4.0\%$  for PMT channel 1, and  $\sim 0.7\%$  and  $1.0\%$  for PMT channel 4 (see the reference light variations in Tables 3.2.1-3.2.2). These long-term RL stability results were similar to the short-term RL variation results, which are given in Appendix 1.
4. As expected, the integral TL light (IL) signal had the worst stability performance in almost all cases. One standard deviation was  $8\%$  for TLD-700 (Table 3.2.1) and  $13\%$  for TLD-600 (Table 3.2.2), and the maximum variation was  $-12\%$  for TLD-700 and  $-27\%$  for TLD-600. The longer the fading time, the smaller the IL signal. Therefore, the worst performance was primarily due to the fading of peaks 2 and 3.

5. The region of interest (ROI) signal of channels 101-200 gave the best stability for TLD-700 (Table 3.2.1,  $1\sigma = 2.5\%$ , maximum variation = 4%). The fact that the magnitude of the ROI signal was not a function of fading time shows that the choice of ROI removed the effect of peak 2 fading in TLD-700. The ROI signal in channels 116-200 was best for TLD-600 (Table 3.2.2,  $1\sigma = 4.8\%$ , maximum variation = -7%). The ROI and peaks 3+4+5 signals of the last run in the TLD-600 neutron exposure were the smallest. This indicated that, at the expense of reduced sensitivity, the channels of the ROI for TLD-600 can be chosen smaller to further reduce the effect of peak 3 fading and better stability can be expected. However, the stability results of the ROI signal for TLD-600 in neutron exposure were already satisfactory. The above results prove that, if the appropriate ROI is chosen, both the stability and the sensitivity can be optimum. The ROI signal can be obtained very easily from setting the calibration region in the reader (see Appendix 1). Therefore, it is very practical to use the ROI signal in routine TLD readouts.
6. For TLD-700, the peaks 3+4+5 or peaks 4+5 signal gave good stability (Table 3.2.1,  $1\sigma < 5\%$ , maximum variation  $< 10\%$ ), but stability of the peak 5 signal was only fair. For TLD-600, the peaks 4+5 and peak 5 signals had slightly better stability than the peaks 3+4+5 signal. However, they showed only fair stability (Table 3.2.2,  $1\sigma \sim 10\%$ , maximum variation  $\sim 20\%$ ). The reasons for these results are that peak 3 fades more in TLD-600 than in TLD-700, and the peak separation option in the CGCD program did not work well, especially in the TLD-600 neutron exposure case. The standard deviation of the 4 TLD's per group for every run is not shown in the tables, but it did not change significantly during reuse in the case of TLD-700. As compared with the TLD-700 case, the standard deviation per group of TL signals of peaks 3+4+5, peaks 4+5, and peak 5 varied by an order of

magnitude between runs for TLD-600 neutron exposures. This also showed that the CGCD program did not work well for neutron-exposed TLD-600.

7. The stability of TLD-700 in high gamma exposure using both TTP1 and TTP3 heatings was compared using the signal of peaks 3+4+5 (Table 3.2.3). For TLD-600 in high neutron exposure, the stability using TTP1, TTP2, and TTP3 heatings were compared. For TLD-700 heating, TTP3 was slightly better than TTP1, but both the TTP1 and TTP3 heatings resulted in good stability. For TLD-600 heating, TTP3 and TTP2 were slightly better than TTP1.

The signals of region of interest and peaks 3+4+5 can have the optimum reuse conditions for TLD's heated with the Harshaw-suggested time-temperature-profiles, regarding the stability, sensitivity, and the readout speed. One standard deviation and the maximum variation of the ROI signal as a function of reuse in the optimum conditions can be within 5% and 10%, respectively. It is suggested that, in routine albedo TLD processing, TTP1 is used to heat TLD-700 chips (elements 2 and 3) and TTP2 is used to heat TLD-600 chips (elements 1 and 4). Only reader anneal with the same TTP's before the use of the TLD's is necessary. The TL signal of region of interest is used, due to its best stability and fast readout. For TLD-700 elements in TTP1 heating, the appropriate ROI is channels 101-200. For TLD-600 elements in TTP2 heating, the appropriate ROI is channels 96-200. The above readout procedure (ROI signals and TTP heating methods) was used in this research. A computer printout of the readout procedure is listed in Appendix 2.

#### Bubble Detector

The BD-100R (sensitivity  $0.7 \text{ bu } \mu\text{Sv}^{-1}$ ) was shown to be reusable up to 24 times in 48 days with the mean response variation less than 15% using a second day

recompression procedure (Jones 1988). The units of bubble response are abbreviated as bu in this dissertation. The hydraulic pressure and time period in their recompression were 6.2 MPa and 1 h, respectively. Toronto General Hospital personnel reused the BD-100R (sensitivity  $0.56 \text{ bu } \mu\text{Sv}^{-1}$ ) for 3 months with a daily recompression procedure (2.8 MPa - 15 h) and no drop of sensitivity was experienced\*. These two results seem to verify the vendor's claim: the BD-100R can be reused for three months, if recompressed daily. The vendor also states that the BDS-1500 is less reusable than the BD-100R, but can be reused at least five times. Besides the above, nothing more has been reported on the reusability of the BD's.

From the operational point of view, it is better that bubble detectors be used for long periods without many recompressions. It is known qualitatively that the less frequent the bubble detector recompression, the less it can be reused. The vendor states that, without recompression, the BD-100R can be used only for one month. The two main purposes in studying the reusability of the bubble detectors were 1). to examine the stability of both the BD-100R and the BDS-1500 as a function of reuse over their usable lifetimes, and 2). to optimize the operational reuse procedure for the bubble detectors, regarding the recompression schedule.

Nine BDS-1500 (sensitivities between  $0.16\text{-}0.55 \text{ bu } \mu\text{Sv}^{-1}$ ) and nine BD-100R (sensitivity  $0.056 \text{ bu } \mu\text{Sv}^{-1}$ ) bubble detectors from the first batch were tested for reusability by tracing their individual sensitivity for six months. To optimize the reuse procedure, the above nine BDS-1500 and nine BD-100R were divided into four groups in four reuse procedures. Three BDS-1500 and three BD-100R were recompressed on

---

\* Poluha W. Personal communication. Morserco Limited. 6620 Kitimat Rd. Mississauga, Ontario L5N2B8, Canada, 1989.

the second day after irradiation with the personal recompression device (PRD) for 0.5 hour. The PRD can recompress one bubble detector at a time and can exert about 5 MPa (725 psi) hydraulic pressure. Three other groups (2 BDS-1500 and 2 BD-100R in each group) were recompressed with the recompression chamber (RC) using a second day recompression, a weekly recompression, and a biweekly recompression procedures, respectively. The RC can recompress eighteen bubble detectors at a time and can exert hydraulic pressure up to 7 MPa.

The BD's were exposed to a  $^{238}\text{Pu}$ -Be source in reproducible positions with a source-detector distance about 50 cm. No correction was made for decay of the source over the test period (0.4%). Since the bubble detector response is dependent on the temperature, constant temperature has to be ensured throughout the test. This was achieved by putting the rezeroed detectors in a place which had the same temperature as the irradiation environment at least one hour before exposure. The temperature was controlled and monitored for every exposure. The temperature was between 20 °C and 24 °C and no temperature dependence correction was made.

The stability index of the BD's is one standard deviation of the response (%) over the period of reuse. The results of the BDS-1500 reusability, using the second day recompression procedure with the PRD for 5 months, are shown in Fig. 3.2.2. Exposure time was 300 s. Two BDS-1500 glass tubes (S.N. 6 and 10) were broken during the recompression procedure and had to be discarded. These detectors showed good stability before breakage ( $1\sigma$  was 10%-15%). The response of the BDS-1500 S.N. 11 decreased slightly after three months. However, the standard deviation of the response was ~ 18% for the first three months (36 reuses), whereas it was ~ 20% over the 6-month period (42 reuses).

ORNL-DWG 89M-9623

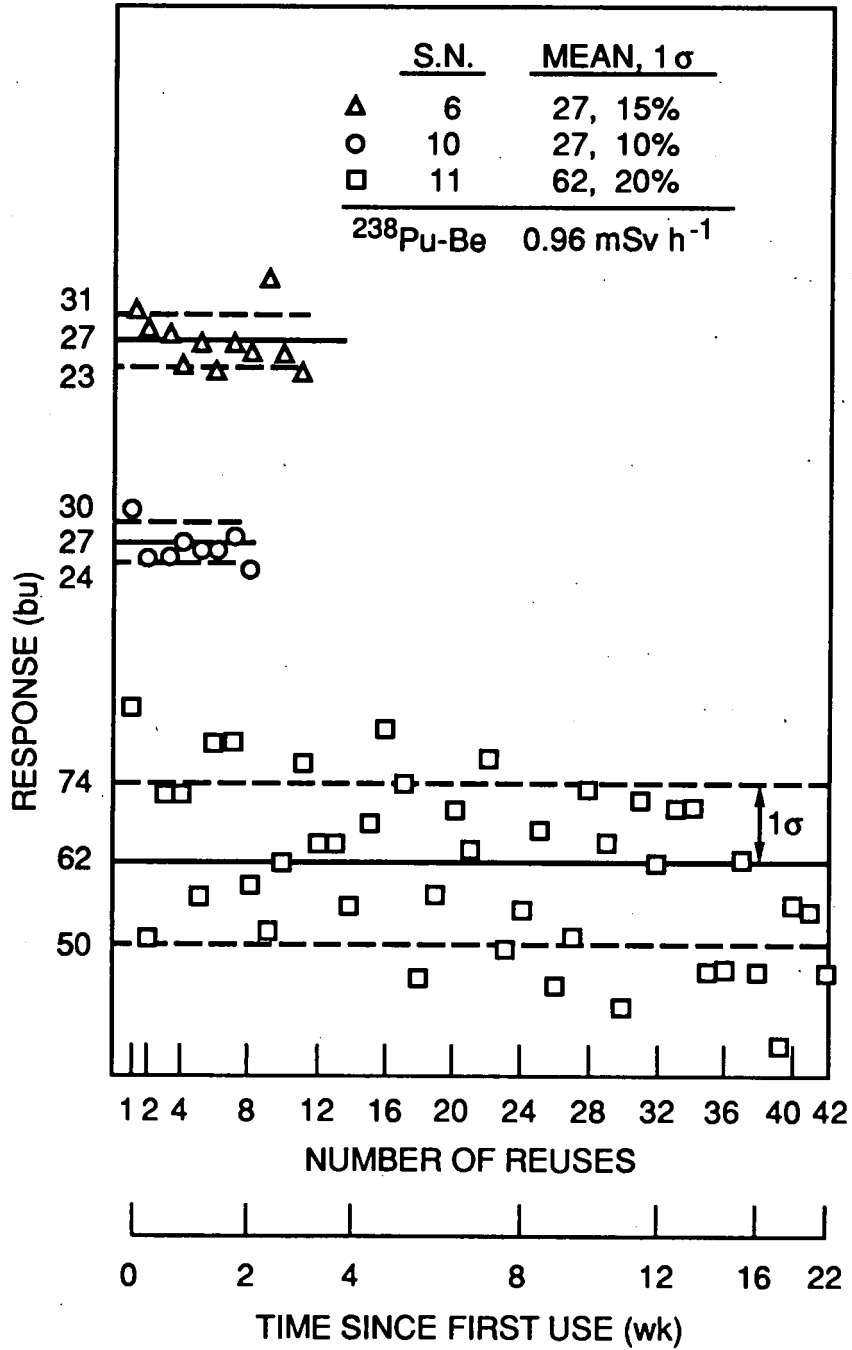


Fig. 3.2.2. Reusability of BDS-1500. Recompressed on the second day with the personal recompression device (5 MPa-0.5 h).

The reusability results of the BDS-1500 using the second day and weekly recompression procedures with the RC (2.8 MPa - 1 h) over a period of six months are shown in Figures 3.2.3 and 3.2.4, respectively. There were 52 reuses and 24 reuses over the 6-month period for the second day and weekly recompression procedures, respectively. Exposure times were 420 s and 1260 s for the second day and weekly recompression procedures, respectively. The BD's using the second day and weekly recompression procedures had similar good stabilities over the first quarter ( $1\sigma \sim 17\%$ ). However, for the 6-month reuse period, the BDS-1500 using the second day recompression procedure showed a slightly better stability ( $1\sigma \sim 17\%$ ) than that using the weekly recompression procedure ( $1\sigma \sim 18\%-22\%$ ).

The 6-month (14 reuses) reusability results of the BDS-1500 using the biweekly recompression procedure (2.8 MPa - 2 h) are shown in Fig. 3.2.5. Exposure time was 500 s. The BDS-1500 using the biweekly recompression procedure showed the poorest stability ( $1\sigma \sim 26\%$ ). It was noted that a few abnormal, non-spherical bubbles (an indication of polymer deterioration) also formed one month after initial neutron exposure during the biweekly recompression test.

The BD-100R from the first batch in all four reuse procedures showed the same bad stability. One typical reusability result of the BD-100R recompressed on the second day with recompression chamber (2.8 MPa - 1 h) are shown in Fig. 3.2.6. About 2 weeks after sensitization of the BD-100R, the sensitivity dropped gradually to  $\sim 1/10$  of the original, and, then, maintained that sensitivity level. The result was much worse than other reported results (Jones 1988). A discussion with Ing revealed that this sensitivity loss problem was due to the difficult production control of the low sensitivity BD-100R (only  $0.056 \text{ bu } \mu\text{Sv}^{-1}$ , about  $1/10$  of those used by Jones). Some superheated droplets may diffuse out of the polymer after sensitization. However, such

ORNL-DWG 89M-9624

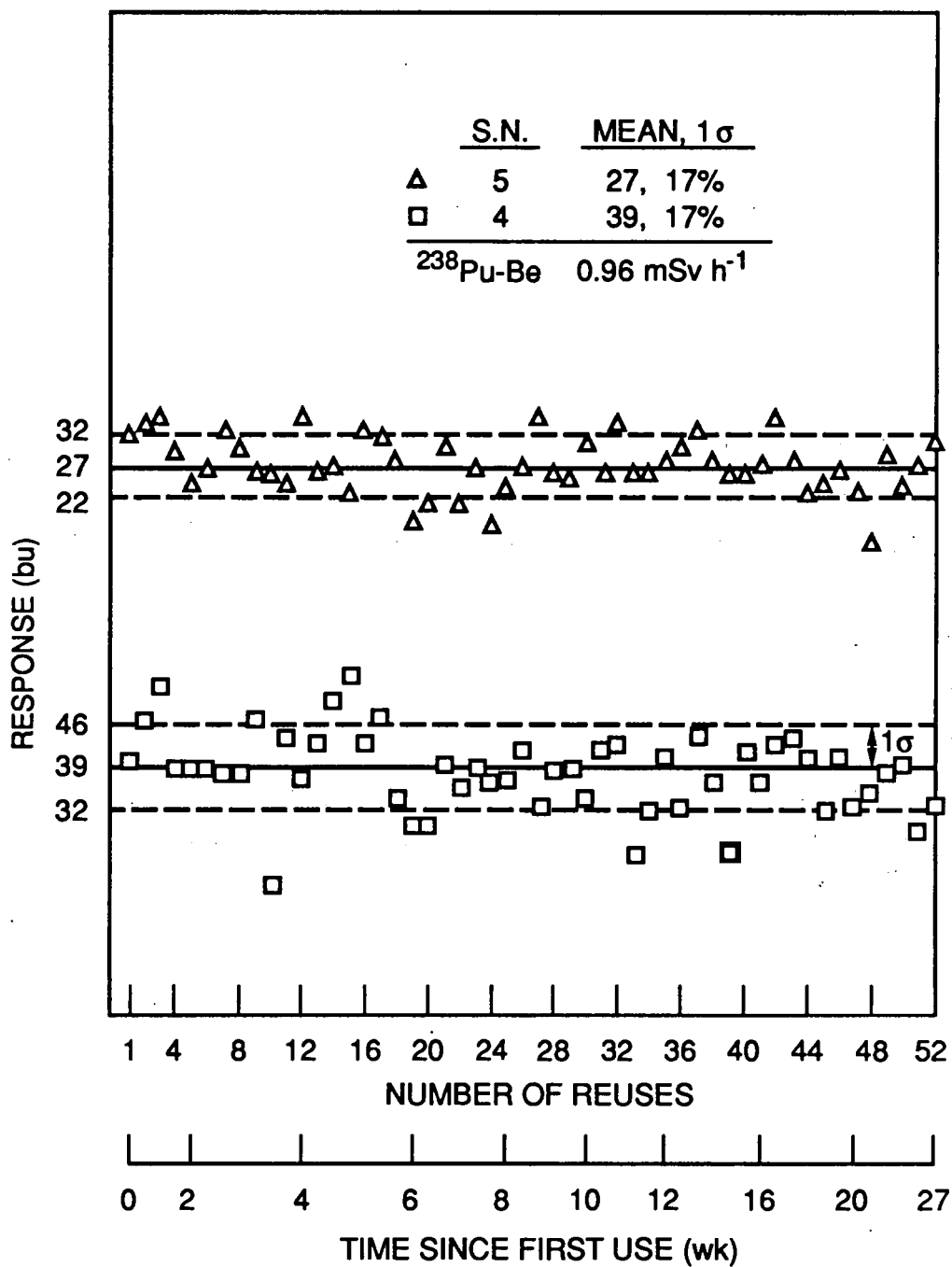


Fig. 3.2.3. Reusability of BDS-1500. Recompressed on the second day (2.8 MPa-1 h).

ORNL-DWG 89M-9625

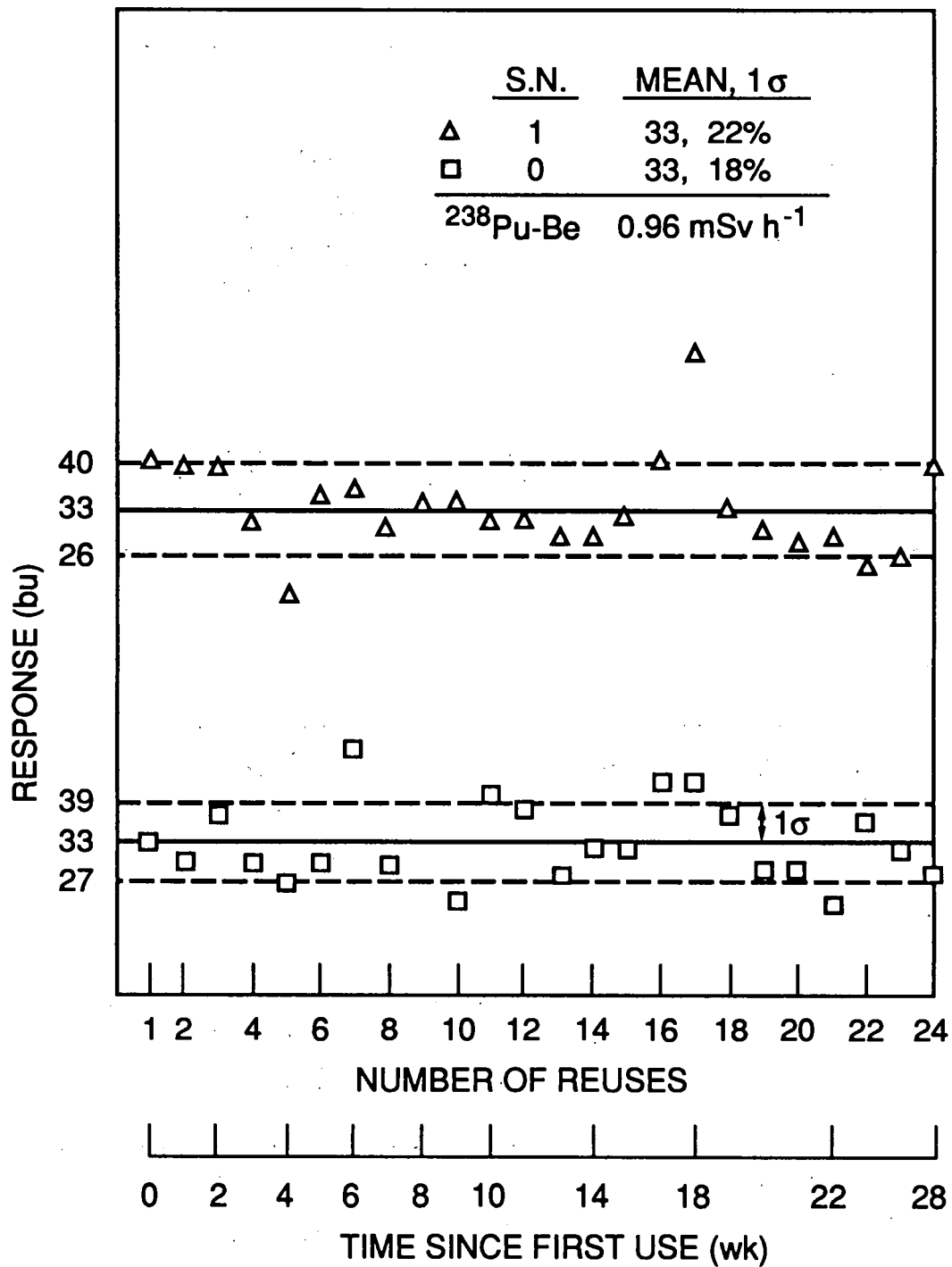


Fig. 3.2.4. Reusability of BDS-1500. Recompressed weekly (2.8 MPa-1 h).

ORNL-DWG 89M-9626

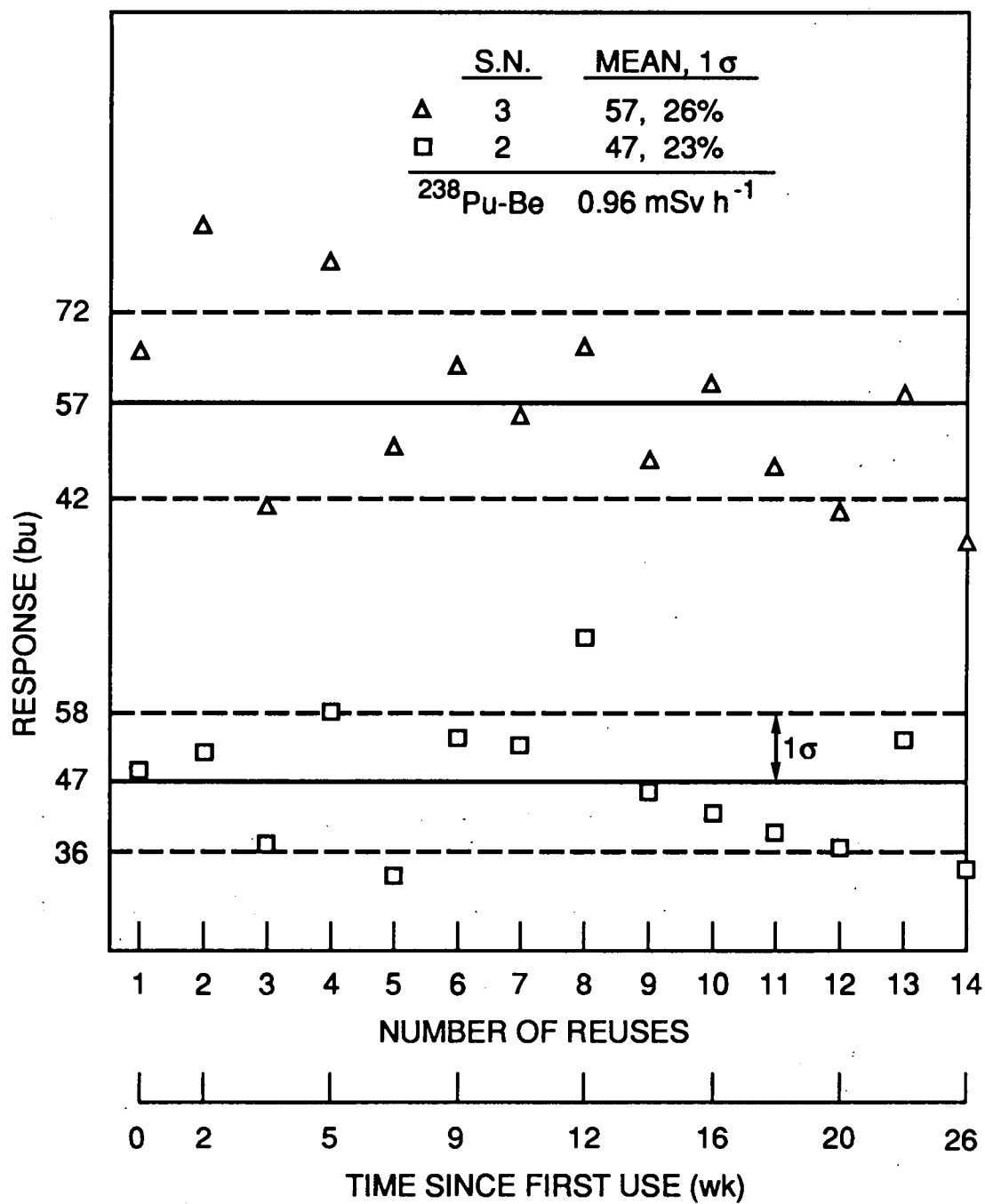


Fig. 3.2.5. Reusability of BDS-1500. Recompressed biweekly (2.8 MPa-2 h).

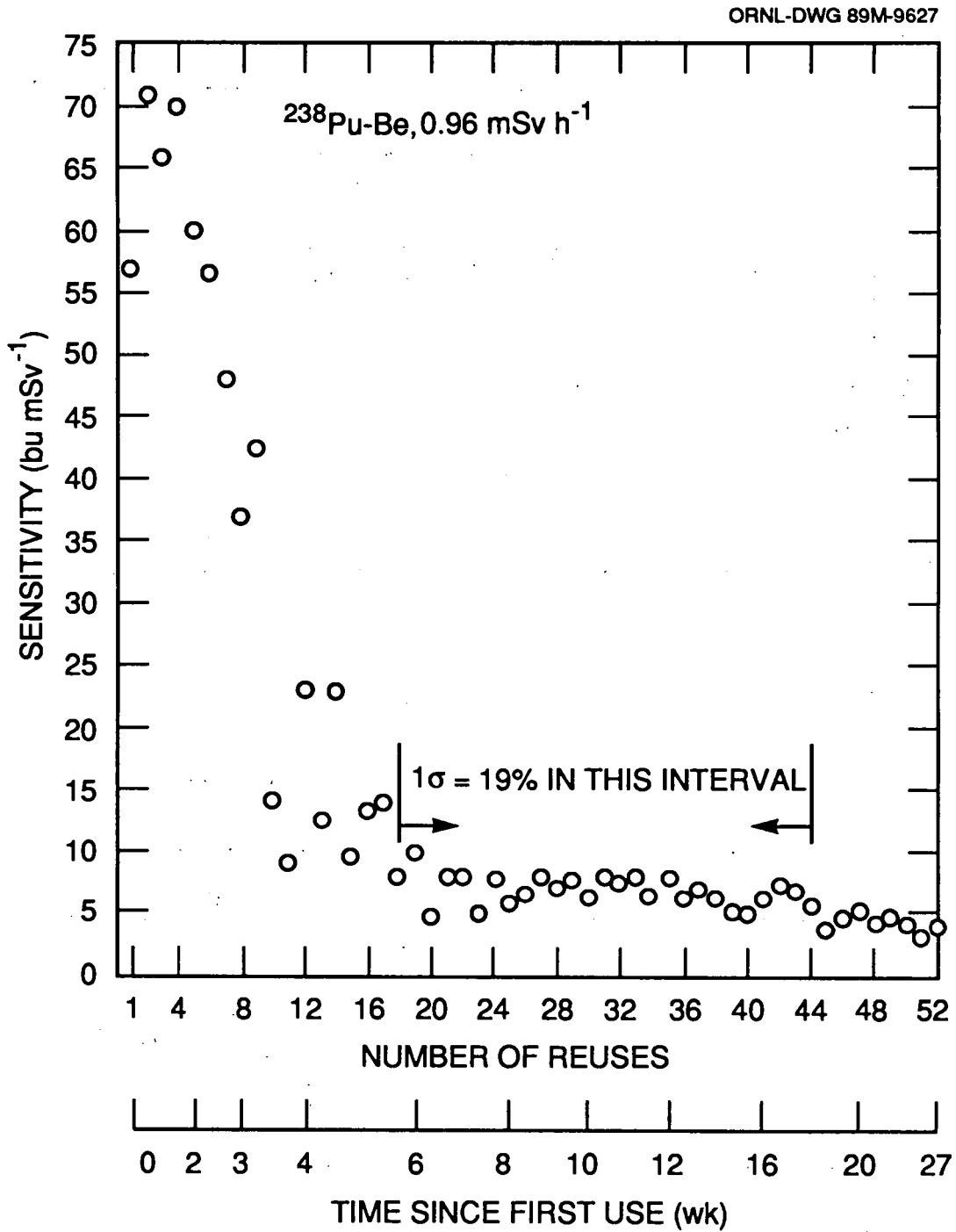


Fig. 3.2.6. Reusability of BD-100R. Recompressed on the second day (2.8 MPa-1 h).

quality problems have been solved to some extent in BTI's recent production procedure.

To check the reusability of the BD-100R with sensitivity in the normal production range and to investigate batch-dependent effects, five BD-100R (sensitivities between 0.085-0.82  $\text{bu } \mu\text{Sv}^{-1}$ ) and four BDS-1500 (sensitivities between 0.1-0.5  $\text{bu } \mu\text{Sv}^{-1}$ ) from the second batch purchased were tested after the first phase reusability test. The 3-month test (20 reuses) was conducted in the same way as in first phase. However, only the second day recompression procedure using the recompression chamber was used. The reusability results of BDS-1500 in the second phase test were similar to those in the first phase and, therefore, are not shown here. The BDS-1500 in the second phase test can be reused for three months with a standard deviation of  $\sim 20\%$ .

The reusability results of the five BD-100R for three months in the second phase test are shown in Fig. 3.2.7. The standard deviations ranged from 15% to 33%. The response of the BD-100R with the lowest sensitivity (0.085  $\text{bu } \mu\text{Sv}^{-1}$ ) decreased slightly and  $1\sigma$  value was 33%. The BD-100R with the sensitivity of 0.15  $\text{bu } \mu\text{Sv}^{-1}$  had a  $1\sigma$  value of 33%. This was due to the first two high data points which might have resulted from statistical variations. The other three BD-100R had a standard deviation no greater than 20%. The BD-100R detectors used in the second test showed no significant sensitivity loss as that in the first phase test.

It is believed that the variation in bubble detector response during the reuse tests is primarily due to expected statistical variations. No significant sensitivity loss of the bubble detector was observed, and all bubbles formed were able to be recompressed during the whole test period. Similar stability results between this study and other reported results (Jones 1988) using different hydraulic pressures and recompression

ORNL-DWG 89M-9628  
 BD-100R SENSITIVITY  
 (bu  $\mu\text{Sv}^{-1}$ )

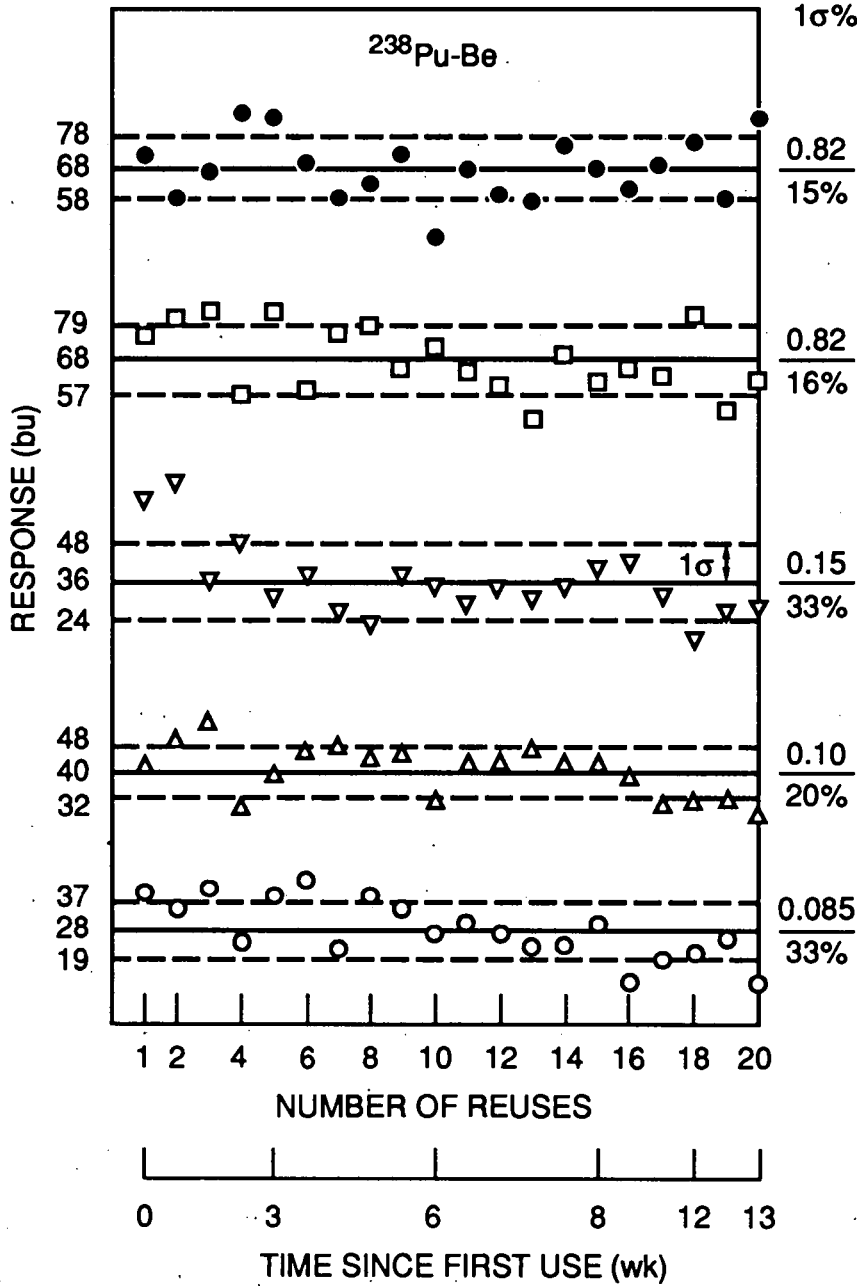


Fig. 3.2.7. Reusability of BD-100R with sensitivity in normal production range and recompressed on the second day.

durations also indicated that the pressure and time period during recompression do not affect the reusability.

Besides the above-mentioned reusability tests, reusability of the bubble detectors (BD-100R and BDS-1500) also has been demonstrated through the use of BD's for other experiments. Practical use of the BD's throughout the research period showed that most of them can be reused for at least three months with good stability. However, a few BD's did show a sensitivity drop, and a sensitivity correction would be required if these BD's were to continue to be used. There was also no bubble fading problem over an 8-month period after irradiation.

### 3.3 LINEARITY OF RESPONSE

Ideally, the dosimeter should have a linear response over a dose equivalent range as wide as possible. In that linear range, only one calibration point is necessary and it can be applied to other exposures. Otherwise, response correction for nonlinearity may be required.

#### Albedo TLD

The linearity of the albedo TLD was examined by irradiating many groups of TLD's (4 TLD's in each group) to different doses with photon and neutron sources. Since both TLD-600 and TLD-700 respond to photon radiation, the linearity of all four elements in a TLD card was checked with  $^{137}\text{Cs}$  irradiations. Photon exposures of bare TLD cards were varied from  $5.16 \mu\text{C kg}^{-1}$  (20 mR) to  $2580 \mu\text{C kg}^{-1}$  (10 R) free in air.

The linearity results are plotted in Fig. 3.3.1 (the data are given in Appendix 3). The mean TL signal (nC) for each element in a group of 4 TLD's is plotted versus the exposure ( $\mu\text{C kg}^{-1}$ ). The percent standard deviation of the 4 TLD's for every data point

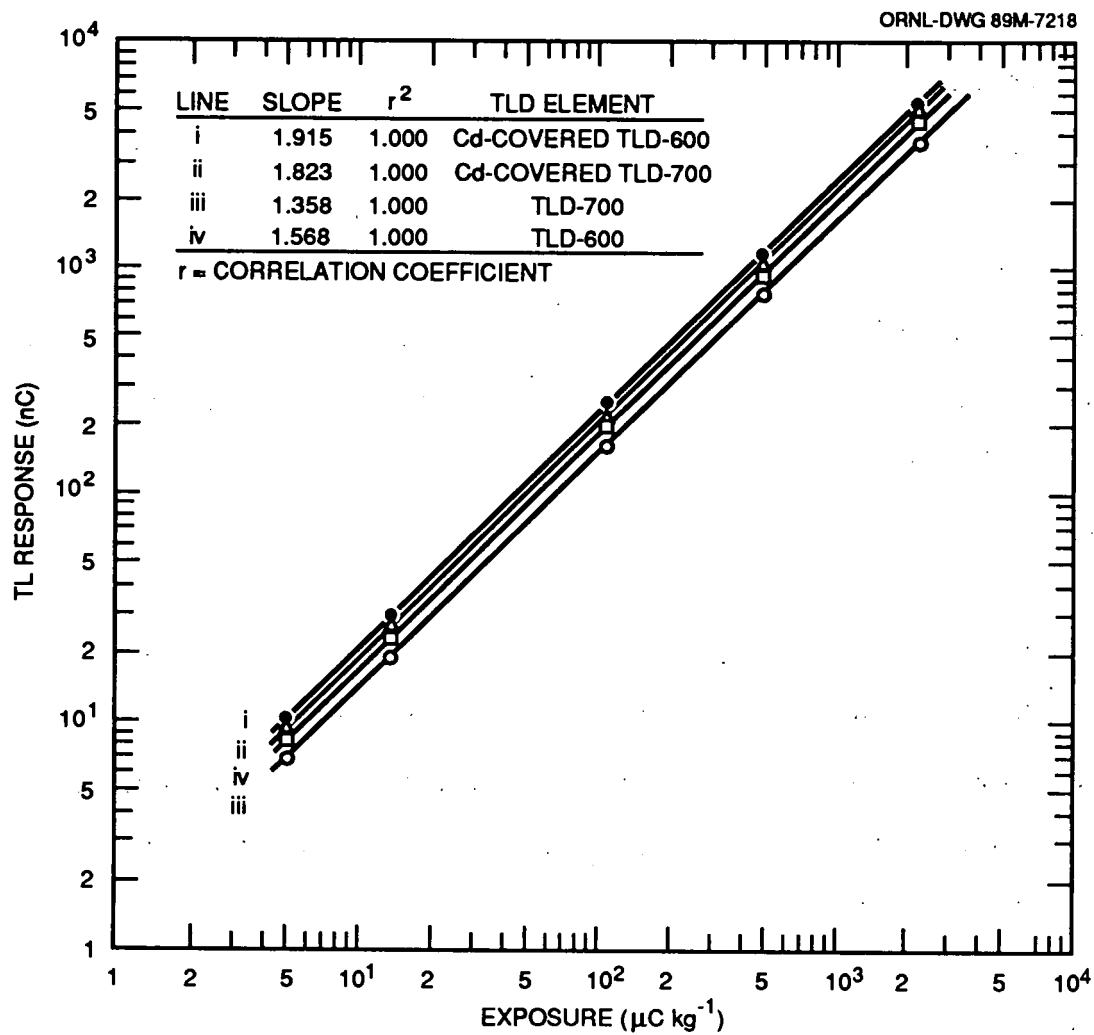


Fig. 3.3.1. Linearity of the four elements in the albedo neutron TLD exposed to a  $^{137}\text{Cs}$  source free in air.

was less than 1.5% for elements 2 and 3, and less than 3.5% for elements 1 and 4. Since the magnitude of error was not a function of dose and was small, the error bars were not plotted in the figure. A linear least squares fit gave the slope (nC per  $\mu\text{C kg}^{-1}$ ) and the  $r^2$  value (square of correlation coefficient) of each line for each element. The residuals of the data points for these linear lines were all less than 3% for elements 2 and 3, and less than 5% for elements 1 and 4. The fit lines, small residuals, and the fact that all  $r^2$  values are equal to 1.000 showed the excellent photon linearity of the albedo TLD over the wide exposure range of interest (3 orders of magnitude). When the TL signals (nC) are converted to TL signals in units of mR by dividing the corresponding reader calibration factor, the four nearly parallel lines in the log-log plot would become one line with a slope of 1.

The neutron linearity was checked with irradiations using the  $^{238}\text{Pu}$ -Be and  $^{252}\text{Cf}$ (PE) sources. Four TLD's as a group were irradiated on the phantom to a specified dose equivalent. The neutron dose equivalents were varied from  $\sim 0.5$  mSv to  $\sim 2$  mSv for  $^{238}\text{Pu}$ -Be and from  $\sim 0.05$  mSv to  $\sim 3.0$  mSv for  $^{252}\text{Cf}$ (PE).

As shown in equations 2.1.4 and 2.1.5, the two TLD-700 elements in a card only play the role of estimating the photon signals of their paired TLD-600 element. Therefore, in neutron exposure the albedo response A and the total response T are the quantities of concern. The mean albedo response A and mean total response T (in units of mR) for each TLD group were plotted versus the neutron dose equivalent. The neutron linearity results for  $^{252}\text{Cf}$ (PE) and  $^{238}\text{Pu}$ -Be exposures are shown in Fig. 3.3.2 and Fig. 3.3.3, respectively (the data are given in Appendix 4). Note that a linear-linear scale was used in Fig. 3.3.3. The standard deviations of the mean A and T responses for all data points in the two figures were all less than 5%. A linear least squares fit gave the slope, sensitivity (mR mSv $^{-1}$ ), and the  $r^2$  values for both A and T

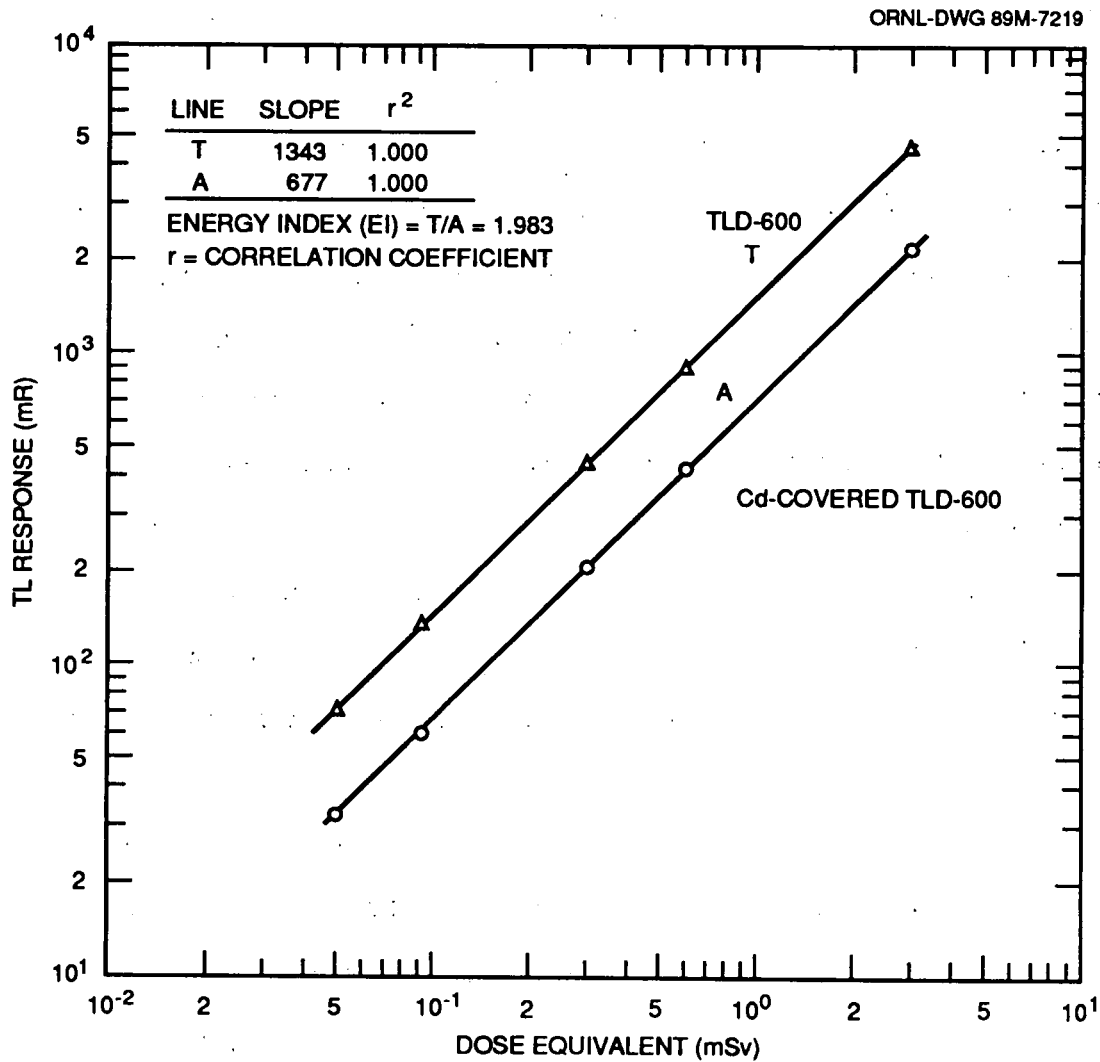


Fig. 3.3.2. Linearity of the albedo neutron TLD exposed to the  $^{252}\text{Cf}(\text{PE})$  neutron source.

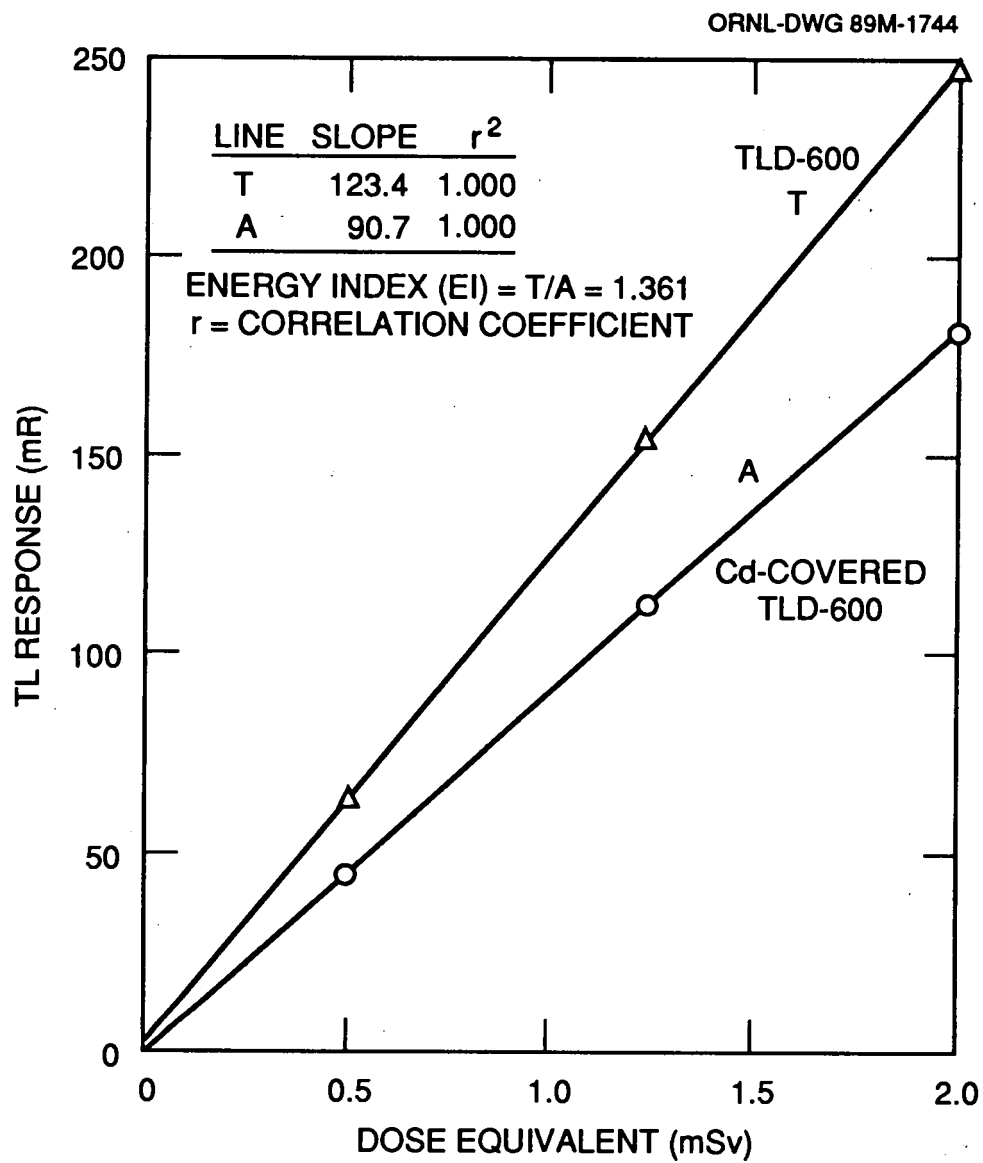


Fig. 3.3.3. Linearity of the albedo neutron TLD exposed to the  $^{238}\text{Pu}$ -Be source.

responses. The  $r^2$  values were equal to 1.000 for both sources. The residuals of the data points were all less than 1% for  $^{238}\text{Pu-Be}$  and 3% for  $^{252}\text{Cf(PE)}$ . These results indicated the excellent neutron linearity of the albedo TLD.

The parallel lines for responses A and T in the log-log plot of Fig. 3.3.2 means that the energy index ( $\text{EI} = T / A$ ) value is constant over the dose equivalent range. The EI value from the slope ratio was 1.98 for  $^{252}\text{Cf(PE)}$  and 1.36 for  $^{238}\text{Pu-Be}$ . The mean EI value from the data was 2.01 for  $^{252}\text{Cf(PE)}$  and 1.39 for  $^{238}\text{Pu-Be}$ . These EI values are expected, since the neutron spectrum of  $^{252}\text{Cf(PE)}$  is "softer" than that of  $^{238}\text{Pu-Be}$ . The sensitivity of the albedo TLD (either T or A) to  $^{252}\text{Cf(PE)}$  neutrons is also about one order of magnitude higher than that for  $^{238}\text{Pu-Be}$  neutrons for the same reason.

#### Bubble Detector

Since the bubble detector does not respond to photons, linearity of the BD's was examined with neutron irradiations using a  $^{238}\text{Pu-Be}$  source. Seven BD-100R and three BDS-1500 bubble detectors were irradiated in reproducible positions, counted, and recompressed on the second day after exposure. The above procedure was repeated several times for three different irradiation times. Because the BD sensitivity is adjustable, it is more reasonable to examine the linear response range in number of bubbles. Therefore, the linearity results are plotted as the mean number of bubbles versus the irradiation time in Fig. 3.3.4. No bubble was produced if the dosimeter was not irradiated. Therefore, the origin of the graph was included in the least squares fit. The  $r^2$  value (0.997 for the BD-100R and 0.998 for the BDS-1500) indicated the good linearity over the bubble response range (20-100 bubbles). One standard deviation and residual values (in %) of the mean response also are shown under each data point (see

ORNL-DWG 89M-1745

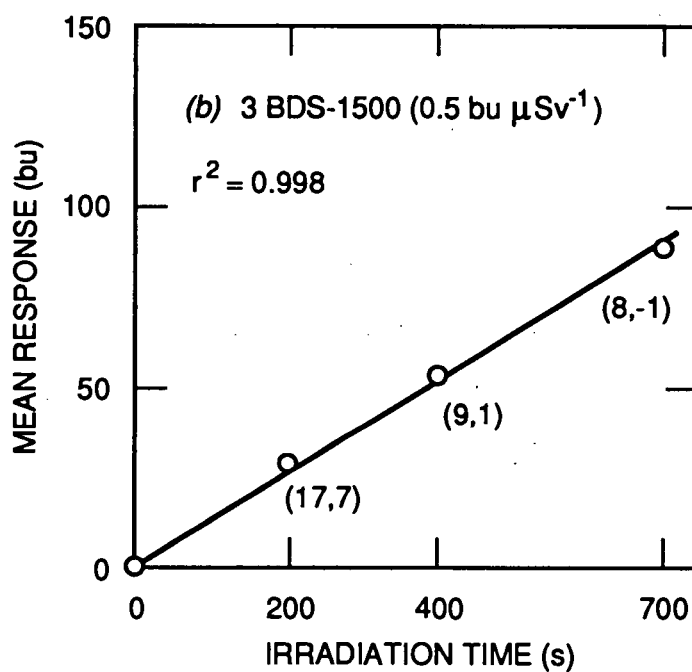
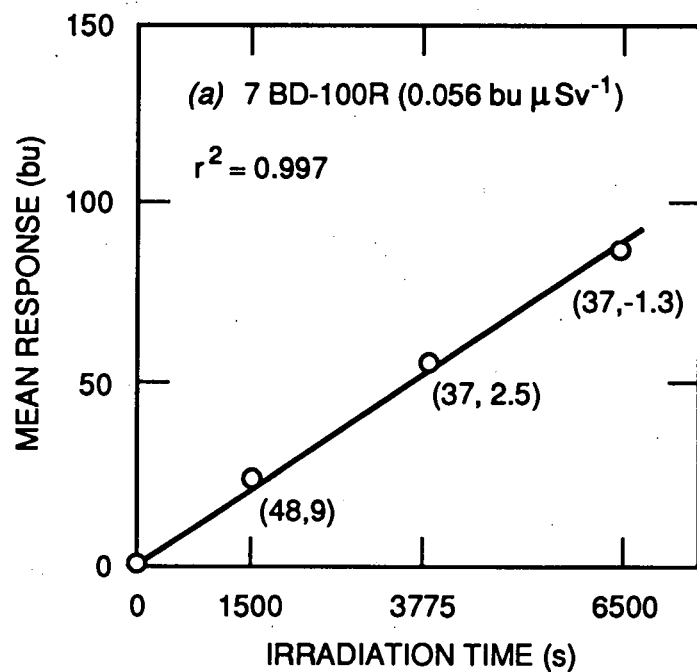


Fig. 3.3.4. Linearity of the bubble detectors exposed to the  $^{238}\text{Pu-Be}$  source. Dose equivalent rate =  $0.96 \text{ mSv h}^{-1}$ . (X, Y): X is  $1\sigma$  in % of the mean response and Y is the residual in % for that data point.

the data, (x,y), in Fig. 3.3.4). The large standard deviation values, especially for the BD-100R, were due to the non-uniform sensitivity of the bubble detectors used.

Perks (Perks et al. 1987) showed a linear response up to about 400 bubbles for the BD-100, using a photographic counting method. Ipe (Ipe and Busick 1987) had similar BD-100 linearity results as obtained here for the BD-100R and the BDS-1500, because the same monitor-magnifying counting system was used. Therefore, from the above results, it is concluded that the response of the BD is linear over the range tested. The upper limit of the linear range is governed by the maximum number of bubbles that can be counted accurately and efficiently. The lower limit of the linear response range is governed by the tolerable statistical error due to the small number of bubbles. The results also indicated that the optimum number of bubbles which can be counted by the visual counting method is 50-80.

### 3.4 LOWER LIMIT OF DETECTION

The lower limit of detection (LLD) for a dosimeter system is the minimum dose equivalent that the dosimeter system can detect reliably. A DOE Order requires that a dosimeter be provided to those persons who are likely to receive an effective dose equivalent exceeding 1 mSv in a year from external sources (USDOE 1988). This implies that a dosimeter's LLD should be no greater than 0.25 mSv (25 mrem), if exchanged quarterly.

#### Albedo TLD

The LLD is dependent on the sensitivity of the dosimeter. Therefore, the albedo TLD has a higher LLD to fast neutrons, e.g.,  $^{252}\text{Cf}$  neutrons, than to slow neutrons, e.g.,  $^{252}\text{Cf}(\text{D}_2\text{O})$  neutrons. The determination of the LLD for the albedo TLD followed

the procedure specified in the DOELAP Standard (USDOE 1986). Ten TLD's were annealed and put on a phantom for storage in the natural background environment for 94 days (close to the quarterly exchange period for the TLD's at ORNL). After storage, the 10 TLD's were processed and the LLD was calculated according to the DOELAP Standard. It was found that the complicated LLD equation (equation 19 in the DOELAP Standard, USDOE 1986) is very close to the following equation:

$$\text{LLD} = 2 t_p S_0, \quad (3.4.1)$$

where  $t_p$  is the abscissa of the student t distribution for  $n-1$  degrees of freedom and a P value of 0.95 (i.e., the probability of false positive results and the probability of false negative results are both 0.05). The  $S_0$  is the standard deviation for the stored ten TLD's. The  $t_p$  is 1.833 and  $S_0$  was 2.1 mR for the ten TLD's. The perpendicular (i.e.,  $0^\circ$ ) irradiation results of the angular dependence tests (Appendix 5) gave the calibration factors ( $\mu\text{Sv mR}^{-1}$ ) of the albedo TLD for  $^{252}\text{Cf}$  and  $^{252}\text{Cf}(\text{D}_2\text{O})$ . The LLD was calculated to be 92  $\mu\text{Sv}$  (9.2 mrem) for the  $^{252}\text{Cf}$  source and 10  $\mu\text{Sv}$  (1 mrem) for the  $^{252}\text{Cf}(\text{D}_2\text{O})$  source for a three-month exchange schedule. The ultra-low LLD can be attributed to the successful use of the ECC correction which greatly reduces the  $S_0$ .

The detection threshold is defined as the minimum dose equivalent for which the reading obtained is significantly different from the reading of the "fresh" dosimeter (ISO 1978). Therefore, the detection threshold of the TLD is similar to the LLD of the "just-annealed" TLD. The detection threshold of the albedo TLD was determined to be 19 mSv (1.9 mrem) for the  $^{252}\text{Cf}$  source.

### Bubble Detector

Because the sensitivity of bubble detector for neutrons above the energy threshold is very high, the LLD is very low. For the highest sensitivity BD used (0.82 bu  $\mu\text{Sv}^{-1}$  for the BD-100R and 0.45 bu  $\mu\text{Sv}^{-1}$  for the BDS-1500), the background count in a week was generally observed to be 0-4 for the BD-100R and 0-2 for the BDS-1500. The LLD for the highest sensitivity BD is, therefore, no greater than 5  $\mu\text{Sv}$  (0.5 mrem) for a weekly reuse schedule. For the lower sensitivity BD, the background count in a week was generally zero. Therefore, the LLD for the BD is close the dose equivalent corresponding to one bubble response.

### 3.5 DETECTION CAPABILITY IN MIXED NEUTRON-GAMMA FIELDS

Many personnel dosimeters detect both neutron and photon radiations and, therefore, the accuracy of the neutron dose equivalent estimate is dependent on the relative magnitudes of the neutron and photon signals of the dosimeter produced by the mixed radiation field. Consequently, the neutron and photon radiation energies, the neutron and photon dose ratios and the dosimeter design all affect the neutron detection capability in mixed neutron-gamma fields. Generally, smaller neutron/gamma dose equivalent ratios ( $n/\gamma$ ) result in a less accurate neutron dose equivalent estimates. Regulations require that the neutron dose equivalent be detectable, if the neutron dose equivalent exceeds one-third of the photon dose equivalent, and that the dosimeters have good performance in such fields (USNRC 1977; USDOE 1986).

### Albedo TLD

The neutron dose equivalent estimate provided by the Harshaw albedo TLD involves the subtraction of the TLD-700 photon signal from the TLD-600 signal.

Therefore, the error in the neutron dose equivalent evaluation can be high in situations in which there is a low  $n/\gamma$  and high energy neutron fields in which the neutron signal is small compared with photon signal in the TLD-600 element (Burgkhardt et al. 1979; Zeman and Snyder 1979).

The mixed field detection capability was tested by irradiating 8 groups of albedo TLD's (4 TLD's per group) to two neutron dose equivalents (0.5 mSv and 1.5 mSv) with four  $n/\gamma$  (3:1, 1:1, 1:3, and 1:10) using both the  $^{238}\text{Pu-Be}$  and  $^{137}\text{Cs}$  sources. The lowest neutron dose equivalent in the DOELAP test is 1.5 mSv (USDOE 1986). However, most albedo TLD's have good accuracy for neutron dose equivalent above 1 mSv and poor accuracy below 0.5 mSv (McDonald and Hadley 1985). The Institute of Nuclear Power Operations (INPO) also suggests that neutron exposure should be monitored for workers who are expected to have 0.3 mSv of neutron dose equivalent in a quarter (INPO 1988). Therefore, besides 1.5 mSv, a dose equivalent level of 0.5 mSv also was chosen to examine the low neutron dose equivalent detection capability of the albedo TLD in mixed fields. To do more than the regulations require, a mixed field of  $n/\gamma = 1:10$  was also included.

Reference pure field exposures were made consisting of a dose equivalent of 1 mSv. For the neutron exposure the  $^{238}\text{Pu-Be}$  source was used whereas  $^{137}\text{Cs}$  was used for the gamma exposure.

The precision, bias, and accuracy of the neutron and gamma responses in these mixed neutron-gamma fields are shown in Tables 3.5.1 - 3.5.3, respectively. Precision is expressed as one standard deviation (in %), which was computed from the 4 TLD's per exposure group. The precision value tells the spread of the four TL response values about their mean value for each group. Bias is expressed as the percentage difference between the mean response of a group in the mixed field and the

ORNL WSM-9195

**Table 3.5.1. Precision of neutron and gamma dose responses in mixed neutron-gamma fields.**

n/ $\gamma$	$H_n$ (mSv)	Neutron (%)		$H_\gamma$ (mSv)	Gamma (%)	
		A	T		A	T
3/1	0.5	5.5	3.0	0.167	3.5	3.4
1/1	0.5	2.4	1.8	0.5	1.0	0.6
1/3	0.5	3.4	1.4	1.5	0.7	0.9
1/10	0.5	24.4	7.8	5.0	1.2	0.4
3/1	1.5	6.4	0.9	0.5	0.7	0.5
1/1	1.5	6.0	2.2	1.5	1.1	0.5
1/3	1.5	7.4	2.7	4.5	0.9	0.7
1/10	1.5	19.2	19.6	15.0	1.2	0.4
Pure $H_n$	1.0	2.3	1.9	0	---	---
Pure $H_\gamma$	0	---	---	1.0	1.1	0.8

1. Percentage is the one standard deviation value computed from 4 TLD's per group.
2. A refers to Cd-covered TLD element, TLD-600 for neutron and TLD-700 for gamma.
3. T refers to no Cd-covered element, TLD-600 for neutron and TLD-700 for gamma.

ORNL WSM-9196

Table 3.5.2. Bias of neutron and gamma dose responses in mixed neutron-gamma fields.

n/ $\gamma$	$H_n$ (mSv)	Neutron (%)			$H_\gamma$ (mSv)	Gamma (%)		
		A	T	T/A		A	T	T/A
3/1	0.5	-2.3	0.2	1.44	0.167	-0.9	-3.5	1.01
1/1	0.5	2.3	0.9	1.38	0.5	0.7	-1.1	1.02
1/3	0.5	7.9	5.1	1.36	1.5	0.9	0.6	1.03
1/10	0.5	8.4	6.9	1.44	5.0	3.2	1.4	1.02
3/1	1.5	-0.2	-1.4	1.39	0.5	-1.7	-4.2	1.01
1/1	1.5	0.1	-0.2	1.40	1.5	1.5	-0.2	1.02
1/3	1.5	0.5	-2.8	1.36	4.5	2.8	2.2	1.03
1/10	1.5	-13.4	-1.2	1.60	15.0	4.0	2.4	1.02
Pure $H_n$	1.0	0	0	1.40	0	---	---	---
Pure $H_\gamma$	0	---	---	---	1.0	0	0	1.03

1. The bias percentage is the difference between the mean response value in each mixed field and the reference response value in pure field, assuming the latter is the true value. (i.e., bias = 0)

ORNL WSM-9197

Table 3.5.3. Accuracy of neutron and gamma dose responses in mixed neutron-gamma fields.

$H_n$ (mSv)	n/ $\gamma$	Neutron (%)		Gamma (%)		Ht (mSv)	Error of Ht (%)	
		A	T	A	T		A	T
0.5	3/1	7.8	3.2	4.4	6.9	0.667	7.0	4.1
0.5	1/1	4.7	2.7	1.7	1.7	1.0	3.2	2.2
0.5	1/3	11.3	6.5	1.6	1.5	2.0	4.0	2.8
0.5	1/10	32.8	14.7	4.4	1.8	5.5	7.0	3.0
1.5	3/1	6.6	2.3	2.4	4.7	2.0	5.6	2.9
1.5	1/1	6.1	2.4	2.6	0.7	3.0	4.4	1.6
1.5	1/3	7.9	5.5	3.7	2.9	6.0	4.8	3.6
1.5	1/10	32.6	20.8	5.2	2.8	16.5	7.7	4.4

1. Accuracy is the sum of absolute value of bias and precision.
2. Ht is the total dose equivalent (neutron + gamma), not including the gammas from neutron source.

true response. Since the true value was not known, the mean response value in the reference field irradiation was assumed to be the true response value. Therefore, the mean response in a pure reference field has a bias of zero (Table 3.5.2). If the mean response value in a mixed field is smaller than the reference value in a pure field, the bias is negative. Accuracy is defined to be the sum of the absolute value of the bias and precision.

The neutron dose equivalent ( $H_n$ ) estimates were made by using both TL responses A and T in this study. The photon dose equivalent ( $H_\gamma$ ) estimate generally is made by using an additional photon dosimeter. However, the photon dose equivalent estimates were made here by using the two TLD-700 elements in the Harshaw albedo TLD (Cd-covered TLD-700 is called A and the other TLD-700 is called T, the same differentiation as the TLD-600 elements). The small gamma component (~ 4.3%) of the  $^{238}\text{Pu}$ -Be source was not included in the total photon dose equivalent. Consequently, for the photon dose equivalent estimates, the response of the TLD-700 in a mixed field was corrected with the reference value of the TLD-700 elements from the pure  $^{238}\text{Pu}$ -Be irradiation results.

Table 3.5.1 shows the gamma precisions in all mixed fields were within 3.5%. The precision in the field of  $n/\gamma = 3:1$  and  $H_\gamma = 0.167$  mSv was the lowest. The precision for exposure in the pure gamma field was about 1%. The gamma precision results illustrated the effective use of the ECC method to correct the individual sensitivity difference of the TLD elements. Table 3.5.2 shows the gamma bias values were all within 4%. The energy index values in mixed fields were close to that in the reference field (1.03). Table 3.5.3 shows the gamma response accuracies were all within about 5%, except in the field with the lowest gamma dose equivalent. The excellent gamma dose detection performance in the mixed neutron-gamma fields can be

attributed to the following reasons: 1). TLD-700 is nearly insensitive to neutrons, 2). the use of ECC, and 3). good stability of the PMT's 2 and 3, which collect the light emitted by the two TLD-700 elements. The stability of the PMT can be seen from the reference light standard deviation values in Appendix 1.

Table 3.5.1 shows the neutron precision ranged from 2.4% to 24.4% for response A and 0.9% to 19.6% for response T, with the lowest precision in the fields with a  $n/\gamma = 1:10$ . The precision attained in the pure  $^{238}\text{Pu-Be}$  neutron field was 2.3% and 1.9% for response A and T, respectively. The precision of response A was worse than that of response T, because the stability of PMT 1 which reads the Cd-covered TLD-600 element was worse than that of PMT 4 which reads the other TLD-600 element (see Appendix 1). The neutron response had worse precision than the gamma response. This was due to 1). an additional photon signal subtraction step is needed to obtain the neutron response, 2). higher instability of the TLD-600 signal due to its narrower region of interest.

Table 3.5.2 shows the neutron bias is larger when the  $n/\gamma$  is lower. Neutron bias was highest in the field with a  $n/\gamma = 1:10$ . The energy index values in the mixed fields were within 3% of that in the pure  $^{238}\text{Pu-Be}$  field, except in the field with a  $n/\gamma = 1:10$  and  $H_n = 1.5$  mSv.

Table 3.5.3 shows the expected trend for neutron response accuracy: the lower the  $n/\gamma$ , the lower the accuracy. The worst neutron response accuracy was about 33% for response A and 21% for response T in the fields with a  $n/\gamma = 1:10$ . The neutron accuracy ranged from 2.3% to 11.3% for the other mixed fields ( $n/\gamma$  from 3:1 to 1:3). The accuracy in the mixed fields with a  $n/\gamma$  from 3:1 to 1:3 indicated that, if the proper energy-dependent calibration factor is applied, the neutron dose equivalent detection performance of the albedo TLD in the mixed fields can be very good. The good

neutron detection capability in the mixed fields also can be attributed to the use of both ECC and RCF corrections, and the PMT's stability.

Although the neutron accuracy in the field with a  $n/\gamma = 1:10$  was about 33%, the accuracy of the gamma dose equivalent (which is 10 times higher than the neutron dose equivalent) estimate was good. Therefore, the total dose equivalent ( $H_t$ , neutron + gamma) estimate was still very good. The accuracy of total dose equivalent estimate can be derived by the equation:  $(A_n H_n + A_\gamma H_\gamma) / H_t$ , where  $A_n$  and  $A_\gamma$  are the accuracy values for neutron and gamma responses, respectively. Table 3.5.3 shows the accuracy of total dose equivalent estimates in all mixed fields were less than 8%.

#### Bubble Detector

The detection principle of the bubble detector requires that the amount of energy locally deposited in the drop be high enough to trigger the vaporization event. The BD-100 was shown to have no response to photons and electrons with energies less than 6 MeV (Ipe and Busick 1987). This is because photons and electrons with energies less than 6 MeV produce only secondary electrons in the detector, and these secondary electrons do not deposit enough energy to induce nucleation events. When the photon and electron energies are higher than 6 MeV, photonuclear reactions and other neutron-producing mechanisms become possible and the bubble detector would have a response to the reaction products. However, the sensitivity of the bubble detector (BD-100) to these radiations is still very small ( $< 2000 \text{ bu Gy}^{-1}$  for 15 MeV bremsstrahlung photons or 20 MeV electrons) due to the low reaction cross sections (Ipe and Busick 1987).

In most of the radiation environment at ORNL, only photons and betas with energies less than 6 MeV are encountered. To verify Ipe's results, two BD-100R and

two BDS-1500 were exposed to  $4.75 \times 10^{-3} \mu\text{C kg}^{-1}$  (18.4 R) of  $^{137}\text{Cs}$  gammas and 0.2 Gy (20 rad) of  $^{90}\text{Sr-Y}$  betas. No response was observed for either irradiation. The results showed that it is not necessary to test the bubble detectors (BD-100R and BDS-1500) in mixed neutron-gamma fields.

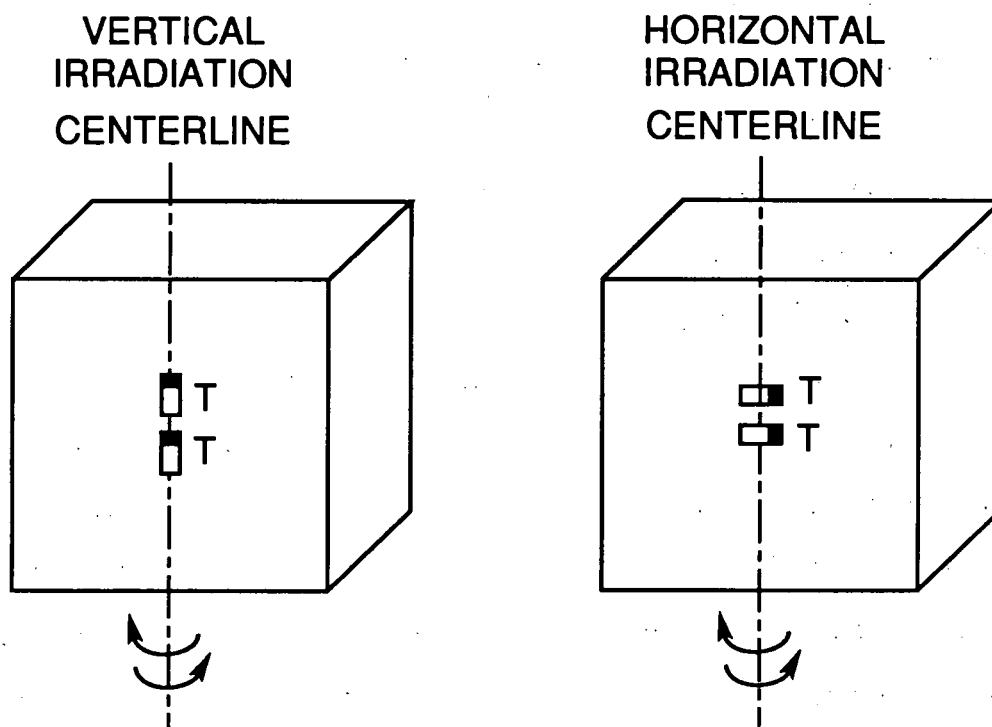
### 3.6 ANGULAR DEPENDENCE

The American National Standard ANSI N13.11-1983 requires that, for every dosimeter design submitted for testing, the processor performance with dosimeter irradiations under nonperpendicular incidence be studied once. A measurement procedure for the angular response study is suggested. However, no pass-fail criterion is specified in ANSI N13.11 (ANSI 1983). The DOELAP also requires the angular response of personnel dosimeters to be measured for front-incident angles between  $0^\circ$  (perpendicular incidence) and  $85^\circ$ . No performance criteria for the angular response are specified in the DOELAP standard either (USDOE 1986). A key reason for this is that the appropriate dose equivalent quantity, which can be used to estimate the effective dose equivalent and the organ dose equivalents in a multidirectional neutron field with reasonable conservatism, has not been agreed upon by the U.S. health physics community. The angular response study for the CPND is described in this section and the results are discussed.

#### Angular Dependence of the Albedo TLD Exposed to Neutrons

The irradiation set-up for the angular response study is shown in Fig. 3.6.1. Two or three TLD's as a group were irradiated on the vertical centerline of a slab phantom at a certain front-incident angle. For vertical irradiation, the top of the dosimeter was toward the top of phantom. For horizontal irradiation, the top of the

ORNL-DWG 89M-1750



▣ DOSIMETER  
 T = TOP OF DOSIMETER

ROTATION ALONG THE VERTICAL AXIS  
 (FRONT FACE CENTERLINE) OF THE PHANTOM  
 (40 x 40 x 15 cm)  
 CLOCKWISE = POSITIVE ANGLE  
 COUNTERCLOCKWISE = NEGATIVE ANGLE

Fig. 3.6.1. Irradiation set-up for the angular response study.

dosimeter was toward the right. For both vertical and horizontal irradiations, clockwise rotation of the phantom about its vertical axis centerline gave positive angles of incidence and counterclockwise rotation gave negative angles. Therefore, the terms of vertical-positive, vertical-negative, horizontal-positive, and horizontal-negative irradiations indicate that the radiations incident upon the TLD's are from the right, left, top, and bottom side of the Harshaw albedo TLD, respectively.

The angular response of the albedo TLD to neutrons was studied by following the DOELAP specified methodology (USDOE 1986). The angles of incidence included  $-85^\circ$ ,  $-60^\circ$ ,  $-30^\circ$ ,  $0^\circ$ ,  $30^\circ$ ,  $60^\circ$ , and  $85^\circ$ . The distance of the source-to-vertical centerline of the phantom was 50 cm for all irradiations. Both  $^{252}\text{Cf}$  and  $^{252}\text{Cf}(\text{D}_2\text{O})$  neutron sources were used in the angular response study. The neutron dose equivalents were 2 mSv for  $^{252}\text{Cf}$  and 0.5 mSv for  $^{252}\text{Cf}(\text{D}_2\text{O})$ , and the irradiation times were the same for all irradiation angles. The irradiations were conducted at the Southwest Radiation Calibration Center of the University of Arkansas. The neutron calibration room is 18.3x18.3x3.7 m. The scattering contribution was calculated to be less than 4% for  $^{252}\text{Cf}$  and 0.9% for  $^{252}\text{Cf}(\text{D}_2\text{O})$ , using the NIST semi-empirical formula (Schwartz and Eisenhauer 1982).

Because the distance between the paired TLD-600 and TLD-700 elements in the Harshaw albedo TLD card is 1.5 cm, the paired elements are different distances from the source in the nonperpendicular vertical irradiations. Therefore, the TLD-700 photon response was corrected using the inverse square law and, then, this signal was subtracted from the total TL signal of the TLD-600 to derive the neutron signal. Then, the neutron responses for nonperpendicular irradiations were normalized to the neutron response at perpendicular incidence. Both responses A and T were studied. Since the

neutron responses are primarily due to albedo neutrons from the phantom, the inverse square law correction was not made in deriving the T/A (EI) values.

The angular response results of the albedo TLD to neutrons from the  $^{252}\text{Cf}$  and  $^{252}\text{Cf}(\text{D}_2\text{O})$  sources are shown in Fig. 3.6.2 and Fig. 3.6.3, respectively. The associated neutron angular dependence data are tabulated in Appendix 5. The energy index (EI) values in the figures were divided by 2, so that they could be included on the same scale. Some results are discussed as follows:

1. The neutron angular dependence of responses A and T in the vertical and the horizontal irradiations for both sources generally followed a bell-shaped (or cosine) response (Figures 3.6.2-3.6.3). The relative responses at  $30^\circ$ ,  $60^\circ$ , and  $85^\circ$  were about 0.9, 0.5-0.7, and 0.2-0.3, respectively. These results agreed well with those reported (Jones et al. 1988).
2. For the vertical irradiations with both sources, the responses A and T had nearly the same angular dependence, and the EI value was nearly constant (1.2-1.3) for all angles (Figures 3.6.2a-3.6.3a). This is due to the symmetry of the two TLD-600 elements in the TLD design in vertical irradiations.
3. For the vertical irradiations with both sources, both responses A and T were higher for negative angles than for positive angles. This was most obvious in  $^{252}\text{Cf}(\text{D}_2\text{O})$  case (see the data in Appendix 5). This is because, for albedo neutrons to reach the TLD-600 elements, there must be less attenuation inside the phantom for negative angles than for positive angles.
4. For the horizontal irradiations with both sources, response A was higher than response T for positive angles and lower for negative angles (Figures 3.6.2b-3.6.3b). Therefore, the EI value was not constant (decreases from about 1.8 at  $-85^\circ$  to about 1.01 at  $85^\circ$ ). This shows that the energy dependence correction, using

ORNL-DWG 89M-1746

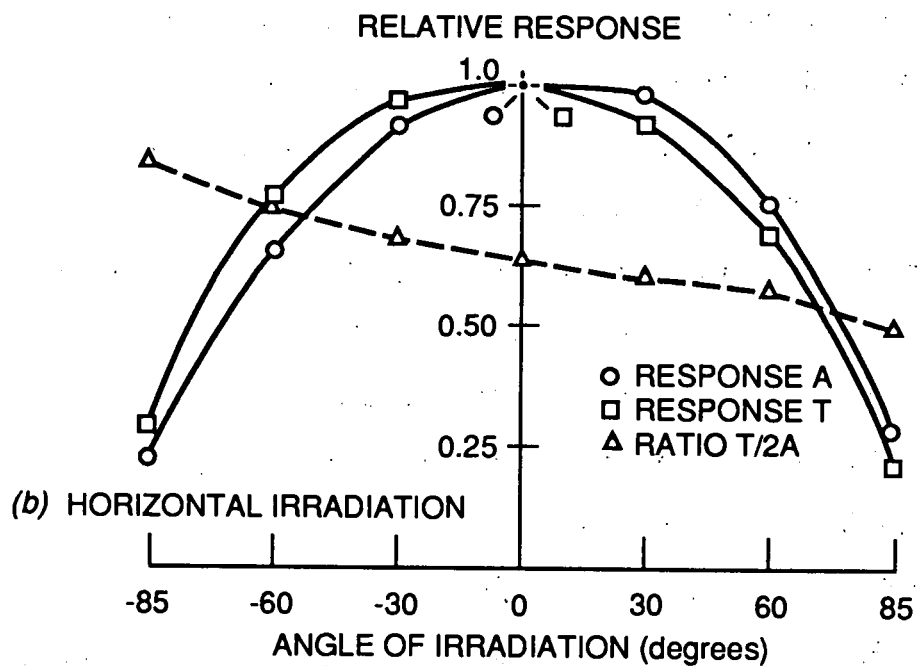
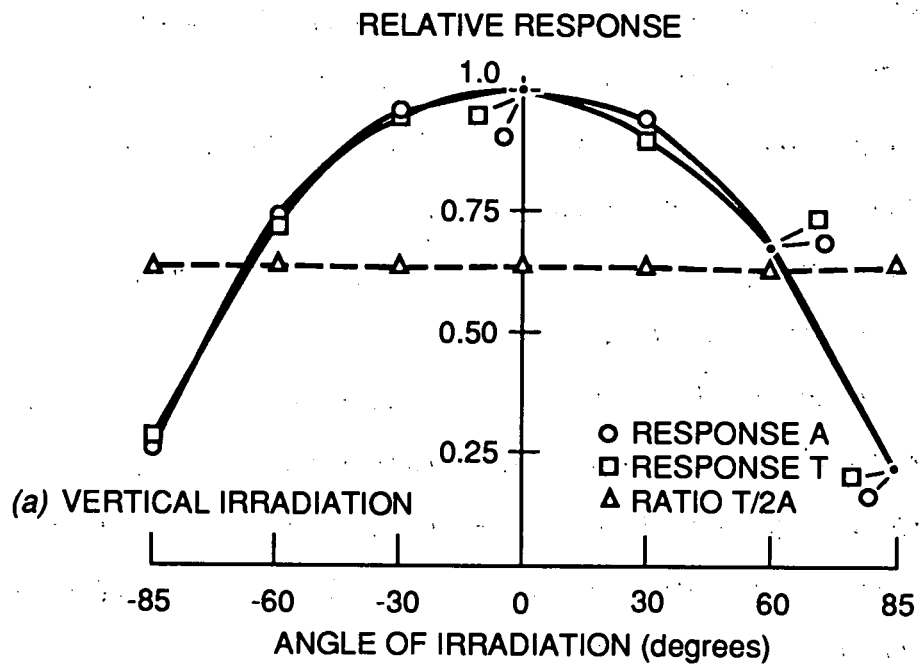


Fig. 3.6.2: Angular response of the albedo TLD to the bare  $^{252}\text{Cf}$  source.

ORNL-DWG 89M-1747

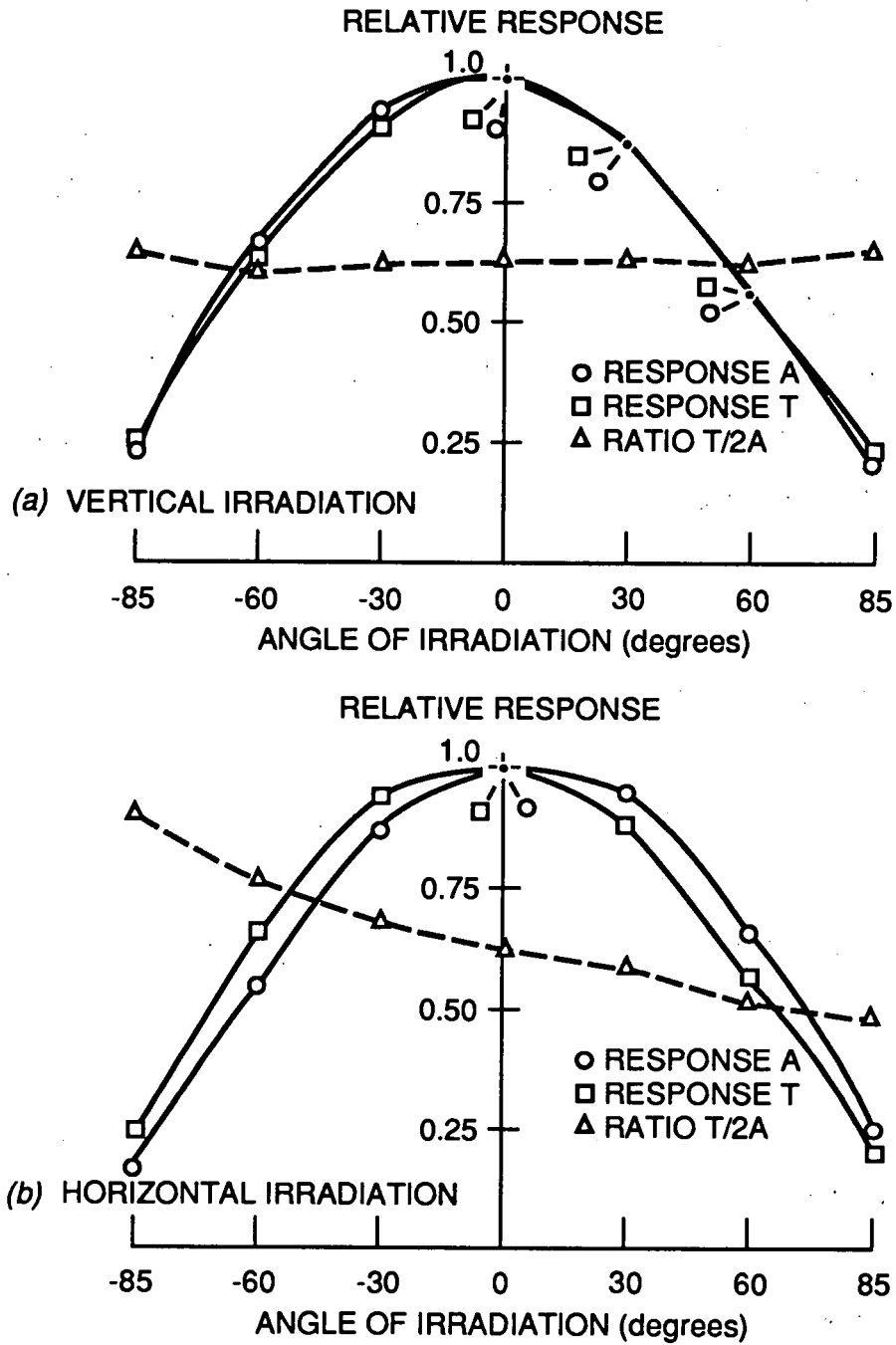


Fig. 3.6.3. Angular response of the albedo TLD to the  $^{252}\text{Cf}(\text{D}_2\text{O})$  source.

the EI value, has a strong angular dependence for the horizontal irradiations. Again, the cause for this comes from the above-mentioned situations of the different attenuation of albedo neutrons inside the phantom. For the horizontal-positive irradiations, albedo neutrons undergo less attenuation in reaching the Cd-covered TLD-600 element than the TLD-600 element (the distance between the two elements is about 2.6 cm).

5. For both the vertical and horizontal irradiations at all incident angles, the responses A and T were lower for the  $^{252}\text{Cf}(\text{D}_2\text{O})$  source than for the  $^{252}\text{Cf}$  source. The relative response at larger angles decreased more rapidly for  $^{252}\text{Cf}(\text{D}_2\text{O})$  than for  $^{252}\text{Cf}$ . This is because  $^{252}\text{Cf}(\text{D}_2\text{O})$  has lower energy neutrons and, consequently, more attenuation of albedo neutrons inside the phantom occurs.

#### Angular Performance Evaluation of the Albedo TLD Exposed to Neutrons

Performance evaluation of the angular response of the dosimeter strongly depends on which dose equivalent quantity is to be measured in personnel monitoring. Traditionally, a dosimeter with an isotropic angular response is desired to measure the maximum dose equivalent quantity. This requirement gives a dose equivalent estimate which is too conservative in most occupational exposures. The reason is explained in the following text.

The effective dose equivalent ( $H_E$ ) is the quantity of interest in today's risk-based radiation protection system. Since  $H_E$  cannot be measured directly, other surrogates which give reasonable and conservative estimates of  $H_E$  are used in practice. The deep dose equivalent, and the ambient dose equivalent (ICRU 1985) quantities are good surrogates in unidirectional fields due to the fact that they are the maximum quantities.

If an albedo TLD is worn in the representative point (i.e., the point which faces the source) on the trunk surface in a unidirectional field, reasonably conservative estimates of  $H_E$  can be made. However, if the albedo TLD is worn in the wrong position (i.e., not the representative point) in a unidirectional field, the dose equivalent would be underestimated. For example, the dose equivalent measured is about 20% of the perpendicular value, if the Harshaw albedo TLD is worn at an angle of  $85^\circ$  to the incident neutrons. Therefore, in a unidirectional field, proper wearing of the dosimeter, or a dosimeter with an isotropic response (which scarcely exists) is necessary for measurement of the maximum dose equivalent quantity.

However, in most occupational exposure situations, the radiation fields are rarely unidirectional due to scattering and movement of the worker within the environment. In such multidirectional neutron fields, traditional maximum dose equivalent estimates obtained by accounting for the angular dependence of the dosimeter or by using a dosimeter with an isotropic response would give an extremely conservative estimate of  $H_E$ . It is the trend in radiation protection that the operational dose equivalent quantity should be more closely linked to the risk-based dose equivalent quantity, i.e.,  $H_E$ . Consequently, a quantity that is a reasonably conservative estimate of  $H_E$  in the multidirectional field is required. The directional dose equivalent quantity,  $H'(10)$ , is advocated to be such quantity by the European dosimetry community (Wagner 1988; Burgkhardt and Piesch 1988) and the personnel at the Pacific Northwest Laboratories (Jones et al. 1988), who proposed to DOE to use this quantity for performance evaluation of the angular response of dosimeters in DOELAP testing.

The directional dose equivalent,  $H'(10)$ , at a point in a radiation field, is defined to be the dose equivalent that would be produced by the corresponding

expanded field in the ICRU sphere at a 10 mm depth on a radius in a specified direction (ICRU 1985). The specified direction usually refers to the zero degree incidence.

The relationship between  $H'(10)$  and  $H_E$  and their angular dependence to monoenergetic and radioisotopic source neutrons have been studied by several investigators. Morhart (Morhart and Burger 1985) showed that, for monoenergetic neutrons in the anterior/posterior (AP) and rotational irradiations,  $H'(10)$  overestimates  $H_E$  by as much as a factor of 4 for about 50 keV neutrons. In lateral irradiation,  $H'(10)$  underestimates  $H_E$  by only about 5% for neutrons with energies less than 30 keV and overestimates  $H_E$  by a factor of 2 at maximum for neutrons with energies above 30 keV. Bartlett (Bartlett 1985) showed, for most neutron spectra encountered in practical fields,  $H'(10)$  overestimates  $H_E$  by as much as 40% in rotational irradiations, and overestimates  $H_E$  by as much as a factor of 2 in isotropic irradiations. Other common dose equivalent quantities, e.g., the ambient dose equivalent, almost always yield much more conservative estimates of  $H_E$ . These results, among others, showed that the  $H'(10)$  quantity is a reasonable estimator of the  $H_E$  quantity, due to the fact that they have similar energy and angular dependence. The angular dependence of the  $H'(10)$  quantity for several monoenergetic neutrons has been calculated (Morhart and Burger 1985). These results predict the angular response that a neutron dosimeter should have, if  $H'(10)$  is adopted to estimate  $H_E$ .

Since  $H'(10)$  is defined using the ICRU sphere phantom, and the Lucite slab phantom is used for routine calibration, correction for different attenuation and backscattering in the two phantoms has to be made (Alberts 1988). This is important, especially for neutrons of energy less than 100 keV, since the secondary radiations inside the phantom produce almost the entire dose. Regretfully, the information required for such correction, as well as a complete set of the fluence-to-directional dose

equivalent conversion factors (both energy and direction), are still unavailable. This deficiency limits the capability to evaluate the performance of the neutron angular response of the dosimeter in terms of the directional dose equivalent quantity.

However, the calculated angular dependence of  $H'(10)$  (Morhart and Burger 1985) and a few angular dependence data of  $H_E$  in the cases of the AP, lateral, and rotational irradiations (ICRP 1987) can aid in assessing roughly the angular performance of the dosimeter. The relative angular dependence of  $H'(10)$  calculated for 1 MeV neutrons incident at  $30^\circ$ ,  $60^\circ$ ,  $85^\circ$ , and  $90^\circ$  are about 99%, 80%, 39%, and 27%, respectively. For 0.1 MeV neutrons, the corresponding relative dependence at these angles are about 94%, 63%, 15%, and 8%. These values were estimated from Figure 4 of a recent paper (Morhart and Burger 1985). Table 17 of the ICRP Publication 51 shows that the relative dependence of  $H_E$  in  $90^\circ$  irradiation for neutrons of 2, 1, and 0.1 MeV are 36%, 23%, and 18%, respectively (ICRP 1987). The relative angular response for the Harshaw albedo TLD at  $85^\circ$  is about 25% for both the  $^{252}\text{Cf}$  and  $^{252}\text{Cf}(\text{D}_2\text{O})$  sources. Considering the above-mentioned correction required, the albedo TLD has an angular response that roughly matches the angular dependence of  $H'(10)$ . The albedo TLD, therefore, would properly measure  $H'(10)$  in a multidirectional field, and, as long as the albedo TLD is worn in the representative position, a reasonably conservative estimate of  $H_E$  can be achieved.

#### Effect of Photon Angular Dependence on the Albedo TLD Response

Because the neutron signal is derived from the signal subtraction process, asymmetry of the holder which shields the paired TLD-600/TLD-700 in the photon vertical irradiation may result in different responses of the paired elements and give a false neutron signal. For example, for a vertical-positive irradiation (i.e., radiation

incident on the right of the TLD holder), the TLD-600 element will have more shielding and, therefore, a reduced response in comparison to the paired TLD-700 element. For the horizontal irradiations, no false neutron signal would be expected due to the symmetry of holder shielding for the paired elements. The effect of the photon angular dependence on the neutron response of the albedo TLD was examined with the  $^{137}\text{Cs}$  and M150 X-ray irradiations.

The photon irradiation set-up was the same as that for the neutron irradiations (Fig. 3.6.1). The source-to-phantom distance was 1 m for the  $^{137}\text{Cs}$  irradiations and 2.2 m for those with X-rays. The phantom was 40x40x15 cm for the  $^{137}\text{Cs}$  and 30x30x15 cm for the X-ray irradiations. The X-ray irradiations (beam code M150, average energy 74.6 keV) were conducted at NIST. The deep dose equivalent delivered was 5.5 mSv for  $^{137}\text{Cs}$  and 4.23 mSv for X-rays. The angles of incidence were  $-85^\circ$ ,  $-60^\circ$ ,  $-30^\circ$ ,  $0^\circ$ ,  $30^\circ$ ,  $60^\circ$ , and  $85^\circ$  for  $^{137}\text{Cs}$ . The angles of incidence for X-rays were  $-60^\circ$ ,  $-40^\circ$ ,  $-20^\circ$ ,  $0^\circ$ ,  $20^\circ$ ,  $40^\circ$ , and  $60^\circ$ . The response difference (TLD-600 minus TLD-700) for each pair was obtained after an inverse square law correction was made. The mean of the absolute values of the pair response difference in a TLD group (2 to 3 TLD's per exposure group) was used to estimate the effect.

The effect of the photon angular dependence on the albedo TLD neutron response is shown in Fig. 3.6.4 for  $^{137}\text{Cs}$  and Fig. 3.6.5 for M150 X-rays (the data are tabulated in Appendix 6). Some conclusions obtained from these results are given below:

1. For the high energy photons from  $^{137}\text{Cs}$  in the vertical irradiations, the effect was small; the biggest difference was  $< 8\%$  at  $85^\circ$  (top figure of Fig. 3.6.4). The mean absolute difference was less than 3% for angles from  $-60^\circ$  to  $60^\circ$ . The cause of this difference was only partly due to the photon angular dependence, since the pair

ORNL-DWG 89M-1748

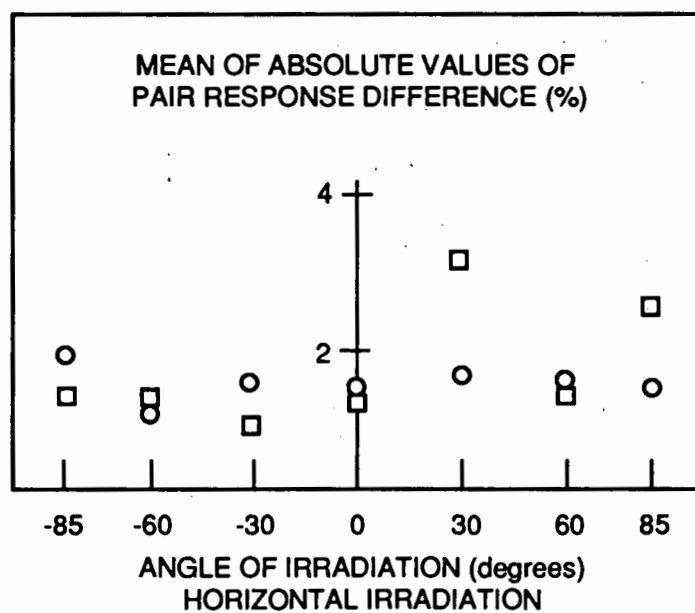
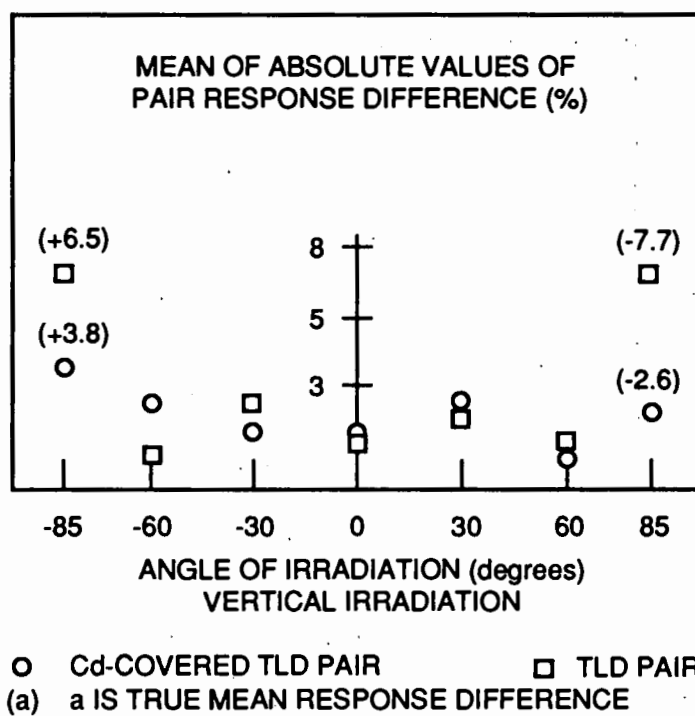


Fig. 3.6.4. The effect of  $^{137}\text{Cs}$  photon angular dependence on the response of the albedo TLD.

ORNL-DWG 89M-1749

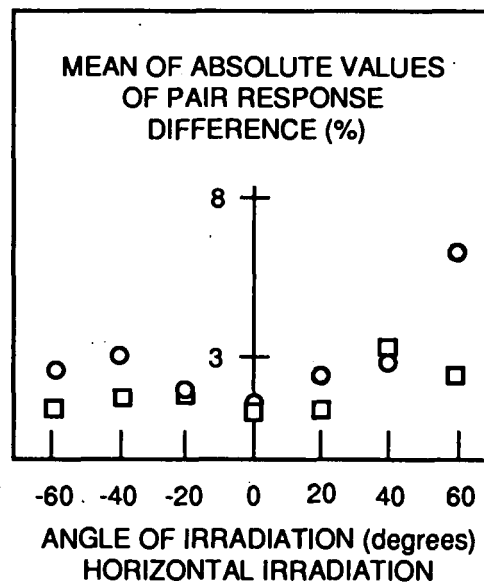
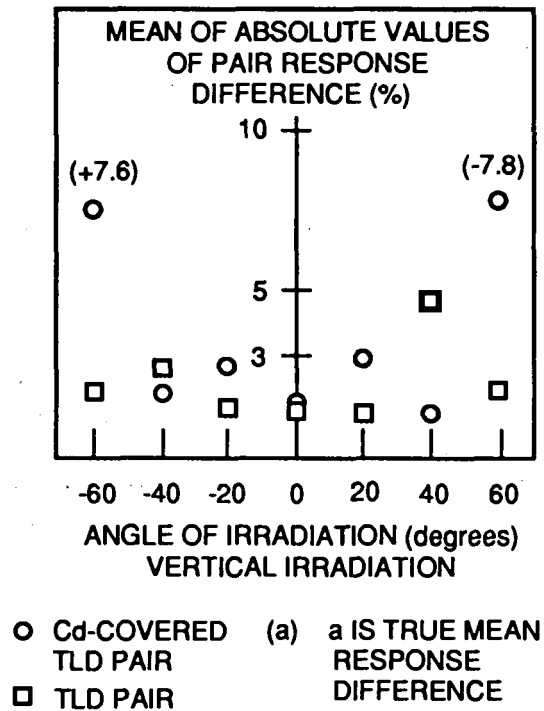


Fig. 3.6.5. The effect of M150 X-ray photon angular dependence on the response of the albedo TLD.

response differences in a TLD group had both negative and positive signs. On the contrary, the differences at  $-85^\circ$  and  $85^\circ$  were caused mainly by the photon angular dependence (i.e., the asymmetry shielding by the TLD holder), since all the pair response differences in the  $85^\circ$  irradiation TLD group had the same positive or negative sign. The true mean difference values are shown in the parentheses above the data point in the figures. For example, the mean response difference for the TLD pair was 6.5% at  $-85^\circ$  and -7.7% at  $85^\circ$ . The mean response difference for the Cd-covered TLD pair was only 3.8% at  $-85^\circ$  and -2.6% at  $85^\circ$ , because of less attenuation in the cadmium sheet than in the plastic holder.

2. For low penetrating X-rays in the vertical irradiations, the effect was higher. The mean absolute difference was less than 5% for angles within  $40^\circ$ . The mean response difference for the Cd-covered TLD pair was 7.6% at  $-60^\circ$  and -7.8% at  $60^\circ$  (top figure of Fig. 3.6.5). Again, due to the same reasons stated above, the differences at  $-60^\circ$  and  $60^\circ$  were caused by the photon angular dependence and the differences for angles within  $40^\circ$  were only partly caused by the angular dependence. The response difference for the Cd-covered TLD pair at  $85^\circ$  was much higher than the response difference of the other TLD pair, due to the higher atomic number (higher attenuation of X-rays) of cadmium compared to plastic.
3. As expected, for both  $^{137}\text{Cs}$  and X-rays in the horizontal irradiations, the effect was small. The mean absolute differences were all less than 4% (two bottom figures of Figures 3.6.4-3.6.5). The slightly large difference at  $60^\circ$  for the M-150 X-rays was caused by one outlier in that data group.

From the above results, it can be seen that the photon angular dependence of the albedo TLD may cause a false neutron response problem (albeit small) only in cases of large vertical angles of irradiation by low energy photons in a unidirectional field. In

multidirectional fields (especially  $2\pi$  rotational or  $4\pi$  isotropic fields), the opposite effect of the photon angular dependence in the positive and negative angles of incidence would compensate each other and, consequently, the pair response difference would be small. Therefore, the effect of the photon angular dependence on the neutron response of the albedo TLD is small in multidirectional fields.

### Bubble Detector

Due to its cylindrical shape, the bubble detector has  $2\pi$  rotational angular independence and a small horizontal angular dependence for "free in air" exposures. There are three reasons that cause the BD to have a small angular dependence difference between the on-phantom and the free-in-air irradiations. These are: 1). the BD has a lower neutron energy threshold and, thus, is much less sensitive to reflected neutrons than to incident neutrons (contrary to the albedo TLD), 2). the fraction of neutrons reflected back to the surface decreases with increasing incident neutron energy, and 3). reflected neutrons exist for every angle of incidence.

The first reason above makes the BD-100R more angular dependent than the BDS-1500. The second reason makes the angular dependence of the BD to  $^{252}\text{Cf}(\text{D}_2\text{O})$  neutrons more pronounced than to neutrons from  $^{252}\text{Cf}$ . The third reason makes the angular response difference be highest between  $0^\circ$  and  $85^\circ$ . Therefore, only the angular responses of the BD-100R to  $^{252}\text{Cf}(\text{D}_2\text{O})$  neutrons at the incidence angles of  $0^\circ$ ,  $85^\circ$ -vertical, and  $85^\circ$ -horizontal were studied. Two BD's were exposed for each angle of incidence. The results showed that the response difference was less than 5% between  $0^\circ$  and  $85^\circ$ -vertical and about 15% between  $0^\circ$  and  $85^\circ$ -horizontal. Considering the statistical variations in the BD response, the angular response of the BD for the on-phantom irradiations can be regarded as isotropic for front-incident

irradiations. The angular dependence of the BD depends on the tube shape. If the  $H'(10)$  quantity is adopted, the BD can be made into a rectangular shape to have the desired bell-shaped angular dependence.

### 3.7 NEUTRON ENERGY DEPENDENCE

The importance of the knowledge of the neutron energy dependence of the CPND to its successful use cannot be overemphasized. A detailed energy dependence study for the CPND was conducted by following ISO/DIS 8529 recommendations (ISO 1986). A total of 11 neutron energies from 2 keV to 14.8 MeV were used. Monoenergetic neutrons at eight energies (0.1, 0.25, 0.565, 1.2, 2.6, 3.2, 5.0, and 14.8 MeV) were provided with a Van de Graaff accelerator at the Pacific Northwest Laboratories (PNL). Three reactor filtered beams (2, 24, and 144 keV) were provided at the National Institute of Standards and Technology (NIST).

#### PNL Irradiations

The characteristics of the monoenergetic neutron fields at PNL which were used for the CPND irradiations are described in Table 3.7.1. The PNL 2 MV Van de Graaff accelerator room is about 8.5x8.5x6.1 m. The neutron producing target was located 3.2 m above the floor center of a 6.1x6.1x2.1 m pit which has an aluminum grid cover. All large neutron scattering objects were at least 2.4 m away from the target. A precision long counter was suspended from an instrument boom that allowed setting of the distance and angle of the counter accurately and easily. The long counter, which was used to monitor the neutron fluences during the CPND irradiations, was at a surface-to-target distance of 92.5 cm and at the same angle as that of the phantom. The phantom was placed on a light cart at a phantom-to-target distance of 50 cm, and an

Table 3.7.1. Characteristics of the monoenergetic neutron fields from the Van de Graaff accelerator at PNL<sup>a</sup>.

Energy (keV)	Energy Uncertainty (%)	Reaction	Projectile Energy (MeV)	Lab. Angle (deg.)	Fluence <sup>b</sup> (10 <sup>6</sup> cm <sup>-2</sup> )	ICRP 21 h $\phi$ (10 <sup>-10</sup> Sv cm <sup>2</sup> )	Neutron Contamination (%)
100 <sup>c</sup>	12	T(p,n) <sup>3</sup> He	1.258	75	8.575	0.579	<1
250 <sup>c</sup>	8.4	T(p,n) <sup>3</sup> He	1.252	45	4.358	1.18	<1
565 <sup>c</sup>	4.8	T(p,n) <sup>3</sup> He	1.494	30	4.600	2.20	<1
1200 <sup>d</sup>	4.6	<sup>12</sup> C(d,n) <sup>13</sup> N	1.588	30	2.936	3.52	<6
2600 <sup>e</sup>	0.3	D(d,n) <sup>3</sup> He	0.584	90	2.493	4.06	<3
3200 <sup>e</sup>	0.8	D(d,n) <sup>3</sup> He	0.824	60	2.480	4.10	<3
5000 <sup>e</sup>	0.9	D(d,n) <sup>3</sup> He	1.830	15	4.956	4.08	<3
14800 <sup>f</sup>	0.1	T(d,n) <sup>4</sup> He	0.754	75	4.909	4.18	<3

a. Irradiation room of PNL is 8.5x8.5x6.1 m. Target is in room center.

b. Total fluence for TLD irradiation.

c. Target is 0.235 mg cm<sup>-2</sup> T-Ti on Cu disk and fluence uncertainty is 10%.

d. Target is 0.518 mg cm<sup>-2</sup> <sup>12</sup>C on Ta disk and fluence uncertainty is 15%.

e. Target is 0.560 mg cm<sup>-2</sup> D-Ti on Cu disk and fluence uncertainty is 15%.

f. Target is 0.235 mg cm<sup>-2</sup> T-Ti on Cu disk and fluence uncertainty is 15%.

appropriate laboratory neutron emission angle relative to the incident charged particle beam. The distance and angle of the phantom relative to the target were chosen to give acceptable uniformity of the radiation field at the irradiation position.

Factors such as the accelerator stability and the neutron output were considered in selecting the projectile energy and neutron emission angle so that neutrons of the appropriate energies could be produced. The  $T(p,n)^3\text{He}$  reaction ( $Q = -0.763$  MeV), with 3 different projectile energies and 3 laboratory angles, was used to generate the 100, 250, and 565 keV neutron fields. The  $^{12}\text{C}(d,n)^{13}\text{N}$  reaction ( $Q = -0.281$  MeV) was used to generate the 1.2 MeV neutron field. The  $D(d,n)^3\text{He}$  reaction ( $Q = 3.27$  MeV), with 3 different projectile energies and 3 laboratory angles, was used to generate the 2.6, 3.2, and 5.0 MeV neutron fields. The  $T(d,n)^4\text{He}$  reaction ( $Q = 17.59$  MeV) was used to generate the 14.8 MeV neutron field.

Titanium targets loaded with tritium and deuterium, with thicknesses of  $0.235$   $\text{mg cm}^{-2}$  and  $0.560$   $\text{mg cm}^{-2}$ , respectively, and a  $^{12}\text{C}$  target with a thickness of  $0.518$   $\text{mg cm}^{-2}$  were used. The projectile beam energy was determined by an analyzing magnet, which was calibrated using the well-known threshold energy of the  $^7\text{Li}(p,n)^7\text{Be}$  reaction. The stated uncertainty in neutron energy (Table 3.7.1) is due to the uncertainty of the projectile energy and the projectile energy loss in the target. The neutron contamination estimate was made with a blank target and provided an estimate of the background and contributions (if any) of competing reactions. Whenever deuteron beam was used, the contamination and the fluence uncertainty were higher due to the  $^{12}\text{C}(d,n)^{13}\text{N}$  reaction in the organic vapor from the vacuum system.

Four TLD's and one set of BD (one BD-100R and one BDS-1500) were irradiated as a group for each energy. The BDS-1500 was not irradiated with neutrons below 1.2 MeV. The BD set was placed in the center of the phantom and the four

TLD's were placed at 90° intervals around the outer edge (about 1 cm away) of the BD. After an appropriate irradiation time, the BD set was replaced by a new BD set. Therefore, there were four TLD's, 2 BD-100R, and 2 BDS-1500 irradiated for every energy. The fluences shown in Table 3.7.1 were obtained from irradiations of the albedo TLD's. The fluence to which the BD's were exposed was less than half of the fluence for the TLD's. The fluence uncertainty was 10% for proton beam reactions and 15% for deuteron beam reactions. The ICRP Publication 21 fluence-to-dose equivalent conversion factors ( $h_\phi$ ) for these neutron energies also are shown in the table (ISO 1986). Room scattered neutron effects for all neutron energies were estimated to be < 5% for the BD's and < 6% for the albedo TLD (Schwartz and Eisenhauer 1982; Lo 1987). The temperature during all irradiations was between 21 °C and 22 °C.

#### NIST Irradiations

Three quasi-monoenergetic filtered neutron beams from the NIST 20 MW reactor were used. The beam characteristics\* are described in Table 3.7.2 (Schwartz 1977). The beams were produced based on the principle that certain materials (filters) have cross section minima (windows) at distinct energies to allow transmission of neutrons in a narrow range of energies. Fission neutrons from the resonant scatterer (manganese for the 2 keV beam; graphite for both the 24 and 144 keV beams) in the core are collimated and pass through the filter located in a beam tube. There are small numbers of neutrons at other energies (i.e., contamination) due to the existence of other

---

\* Schwartz, R. B. Personal communication. A155 Reactor, NIST, Gaithersburg, MD 20899, 1989.

Table 3.7.2. Characteristics of the reactor filtered beams at NIST.

Energy (keV)	Main Filter <sup>a</sup> Material	FWHM (%)	Contamination <sup>b</sup> keV (%)	Fluence <sup>c</sup> (cm <sup>-2</sup> )	ICRP 21 h $\phi$ (10 <sup>-10</sup> Sv cm <sup>2</sup> )
2	Sc	35.0	29, others (4.4)	$4.9 \times 10^7$	0.0943
24	Fe-Al	8.3	>100 (2.9)	$2.578 \times 10^7$	0.193
144	Si	17.4	54 (0.33)	$1.307 \times 10^7$	0.773

a. Secondary filter of Ti is added for the 2 and 144 keV beams to suppress the contamination peaks.

b. See text for contamination description.

c. Nominal beam fluence. Uncertainty is about 10% to 15%.

windows in the filter. An additional titanium filter was used for the 2 keV and 144 keV beams to suppress these contamination neutrons.

The beam spectra and intensities were characterized by using  $^{10}\text{BF}_3$  counter (for 2 keV beam) and recoil proton proportional counter (for 24 and 144 keV beams). The scandium filtered beam had 95.6% of the fluence at 2 keV (full width half maximum (FWHM) = 35%), 1.3% at 29 keV, and the rest at other high energies. The iron-aluminum filtered beam had 97.1% of the fluence at 24 keV (FWHM = 8.3%) and 2.9% at energies between 50 and 400 keV. The silicon filtered beam had 99.7% of the fluence at 144 keV (FWHM = 17.4%) and 0.3% at 54 keV. Corrections of the albedo TLD and the bubble detector responses for these contamination neutrons were made in the energy dependence study. The gamma dose equivalent components of the beams were all less than 1% of the neutron dose equivalent.

Four TLD's and two BD-100R detectors were exposed to each beam. Two BDS-1500 detectors were exposed only to the 144 keV beams. Since the beam diameter was small (5 cm), the beam was moved in a raster to cover a 25 cm square area centered on the phantom. The four TLD's were placed at 90° intervals around the inner edge of a 15x15 cm square. The BD's were placed in the phantom center. The fluence uncertainty was about 10% to 15%. Control CPND measurements outside the beam were made to estimate the scattered component. The temperature during all irradiations was between 21 °C and 22 °C.

### Energy Dependence Results

The results of the energy response studies for the albedo TLD and the BD's from the monoenergetic neutron irradiations at PNL and NIST are shown in Table 3.7.3. The energy response per unit fluence for the CPND is plotted as curves with

Table 3.7.3. Energy responses per unit fluence of the albedo TLD and the bubble detectors (BD-100R and BDS-1500), and the 9"-to-3" sphere response ratio for the ISO reference neutron radiations.

Energy (keV)	9"/3" <sup>a</sup>	TLD ( $10^{-5}$ mR cm <sup>2</sup> )			BD ( $10^{-5}$ bu cm <sup>2</sup> ) <sup>b</sup>	
		A	T	EI	BD-100R	BDS-1500
2	0.11	6.36	7.78	1.223	0.04	-
24	0.19	5.22	6.84	1.311	0.02	-
100	0.28	5.43	6.58	1.212	0.82	-
144	0.35	5.79	7.05	1.217	1.54	0
250	0.53	5.02	6.17	1.229	3.21	-
565	1.0	4.25	5.25	1.235	6.45	-
1200	1.8	3.15	4.09	1.297	6.47	2.67
2600	2.7	2.26	2.86	1.264	5.05	5.97
3200	3.6	2.04	2.62	1.285	4.48	4.42
5000	4.5	1.37	1.71	1.247	2.89	4.93
14800	8.2	0.86	1.10	1.282	4.72	5.57

a. First five points were estimated from a published graph (Griffith et. al. 1979).

b. The nominal sensitivities of both the BD-100R and BDS-1500 are normalized to 0.1 bu  $\mu\text{Sv}^{-1}$  from the BTI <sup>238</sup>Pu-Be source.

experimental points in Fig 3.7.1. The step functions shown in Fig. 3.7.1 are the average sensitivity values used in the CPND algorithm and will be explained in Chapter 4. Using the ICRP Publication 21 fluence-to-dose equivalent conversion factors, the energy response per unit dose equivalent for the CPND is plotted in Fig. 3.7.2. These response functions are shown for bubble detectors having a nominal sensitivity of 0.1 bubble per  $\mu\text{Sv}$  to BTI's  $^{238}\text{Pu-Be}$  source. This source is used to determine the sensitivities of the BD's and for the quality assurance irradiations of the BD's at BTI.

From a closer comparison of Figures 3.7.1 and 3.7.2, it can be seen that the BD-100R and the BDS-1500 bubble detectors function more like a "fluence dosimeter" (i.e., response per unit fluence is energy independent) than a "dose equivalent dosimeter" (i.e., response per unit dose equivalent is energy independent). The fluence response of the albedo TLD also has less variation over the energy range than its dose equivalent response. Energy dependence results for the bubble detectors agreed with those reported (Ing and Tremblay 1988; Perks et al. 1988; Ipe et al. 1988). The BD-100R energy dependence result in this study was the one first reported and it was very close to that of the BD-100. The albedo TLD results also agreed well with the calculated results (Alsmiller and Barish 1974).

The  $9^{1/3}$  ratios for the energy points also are given in Table 3.7.3. The ratios for energies less than 565 keV were estimated from a published graph (Griffith et al. 1979) and the rest were the measured values from former PDIS studies\*. A plot of the calibration factor of the Harshaw albedo TLD (response A) versus the  $9^{1/3}$  value is shown in Fig. 3.7.3. Two equations were fit to the data points. The calibration factor

---

\* T. A. Rhea. Personal communication. Science Applications International Corporation. 800 Oak Ridge Turnpike, P.O. Box 2501, Oak Ridge, TN 37831, 1989.

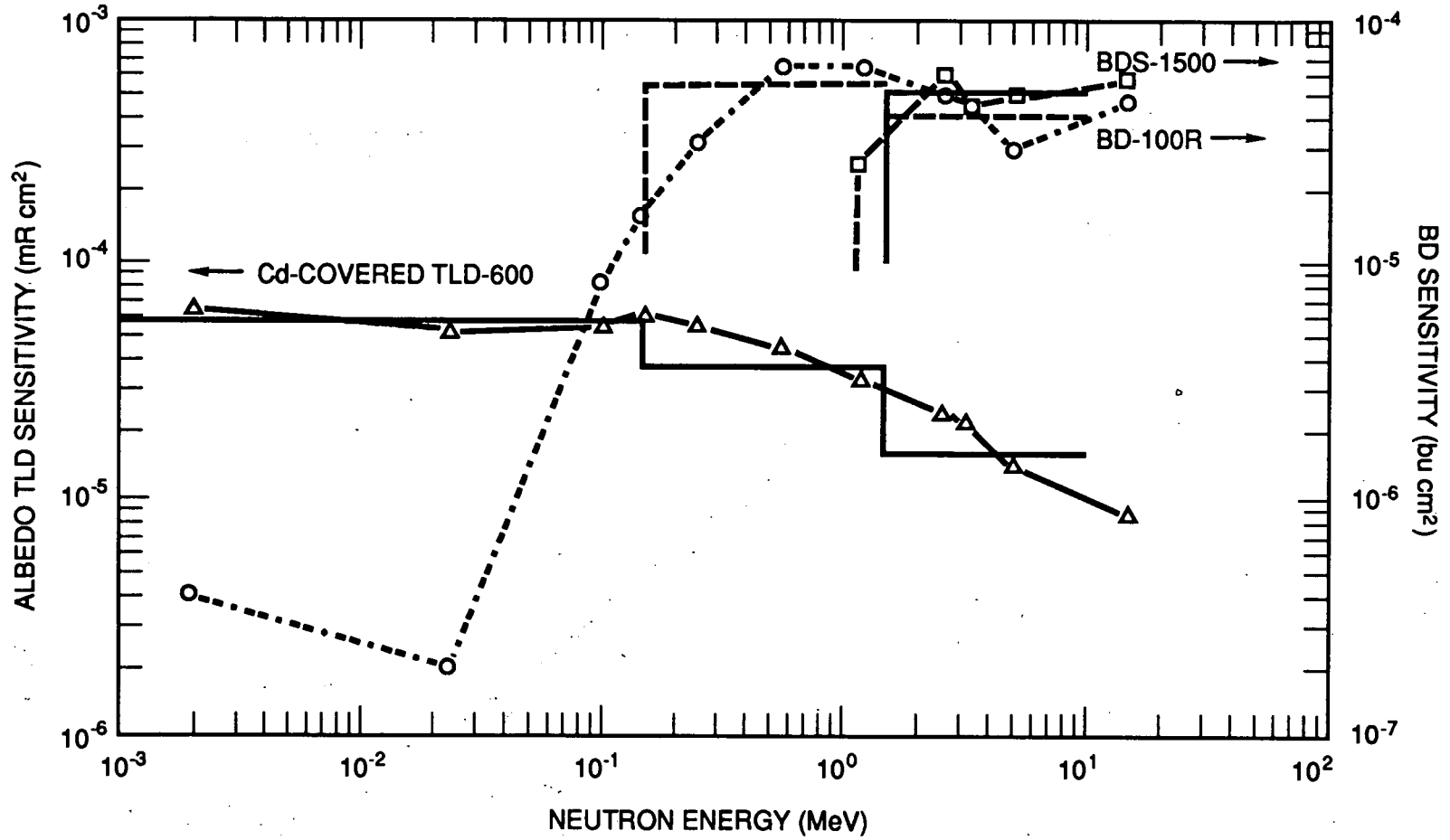


Fig. 3.7.1. Neutron energy response per unit fluence of the CPND. Curves with points: monoenergetic neutron irradiation results. Step functions: average sensitivity values.

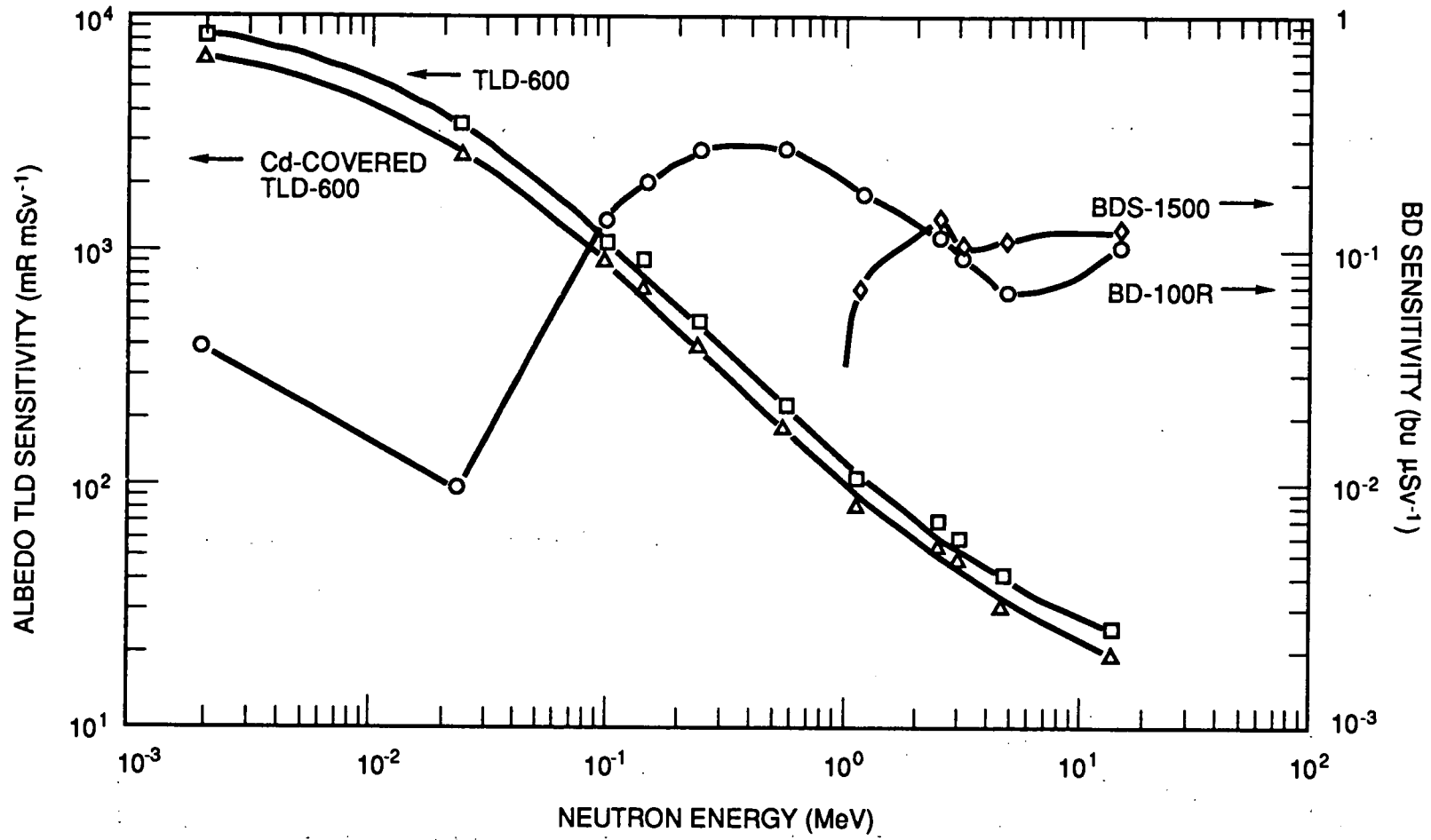


Fig. 3.7.2. Neutron energy response per unit dose equivalent of the CPND.

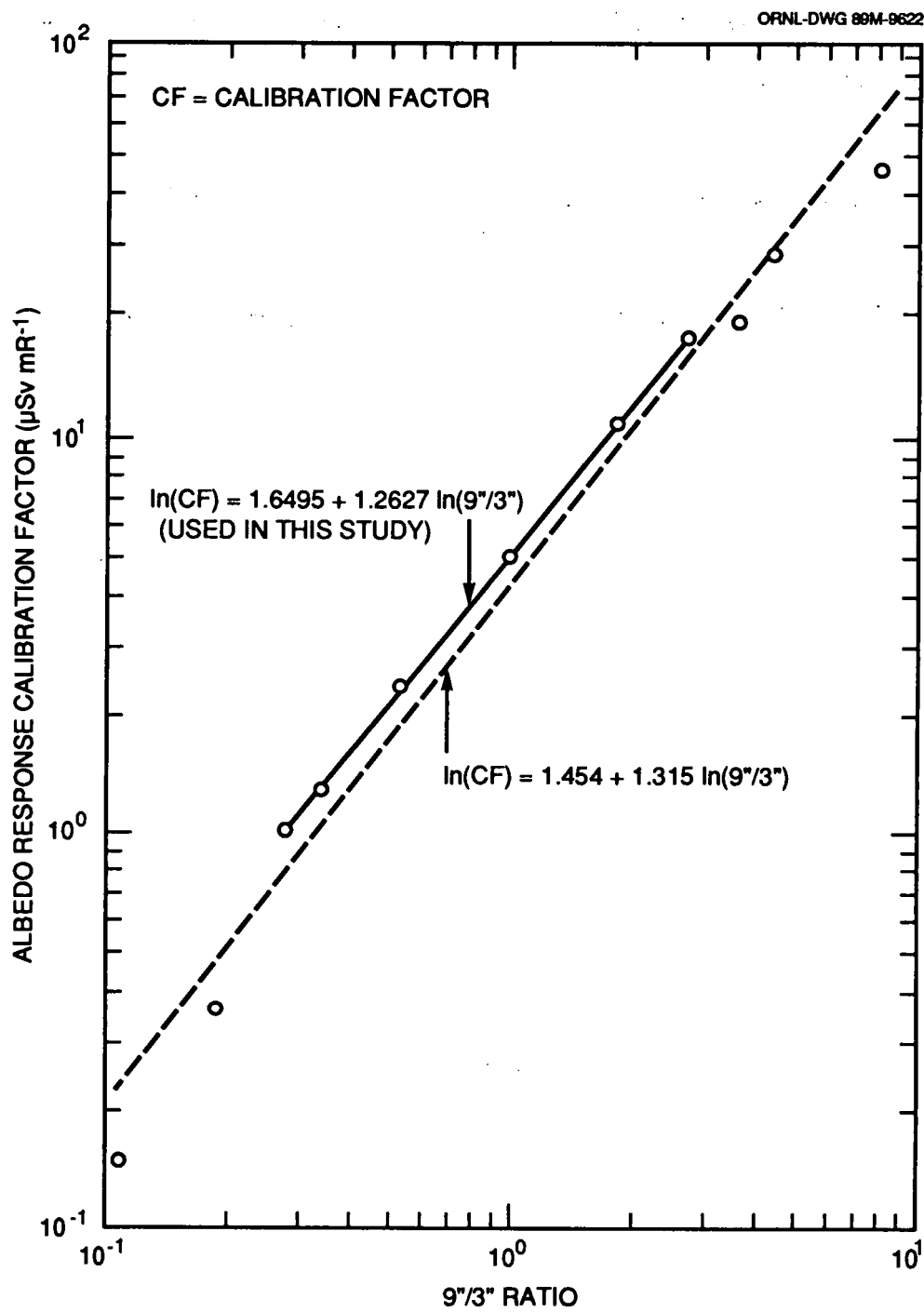


Fig. 3.7.3. The relationship between the calibration factor of the albedo TLD (Cd-covered TLD-600) and the 9''/3'' response ratio.

derived from these two lines were different by about 20%. The upper line was used to derive the calibration factor (CF in  $\mu\text{Sv mR}^{-1}$ ) based on the 9"/3" calibration technique, because it fit the data better in the region of interest. The equation for this fit is:

$$\ln(\text{CF}) = 1.6495 + 1.2627 \ln(9"/3"), \quad (3.7.1)$$

where the CF can be applied to the response A to derive the dose equivalent.

## CHAPTER IV

### DOSE EQUIVALENT EVALUATION ALGORITHM FOR THE CPND AND ITS OPERATIONAL USAGE

Since spectrometric capability and universal applicability were two of the main design objectives for the CPND, it was essential that rough spectral information be extracted from the responses of the four detector components (i.e., two TLD-600 elements, one BD-100R, and one BDS-1500). The spectral stripping and dose equivalent evaluation algorithm and the operational usage of the CPND are presented in this chapter.

#### 4.1 DOSE EQUIVALENT EVALUATION ALGORITHM

Unfolding of the neutron spectrum can be accomplished by using the three energy response functions of the albedo TLD, the BD-100R, and the BDS-1500 which are shown as curves with experimental points in Fig. 3.7.1. Average sensitivity concept was used in the CPND algorithm.

##### Average Sensitivity of the CPND

Since neutrons in radiation protection situations rarely have energies exceeding 10 MeV, the upper limits for the spectrum and the response functions were set at 10 MeV. The spectrum was divided into four intervals: 0.025-0.4 eV, 0.4 eV - 0.15 MeV, 0.15-1.5 MeV, and 1.5-10 MeV, according to the energies of the cadmium cut-off (0.4 eV) and the two thresholds of the two BD's (0.15 and 1.5 MeV). Neutrons within the energy intervals of 0.025-0.4 eV, 0.4 eV - 0.15 MeV, 0.15-1.5 MeV, and 1.5-10 MeV are called thermal, slow, medium, and fast neutrons, respectively in this

research. Since the CPND may be applied in unknown fields where no prior information on spectral shape is available, the average sensitivities of the albedo TLD and the two BD's for each energy interval were derived based on the assumption of constant fluence per unit energy within each energy interval.

The results in Fig. 3.7.1 show that the response functions of the two bubble detectors can be approximated with appropriate step functions which have constant sensitivities over certain energy intervals. The average sensitivity of the BDS-1500 is  $5.0 \times 10^{-5}$  bu  $\text{cm}^2$  with a threshold of 1.5 MeV, i.e., the BDS-1500 is assumed to respond, with a constant sensitivity, only to fast neutrons. The average sensitivity of the BD-100R is  $4.0 \times 10^{-5}$  bu  $\text{cm}^2$  for fast neutrons, and  $5.1 \times 10^{-5}$  bu  $\text{cm}^2$  for medium neutrons. The threshold of the BD-100R is taken to be 150 keV. The maximum difference at any energy between the response function values and these average sensitivities was less than 20% for the BDS-1500 and 25% for the BD-100R, respectively.

The response function of the albedo TLD (i.e., the albedo response A) in Fig. 3.7.1 can be fit with appropriate equations in three energy intervals (0.4 eV - 0.15 MeV, 0.15-1.5 MeV, and 1.5-10 MeV). A particular form ( $A = kE^n$ , where E is energy in keV, k and n are constants) was chosen for the equation because the energy response of the albedo TLD is approximately linear in the log-log plot over these intervals. The fit equations are shown in Table 4.1.1. The sensitivity differences between the response functions and the fit equations were about 5%. A simple integration of the fit equation over the energy interval yields the average sensitivity for that interval. The average sensitivity derived for the response A (shown as the step functions in Fig. 3.7.1) is  $1.6 \times 10^{-5}$  mR  $\text{cm}^2$  for fast neutrons,  $3.8 \times 10^{-5}$  mR  $\text{cm}^2$  for medium neutrons, and  $5.6 \times 10^{-5}$  mR  $\text{cm}^2$  for slow neutrons.

Table 4.1.1. The fit response function for the albedo TLD and the equations for the ICRP Publication 21 fluence-to-dose equivalent conversion factors over the energy intervals.

Quantity and Equation	Energy Interval	Coefficient
Albedo Response Function A ( $10^{-5}$ mR cm <sup>2</sup> ) A = kE <sup>n</sup>	0.025-0.4 eV	A = constant = 14.7
	0.4 eV - 0.15 MeV	k = 6.23, n = -0.0276
	0.15-1.5 MeV	k = 24.18, n = -0.2839
	1.5-10 MeV	k = 144.3, n = -0.5352
Fluence-to-Dose Equivalent Conversion Factor ( $10^{-10}$ Sv cm <sup>2</sup> ) $h_{\phi} = pE^m$	0.025-0.4 eV	$h_{\phi} = 0.11$
	0.4 eV - 10 keV	$h_{\phi} = 0.102$
	10 keV - 1 MeV	p = 0.01679, m = 0.7673
	1-2 MeV	p = 0.5097, m = 0.2706
	2-10 MeV	$h_{\phi} = 4.06$

1. E is neutron energy in keV.

It is desirable to measure the thermal neutron component in the field. The response difference of the two TLD-600 elements (i.e., T-A) in the Harshaw albedo TLD can serve the purpose. Differing in sensitivity levels, all types of albedo TLD's have similar energy dependence. From the calculated energy dependence (Fig. 3 of Alsmiller and Barish 1974), sensitivity ratios between thermal neutrons and higher energy neutrons for an albedo type TLD were derived. Based on these calculated ratios, the thermal neutron sensitivity of the Harshaw albedo TLD can be obtained by extrapolation from the experimental results for high energy neutron sensitivity in Fig. 3.7.1. Using the above comparison method, the average thermal neutron sensitivity for the response A was calculated to be  $14.7 \times 10^{-5}$  mR cm<sup>2</sup>. Using an albedo factor of 0.8 for thermal neutrons (Alsmiller and Barish 1974), the average thermal neutron sensitivity for the response T was calculated to be  $33.1 \times 10^{-5}$  mR cm<sup>2</sup>. The response difference of T minus A is a measure of the incident thermal neutron component and the thermal neutron sensitivity value for T-A is then  $18.4 \times 10^{-5}$  mR cm<sup>2</sup>.

From measurements obtained using the multisphere spectrometer and the CPND in working environments at ORNL, the response T-A also can be related to thermal neutrons of the field. The average sensitivity for response T-A for thermal neutrons was found to be  $19.7 \times 10^{-5}$  ( $1\sigma = 33\%$ ) mR cm<sup>2</sup> from such field measurements. The measured value agreed with the calculated value used in this study. The average sensitivities for the CPND over the four energy intervals are presented in Table 4.1.2.

#### Spectral Unfolding and Dose Equivalent Evaluation

There are many mathematical methods for converting the measured responses of the CPND to the desired spectrum using the response functions. Since the CPND has only four measured responses and it is designed to provide crude spectral information

Table 4.1.2. The average sensitivities of the albedo TLD and the bubble detectors and the average fluence-to-dose equivalent conversion factors over the four neutron energy intervals.

Response	0.025-0.4 eV	Average Sensitivity		
		0.4 eV - 0.15 MeV	0.15-1.5 MeV	1.5-10 MeV
Albedo Response <sup>a</sup>	14.7	5.6	3.8	1.6
Response: T-A <sup>a</sup>	18.4	-	-	-
BD-100R <sup>b</sup>	-	-	5.1	4.0
BDS-1500 <sup>b</sup>	-	-	-	5.0
Average $h_\phi$ ( $10^{-10}$ Sv cm <sup>2</sup> )	$h_t$ 0.11	$h_s$ 0.45	$h_m$ 2.66	$h_f$ 4.05

a. Units =  $10^{-5}$  mR cm<sup>2</sup>.

b. Units =  $10^{-5}$  bu cm<sup>2</sup>.

for personnel monitoring purposes, complicated manipulation of the four responses and the response functions with computer codes is not practical or necessary. Therefore, a simple stripping method was used in deriving the neutron spectrum.

Knowing the average sensitivities of the four responses for the four energy intervals (Table 4.1.2) from the assumption of constant fluence per unit energy within each interval, the following four simultaneous equations can be established:

$$BS = 5.0 \phi_f 10^{-5}, \quad (4.1.1)$$

$$BR = (4.0 \phi_f + 5.1 \phi_m) 10^{-5}, \quad (4.1.2)$$

$$T-A = 18.4 \phi_t 10^{-5}, \quad (4.1.3)$$

$$A = (1.6 \phi_f + 3.8 \phi_m + 5.6 \phi_s + 14.7 \phi_t) 10^{-5}, \quad (4.1.4)$$

where BS, BR, T, A = the measured neutron responses for the BDS-1500, the BD-100R, the TLD-600, and the Cd-covered TLD-600, respectively. BD and BR are in units of number of bubbles, normalized to unit sensitivity ( $0.1 \text{ bu } \mu\text{Sv}^{-1}$ ). T and A are in units of mR; and

$\phi_f, \phi_m, \phi_t, \phi_s$  = the fluences of fast, medium, thermal, and slow neutrons, respectively ( $\text{cm}^{-2}$ ).

Starting with equation 4.1.1 and continuing down through equation 4.1.4, the fluence of fast, medium, thermal, and slow neutrons can be stripped consecutively and a 4-interval fluence spectrum can be obtained.

To derive the dose equivalent from the 4-interval spectrum, the average fluence-to-dose equivalent conversion factors for the corresponding four energy intervals were used. The ICRP Publication 21 fluence-to-dose equivalent conversion factor curve was

divided into five energy intervals. The conversion factors in each interval was fit with a constant or an equation:  $h_{\phi} = pE^m$ , where  $p$  and  $m$  are constants (see Table 4.1.1). The particular form and energy intervals were chosen because the conversion factor curve is roughly linear in the log-log plot over these intervals. The differences between the conversion factors and the fit equation values were within 3%. The average fluence-to-dose equivalent conversion factor for each CPND energy interval was derived by a simple integration of the fit equations or the constant over appropriate energies. The average conversion factor is  $4.05 \times 10^{-10}$  Sv cm<sup>2</sup> ( $h_f$ ) for fast neutrons,  $2.66 \times 10^{-10}$  Sv cm<sup>2</sup> ( $h_m$ ) for medium neutrons,  $0.45 \times 10^{-10}$  Sv cm<sup>2</sup> ( $h_s$ ) for slow neutrons, and  $0.11 \times 10^{-10}$  Sv cm<sup>2</sup> ( $h_t$ ) for thermal neutrons (the values are shown in Table 4.1.2). Then, the dose equivalents for every neutron interval and the total dose equivalent,  $H$  (Sv), can be derived by equation 4.1.5.

$$H = \phi_f h_f + \phi_m h_m + \phi_s h_s + \phi_t h_t. \quad (4.1.5)$$

The above spectral stripping and dose equivalent evaluation algorithm is simple enough to be done by hand calculation. A major error of this algorithm comes from the average sensitivities which were derived based on the necessary assumption of constant fluence per unit energy within each interval. If prior spectral information can be obtained from other references, better average sensitivity values can be used to unfold a more accurate spectrum. It is known that the spectrum estimate errors will accumulate with successive stripping steps, i.e., from equation 4.1.1 to equation 4.1.4. Therefore, the slow and medium neutron estimates are expected to have higher errors than those of the fast and thermal neutron estimates. Fortunately, slow neutrons

usually do not contribute significantly to the total dose equivalent due to the small  $h_s$  value.

The CPND with the above algorithm can measure a crude 4-interval fluence spectrum covering energies from 0.025 eV to 10 MeV. If a new set of fluence-to-dose equivalent conversion factors is adopted in the future, dose equivalent can still be derived by using new average  $h_\phi$  values.

#### 4.2 OPERATIONAL USAGE

The use of the CPND should benefit most external dosimetry programs by providing important spectral information so that more accurate estimates of the neutron dose equivalent can be achieved. The instant visible bubble responses of the two highly sensitive BD's can be used to alert the worker and the health physicist to an unexpected exposure. Timely control of the exposure also can be achieved through the use of the BD-100R which measures a large proportion of the neutron dose equivalent. A more active and effective ALARA (as low as reasonably achievable) radiation protection program can result from the the use of the CPND.

The personnel to be badged with the CPND should be those who are likely to be in the following situations: receiving high neutron exposures, exposed to a large component of neutrons with energies higher than 100 keV, exposed to a variety of neutron sources, or whose dose equivalent estimates may not be appropriate using current dosimetry techniques.

The routine procedure for the use of the CPND is: exchange and readout the albedo TLD quarterly by following the optimum TLD readout procedure (Section 3.2) and the signal processing procedure (Section 2.1); anneal the TLD's in the Harshaw

reader before the issue of the TLD's; readout and recompress the bubble detectors at least every week.

The CPND should be worn only during working hours. Use of the CPND in extreme temperature ( $< 15\text{ }^{\circ}\text{C}$  or  $> 30\text{ }^{\circ}\text{C}$ ) for a long periods of time ( $> 0.5\text{ h}$ ) should be noted.

## CHAPTER V

### REFERENCE NEUTRON SPECTRA AND DOSIMETRY

Various reference spectra with different energies and intensities were developed and used to evaluate the CPND performance. The development of these reference spectra is presented in this chapter.

#### 5.1 SPECTROMETER SYSTEM

The Bonner multisphere spectrometer (BMS) is a set of hydrogenous spheres of various diameters, each with a thermal neutron counter at the sphere center. The smaller detectors have higher responses to low energy neutrons and the larger detectors, which moderate more fast neutrons to thermal neutrons, have higher responses to high energy neutrons. The different energy responses of the detectors form the basis for the spectrometric capability of the multisphere spectrometer (Awschalom and Sanna 1985).

The BMS is widely used for reference neutron spectrometry for health physics purposes due to its high sensitivity, wide energy range (0.025 eV - 15 MeV), isotropic response, and simplicity of operation. The spectral resolution of the BMS is not fine, but it is adequate for dose equivalent determination. The primary disadvantage of the BMS is that complicated data manipulation using computer codes is required to unfold the spectrum from the measured detector responses.

#### BMS from EML

For characterization of neutron spectra in working areas, the above advantages and a good gamma discrimination capability are essential. Consequently, the BMS

from the Environmental Measurements Laboratory (EML), New York, was used in this study. The field characterization work was undertaken in collaboration with Dr. Ferenc Hajnal of EML.

The BMS consists of twelve detectors. Detectors no. 1 and no. 2 are a 2.54 cm radius spherical  $^{10}\text{BF}_3$  proportional counter and have no moderator. Detectors no. 3 to no. 12 have a  $^{10}\text{BF}_3$  counter surrounded by a spherical shell of polyethylene with a radial thickness ranging from 1.19 cm (detector no. 3) to 12.42 cm (detector no. 12). For all detectors except detector no. 1, a 0.76 mm thick spherical shell of cadmium also encloses the outer periphery to suppress the detector response to thermal neutrons and to provide better energy resolution. The response difference of detector no. 1 and detector no. 2 gives the thermal neutron component.

The detector output signal was connected directly to a preamplifier and, then, to an amplifier in a remote area away from the measurement point. The signals were accumulated in a multichannel analyzer (MCA). The  $^{10}\text{BF}_3$  proportional counter is very sensitive and has very good photon signal discrimination due to the  $^{10}\text{B}(n,\alpha)^7\text{Li}$ ,  $Q = 2.8$  MeV, reaction. Simple selection of the integral over the signal spectrum above a certain threshold on the MCA gives the neutron response. This fast response readout of the BMS, together with the ultra-high sensitivity (can measure the natural neutron background), greatly speed up the measurement process even in low intensity fields.

### Spectral Unfolding

For a neutron spectrum  $\phi(E)$ , the response of the  $i$ th detector,  $C_i$ , is given by:

$$C_i = \int R_i(E) \phi(E) dE, \quad i = 1, 2, \dots, N \quad (5.1.1)$$

where  $R_i(E)$  is the energy response function of the  $i$ th detector and  $N$  is the number of detectors ( $N=12$  for the BMS). If  $R_i(E)$  is known for every detector, the  $\phi(E)$  can be unfolded from the measured responses,  $C_i$ 's, of the twelve detectors.

There are many mathematical methods which can be used to solve for the  $\phi(E)$  from the above integral (Cross and Ing 1987; Routti and Sandberg 1985). Most methods adopt two approximations; both the continuous functions,  $\phi(E)$  and  $R_i(E)$ , are approximated by a set of values,  $\phi_j$  and  $R_{ij}$  respectively, in  $m$  finite energy intervals. Equation 5.1.1 can be rewritten in a discrete form as the following equation:

$$C_i = \sum_j R_{ij}(E) \phi_j(E), \quad i = 1, \dots, N, \text{ and } j = 1, \dots, m. \quad (5.1.2)$$

A set of 12 linear equations with the  $C_i$  and  $R_{ij}$  values corresponding to the 12 detectors can be obtained for the BMS. To have better spectral resolution, the number of energy intervals generally is set to be larger than the number of detectors (i.e.,  $m > N$ ) and equation 5.1.2 becomes undefined. Some conditions of the spectrum, e.g., non-negativity, bounded, smoothness, and shape are assumed to derive a physically meaningful spectrum.

An iterative unfolding code, TWOGO (developed by Hajnal), was used to solve equation 5.1.2 in analyzing the BMS measurements. The details of the code can be found elsewhere (Hajnal 1981). The basic principle of the iteration code is that a reasonable guess of the initial spectrum is made, the responses of the 12 detectors are calculated, and the spectrum is improved by comparing the calculated responses with the measured responses, and an iteration process is continued until a satisfactory spectrum is obtained.

Two different algorithms to modify the spectrum are applied in the code. One of the algorithms is used on each alternate iteration. This provides faster convergence and more stable solutions than can be obtained by using only one algorithm (Hajnal 1981). The iteration process is terminated either when the ratio of the coefficient of variation in terms of the measured and calculated responses is unity, or when the average absolute fractional difference between the measured and the calculated responses is less than the average measurement error. The performance of the TWOGO program has been tested satisfactorily with both pseudo and real spectra of reactors, fission sources, and cosmic-rays (Hajnal 1981).

#### Response Functions of the BMS

One of the critical factors for accurate spectrometry with the BMS is the accuracy of its response functions, i.e., the responses of the detectors as a function of neutron energy. The response functions for the BMS in the TWOGO code were calculated by Maerker, based on an adjoint ANISN calculation (Maerker et al. 1971a), and were verified by another Monte Carlo calculation (Burgart and Emmett 1972).

The calculated response functions for the 11 detectors (no. 2 - no. 12) of the BMS are plotted in Fig. 5.1.1. Detector no. 1 has same response function as that of detector no. 2, except that detector no. 1 is sensitive to thermal neutrons. Note from the figure that the energy at which the detector has its peak response increases as the detector size increases. Detector no. 12 also has a fluence energy response curve similar to the fluence-to-dose equivalent conversion factor curve. The response of detector no. 12, therefore, can be used for a quick estimate of the dose equivalent rate in the field.

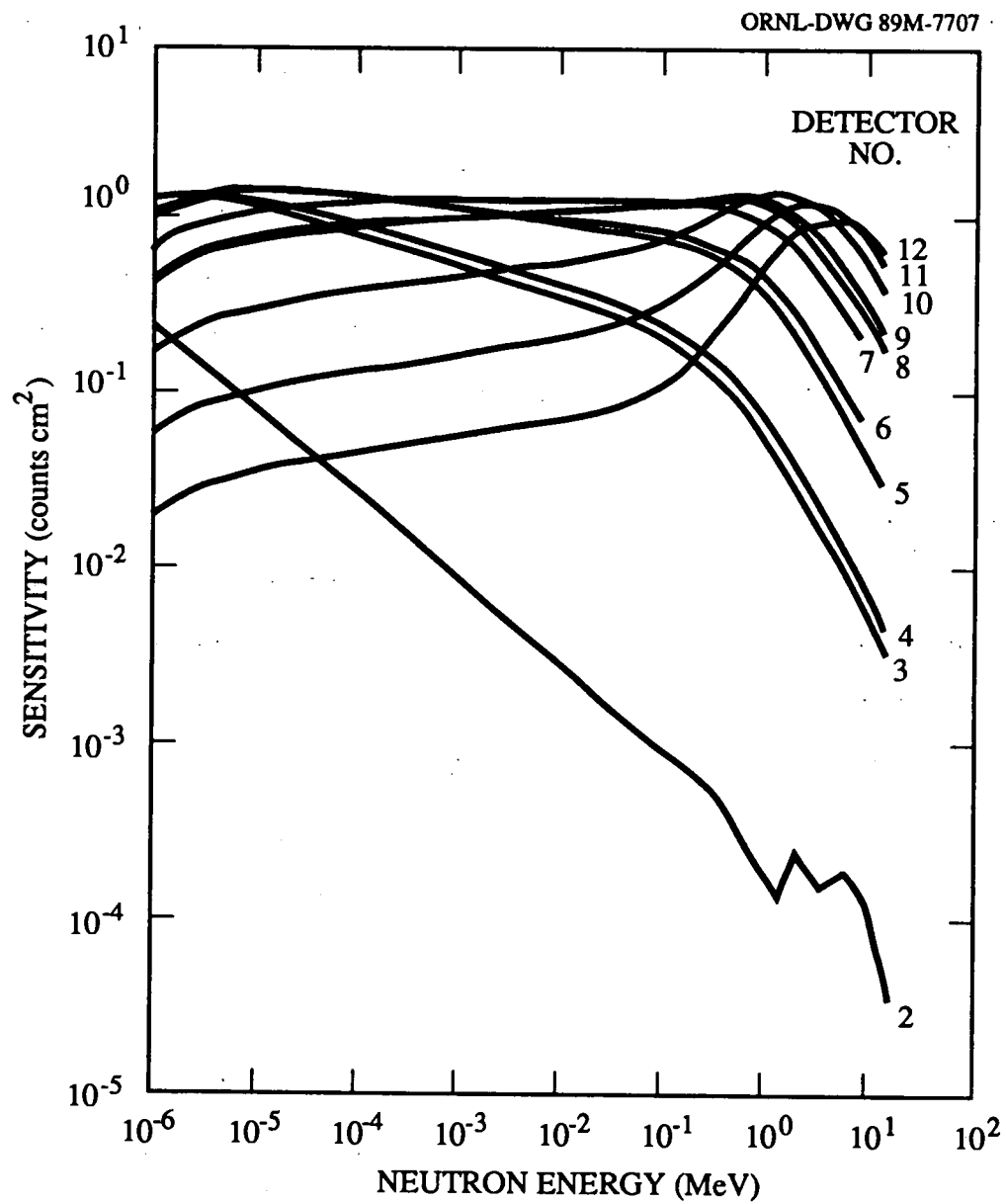


Fig. 5.1.1. Response functions of the Bonner multisphere spectrometer (<sup>10</sup>BF<sub>3</sub> gas spherical counter).

Minor shortcomings of this, and other BMS systems, can be inferred from the response functions shown in Fig. 5.1.1. The first shortcoming is that the response functions are smoothly varying and, therefore, the unfolded spectrum also will be smooth and detailed spectral information (e.g., sharp peaks) will be lost from the unfolding process. The second shortcoming is that no peak response occurs between about 20 eV - 300 keV. Therefore, the energy resolution and the spectrum estimate will lack accuracy in this energy interval.

### Calibration of the BMS

The response functions of the BMS were calculated based on certain detector characteristics, e.g., the  $^{10}\text{B}/\text{B}$  atom ratio of  $\text{BF}_3$  gas, the  $\text{BF}_3$  gas pressure, and the polyethylene sphere density. The actual detectors may differ from these assumed characteristics. Therefore, the calculated response function generally is used only to indicate the relative energy dependence of the detector. The absolute neutron detection efficiency of each detector must be determined. This determination can be made by calibrating the BMS in a reference radiation field; the free-field (i.e., scatter-free field) from a well-known neutron source with a known emission rate.

Calibration of the BMS was undertaken in a low-scattering room at EML. A  $^{252}\text{Cf}$  source (ID: SRCF-185-Z), with a neutron output calibrated by comparison with a source at NIST, was used for the calibration. Theoretical free-field responses (efficiencies) of the 12 detectors to the known spectrum of the  $^{252}\text{Cf}$  source were calculated from equation 5.1.2. The purpose of the BMS calibration is to compare the above calculated efficiencies with the measured free-field efficiencies and to derive an efficiency correction factor for each detector. To measure the free-field efficiencies for

the detectors, scattering effects during calibration must be considered. This scattering correction was made by use of the measurement method described below.

Measurements of the variation of the detector response as a function of the source-to-detector distance were made for all 12 detectors. Source-to-detector distances from 15 to 170 cm were used. Several models (Maerker et al. 1971b; Thompson and Lavender 1973; Hunt 1984) were applied to analyze the measured response data, determine scattered components, and derive the free-field efficiencies. The results from different models were similar. Hunt's model showed the best results and, therefore, was used in scattering correction.

In Hunt's model, the response of a spherical detector at a source-to-detector distance of  $d$  cm,  $C(d)$  (counts  $s^{-1}$ ), is given by:

$$C(d) = (S F(\theta) / 4\pi d^2) F_1(d) F_2(d) \epsilon, \quad (5.1.3)$$

where  $S$  = source strength ( $s^{-1}$ );

$F(\theta)$  = source anisotropy factor;

$F_1(d)$  = geometry correction term;

$F_2(d)$  = scattering correction term; and

$\epsilon$  = detector efficiency (counts  $cm^2$ ).

The source anisotropy factor,  $F(\theta)$ , corrects for anisotropic neutron emission. A value of 1.037 was used for the SRCF-185-Z  $^{252}\text{Cf}$  source in this study (Schwartz and Eisenhauer 1982). The geometry factor,  $F_1(d)$ , corrects for non-uniform illumination of the detector at short distances.  $F_1(d)$  was estimated by using equation 3 of the literature (Hunt 1984).

Assuming that the room-scatter component is constant in a region near the source, and that the air-scatter component is inversely proportional to the distance, the scattering correction term,  $F_2(d)$ , is given by:

$$F_2(d) = (1 + A d + R d^2), \quad (5.1.4)$$

where  $A d$  = fractional component due to air scattering; and

$R d^2$  = fractional component due to room scattering.

Combining equation 5.1.4 and equation 5.1.3 gives the following equation:

$$C(d) 4\pi d^2 / F_1(d) = (S F(\theta) \epsilon) (1 + A d + R d^2). \quad (5.1.5)$$

Therefore, the measurement response data  $C(d)$ , after being corrected for the inverse square law reduction and applying the geometry factor  $F_1(d)$ , can be fit to a second-order polynomial function of  $d$  using a least squares technique. The least squares fit provides the constant  $SF(\theta)\epsilon$ , the air scattering  $A$ , and the room scattering  $R$  components. Knowing the source strength  $S$  and the anisotropy factor  $F(\theta)$ , the measured scatter-free efficiency  $\epsilon$  can be derived. A simple comparison between the measured efficiency and the calculated efficiency (both in scatter-free conditions) gives the efficiency correction factor for each detector.

A  $^{252}\text{Cf}$  spectrum was unfolded from the measured scatter-free responses using the TWOGO code after calibration of the BMS. A comparison of the unfolded spectrum obtained in the BMS measurements and the reference  $^{252}\text{Cf}$  spectrum (IAEA 1985) is shown in Fig. 5.1.2. The figure clearly shows that the calibrated BMS and the TWOGO code can produce very good spectrometry results. Not only was the

ORNL-DWG 89M-9675

	SOURCE STRENGTH ( $s^{-1}$ )	H ( $mSv\ h^{-1}$ )	AVERAGE ENERGY (MeV)
REFERENCE	$4.80 \times 10^6$	0.0458	2.1
BMS	$4.94 \times 10^6$	0.0473	2.1

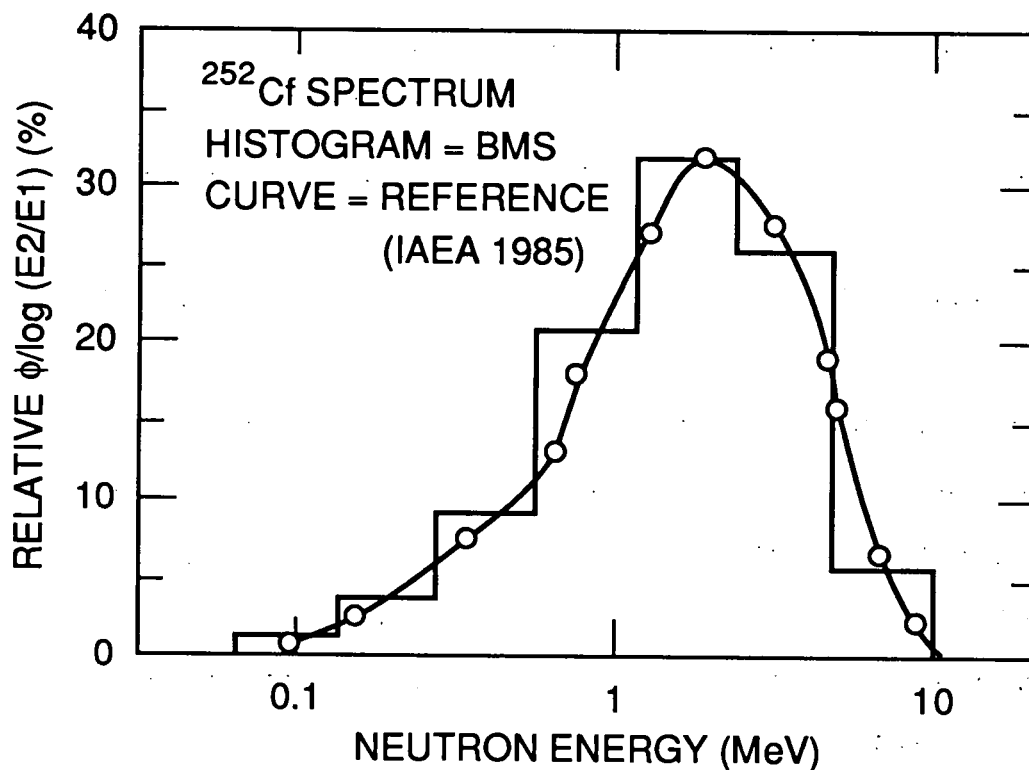


Fig. 5.1.2. Comparison of the reference spectrum and the unfolded spectrum from the Bonner multisphere spectrometer for the  $^{252}\text{Cf}$  source.

$^{252}\text{Cf}$  spectrum correctly unfolded, but the integral quantities of source strength, dose equivalent rate, and average energy for the EML  $^{252}\text{Cf}$  source derived by the BMS measurements agreed with the reference values to within about 3%. The stability of the BMS was checked with constant and reproducible irradiations using the  $^{241}\text{Am}$ -Be source at EML.

## 5.2 REFERENCE SPECTRA AND DOSIMETRY AT TRU

The neutron spectra in five work areas at ORNL were characterized with the calibrated Bonner multisphere spectrometer from EML.

### TRU Neutron Fields

The Transuranium Processing Plant (TRU) and the High Flux Isotope Reactor (HFIR) were built at ORNL to provide gram quantities of the transuranium elements and milligram quantities of the transcalifornium elements. The ground floor map of TRU, which was recently renamed as the Radiochemical Engineering Development Center, is shown in Fig. 5.2.1. The six locations of TRU in which neutron spectra were measured with the BMS also are shown in the figure.

The targets that are irradiated at HFIR are processed at TRU. The desired heavy elements are separated from the waste in cubicle 7 (abbreviated as cub in Fig. 5.2.1). The waste is transferred manually to a storage area through a conduit in the transfer cubicle. The elements Bk, Cf, Es, and Fm are extracted in cubicles 4 through 6. In cubicle 1, the elements Pu, Am, and Cm are made into targets and recycled to HFIR for irradiation.

The reprocessing of irradiated fuels presents the concern of radiation protection against neutrons which result from spontaneous fission or ( $\alpha$ ,n) reactions in elements

ORNL-DWG 89M-10602

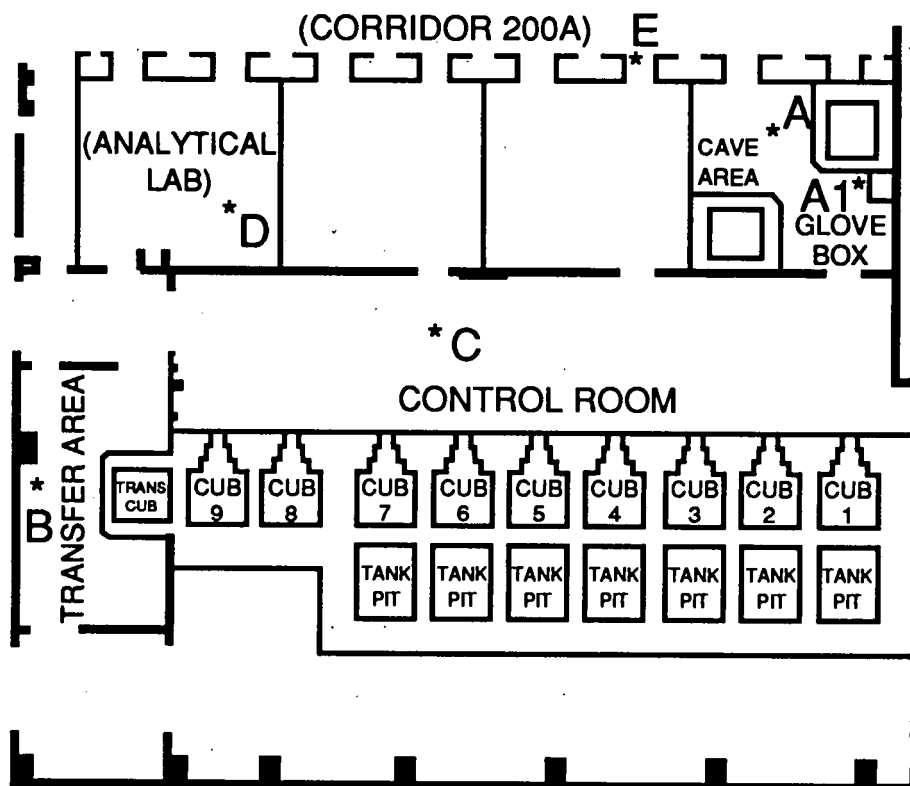


Fig. 5.2.1. Locations in the Transuranium Processing Plant (TRU) in which spectra were characterized with the Bonner multisphere spectrometer. Analytical laboratory and corridor 200A are on the second floor.

Cf, Cm, and Pu. The various operational procedures and different degrees of shielding mean that a wide range of neutron spectra are encountered at TRU. The intensity and directionality of the neutron fields to which the workers are exposed also may be a function of occupancy time and position.

Before field characterization with the BMS, a complete field survey was made at TRU with the Eberline 9" and 3" spheres and bare BF<sub>3</sub> detectors to determine critical points for further characterization. These survey results are given in Appendix 7. Priority of the fields to be characterized was determined from the radiation protection point of view and from the view point of using the fields to evaluate the CPND performance. A total of six fields were characterized with the BMS (see the locations marked with \* in Fig. 5.2.1). During field characterization, surveys with the same Eberline detectors (9", 3", and bare BF<sub>3</sub>) also were made (data also are included in Appendix 7). These were used to check whether the intensity (use 9" response) or the quality (use 9"/3") of the field changed after the field characterization.

Cell A in the cave area (site A) has heavy shielding of water and leaded glass. The glove box (site A1) next to the cell A is only lightly shielded. The small size of the cave area also causes serious scattering for both survey sites. The BMS measurement in the waste transfer area (site B) was made in front of the conduit exit which had less shielding and, therefore, a higher energy spectrum was expected. The BMS measurement in the control room (site C) was made next to the operator's desk location. This location received much of the exposure through the door of a chemical laboratory. This location had the highest dose rate in the control room and a moderated spectrum was expected. The glove box in the analytical laboratory (site D) had little shielding and less scattering due to the large room and, therefore, a high energy spectrum was expected. The measurement at site E (corridor 200 A) was made only to

relieve some worker concern and the result was not used to test the CPND. All survey locations were on the first floor except the analytical laboratory and the corridor 200 A which were on the second floor of TRU.

#### Field Characterization with the BMS

The locations of the BMS measurements in the radiation fields were all recorded. At least two measurements were taken using each detector. The time for each measurement was 100 seconds and the total measurement time for each field was about 1 hour.

The measurement error for a detector was taken to be one standard deviation or the root square of the mean detector response, whichever is larger. The measurement errors were all less than 5% (most errors < 3%), except for detector no. 2 in the waste transfer area (7%), control room (19%), and analytical laboratory (8%). The larger errors for detector no. 2 response in these three sites were resulted from the small amount of low energy neutrons in these fields.

The relative detector responses (normalized to the maximum detector response) of the BMS for each field are plotted versus the radial thicknesses of the polyethylene spheres in Fig. 5.2.2. Such plots should be smooth and, therefore, can be used to identify any measurement outliers. The smooth curves in Fig. 5.2.2 show that the measurements were good. The plot also shows that the spectrum for the analytical laboratory was the most energetic, and the control room was the least energetic (not including the corridor 200A). The relative detector response of the BMS for the TRU fields, together with the detector characteristics, are given in Appendix 8.

Unfolding of the spectrum using the TWOGO code requires an estimate of the spectrum from which to start. To ensure better unfolding results, a 1/E spectrum and a

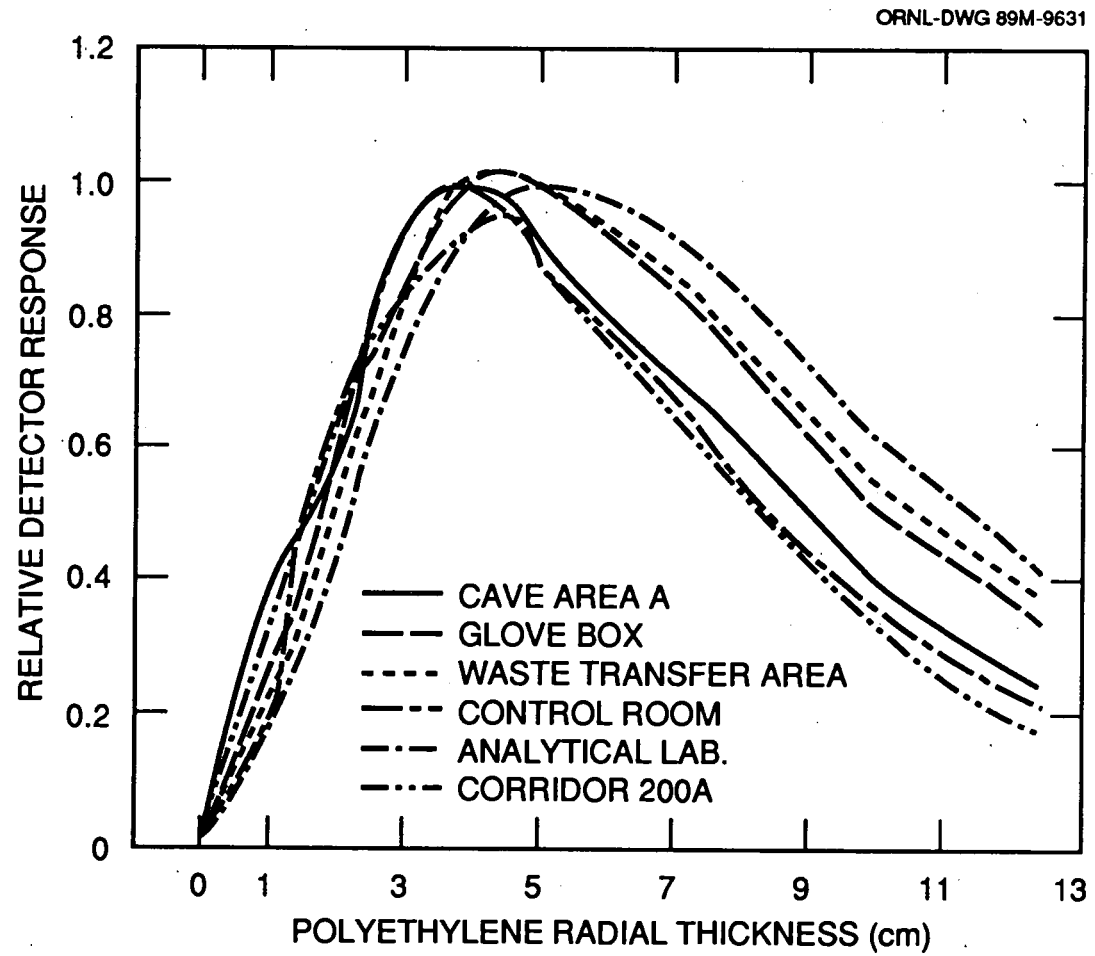


Fig. 5.2.2. Relative detector response of the Bonner multisphere spectrometer for the neutron fields at the Transuranium Processing Plant, ORNL.

spectrum of  $^{252}\text{Cf}$  moderated with a 15 cm radius polyethylene sphere (Thorngate 1987) were both tried. While both beginning spectra produced similar results, the latter produced a spectrum which had a slightly smaller differences between the measured and calculated detector responses and also converged faster. Therefore, the spectra unfolded with the latter input spectrum were used.

Spectra of the TRU fields evaluated with the BMS are shown in Figures 5.2.3 - 5.2.7. The associated data are tabulated in Appendix 9. Neutron flux per unit logarithmic energy interval,  $\phi/\log(E2/E1)$ , versus the neutron energy was plotted in 26 energy groups (0.025 eV - 20.5 MeV). E2 and E1 are the upper and lower bounds for each energy group, respectively. Plotting the spectrum in this way has the advantage that the area under the curve between any two energies is proportional to the flux magnitude between those energies. Visualization of the spectrum is easier. A linear scale on the ordinate, instead of several decades of a logarithmic scale, can be used. Therefore, all the spectral results in this research were plotted in this way.

Since the fields were used to test the CPND, the detailed 26-energy-group spectrum for each field was divided into 4 energy intervals; fast (1.5-10 MeV), medium (0.15-1.5 MeV), slow (0.4 eV - 0.15 MeV), and thermal (0.025-0.4 eV). The 4-interval spectrum is more useful and comparable to the crude spectrum derived with the CPND. The results in terms of flux, dose equivalent rate, and average fluence-to-dose equivalent conversion factor for each energy interval in every field are shown in Table 5.2.1.

Although the high energy neutron component (fast and medium neutrons) was only 20%-60% of the total fluence, it contributed 83%-95% of the total dose equivalent for all fields. The thermal neutron component was 7% (analytical laboratory) to 43% (cave area A) of the total fluence, but it contributed only 7% (cave area A) at most of the

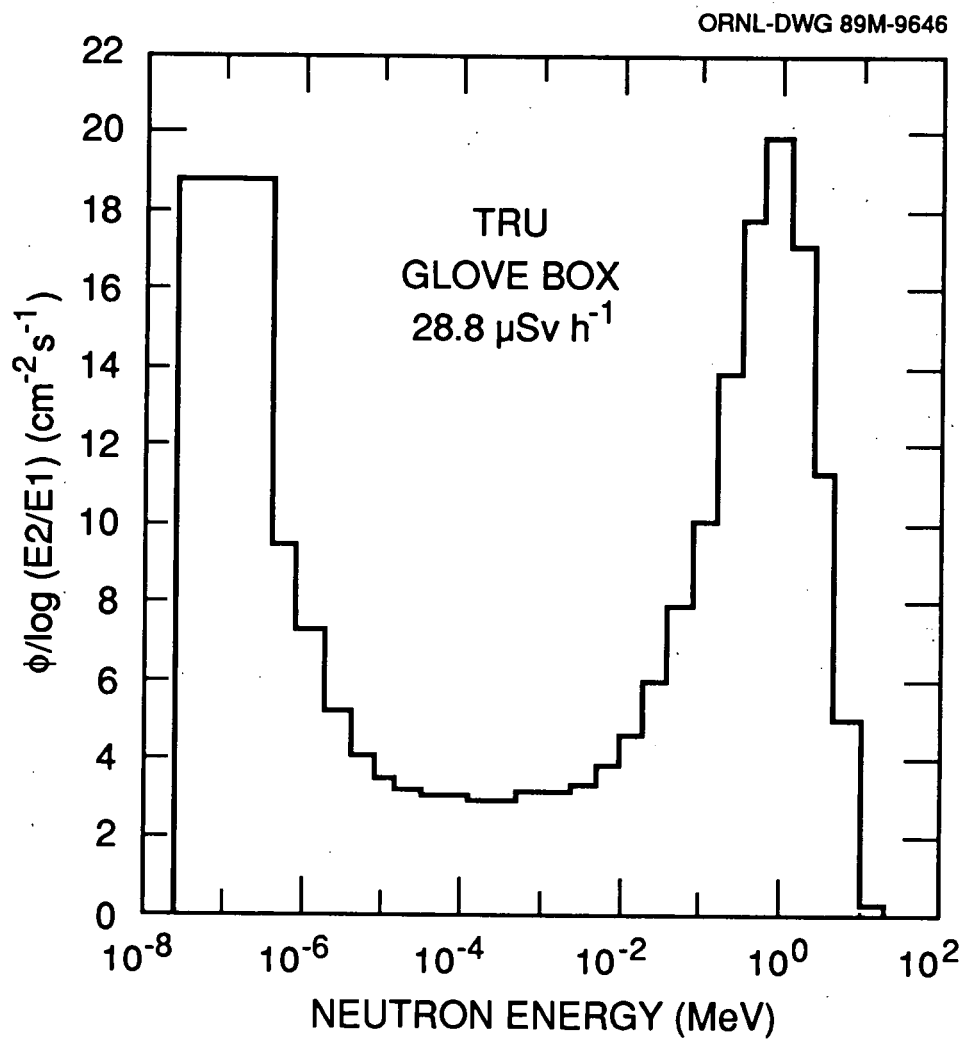


Fig. 5.2.3. Neutron spectrum at the glove box, TRU, measured with the Bonner multisphere spectrometer.

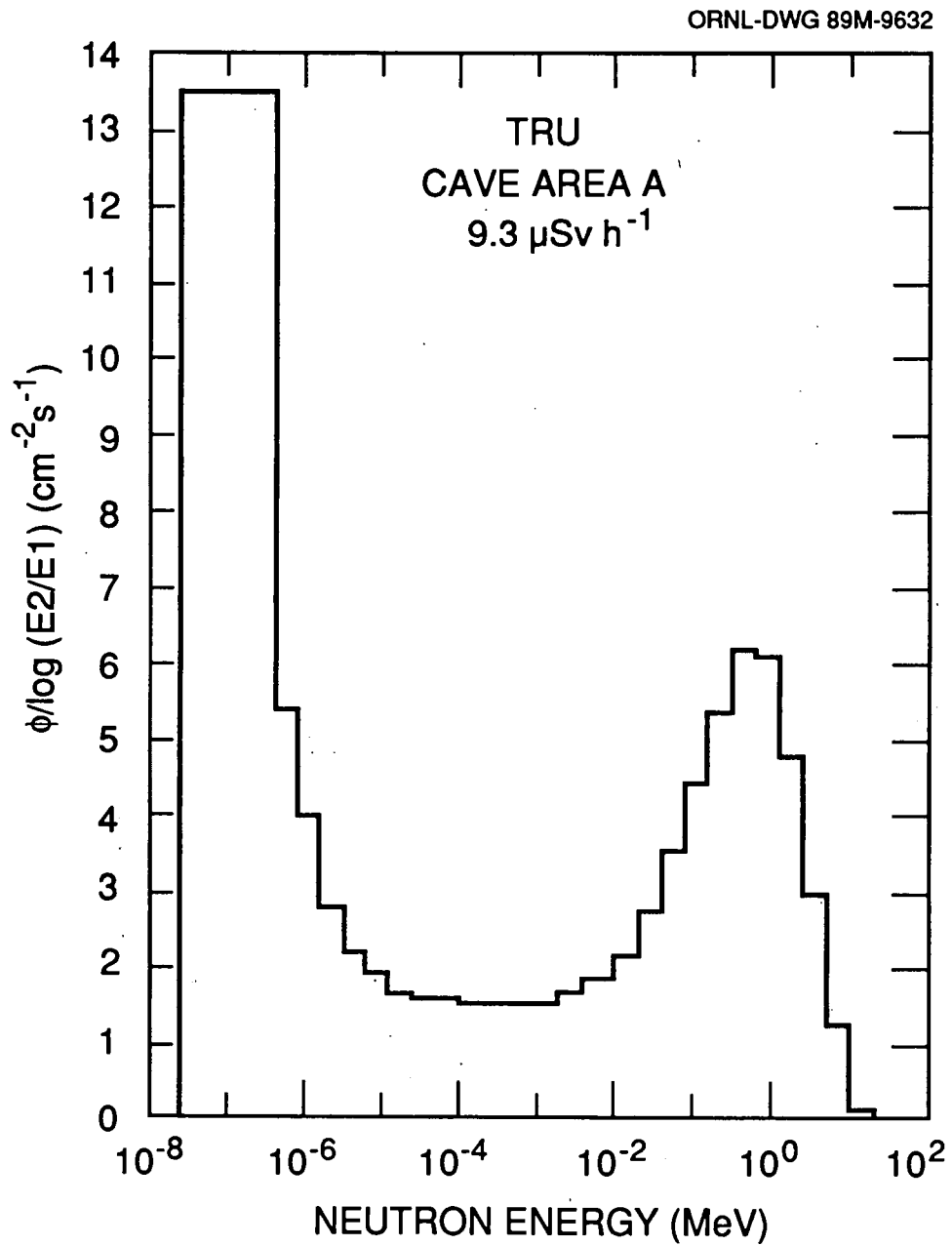


Fig. 5.2.4. Neutron spectrum in the cave area A, TRU, measured with the Bonner multisphere spectrometer.

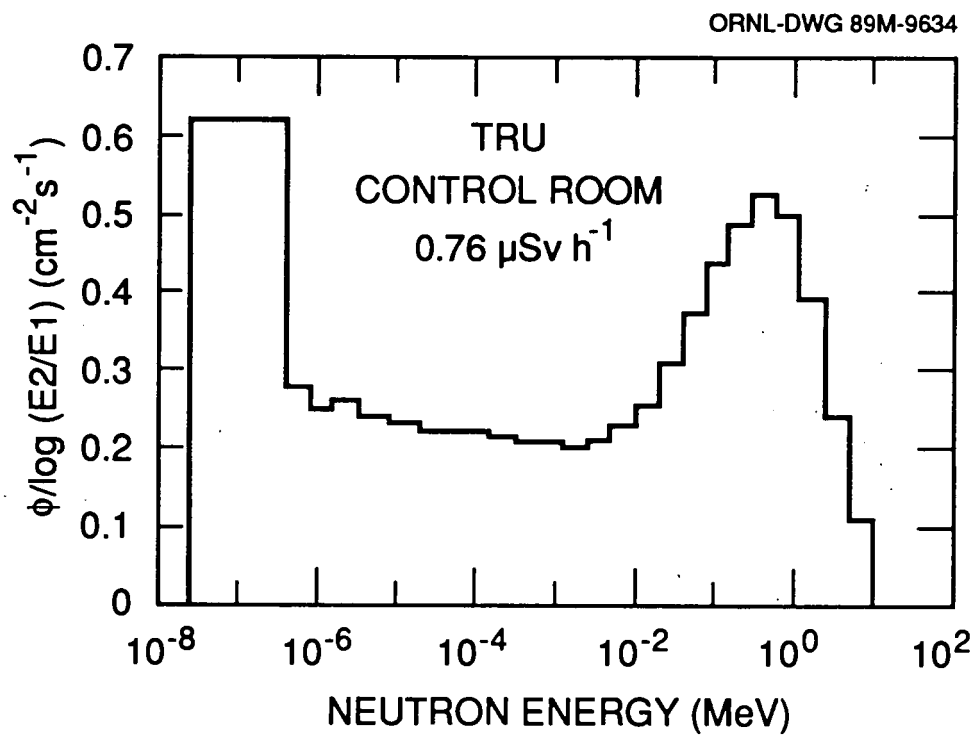


Fig. 5.2.5. Neutron spectrum in the control room, TRU, measured with the Bonner multisphere spectrometer.

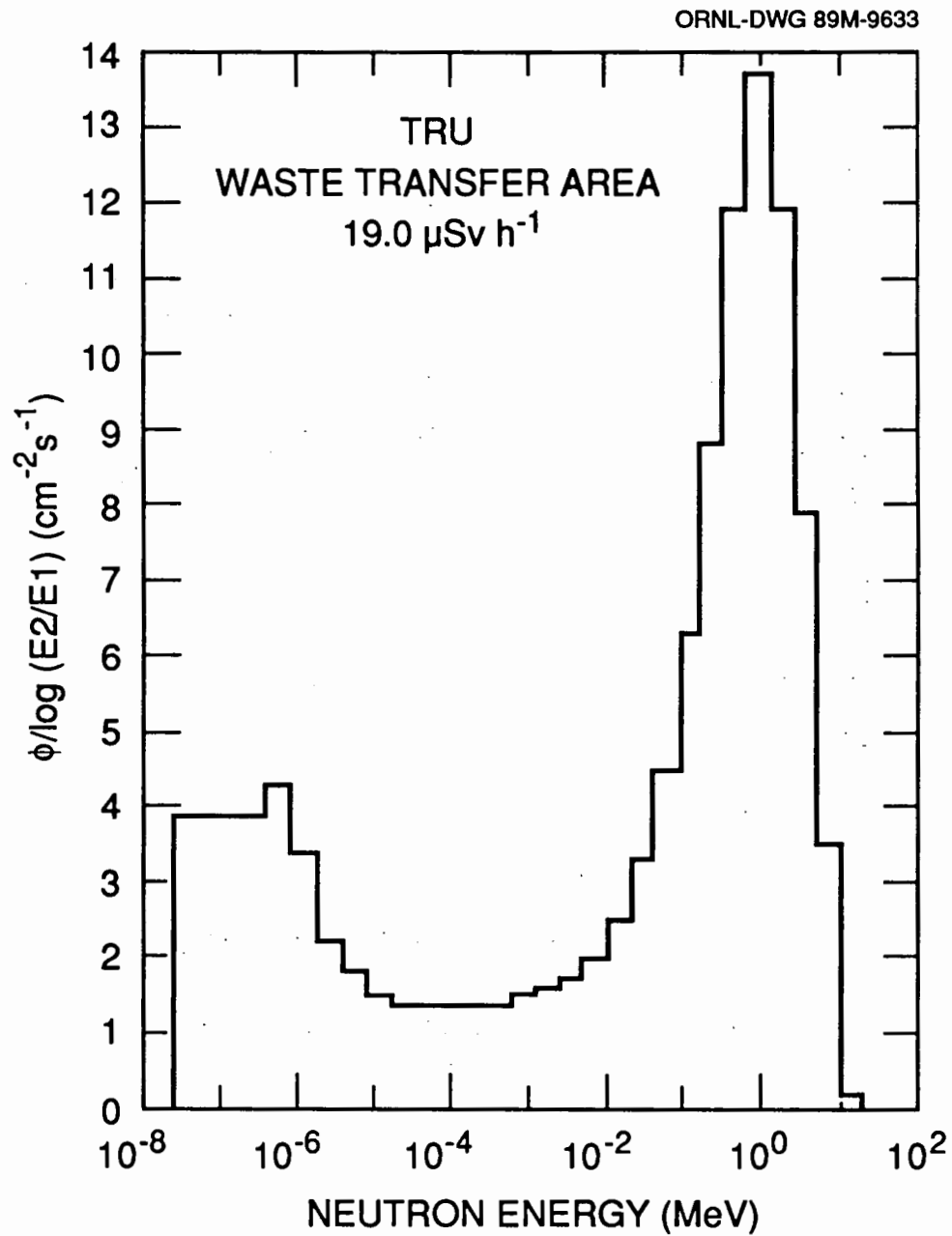


Fig. 5.2.6. Neutron spectrum in the waste transfer area, TRU, measured with the Bonner multisphere spectrometer.

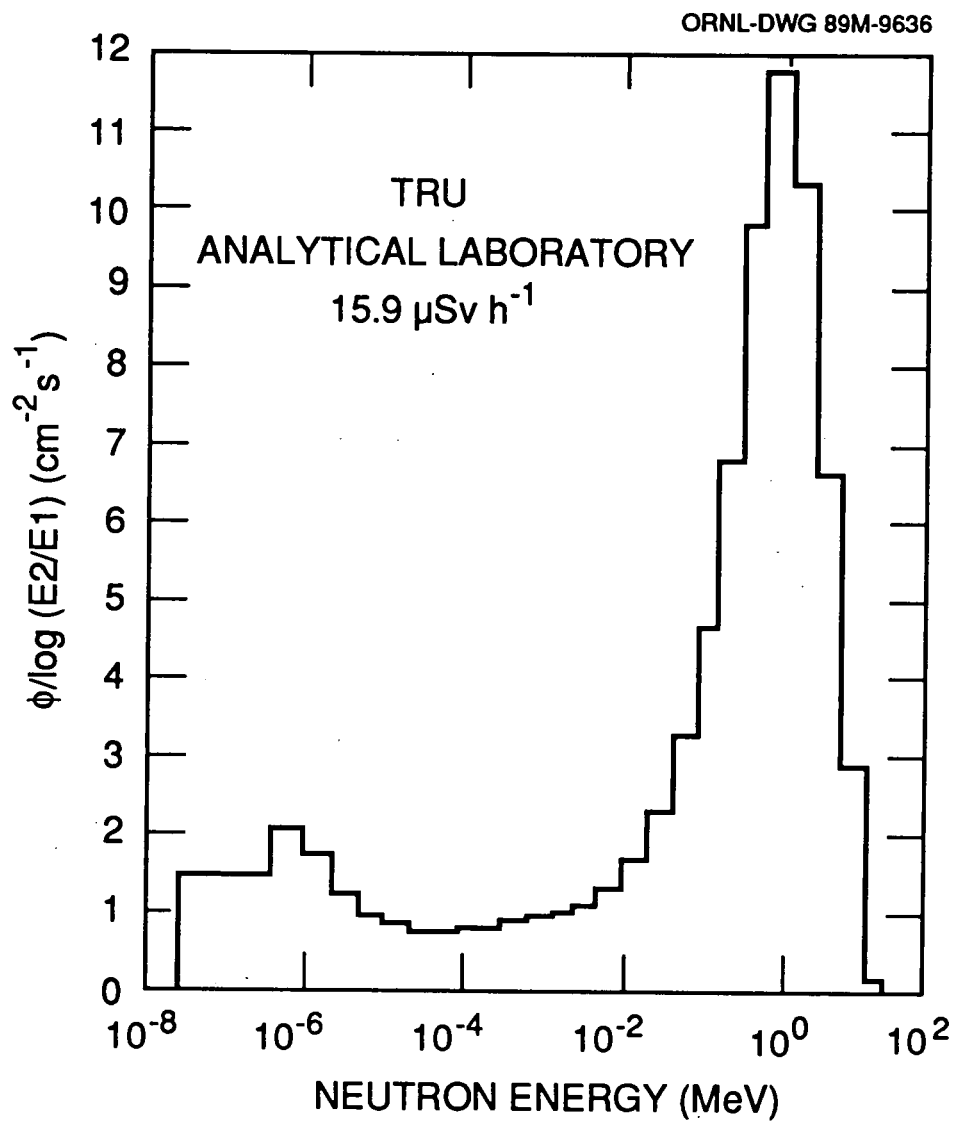


Fig. 5.2.7. Neutron spectrum in the analytical laboratory, TRU, measured with the Bonner multisphere spectrometer.

ORNL WSM-10125

Table 5.2.1. Reference neutron spectra measured with the Bonner multisphere spectrometer at TRU.

Quantity	Glove Box	Cave Area A	Control Room	Waste Transfer	Analytical Laboratory
H ( $\mu\text{Sv h}^{-1}$ )	28.80	9.30	0.760	19.00	15.90
Fast	13.00	3.53	0.287	9.00	7.69
Medium	13.00	4.20	0.350	8.80	7.42
Slow	1.89	0.92	0.093	1.01	0.72
Thermal	0.91	0.65	0.030	0.19	0.07
Flux ( $\text{cm}^{-2} \text{s}^{-1}$ )	76.10	38.40	2.860	35.90	25.20
Fast	9.07	2.47	0.201	6.30	5.39
Medium	16.90	5.73	0.487	11.33	9.41
Slow	27.16	13.71	1.413	13.47	8.54
Thermal	22.97	16.49	0.759	4.80	1.86
$h\phi(10^{-10} \text{ Sv cm}^2)$					
Fast	3.98	3.97	3.97	3.97	3.97
Medium	2.14	2.04	2.00	2.16	2.19
Slow	0.19	0.19	0.18	0.21	0.23
Thermal	0.11	0.11	0.11	0.11	0.11
Mean Energy (MeV)	0.55	0.31	0.34	0.80	0.97

total dose equivalent for all fields. This was expected, since the fluence-to-dose equivalent conversion factors for high energy neutrons were much higher than those for low energy neutrons. This reflects the fact that the high energy neutron component must be measured correctly for accurate neutron dose equivalent estimation.

The average fluence-to-dose equivalent conversion factor of each energy interval (except the thermal neutrons) for all fields was smaller than the corresponding conversion factor used in the CPND algorithm (see the average  $h_{\phi}$  values in Tables 5.2.1 and 4.1.2). This was because, for the spectrum in the field, the fluence per unit energy within each interval was certainly not constant and more neutrons were distributed in lower end of the interval.

The measured 4-interval spectra in the TRU fields, summarized in Table 5.2.1, were used as the references for the field test of the CPND.

### 5.3 REFERENCE SPECTRA AND DOSIMETRY AT RADCAL

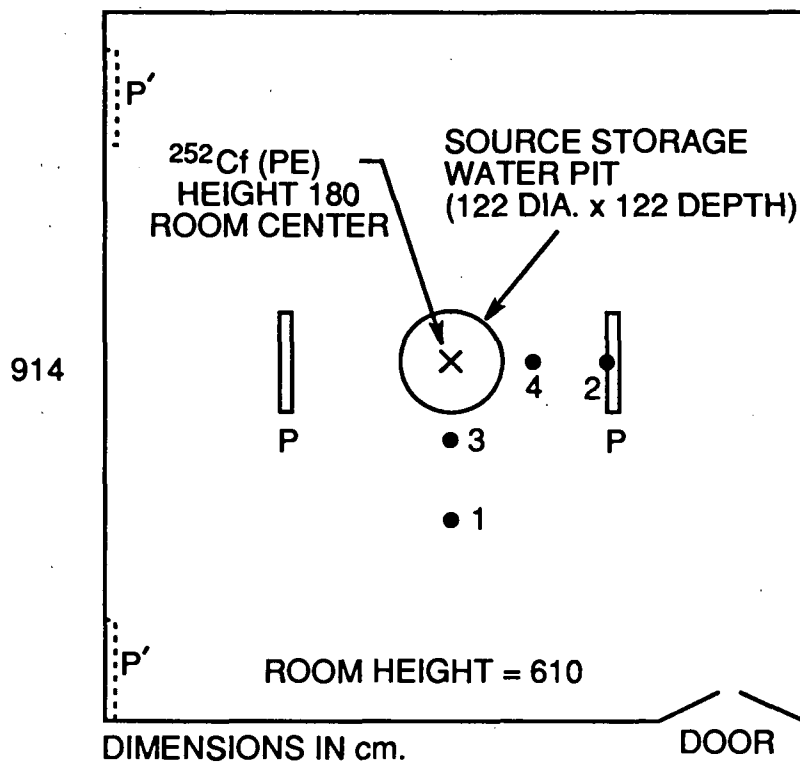
Four radioisotopic sources,  $^{252}\text{Cf}(\text{PE})$ ,  $^{238}\text{Pu}\text{-Be}$ ,  $^{252}\text{Cf}(\text{D}_2\text{O})$ , and  $^{252}\text{Cf}(\text{D}_2\text{O}, \text{no Cd})$ , at the RADCAL facility were used as references in both the laboratory tests and the fourteenth PDIS for performance evaluation of the CPND. The  $^{252}\text{Cf}(\text{D}_2\text{O}, \text{no Cd})$  source is the  $^{252}\text{Cf}(\text{D}_2\text{O})$  source without the cadmium shell.

#### $^{252}\text{Cf}(\text{PE})$

The spectrum of the  $^{252}\text{Cf}(\text{PE})$  source in the RADCAL neutron room was measured with the BMS. A floor map of the neutron room is shown in Fig. 5.3.1. The room is 9.1x8.7x6.1 m. The source was in the room center position (height 1.8 m) for irradiation. The spectra were measured at source-to-detector distances of 1 m and 2 m (positions no. 2 and 4 in Fig. 5.3.1). Two large Lucite slab phantoms

ORNL-DWG 89M-7712

874



1 AND 2 = 200 cm FROM SOURCE  
 3 AND 4 = 100 cm FROM SOURCE  
 P = BIG LUCITE PHANTOM POSITION FOR 1 AND 3  
 P' = BIG LUCITE PHANTOM POSITION FOR 2 AND 4

Fig. 5.3.1. Neutron irradiation room at the RADCAL facility and positions characterized with the multisphere spectrometer.

(125x91x10 cm) were utilized in an experiment involving irradiations of a large number of dosimeters. Spectra were measured at positions no. 1 and 3 when the large phantoms were in the irradiation positions. However, only the spectra without the two large phantoms in place (i.e., positions no. 2 and 4) were used to test the CPND.

The relative detector response is plotted versus the radial thickness of the polyethylene sphere in Fig. 5.3.2. The smooth curves show that the measurements were good and the spectrum at 1 m had a higher average energy than the spectrum at 2 m. The relative detector response of the BMS for the above four positions are tabulated in Appendix 10.

The unfolded 26-energy-group spectra of the  $^{252}\text{Cf}(\text{PE})$  at 1 m and 2 m are plotted in Fig. 5.3.3. The associated spectral data are given in the last two columns of Appendix 9. The 26-energy-group spectra were divided into 4-interval spectra for comparison with the CPND results. The reference 4-interval spectra results are shown in Table 5.3.1. The dose equivalent rate was  $1.875 \text{ mSv h}^{-1}$  at 1 m and  $0.576 \text{ mSv h}^{-1}$  at 2 m. The high energy neutron component was only  $\sim 35\%$  of the total fluence, but it contributed over 91% of the dose equivalent. The mean energy of the spectrum was 0.86 MeV at 1 m and 0.65 MeV at 2 m. The average fluence-to-dose equivalent conversion factor of each energy interval was smaller than the corresponding average conversion factor used for the CPND. The "softness" of the spectrum at 2 m also resulted in the smaller average conversion factors.

#### $^{238}\text{Pu}\text{-Be}$ , $^{252}\text{Cf}(\text{D}_2\text{O})$ , and $^{252}\text{Cf}(\text{D}_2\text{O}, \text{no Cd})$

The spectra of the  $^{238}\text{Pu}\text{-Be}$ , and  $^{252}\text{Cf}(\text{D}_2\text{O})$  are well-known from the literature. The spectrum of  $^{238}\text{Pu}\text{-Be}$  was obtained from the work of Block et al. (Block et al. 1967). The spectrum of  $^{252}\text{Cf}(\text{D}_2\text{O})$  was obtained from a previous

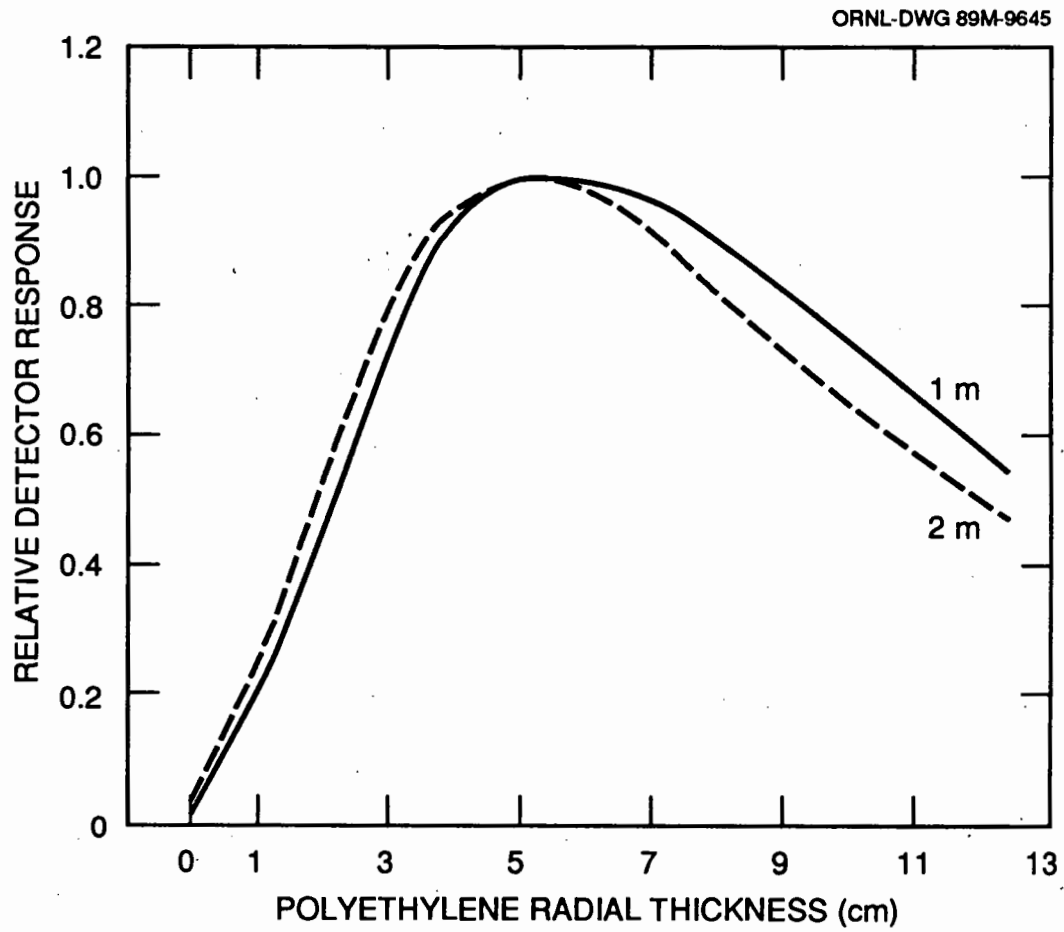


Fig. 5.3.2. Relative detector response of the Bonner multisphere spectrometer for the neutron spectra of the RADCAL  $^{252}\text{Cf}(\text{PE})$  source.

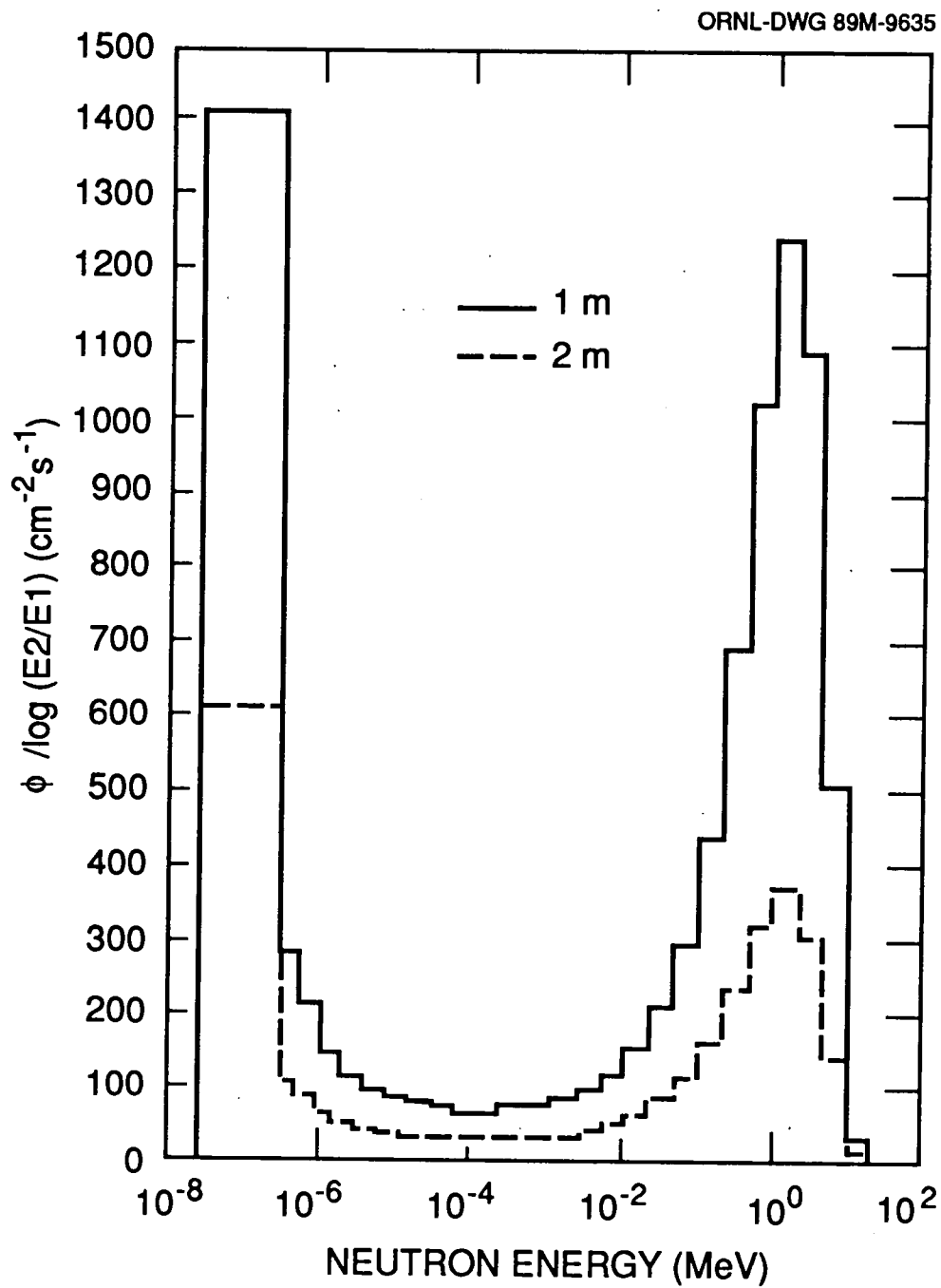


Fig. 5.3.3. Neutron spectrum of the RADCAL  $^{252}\text{Cf}(\text{PE})$  source measured with the Bonner multisphere spectrometer.

ORNL WSM-10126

Table 5.3.1. Reference neutron spectra at RADCAL.

Quantity	<sup>252</sup> Cf (PE) <sup>a</sup>		<sup>238</sup> Pu-Be <sup>b</sup>	<sup>252</sup> Cf (D <sub>2</sub> O) <sup>c</sup>
	1 m	2 m	1 m	0.75 m
H (mSv h <sup>-1</sup> )	1.875	0.576	0.241	18.46
Fast	1.128	0.323	0.200	10.89
Medium	0.628	0.202	0.041	4.83
Slow	0.051	0.022	0	2.73
Thermal	0.068	0.029	0	0
Flux (cm <sup>-2</sup> s <sup>-1</sup> )	3957	1524	181	56510
Fast	786	225	140	7538
Medium	743	246	41	6784
Slow	708	311	0	42188
Thermal	1720	742	0	0
$h\phi(10^{-10} \text{ Sv cm}^2)$				
Fast	3.99	3.98	3.97	4.01
Medium	2.35	2.29	2.78	1.98
Slow	0.20	0.19	0	0.18
Thermal	0.11	0.11	0	0
Mean Energy (MeV)	0.86	0.65	4.00	0.55

a. Bonner multisphere measurement results, (March 2, 1989).

b. Calculated from the literature (Block et al. 1967), (May 1, 1989).

c. Calculated from the literature (IAEA 1985) with the NDS-107 <sup>252</sup>Cf source. If the NDS-87 <sup>252</sup>Cf source is used, the source strength is 32.7% of that of NDS-107, (May 1, 1989).

publication (IAEA 1985). These theoretical spectra were folded into 4-interval spectra and the results are shown in Table 5.3.1.

The  $^{238}\text{Pu}$ -Be neutron spectrum has a mean energy of 4 MeV and has no neutrons less than 150 keV (i.e., no slow and thermal neutrons). The fast neutron component is ~ 77% of the total fluence, and it contributes ~ 83% of the total dose equivalent. The dose equivalent rate of the  $^{238}\text{Pu}$ -Be source in the aluminum-walled room at RADCAL was  $0.241 \text{ mSv h}^{-1}$  at 1 m. The average conversion factor for medium neutrons ( $2.78 \times 10^{-10} \text{ Sv cm}^2$ ) was higher than the corresponding value ( $2.66 \times 10^{-10} \text{ Sv cm}^2$ ) used for the CPND.

The fast neutron component of  $^{252}\text{Cf}(\text{D}_2\text{O})$  is ~ 13% of the total fluence, and it contributes ~ 59% of the total dose equivalent. The slow neutron component is ~ 75% of the total fluence, but it contributes only ~ 15% of the dose equivalent. The mean energy is lowered from 2.1 MeV for  $^{252}\text{Cf}$  to 0.55 MeV for  $^{252}\text{Cf}(\text{D}_2\text{O})$  due to the presence of the moderation. The dose equivalent rates of the  $^{252}\text{Cf}(\text{D}_2\text{O})$  source in the neutron room at RADCAL were  $18.46 \text{ mSv h}^{-1}$  (NDS-107  $^{252}\text{Cf}$ ) or  $6.036 \text{ mSv h}^{-1}$  (NDS-87  $^{252}\text{Cf}$ ) at 0.75 m.

It should be noted that the above-mentioned reference spectra for the  $^{238}\text{Pu}$ -Be and the  $^{252}\text{Cf}(\text{D}_2\text{O})$  sources are based on the scatter-free spectra, i.e., unscattered spectra. The unscattered spectrum is useful to evaluate the spectrometric capability of the CPND. However, information on the scattered radiation contributions to the total dose equivalent of the sources at RADCAL should be assessed so that a more accurate estimate of the reference dose equivalent can be used for the CPND test. The assessment was made by using both measurement and calculation methods (Schwartz and Eisenhauer 1982).

A series of measurements was made for each source with the Eberline 9" remmeter at several distances. After correction for the calculated air scattering fraction, the 9" remmeter response (D) was plotted versus distance from the source (r) in a linear plot of  $Dr^2$  versus  $r^2$ . A least squares fit to data provided the intercept (9" remmeter response per unit distance to the unscattered source,  $D_0$ ) and the slope ( $D_0S$ , where S is the fractional room scattering at unit distance). Since the 9" remmeter can measure the dose equivalent roughly, the measured S values can be used to estimate the influence of the scattered radiation component on the dose equivalent.

The empirical equations (Schwartz and Eisenhauer 1982) were used to calculate the increase in the dose equivalent due to scattered radiation. Increase in response for both a 9" remmeter and a "dose equivalent meter" were calculated. Calculated results for the 9" remmeter were used to compared with the measured 9" remmeter results. The  $^{238}\text{Pu}$ -Be source was located in the aluminum room and, therefore, a single-surface reflection model was used for the calculation. Since the parameters required in the calculation for the  $^{238}\text{Pu}$ -Be source were not available in the literature, the parameters of the  $^{252}\text{Cf}$  source were used in the scattering calculation for the  $^{238}\text{Pu}$ -Be source. The  $^{252}\text{Cf}(\text{D}_2\text{O})$  and  $^{252}\text{Cf}(\text{D}_2\text{O}, \text{no Cd})$  sources were located in the neutron room and, therefore, an enclosed-room model was used for the calculation.

The two spectra of the  $^{252}\text{Cf}(\text{D}_2\text{O})$  and  $^{252}\text{Cf}(\text{D}_2\text{O}, \text{no Cd})$  sources are the same, except the latter has an additional thermal neutron component which is 11.5% of the total fluence. Using a fluence-to-dose equivalent conversion factor of  $0.107 \times 10^{-10}$  Sv  $\text{cm}^2$  for thermal neutrons, the dose equivalent rate of the  $^{252}\text{Cf}(\text{D}_2\text{O}, \text{no Cd})$  source was calculated to be 1.5% higher than that of the  $^{252}\text{Cf}(\text{D}_2\text{O})$  source. The scattering fraction of the  $^{252}\text{Cf}(\text{D}_2\text{O}, \text{no Cd})$  source at RADCAL also was estimated with both the

9" remmeter measurements and the calculations by using the parameters of the  $^{252}\text{Cf}(\text{D}_2\text{O})$  source.

The estimates of the scattered radiation component of the three neutron sources at RADCAL are summarized in Table 5.3.2. The 9" measurement results agreed with the calculated 9" results for the  $^{252}\text{Cf}(\text{D}_2\text{O})$  and the  $^{252}\text{Cf}(\text{D}_2\text{O}, \text{no Cd})$  sources, but not for the  $^{238}\text{Pu-Be}$  source. This could be due to the use of the parameters of the  $^{252}\text{Cf}$  source for the calculation of the  $^{238}\text{Pu-Be}$  source. Calculation of the scattered fraction of the dose equivalent for every source was smaller than the 9" remmeter results, except for  $^{238}\text{Pu-Be}$ . These estimates showed that a scattered correction had to be made to obtain an accurate reference dose equivalent, especially for the  $^{252}\text{Cf}(\text{D}_2\text{O})$  source at 1.5 m.

Because the results from both the measurements and calculations for the 9" remmeter agreed with each other, the calculation method should be reliable. Also the 9" remmeter can only measure the dose equivalent roughly and the "dose equivalent meter" can measure the dose equivalent exactly. Therefore, the calculated scattered fraction of the "dose equivalent meter" response was used to estimate the increase of the dose equivalent. The total dose equivalent rate and the unscattered dose equivalent rate for each source are shown in Table 5.3.2.

ORNL-DWG 89M-9676

Table 5.3.2. Estimates of scattered neutron components for the neutron sources at RADCAL for the PDIS 14.

Method	$^{252}\text{Cf}(\text{D}_2\text{O})$			$^{252}\text{Cf}(\text{D}_2\text{O}, \text{no Cd})$	$^{238}\text{Pu-Be}$
	0.75 m	1 m	1.5 m	0.75 m	1 m
9" Measurement <sup>a</sup>	0.086 (0.069)	0.145 (0.122)	0.310 (0.275)	0.090 (0.073)	0.05 (0.04)
9" Calculation <sup>b</sup>	0.09 (0.072)	0.154 (0.128)	0.333 (0.288)	0.09 <sup>c</sup> (0.072)	0.09 <sup>d</sup> (0.08)
H Calculation <sup>b</sup>	0.05 (0.04)	0.09 (0.073)	0.19 (0.164)	0.05 <sup>c</sup> (0.04)	0.05 <sup>d</sup> (0.04)
Unscattered H (mSv h <sup>-1</sup> ) 5/1/1989	18.46	10.38	4.61	18.75	0.241
Total H <sup>e</sup> (mSv h <sup>-1</sup> )	19.38	11.31	5.49	19.69	0.253

1. Value in parentheses is the room scattering fraction.

a. 9" sphere responses as a function of distance and a plot of  $\text{Dr}^2$  vs.  $r^2$ .

b. NIST empirical formula and an equivalent radius = 5.5 m.

c. Used parameters of  $^{252}\text{Cf}(\text{D}_2\text{O})$ .

d. Used parameters of bare  $^{252}\text{Cf}$ .

e. Based on scattering estimate from H calculation.

## CHAPTER VI

### PERFORMANCE EVALUATION OF THE CPND

The performance (mainly the capabilities of spectrometry and dose equivalent measurement) of the CPND was evaluated by *in-situ* field tests, calibration laboratory radioisotopic source tests, and by participating the 14th PDIS. Comparison of the dose equivalent measured in these tests with the CPND, a Harshaw albedo TLD, a Panasonic TLD, and a 9" remmeter was made to show the superiority of the CPND.

#### 6.1 TRU FIELD TESTS

The first type of test was to evaluate the CPND performance in practical radiation fields in the TRU facility.

##### CPND Field Measurements

One major difference between the TRU neutron fields and the RADCAL radioisotopic source fields is the directionality of the fields. Due to more scattering in the smaller rooms and the more distributed sources at TRU, the fields at TRU are more multidirectional than those at RADCAL. Therefore, scattered radiation contributes a larger proportion of the total fluence (or dose equivalent) in the fields at TRU.

Since the BMS has isotropic response, it can measure the summation of neutrons from all directions. For this reason, comparison of the BMS and the CPND required dosimeters to be mounted on both sides of the phantom during the TRU field measurements. After characterization of the radiation fields with the BMS, four CPND's were put on the phantom in the same position as the BMS for every field. Two CPND's on the front side of the phantom faced the source and received more

exposure than the two CPND's on the back side. Four Panasonic albedo TLD's, model UD-809AS type, also were exposed in every field except that in the waste transfer area. One CPND was worn by an operator who spent most of his time in the control room. The operator's exposure was used solely for comparison with the results obtained in the control room.

During the CPND field measurements, the BD's were counted and recompressed every three to four days so that the number of bubbles could be counted easily. The measurement time for each field ranged from 119 h to 549 h. The temperature during the measurements was within 19 °C - 23 °C, except the control room temperature was higher (23 °C - 26 °C). Field survey with the Eberline 9" sphere, 3" sphere, and bare  $^{10}\text{BF}_3$  detectors also were made during the CPND field measurements. The photon intensity was measured with a calibrated GM counter. The TRU field measurements are summarized in Table 6.1.1. Again, the bubble detector responses have been normalized to unit sensitivity ( $0.1 \text{ bu } \mu\text{Sv}^{-1}$ , or  $1 \text{ bu mrem}^{-1}$ ).

#### Spectrometric Performance of the CPND

The 4-interval spectra for the TRU fields evaluated with the CPND measurements are shown in Table 6.1.2. The comparisons between the two 4-interval spectra, as well as the dose equivalents, measured with the CPND's (front + back) and the BMS (Table 5.2.1) for all fields are presented in Figures 6.1.1 through 6.1.5. Generally speaking, the spectra evaluated with the CPND agreed well with those from the BMS measurements. The CPND successfully measured both a low energy spectrum (Fig. 6.1.2) and high energy spectra (Fig. 6.1.4 and Fig. 6.1.5). As mentioned in Section 4.1, a major error in the spectrum estimate using the CPND algorithm is the use of average sensitivities which were derived based on the

ORNL WSM-10127

Table 6.1.1. Data from the CPND measurements in the TRU neutron fields.

Detector or Quantity	Glove Box	Cave Area A	Control Room	Control <sup>b</sup> Room	CR <sup>a</sup> Operator	Waste Transfer	Analytical Laboratory
<b>CPND. Front<sup>c</sup></b>							
Albedo TLD (mR)	2837.3	1404.8	171.7	48.2	170.8	1180.6	1127.5
EI of TLD	1.69	2.023	1.52	1.70	1.56	1.42	1.352
BD-100R (bu)	424	114	51.0	10.6	63.3	389	402
BDS-1500 (bu)	320	63	24.2	5.9	40.2	177	270
<b>CPND. Back<sup>d</sup></b>							
Albedo TLD (mR)	1439.9	459.9	97.9	30.0	---	477.2	530.2
EI of TLD	1.65	1.728	0.64	1.53	---	1.53	1.353
BD-100R (bu)	264	49.8	14.3	4.5	---	99	101
BDS-1500 (bu)	133	10.7	9.1	2.1	---	38	44
Time (h)	271.5	182.3	362.2	119.3	549.1	227.9	297.3
Temperature (°C)	19-21	19-21	23-26	24	20-26	21-22	21-23
<b>9", 3" &amp; Bare<sup>10</sup>BF<sub>3</sub><sup>e</sup></b>							
9" (cpm)	162	65.7	6.7	6.0	---	96.5	98.3
9"/3"	0.38	0.29	0.31	0.32	---	0.42	0.63
9"/Bare	0.53	0.25	0.57	0.51	---	1.46	2.95
Photon Intensity, n/γ	0.64	2.80	0.75	---	0.75	1.90	2.30
(μC kg <sup>-1</sup> h <sup>-1</sup> )	1.16	0.086	0.026	---	0.026	0.258	0.181

a. Second set of measurements.

b. The operator spent most of the time in the control room (CR) and wore one CPND on his chest.

c. Two CPND's on the front side of phantom facing the source.

d. Two CPND's on the back side of phantom receiving less exposure than the front.

e. Eberline Remmeter.

ORNL WSM-10128

Table 6.1.2. Spectrum results obtained with the CPND at TRU.

Quantity	Glove Box	Cave Area A	Control Room	Control <sup>a</sup> Room	CR Operator	Waste Transfer	Analytical Laboratory
Flux (cm <sup>-2</sup> s <sup>-1</sup> ) <sup>b</sup>	39.92	20.87	2.165	1.703	1.51	25.36	20.24
Fast	6.55	1.92	0.370	0.275	0.41	4.32	5.05
Medium	3.37	1.91	0.478	0.269	0.31	5.91	3.41
Slow	19.11	5.14	0.945	0.779	0.53	11.85	9.76
Thermal	10.88	11.90	0.372	0.360	0.26	3.28	2.02
H (μSv h <sup>-1</sup> ) <sup>b</sup>	16.30	5.92	1.165	0.802	0.98	14.00	12.29
Fast	9.55	2.80	0.541	0.401	0.59	6.29	7.36
Medium	3.22	1.82	0.456	0.257	0.30	5.66	3.27
Slow	3.10	0.83	0.153	0.130	0.08	1.92	1.58
Thermal	0.43	0.47	0.015	0.014	0.01	0.13	0.08
Flux (cm <sup>-2</sup> s <sup>-1</sup> ) <sup>c</sup>	20.80	8.64	1.049	0.956	---	8.66	8.28
Fast	2.72	0.33	0.139	0.098		0.93	0.82
Medium	3.16	1.23	0.106	0.129		1.64	1.21
Slow	9.71	4.31	0.543	0.481		4.62	5.30
Thermal	5.21	2.77	0.261	0.248		1.67	0.95
H (μSv h <sup>-1</sup> ) <sup>c</sup>	8.78	2.46	0.403	0.354	---	3.74	3.26
Fast	3.97	0.48	0.203	0.143		1.35	1.20
Medium	3.03	1.18	0.102	0.123		1.57	1.16
Slow	1.57	0.70	0.088	0.078		0.75	0.86
Thermal	0.21	0.10	0.010	0.010		0.07	0.04

a. Second set of measurements.

b. Result of the CPND's on the front of phantom.

c. Result of the CPND's on the back of phantom.

ORNL-DWG 89M-9643

$H(\mu\text{Sv h}^{-1})$	TOTAL	THERMAL	SLOW	MEDIUM	FAST
BMS	28.8	0.91	1.89	13.0	13.0
CPND	25.1	0.64	4.67	6.3	13.5

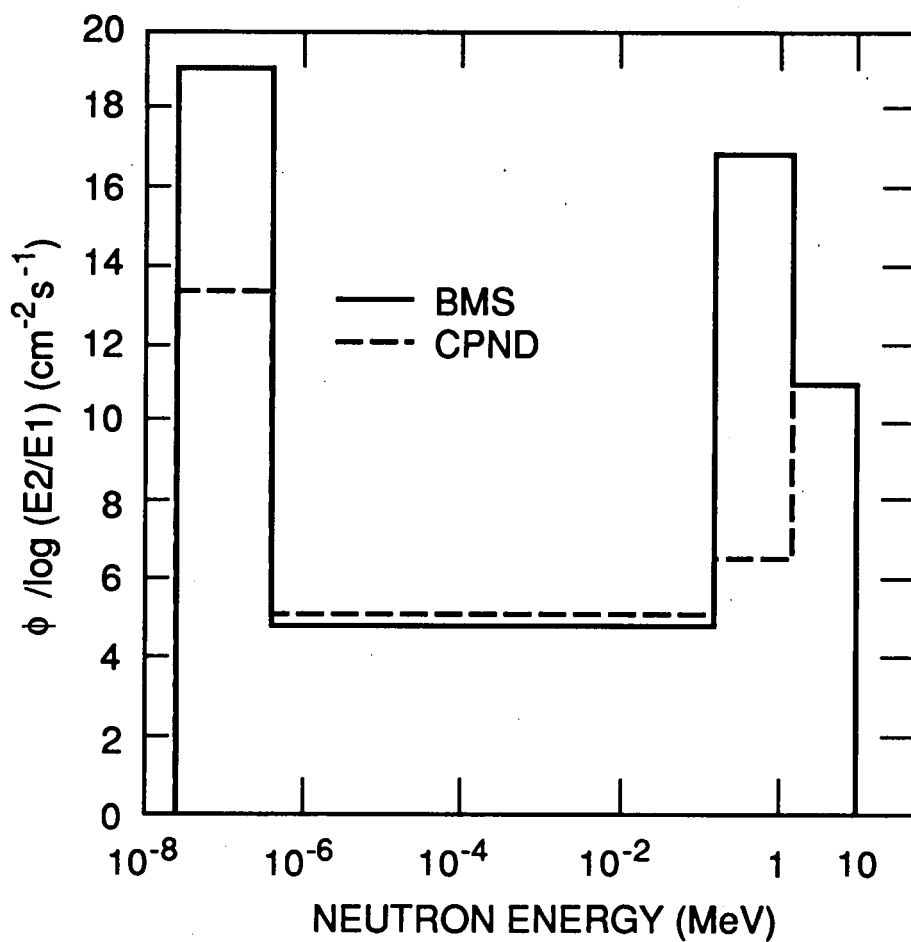


Fig. 6.1.1. Comparison of the spectrum and dose equivalent evaluated with the CPND and the multisphere spectrometer at the glove box, TRU.

ORNL-DWG 89M-9644

H( $\mu\text{Sv h}^{-1}$ )	TOTAL	THERMAL	SLOW	MEDIUM	FAST
BMS	9.3	0.65	0.92	4.20	3.53
CPND	8.4	0.57	1.53	3.00	3.28

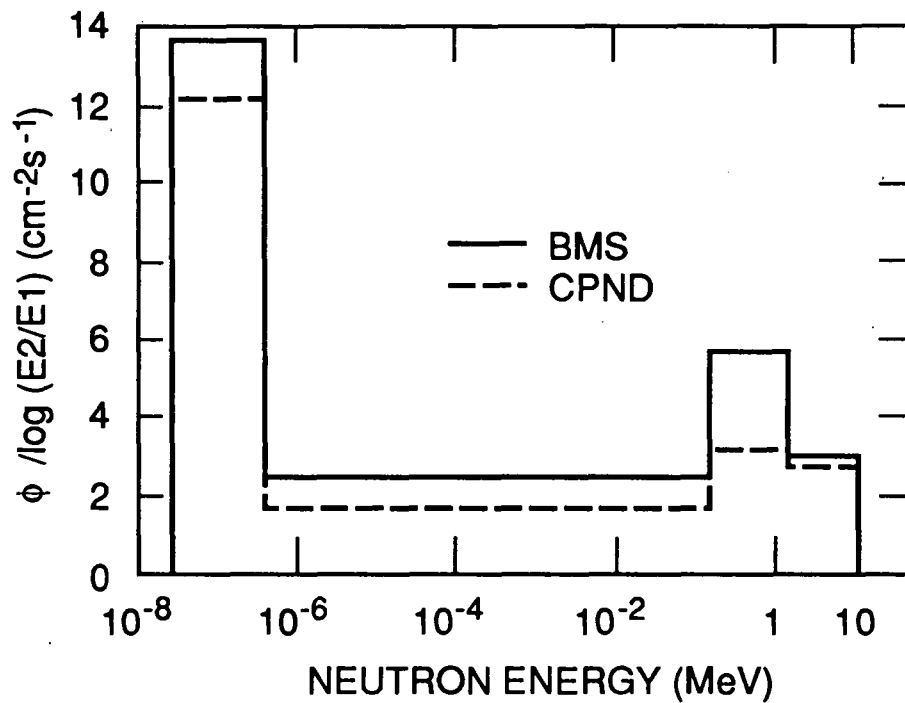


Fig. 6.1.2. Comparison of the spectrum and dose equivalent evaluated with the CPND and the multisphere spectrometer in the cave area A, TRU.

ORNL-DWG 89M-9641

H(mSv h <sup>-1</sup> )	TOTAL	THERMAL	SLOW	MEDIUM	FAST
BMS	0.76	0.030	0.093	0.350	0.287
CPND	1.156	0.024	0.208	0.380	0.544

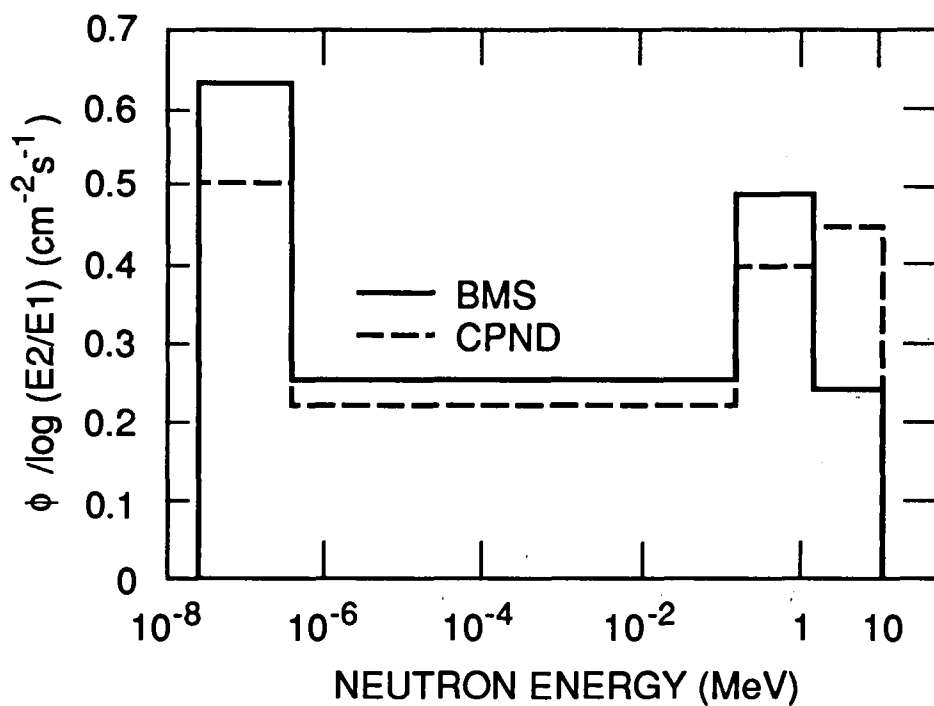


Fig. 6.1.3. Comparison of the spectrum and dose equivalent evaluated with the CPND and the multisphere spectrometer in the control room, TRU.

ORNL-DWG 89M-9642

H( $\mu\text{Sv h}^{-1}$ )	TOTAL	THERMAL	SLOW	MEDIUM	FAST
BMS	19.0	0.19	1.01	8.80	9.00
CPND	17.7	0.20	2.67	7.23	7.64

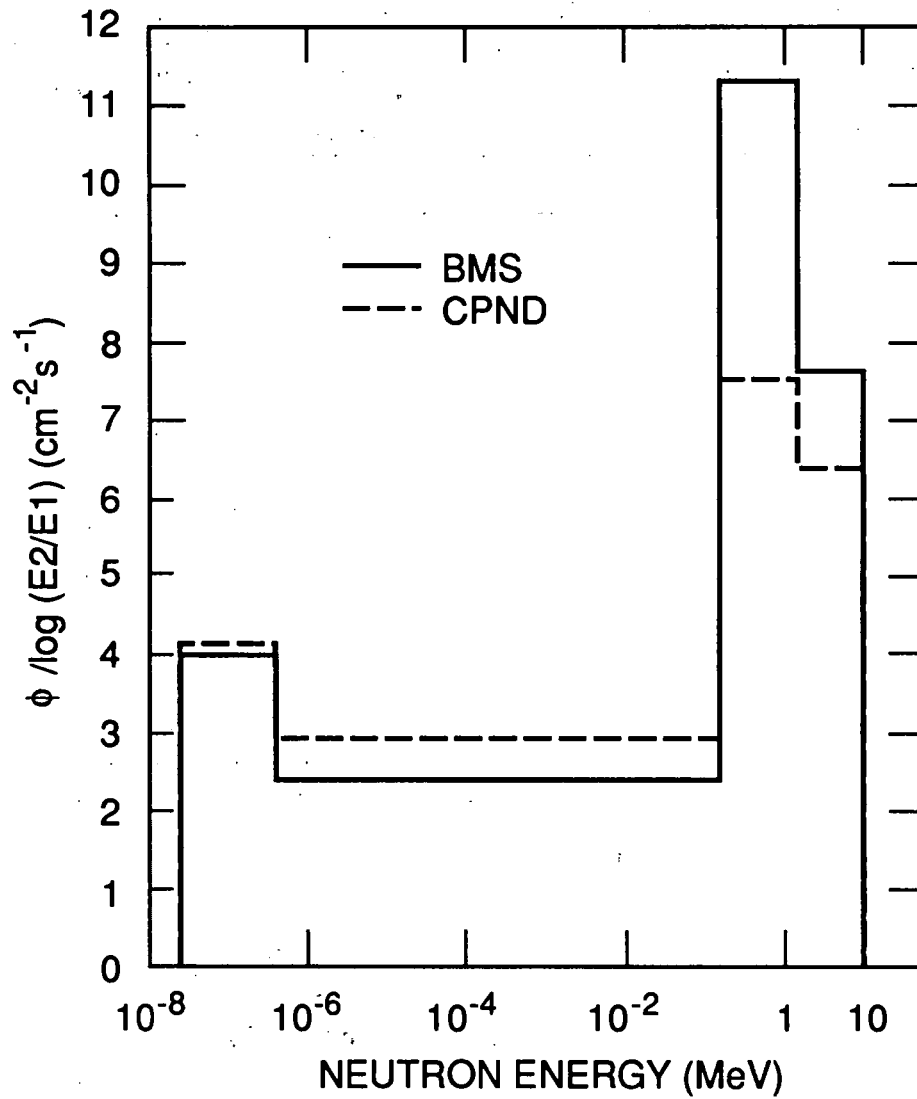


Fig. 6.1.4. Comparison of the spectrum and dose equivalent evaluated with the CPND and the multisphere spectrometer in the waste transfer area, TRU.

ORNL-DWG 89M-9639

$H(\mu\text{Sv h}^{-1})$	TOTAL	THERMAL	SLOW	MEDIUM	FAST
BMS	15.9	0.07	0.72	7.42	7.69
CPND	15.6	0.12	2.44	4.43	8.56

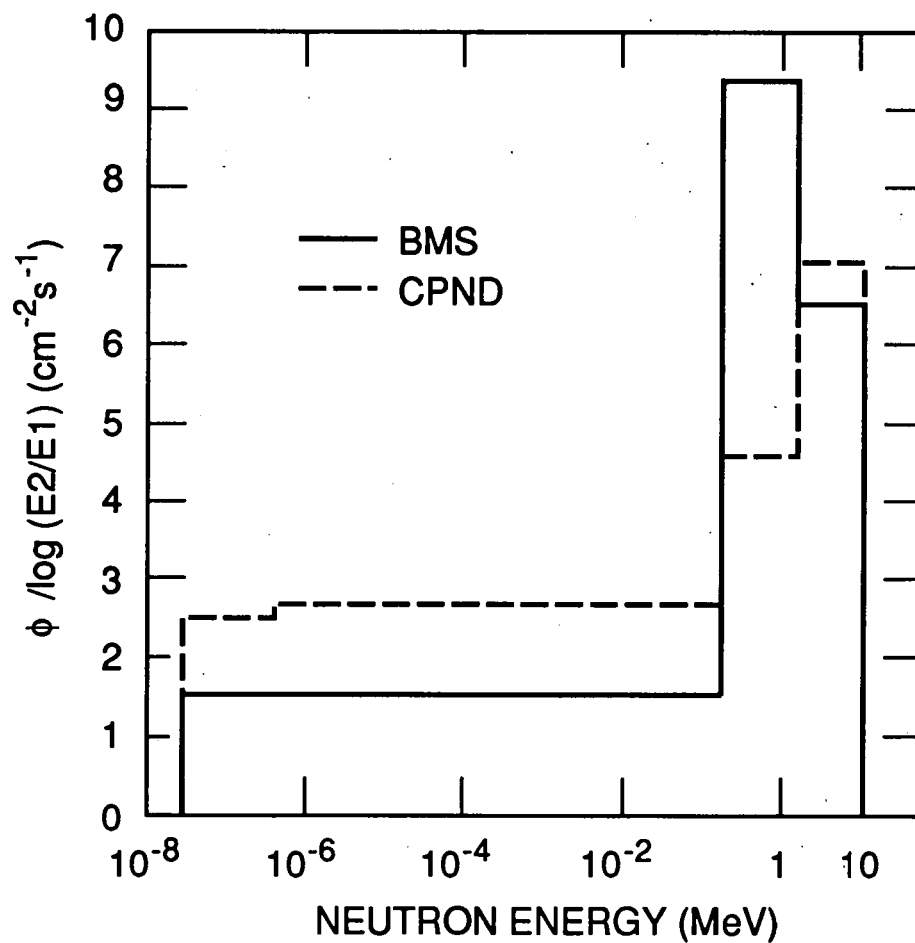


Fig. 6.1.5. Comparison of the spectrum and dose equivalent evaluated with the CPND and the multisphere spectrometer in the analytical laboratory, TRU.

assumption of constant fluence per unit energy within each neutron interval for the unknown spectrum. The fact that the shape of the field spectrum differs from the assumed shape introduces errors in the spectrum estimate.

From the spectrum comparison, it is seen that the estimates for the fast and the thermal neutron components were more accurate than those for the medium and the slow neutron components. There are three reasons for this. First, as mentioned in Section 5.1, the BMS has less measurement accuracy in the neutron interval between 20 eV - 300 keV and, therefore, the reference spectrum in this interval (slow and medium neutrons) is subject to higher error. Second, using the spectral stripping algorithm for the CPND, the estimates of slow and medium neutrons will have higher errors than those of fast and thermal neutrons. The third reason is due to the multidirectional characteristic of the field and the fact that the BMS has isotropic response, but the albedo TLD response is angular dependent. Because of the bell-shaped angular dependence of the albedo TLD component, the CPND will measure low compared to the BMS under large-angle (e.g., 90°) irradiations. It can be expected that the more isotropic the field, the lower the CPND would measure relative to the BMS results. This can be supported by the following results. The ratio of the front-side dose equivalent to the total dose equivalent (front+back) from the CPND measurements was used as an index of the field directionality. The more isotropic the field, the lower the directionality index. A laboratory source with little scattering would have a directionality index close to 1. From Table 6.1.2, the directionality index was found to be 0.65 for the glove box, 0.71 for the cave area A, 0.79 for the waste transfer area, and 0.79 for the analytical laboratory. From Figures 6.1.1 - 6.1.5, the ratio of the dose equivalent rates measured between the CPND and the BMS was 0.87 for the glove box, 0.90 for the cave area A, 0.93 for the waste transfer area, and 0.98 for the

analytical laboratory. A comparison of the directionality index with the dose equivalent ratio for the TRU fields confirmed that the lower the directionality index, the lower the dose equivalent ratio. In large-angle irradiations, most neutrons are low energy scattered neutrons. Because of this, the estimates of medium and slow neutrons will have higher errors than those of fast and thermal neutrons in multidirectional fields.

Compared with the BMS results, the CPND underestimated the dose equivalent by less than 13% for all fields at TRU, except the control room. This underestimation could possibly be due to field characteristics, e.g., multi-directionality and non-uniform spatial dose intensity.

The first measurement in the control room with the CPND overestimated the dose equivalent by 107%. The second CPND measurement in the control room overestimated the dose equivalent by about 53%. Two reasons were believed to be the cause for these overestimates. First, after the BMS field characterization, the dose equivalent rate in the control room increased due to a source inventory change in the adjacent chemical laboratory. This could be supported by the evidence of an increase of the 9" remmeter response by ~ 40% from the field survey data (compare the 9" remmeter response of 4.3 cpm in Appendix 7 and 6 cpm in Table 6.1.1). Second, the temperature in the control room was ~ 4 °C higher than in other fields and, therefore, it could increase the responses of the BD's by up to 20%.

#### Dose Equivalent Measurement Comparison

One point is worthy of being mentioned before the discussion of the dose equivalent measurement capability of the CPND. Since high energy neutrons contribute most of the total dose equivalent, the response of the BD-100R, when converted to dose equivalent by the nominal sensitivity, can be used to provide a rough

estimate of the total dose equivalent. The total dose equivalent estimated by the sum of the responses of the BD-100R (front + back) had an error less than 13% for all fields except the control room (see Table 6.1.1). This capability could be a bonus in terms of using the CPND, since it gives the worker a quick estimate of the dose equivalent without requiring the evaluation of the CPND algorithm by a health physicist.

A comparison of the dose equivalent measured with five different detector systems for the TRU fields is presented in Table 6.1.3. The BMS results were used as a reference against which the performance of other detectors were evaluated. The Eberline 9" remmeter was included to show the performance of a routine survey instrument. A calibration factor of 0.17 ( $1\sigma=15\%$ )  $\mu\text{Sv h}^{-1} \text{cpm}^{-1}$  was used to convert the response of the 9" remmeter (cpm) to the dose equivalent. This value was derived based on a comparison between the 9" remmeter response and the dose equivalent rate measured with the BMS during the TRU field characterization. The 9" remmeter also showed an increase of the dose equivalent in the control room during the CPND measurement (34% in the second measurement). For the remaining four fields, the differences in the dose equivalents measured between the 9" remmeter and the BMS were < 20%.

There were three types of dosimeters in the comparison: the CPND, a Harshaw albedo TLD, and a Panasonic albedo TLD. Except for the measurements in the control room, the CPND underestimated the dose equivalents measured with the BMS by less than 13%.

The calibration factor of the Harshaw albedo TLD for each radiation field was derived by using equation 3.7.1 and the 9"/3" value in Table 6.1.1. The same calibration factor was applied to the TLD's on both sides of the phantom. Table 6.1.3 shows that the differences in the dose equivalents measured between the Harshaw

ORNL WSM-10129

Table 6.1.3. Comparison of the dose equivalent rates measured with different detector systems in the TRU fields ( $\mu\text{Sv h}^{-1}$ ).

Method	Glove Box	Cave Area A	Control Room	Control <sup>a</sup> Room	CR Operator	Waste Transfer	Analytical Laboratory
Multisphere	28.8	9.3	0.76	0.76	0.76	19.0	15.9
9" Remmeter	27.5	11.2	1.14	1.02	---	16.4	16.7
Difference <sup>b</sup>	-5%	+20%	+50%	+34%	---	-14%	+5%
CPND	25.1	8.38	1.57	1.16	---	17.7	15.6
Difference	-13%	-10%	+107%	+53%	---	-7%	-2%
Front	16.30	5.92	1.165	0.802	0.98	14.00	12.29
Back	8.78	2.46	0.403	0.354	---	3.74	3.26
Harshaw TLD	24.1	11.2	0.87	0.81	---	12.7	16.1
Difference	-16%	+20%	+14%	+7%	---	-33%	+1%
Calibration Factor <sup>c</sup>	1.534	1.090	1.186	1.235	1.186	1.740	2.884
Front	16.00	8.40	0.54	0.499	0.37	9.02	10.94
Back	8.14	2.75	0.33	0.310	---	3.64	5.14
Panasonic TLD	38.5	15.0	1.0	0.50	---	---	4.1
Difference	+34%	+61%	+32%	-34%	---	---	-74%
Front	31.6	11.36	0.65	0.29	---	---	2.81
Back	6.9	3.64	0.35	0.21	---	---	1.26

a. Second measurement.

b. Relative to the multisphere results.

c. From Fig. 3.7.3. Units =  $\mu\text{Sv mR}^{-1}$ .

albedo TLD and the BMS were < 33%. The results obtained in the control room seemed good (7% difference in the second measurement). However, this "good" result was probably incorrect due to the fact that the dose equivalent in the control room should be 40% higher as mentioned in last section.

Disadvantages of using the  $9''/3''$  calibration method for the Harshaw albedo TLD can be seen from Table 6.1.3. The calibration factors (units:  $\mu\text{Sv mR}^{-1}$ ) for the TRU fields varied from 1.09 to 2.88. Therefore, if a mean calibration factor has to be used for the TLD's used in the TRU fields for personnel monitoring, it may introduce an error as high as 70%. Also, the uncertainty associated with the  $9''/3''$  measurement value is generally around 5-15%, depending on the field intensity. The  $9''/3''$  value in a ultra-low intensity field may have an error as high as 50% (e.g., the response of the  $9''$  sphere in the control room was only 6 cpm). Such errors in the use of  $9''/3''$  ratios would certainly introduce a higher error in the calibration factor.

The model UD-809AS Panasonic TLD is currently being used at ORNL. The Panasonic TLD has four elements of  $\text{Li}_2\text{B}_4\text{O}_7$ . Element 1 is enriched in  ${}^7\text{Li}$  and  ${}^{11}\text{B}$  and is insensitive to neutrons. Elements 2, 3, and 4 are enriched in  ${}^6\text{Li}$  and  ${}^{10}\text{B}$  and are very sensitive to thermal neutrons. The four elements have different filters in front and behind the elements. Elements 1 and 3 are shielded by cadmium both in front and back. Element 2 is shielded by tin in front and by cadmium in back. Element 4 is shielded by cadmium in front and by tin in back. The function of element 4 of the Panasonic TLD is similar to that of the Cd-covered TLD-600 element of the Harshaw TLD. With the different filtrations, each element responds to a different part of the incident neutron spectrum.

After the response of element 1 is used for photon signal subtraction, the neutron responses of elements 2, 3, and 4 can be used to derive three neutron dose

equivalent data (H2, H3, and H4 for elements 2, 3, and 4, respectively) using a set of three corresponding calibration factors. ORNL has a data bank of 17 sets of calibration factors for 17 different spectra for the three elements (2, 3, and 4). Two algorithms are used to determine the correct dose equivalent using this data bank. These two algorithms are based on the same principle; the three elements should give same dose equivalent estimate with the set of calibration factors from the correct spectrum.

The first algorithm is applied when the source of exposure is known and the source spectrum is in the data bank. The corresponding set of calibration factors for the source is applied to the responses of the three elements. The mean dose equivalent obtained from the three elements is used. The second algorithm is applied when the source is unknown or the source is not in the data bank. The values of H2, H3, and H4 for all 17 spectra are calculated from the responses of the three elements. The spectrum which gives the smallest standard deviation of the H2, H3, and H4 is determined, and the mean dose equivalent is used. If the standard deviation values are close for some spectra, the spectrum for which the H3/H4 ratio is closest to unity is used. The dose equivalents in the TRU fields obtained with the Panasonic TLD's were determined by use of the second algorithm. The dose equivalent differences measured between the Panasonic TLD and the BMS ranged from 32% - 74%.

Considering the difficulties in the field measurements, the performance results of the CPND in the TRU fields showed that the CPND can measure successfully not only the correct spectral shape, but also the correct dose equivalent. The performance of the CPND was comparable to the 9" remmeter. The CPND had better performance than the Harshaw TLD and the Panasonic TLD. These results were confirmed by the RADCAL radioisotopic source tests (see below). The field tests also proved that the CPND could measure very low dose equivalent rates for long exposure times. The

CPND, therefore, can be used in real and practical radiation fields which exist in typical work environments.

## 6.2 RADCAL RADIOISOTOPIC SOURCE TESTS

The CPND performance was evaluated at the RADCAL facility with radioisotopic sources. Single-source and multi-source exposures were made to evaluate further the spectrometric capability of the CPND. Finally, the CPND was exposed to six radiation fields in the fourteenth PDIS as an independent blind test.

### Single-Source and Multi-Source Exposure Tests

The data for the CPND measurements using the radioisotopic neutron sources at RADCAL and the associated 9"/3" measurement results are shown in Table 6.2.1. Three single-source exposures and two multi-source exposures were conducted. At least three CPND's were irradiated on the front side of the phantom for each exposure.

The measurement results of the Eberline detectors (9" sphere, 3" sphere, and bare  $^{10}\text{BF}_3$  detector) indicated that the  $^{252}\text{Cf}(\text{PE})$  source has a large component of thermal neutrons (9"/bare = 0.30), and the  $^{238}\text{Pu}\text{-Be}$  source has a large fast neutron component (9"/3" = 3.06) and a small thermal neutron component (9"/bare = 27.19). The 9"/3" measurement is not applicable in the situations of multi-source exposure.

Comparison of the spectrum and dose equivalent evaluated with the CPND and the reference values for the radioisotopic source exposures at RADCAL are shown in Figures 6.2.1 - 6.2.5. The reference spectral values are from Table 5.3.1. Remember these reference spectra represent the unscattered radiation component only. The  $^{252}\text{Cf}(\text{PE})$  source is an exception to this since the reference spectrum was measured with the BMS and, therefore, the scattered component is included.

ORNL WSM-10130

Table 6.2.1. Data from the CPND measurements for the neutron sources at RADCAL.

Response	$^{252}\text{Cf}$ (PE) (2 m, 90 min)	$^{238}\text{Pu}$ -Be (1 m, 158 min)	$^{252}\text{Cf}$ ( $\text{D}_2\text{O}$ ) <sup>a</sup> (0.75 m, 8 min)	Mixture <sup>b</sup>	Mixture <sup>c</sup>
<b>CPND</b>					
Albedo TLD (mR)	544	44.6	2256.2	485.3	965.9
EI of TLD	1.97	1.35	1.24	1.34	1.437
BD-100R (bu)	91.1	72.2	216	63.9	520.5
BDS-1500 (bu)	50.7	74.2	191	55.5	496.4
<b>9", 3", &amp; Bare <math>^{10}\text{BF}_3</math></b>					
9" (cpm)	3110	1142	13717		
9"/3"	0.54	3.06	0.26	Unknown	Unknown
9"/Bare	0.30	27.19	0.94		

a. PDIS 14 run no. 5.

b.  $^{238}\text{Pu}$ -Be + NDS-87  $^{252}\text{Cf}$  ( $\text{D}_2\text{O}$ ).c.  $^{252}\text{Cf}$ (PE) + NDS-87  $^{252}\text{Cf}$  ( $\text{D}_2\text{O}$ ) +  $^{238}\text{Pu}$ -Be.

ORNL-DWG 89M-9637

DISTANCE	H(mSv h <sup>-1</sup> )	TOTAL	THERMAL	SLOW	MEDIUM	FAST
1 m	BMS	1.875	0.068	0.051	0.628	1.128
	CPND	2.098	0.059	0.092	0.355	1.592
2 m	BMS	0.576	0.029	0.022	0.202	0.323
	CPND	0.508	0.021	0.037	0.176	0.274

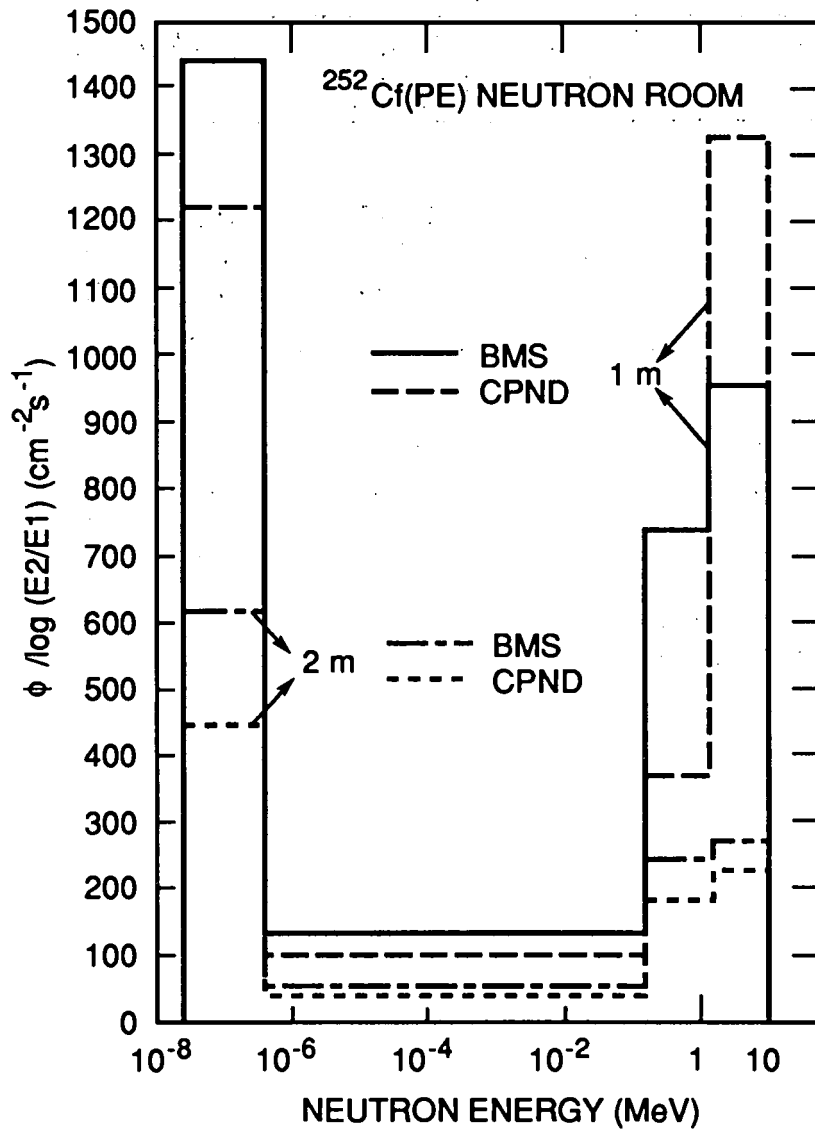


Fig. 6.2.1. Comparison of the spectrum and dose equivalent evaluated with the CPND and the multisphere spectrometer for the <sup>252</sup>Cf(PE) source at RADCAL.

ORNL-DWG 89M-9640

H(mSv h <sup>-1</sup> )	TOTAL	THERMAL	SLOW	MEDIUM	FAST
REFERENCE	0.241	0	0	0.041	0.200
CPND	0.266	0.014	0	0.025	0.227

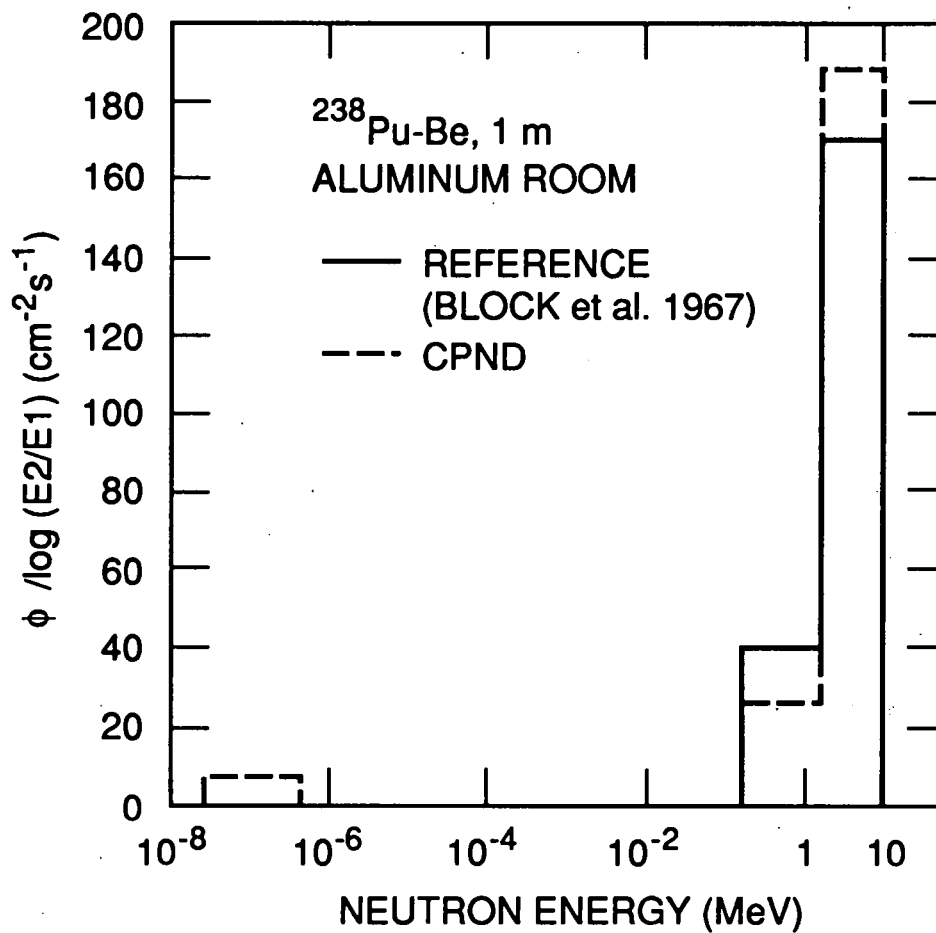


Fig. 6.2.2. Comparison of the spectrum and dose equivalent evaluated with the CPND and the reference value for the <sup>238</sup>Pu-Be source at RADCAL.

ORNL-DWG 89M-9638

H(mSv h <sup>-1</sup> )	TOTAL	THERMAL	SLOW	MEDIUM	FAST
REFERENCE	18.46	0	2.74	4.83	10.89
CPND	24.68	0.23	10.38	2.47	11.60

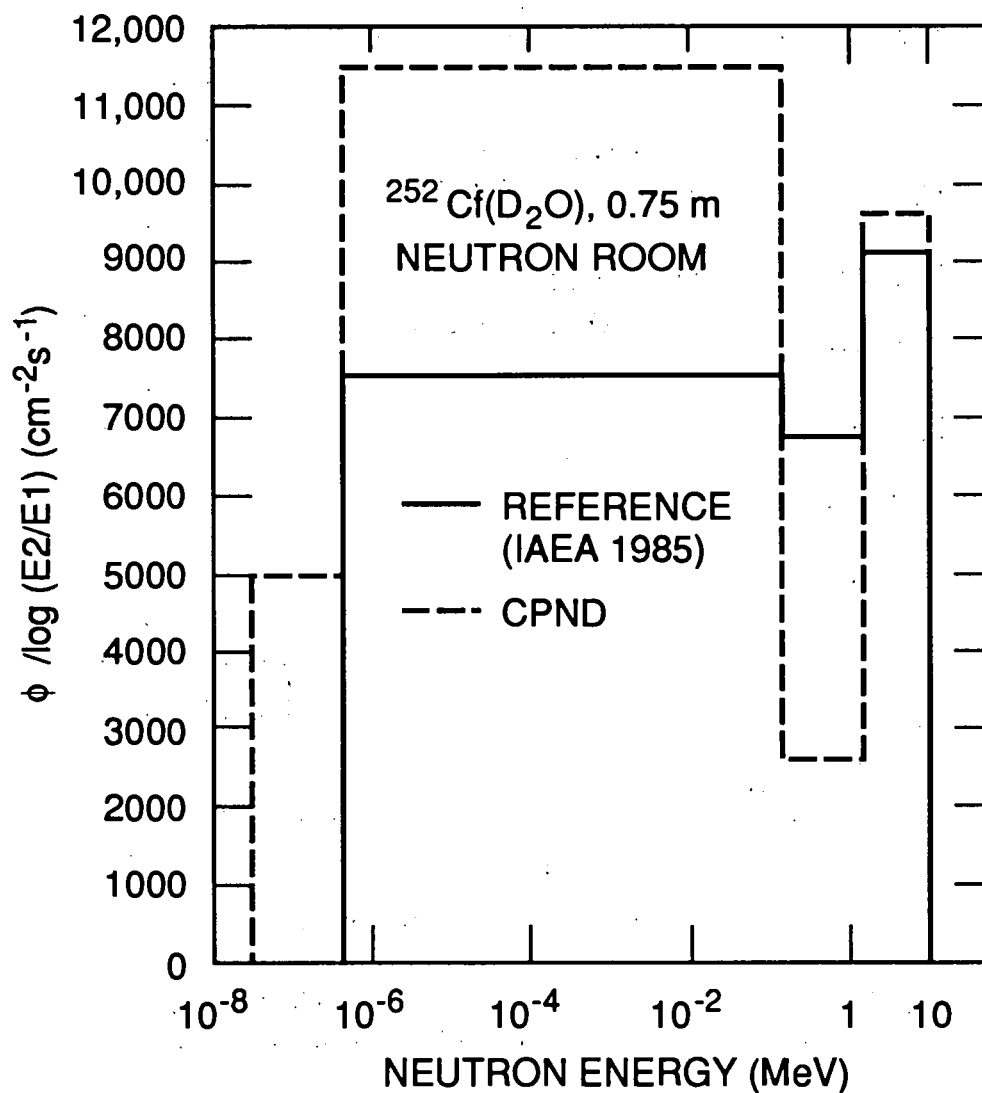


Fig. 6.2.3. Comparison of the spectrum and dose equivalent evaluated with the CPND and the reference value for the <sup>252</sup>Cf(D<sub>2</sub>O) source at RADCAL.

ORNL-DWG 89M-9629

$H(\text{mSv h}^{-1})$	TOTAL	THERMAL	SLOW	MEDIUM	FAST
REFERENCE	0.454	0	0.038	0.100	0.316
CPND	0.547	0.007	0.172	0.800	0.300

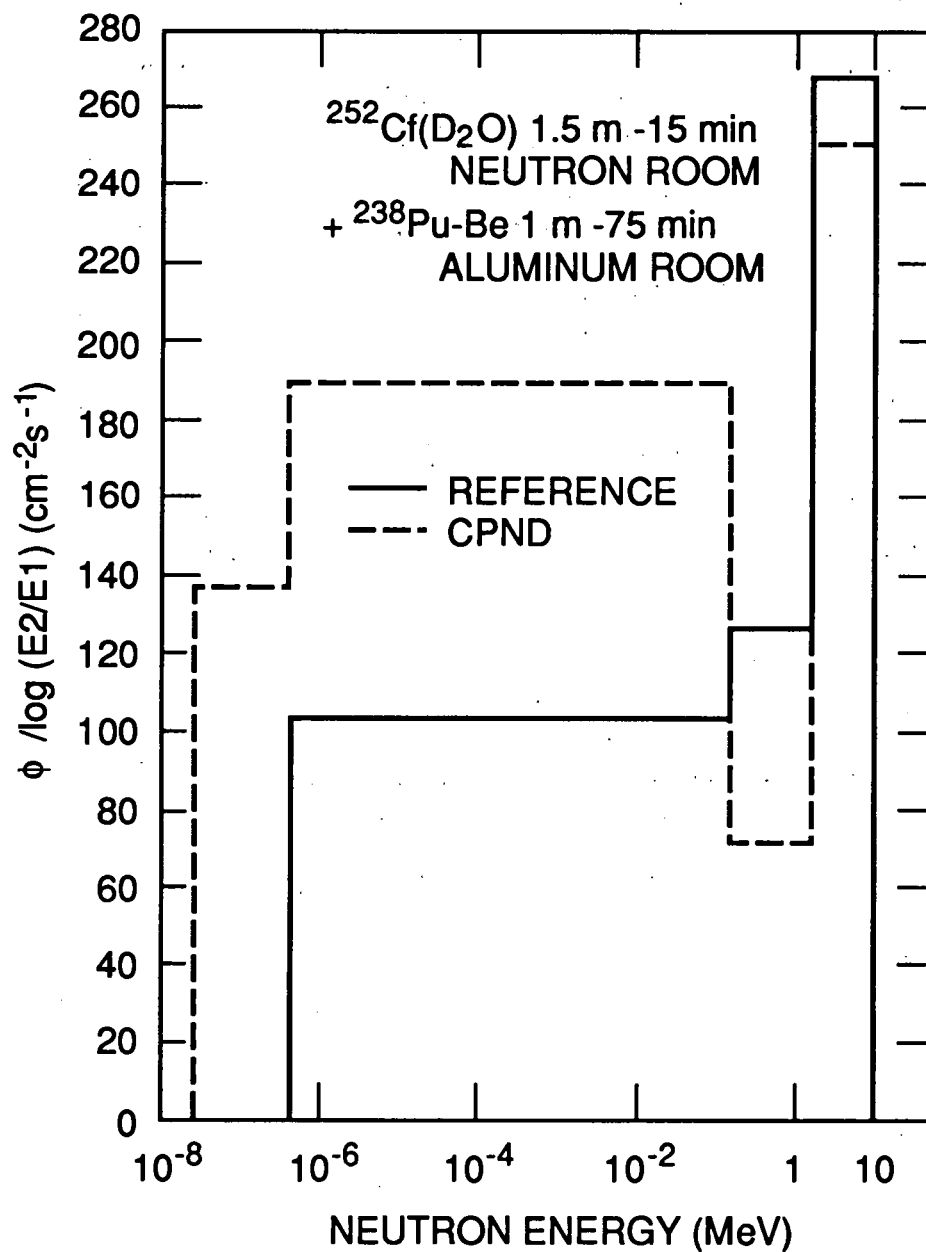


Fig. 6.2.4. Comparison of the spectrum and dose equivalent evaluated with the CPND and the reference values for a mixture of two sources at RADCAL.

ORNL-DWG 89M-9630

$H(\text{mSv h}^{-1})$	TOTAL	THERMAL	SLOW	MEDIUM	FAST
REFERENCE	0.274	0.0013	0.0043	0.0534	0.2152
CPND	0.294	0.0015	0.0178	0.0379	0.2365

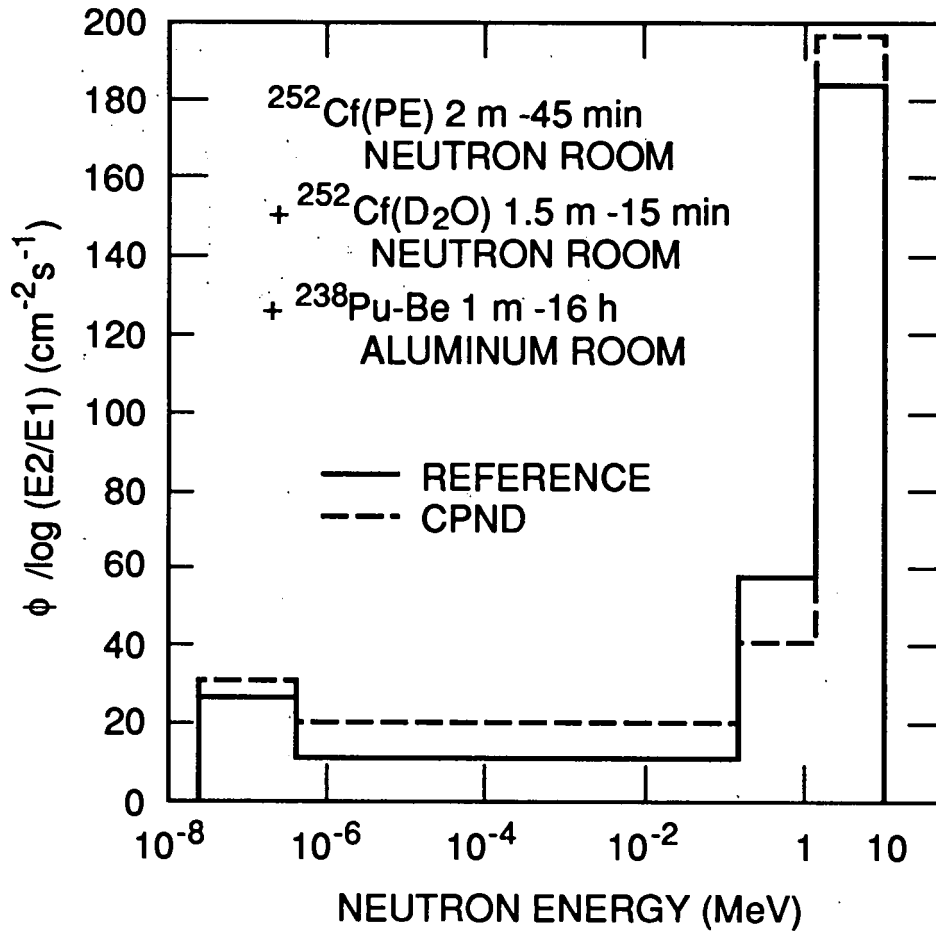


Fig. 6.2.5. Comparison of the spectrum and dose equivalent evaluated with the CPND and the reference values for a mixture of three sources at RADCAL.

The U-shape spectrum from the  $^{252}\text{Cf}(\text{PE})$  source which was measured accurately with the CPND is shown in Fig. 6.2.1. The dose equivalent estimated with the CPND was different by 12% at 1 m and -12% at 2 m from that obtained with the BMS. The difference of the CPND measurement at 2 m was partly due to the large scattered component at 2 m in the neutron room at RADCAL. Because the CPND on the front side of the phantom would respond low to the scattered neutrons from the back side of the phantom, the CPND measured low at 2 m compared with the BMS.

The energetic neutron spectrum from the  $^{238}\text{Pu}\text{-Be}$  source in the low-scattering aluminum-walled room which was measured accurately with the CPND is shown in Fig. 6.2.2. The difference in the dose equivalent obtained was 10%, when compared with the reference unscattered radiations only. If the scattered fraction of 5% at 1 m in the aluminum room is included in the reference dose equivalent (see Table 5.3.2), the measurement difference becomes only 5%.

The moderated spectrum from the  $^{252}\text{Cf}(\text{D}_2\text{O})$  source which was measured with the CPND is shown in Fig. 6.2.3. Again, the overestimate of the slow and the thermal neutron components by the CPND was because the scattered radiations were not included in the reference spectrum. The dose equivalent estimate difference was 34%, compared with the reference unscattered radiations only. If the scattered fraction of 5% at 0.75 m in the neutron room is included in the reference values (see Table 5.3.2), the measurement difference is reduced to 27%.

The composite spectrum from a mixture of two exposures to  $^{252}\text{Cf}(\text{D}_2\text{O})$  and  $^{238}\text{Pu}\text{-Be}$  which was measured with the CPND is shown in Fig. 6.2.4. The distance and exposure time were 1.5 m - 15 min for  $^{252}\text{Cf}(\text{D}_2\text{O})$  in the neutron room and 1 m - 75 min for  $^{238}\text{Pu}\text{-Be}$  in the aluminum room. Again, the overestimate of the slow and the thermal neutron components was because the scattered radiations were not included

in the reference spectrum. The dose equivalent estimate difference for the CPND was about 20%, compared with the reference value. The difference is reduced to 7%, if the scattered components of the two sources, 5% for  $^{238}\text{Pu-Be}$  and 19% for  $^{252}\text{Cf}(\text{D}_2\text{O})$ , are included in the reference values.

The composite spectrum from a mixture of three exposures to  $^{252}\text{Cf}(\text{PE})$ ,  $^{252}\text{Cf}(\text{D}_2\text{O})$ , and  $^{238}\text{Pu-Be}$  which was measured accurately with the CPND is shown in Fig. 6.2.5. The distance and exposure time were 2 m - 45 min for  $^{252}\text{Cf}(\text{PE})$  in the neutron room, 1.5 m - 15 min for  $^{252}\text{Cf}(\text{D}_2\text{O})$  in the neutron room, and 1 m - 16 h for  $^{238}\text{Pu-Be}$  in the aluminum room. The difference in the dose equivalent estimate was only 7%, compared with the reference unscattered radiations. If scattered components are included in the reference values, the difference would be only ~ 1%.

The dose equivalent rates measured with 6 different methods are compared and summarized in Table 6.2.2. The first five methods are the same as those in Table 6.1.3. The reference dose equivalent rates for  $^{252}\text{Cf}(\text{PE})$  are from the BMS measurements. The reference dose equivalent rates for the remaining sources are the sum of the unscattered and scattered components from calculated results (see Table 5.3.2). The 9"/3" values used for the 9"/3" calibration method are from Table 6.2.1. For the Panasonic TLD, the second algorithm was used to derive the dose equivalent. The 6th method used the Harshaw albedo TLD and the energy index (EI) correction. The relationship between the EI value and the calibration factor (CF) for the Harshaw albedo TLD was obtained from the TRU field calibration. The relationship is:  $\text{CF} = 7.36 - 3.30 \text{EI}$ , where the EI and the CF ( $\mu\text{Sv mR}^{-1}$ ) values are given in Tables 6.2.1 and 6.2.2, respectively.

Compared with the reference values, the differences in the dose equivalent estimated by the 9" remmeter were less than 23% for the single-source exposures. The

ORNL-DWG 89M-9678

Table 6.2.2. Comparison of the dose equivalent rates measured with different detector systems for the neutron sources at RADCAL ( $\text{mSv h}^{-1}$ ).

Method	$^{252}\text{Cf (PE)}$	$^{252}\text{Cf (PE)}$	$^{238}\text{Pu-Be}$	$^{252}\text{Cf (D}_2\text{O)}$	Mixture <sup>c</sup>	Mixture <sup>d</sup>
	1 m <sup>a</sup>	2 m	1 m	0.75 m <sup>b</sup>		
Reference <sup>e</sup>	1.88	0.576	0.253	19.38	0.512	0.290
9" Remmeter	1.662	0.529	0.194	23.25	Unknown	Unknown
Difference <sup>f</sup>	-11%	-8%	-23%	+20%		
CPND	2.098	0.508	0.266	24.68	0.547	0.294
Difference	+12%	-12%	+5%	+27%	+7%	+1%
Harshaw TLD <sup>g</sup>	3.624	0.867	0.362	18.45		
Difference	+93%	+51%	+43%	-5%		
Calibration Factor (9"/3")	3.55	2.39	21.36	1.09	Unknown	Unknown
Panasonic TLD	1.35	---	0.211	14.33	0.282	---
Difference	-28%	---	-17%	-26%	-45%	---
Harshaw TLD <sup>h</sup>	0.878	0.311	0.049	55.33	0.951	0.149
Difference	-53%	-46%	-81%	+186%	+86%	-49%
Calibration Factor (EI)	0.859	0.859	2.91	3.27	2.94	2.62

a. PDIS 14 run no. 2.

b. PDIS 14 run no. 5.

c. NDS-87.  $^{252}\text{Cf(D}_2\text{O)}$  +  $^{238}\text{Pu-Be}$ .d.  $^{252}\text{Cf(PE)}$  + NDS-87  $^{252}\text{Cf(D}_2\text{O)}$  +  $^{238}\text{Pu-Be}$ .e. Multisphere spectrometer results for  $^{252}\text{Cf(PE)}$ . References for the remaining are from relevant literature.

f. Relative to the reference value.

g. From 9"/3" calibration, i.e., Fig. 3.7.3.

h. From energy index method.

Eberline 9" remmeter can integrate the dose equivalent only over finite times (5 min is maximum). Therefore, the 9" remmeter cannot measure the accumulated dose equivalent in practical situations involving multi-source exposure over long period of times, e.g., weeks. The CPND had comparable performance with the 9" remmeter in single-source exposures. The differences in the dose equivalents obtained with the CPND and the references were all less than 27%. In exposures to mixtures of sources, the CPND measurements had very good results (the differences were less than 7%).

Compared with the reference values, the dose equivalent estimate differences for the Harshaw albedo TLD, based on the 9"/3" calibration, were large. The difference in the  $^{252}\text{Cf}(\text{PE})$  source was 93% at 1 m, and 51% at 2 m. This large overestimation was because that the large thermal neutron component of the  $^{252}\text{Cf}(\text{PE})$  source greatly increases the albedo response. The large difference (43%) for the Harshaw TLD when exposed to the  $^{238}\text{Pu}\text{-Be}$  source was due to the very energetic spectrum characteristics of the source. This method cannot measure the dose equivalents in multi-source exposures because the 9"/3" value is unknown.

The dose equivalent estimates using the Panasonic TLD had fair results for all exposures (differences < 45%). The dose equivalent estimates using the Harshaw albedo TLD, based on the EI correction, had poor results (difference was as high as 186%).

From the above comparison, the performance of the CPND has been demonstrated to be superior to other dosimeters, especially in the situations of multi-source exposure.

#### Fourteenth PDIS Test

The 14th PDIS was held in the DOSAR facility during May 1-5, 1989. Six exposures were made with different sources and irradiation conditions to examine dosimeter performance under a variety of conditions. Run 1,  $^{252}\text{Cf}(\text{D}_2\text{O})$  at 1.5 m, total exposure 0.82 mSv, was a standard low dose equivalent exposure. Run 2,  $^{252}\text{Cf}(\text{PE})$  at 1 m, total exposure 0.6 mSv and  $n/\gamma = 1:3$ , was an uncommon source to most participants. This source was used to examine the detection capability of participant's dosimeters in mixed neutron-gamma fields and unknown source conditions. Run 3,  $^{252}\text{Cf}(\text{D}_2\text{O})$  at 0.75 m, total exposure 2.58 mSv and an angle of incidence of  $60^\circ$ , was used to examine the angular dependence of the dosimeters. Run 4,  $^{252}\text{Cf}(\text{D}_2\text{O}, \text{no Cd})$  at 0.75 m, total exposure 2.63 mSv, was to examine the ability of dosimeters to discriminate against thermal neutrons. Run 5,  $^{252}\text{Cf}(\text{D}_2\text{O})$  at 0.75 m, total exposure 2.58 mSv, also was a standard high dose equivalent exposure. Run 6,  $^{238}\text{Pu}\text{-Be}$  at 1 m, total exposure 0.44 mSv, was intended to examine the dosimeter performance exposed to high energy neutrons in a very low dose equivalent exposure. The  $9\frac{2}{3}$ " value and source information for every source was provided to participants.

The 14th PDIS was used as an independent blind test for the CPND. The ORNL Panasonic TLD results for the 14th PDIS were included for comparison. Table 6.2.3 shows a comparison of the CPND, the Harshaw TLD, and the Panasonic TLD results for the 14th PDIS. Three dosimeters were irradiated for each run. One standard deviation of the dose equivalent measured with the dosimeters is called the precision (S). The difference between the mean dose equivalent measured by the three dosimeters and the reference value is called the bias (B). The sum of the absolute value of the bias and the precision is the accuracy level (L).

Table 6.2.3. Performance results of the CPND in the PDIS 14.

Run Number	Source Description	CPND			Harshaw TLD			Panasonic TLD		
		B	S	L	B	S	L	B	S	L
1.	$^{252}\text{Cf}$ ( $\text{D}_2\text{O}$ ) 0.82 mSv	0.403	0.097	0.50	-0.099	0.026	0.13	-0.146	0.038	0.18
2.	$^{252}\text{Cf}$ (PE) 0.6 mSv, $n/\gamma = 1/3$	0.119	0.070	0.19	0.933	0.024	0.96	-0.280	0.156	0.44
3.	$^{252}\text{Cf}$ ( $\text{D}_2\text{O}$ ) $60^\circ$ 2.58 mSv	0.048	0.051	0.10	-0.302	0.042	0.34	-0.473	0.052	0.52
4.	$^{252}\text{Cf}$ ( $\text{D}_2\text{O}$ , no Cd) 2.63 mSv	0.183	0.024	0.21	0.205	0.018	0.22	-0.323	0.021	0.34
5.	$^{252}\text{Cf}$ ( $\text{D}_2\text{O}$ ) 2.58 mSv	0.281	0.073	0.35	-0.047	0.032	0.08	-0.260	0.006	0.27
6.	$^{238}\text{Pu}$ -Be 0.44 mSv	0.141	0.115	0.26	0.455	0.002	0.46	-0.159	0.690	0.85

B = bias, S = one standard deviation, L =  $|B| + S$ .

The dose equivalent derived by the Harshaw TLD was based on the 9"/3" calibration method. The dose equivalent derived by the Panasonic TLD was based on the use of first algorithm, i.e., the source is known. The Harshaw TLD had good precision ( $S < 5\%$  for every run) due to the use of the ECC and RCF corrections. The precision of the CPND was higher ( $< 12\%$ ) due to the statistical variation of the bubble detector response. The Panasonic TLD had an unacceptable precision for run 6 (69%) since the dose equivalent for this exposure was very low.

The bias results for the CPND were better than either the Harshaw TLD or the Panasonic TLD. The positive bias of the CPND was less than  $\sim 40\%$  for all runs. The Harshaw TLD had a bias of 93% for run 2 due to the large thermal neutron component, and had a bias of 46% for run 6 due to the low dose equivalent. The Panasonic TLD had a negative bias ranging from 15% to 47%.

The CPND had better accuracy (i.e., lower L value) than the Harshaw and Panasonic TLD's for runs 2, 3, 4, and 6. The L value of the CPND was within 0.5 for all runs. The overall performance of the CPND is superior to the Harshaw TLD and the Panasonic TLD. This comparison was based on the fact that the source information was known for the Harshaw TLD and the Panasonic TLD, but not for the CPND. Therefore, if the source is not known, the CPND could outperform the Harshaw and Panasonic albedo TLD's by an even greater margin.

The CPND for run 1 had a large bias of 0.40, i.e., the CPND overestimated the reference value by 40%. This was the biggest error in the dose equivalent measurements using the CPND in this research. An explanation for this overestimation is given below. The reference dose equivalent for run 1,  $^{252}\text{Cf}(\text{D}_2\text{O})$  at 1.5 m, total dose equivalent of 0.82 mSv, was the sum of the unscattered component (0.69 mSv) and a calculated scattered component (19%, i.e., 0.13 mSv). The calculation model

assumes the room scattering component is constant, and the validity of this assumption is in doubt for distances greater than 20% of the equivalent radius of the irradiation room (i.e., 1.1 m in the RADCAL neutron room). Therefore, the actual scattered fraction of  $^{252}\text{Cf}(\text{D}_2\text{O})$  at 1.5 m could be higher than the calculated 19%. If the scattered fraction of 31% from the 9" sphere measurements is used (Table 5.3.2), the reference dose equivalent for run 1 would be 0.90 mSv and the bias for the CPND would be lowered to 28%. Then, the CPND would have comparable performance with the Harshaw TLD and the Panasonic TLD for the run 1 test. Also in that case, the bias of the CPND in run 1 and run 5 (both were  $^{252}\text{Cf}(\text{D}_2\text{O})$  exposures) would be the same (28%).

The tests of the 14th PDIS proved that the CPND had good performance in a very low dose equivalent measurement (run 6), in a mixed n/ $\gamma$  field measurement (run 2), in the angular dependence test (run 3), and in high dose equivalent measurements (runs 4 and 5).

## CHAPTER VII

### SUMMARY AND CONCLUSIONS

The development, characterization, and performance evaluation of the CPND is summarized below. Following the summary, conclusions based on the research are presented.

#### 7.1 SUMMARY

Each major part of the research is summarized and recommendations for additional work are presented.

##### Research Summary

Growing regulatory and legal pressures of radiation protection have been demanding more accurate, sensitive, and reliable personnel dosimetry. Compared with photon dosimetry, neutron dosimetry remains unsatisfactory since no single neutron detector has all the desired characteristics to meet the complex needs, especially the required energy response. A new combination personnel neutron dosimeter (CPND) has been developed at the Oak Ridge National Laboratory to cope with the problems.

Based on extensive review of the literature and detailed consideration of the research objectives, two bubble detectors (one BD-100R and one BDS-1500) were chosen to be combined with a Harshaw albedo TLD to form the CPND. Besides being more applicable in all kinds of exposure situations, the CPND was designed to have a crude spectrometric capability, much higher sensitivity, and better angular response.

The CPND has been characterized comprehensively and the results showed that the CPND has the desired personnel neutron dosimeter characteristics. The albedo

TLD in the CPND can be reused for several years and the BD's can be reused for at least six months with satisfactory stability. The minimum linear response range is three orders of magnitude for the albedo TLD and is 2 orders of magnitude for the BD's. With the albedo TLD sensitive to low energy neutrons and the bubble detectors sensitive to high energy neutrons, the CPND is very sensitive to neutrons of any energy and the LLD is only 10  $\mu$ Sv (1 mrem). The BD has no response to photons and the albedo TLD has good photon discrimination in a field with a neutron to gamma dose equivalent ratio of 1:10. Therefore, the CPND has very good neutron dose equivalent measurement ability in mixed neutron-gamma fields. The albedo TLD has a bell-shaped angular dependence and the BD has a nearly isotropic response. Therefore, as long as the CPND is worn in the appropriate position, it can provide a reasonably conservative and accurate estimate of the dose equivalent. The energy dependence of the albedo TLD agreed with the calculated one (Alsmiller and Barish 1974). The energy response per unit fluence of the BD can be regarded as flat within a certain interval for neutrons above the energy threshold of the BD.

In routine operational usage of the CPND, it is suggested that the albedo TLD's be exchanged and readout every quarter using the optimum procedure developed in this research, and the BD's evaluated every week and reused. Due to the instant bubble readout ability of the BD's, workers could read their BD's periodically when in radiation areas to ensure the exposures are consistent with expectations. The BD-100R also can be used as an "alarm" detector. Daily accounting of the approximate accumulated dose equivalent can easily be accomplished by using the BD-100R response to ensure proper exposure control. A more active and effective ALARA program can be achieved through the use of the BD's in the CPND.

The CPND has a 4-interval spectrometric capability, utilizing the different energy response functions of the CPND components. This is a unique and very valuable feature for the CPND as a personnel neutron dosimeter. The performance (mainly the spectrometry and the dose equivalent measurement) of the CPND was evaluated rigorously by an *in-situ* field tests, calibration laboratory radioisotopic source tests, and the 14th PDIS.

Before the performance evaluation of the CPND, various reference spectra (regarding the energy, dose equivalent rate, directionality) for the tests were developed by using either measurements or calculations. Five radiation fields at the ORNL's TRU facility and two spectra of the  $^{252}\text{Cf}(\text{PE})$  source at RADCAL were characterized by measurements with a calibrated Bonner multisphere spectrometer. Three known spectra and associated dosimetric data from the  $^{252}\text{Cf}(\text{D}_2\text{O})$ ,  $^{252}\text{Cf}(\text{D}_2\text{O}, \text{no Cd})$  and  $^{238}\text{Pu}\text{-Be}$  sources at the RADCAL facility were calculated.

The *in-situ* field tests showed that the CPND can measure different energy neutron spectra, can be used for very low dose equivalent measurements, and can be used in practical working fields. The differences in the dose equivalents measured between the CPND and the BMS in the TRU fields were less than 13%. The RADCAL radioisotopic source tests further demonstrated the spectrometric capability of the CPND in the single-source and multi-source exposures. Compared with the reference values, the differences in the dose equivalent estimates with the CPND were less than 27% in these tests. The superiority of the CPND over other types of dosimeters was most distinguished by the multi-source (mixture) and unknown source exposures. The 14th PDIS, an independent blind test, also proved the dose equivalent measurement ability of the CPND under six exposure conditions (accuracy was better than 50%).

### Recommendations for Further Development of the CPND

A few improvements to the CPND are suggested. The major error in the use of the CPND comes from the 4-interval spectral stripping algorithm which uses the average sensitivity concept. The average sensitivity values are derived based on the assumption of constant fluence per unit energy within each interval. To reduce the error, other spectral unfolding methods, e.g., the one used for the multisphere spectrometer, can be used to obtain the spectrum in more energy intervals. The current size of the bubble detector and the albedo TLD can be reduced further. More bubble detectors with different energy thresholds can be used to increase the spectral resolution. More bubble detectors with different sensitivities can be used to increase the linear response range. A holder with better thermal insulation can be developed so that the CPND can be used in environments without temperature control for extended periods of time. The temperature dependence of the BD sensitivity also can be studied with the idea of providing temperature correction. The quality of the BD (batch uniformity, sensitivity stability, and useful lifetime) can be improved. The shape of the vial for the BD can be tailored so that the angular response of the BD follows the desired angular dependence of the  $H'(10)$  quantity. The capabilities of a compact CPND with the improved features can be enhanced greatly. It is encouraging that all these potential improvements appear to be feasible.

### 7.2 CONCLUSIONS BASED ON THIS RESEARCH

The characterization and performance evaluation of the CPND in this research has demonstrated that a passive, small, lightweight, and practical personnel neutron dosimeter with spectrometric capability has been developed successfully. The CPND can, without prior knowledge of the neutron spectrum or calibration in the working

field, provide an accurate estimate of the dose equivalent. With expected advances in bubble detectors, the minor problems of the BD (e.g., temperature dependence, dynamic range, quality control, and cost) will be solved. It is expected that, in the very near future, the CPND will fulfill a major need in personnel neutron monitoring.

## REFERENCES

- Alberts, W. G. Response of an albedo neutron dosimeter to  $^{252}\text{Cf}$  neutrons on various phantoms. *Radiat. Prot. Dosim.* 23:183-186; 1988.
- Alsmiller, R. G.; Barish, J. The calculated response of  $^6\text{LiF}$  albedo dosimeters to neutrons with energies  $\leq 400$  MeV. *Health Phys.* 26:13-28; 1974.
- American National Standards Institute. Personnel dosimetry performance - criteria for testing. New York, NY: ANSI; ANSI N13.11; 1983.
- Apfel, R. E. The superheated drop detector. *Nucl. Instrum. and Meth.* 162:603-608; 1979.
- Apfel, R. E.; Roy, S. C. Investigation on the applicability of superheated drop detectors in neutron dosimetry. *Nucl. Instrum. and Meth. in Phys. Res.* 219:582-587; 1984.
- Apfel, R. E.; Roy, S. C.; Lo, Y.-C. Prediction of the minimum neutron energy to nucleate vapor bubbles in superheated liquids. *Physical Review A* 31:3194-3198; 1985.
- Apfel, R. E.; Lo, Y.-C. Practical neutron dosimetry with superheated drops. *Health Phys.* 56:79-83; 1989.
- Awschalom, H.; Sanna, R. S. Application of Bonner sphere detectors in neutron field dosimetry. *Radiat. Prot. Dosim.* 10:89-101; 1985.
- Bartlett, D. T. Inter-relationships of the proposed ICRU operational radiological protection quantities and effective dose equivalent for practical radiation fields. *Radiat. Prot. Dosim.* 12:155-157; 1985.
- Block, S.; Bryan, J.; Prevo, C.; Montan, D. Laboratory sources enhanced in 0.5 eV to 200 keV neutrons for instrument evaluation. *Health Phys.* 13:1025-1031; 1967.

- Brackenbush, L. W.; Endres, G. W. R.; Selby, J. M.; Vallario, E. J. Personnel neutron dosimetry at Department of Energy facilities. Richland, WA: Pacific Northwest Laboratories; PNL-3213; 1980.
- Brackenbush, L. W.; McDonald, J. C.; Endres, G. W. R.; Quam, W. Mixed field dose equivalent measuring instruments. *Radiat. Prot. Dosim.* 10:307-318; 1985.
- Burgart, C. E.; Emmett, M. B. Monte Carlo calculations of the response functions of Bonner ball neutron detectors. Oak Ridge, TN: Oak Ridge National Laboratory; ORNL-TM-3739; 1972.
- Burgkhardt, B.; Heinzelmann, M.; Piesch, E.; Viragh, E. Statistical errors of dose estimation in personnel neutron monitoring with albedo dosimeters. *Nucl. Instrum. and Meth.* 160:533-540; 1979.
- Burgkhardt, B.; Piesch, E. A computer assisted evaluation technique for albedo thermoluminescence dosimeters. *Radiat. Prot. Dosim.* 2:221-230; 1982.
- Burgkhardt, B.; Piesch, E. Field calibration technique for albedo neutron dosimeters. *Radiat. Prot. Dosim.* 23:121-126; 1988.
- Casson, W. H.; Sims, C. S. A new dosimeter calibration laboratory at ORNL. Oak Ridge, TN: Oak Ridge National Laboratory; ORNL-TM-10971; 1988: 206-210.
- Cross, W. G.; Ing, H. Neutron spectroscopy. In: Kase, K. R.; Bjarngard, B. E.; Attix, F. H., ed. *The dosimetry of ionizing radiation*. 2nd ed. Vol. II, New York, NY: Academic Press; 1987: 91-167.
- Dajko, G.; Somogyi, G. Fast neutron spectrometry based on proton detection in CR-39 detector. *Nucl. Tracks* 12:607-610; 1986.
- Driscoll, C. M. H.; Richards, D. J. Reader annealing of LiF chips. *Radiat. Prot. Dosim.* 18:99-100; 1987.

- Endres, G. W. R. Neutron dosimetry at commercial nuclear plants. Richland, WA: Pacific Northwest Laboratories; PNL-3585; 1981.
- Gibson, J. A. B. Individual neutron dosimetry. *Radiat. Prot. Dosim.* 23:109-115; 1988.
- Griffith, R. V.; Hankins, D. E.; Gammage, R. B.; Tommasino, L.; Wheeler, R. V. Recent developments in personnel neutron dosimeters - a review. *Health Phys.* 36:235-260; 1979.
- Griffith, R. V.; McMahon, T. A. Progress on development of a passive personnel dosimeter / spectrometer-DOSPEC. Richland, WA: Pacific Northwest Laboratories; PNL-SA-10714; 1982: 103-119.
- Griffith, R. V. Review of the state of the art in personnel neutron monitoring with solid state detectors. *Radiat. Prot. Dosim.* 23:155-160; 1988a.
- Griffith, R. V. The next decade in external dosimetry. *Health Phys.* 55:177-189; 1988b.
- Hajnal, F. An iterative nonlinear unfolding code: TWOGO. New York, NY: Environmental Measurements Laboratory; EML-391; 1981.
- Hankins, D. E.; Homann, S. G.; Westermark, J. Personnel neutron dosimetry using electrochemically etched CR-39 foils. Livermore, CA: Lawrence Livermore National Laboratory; UCRL-53833; 1987.
- Hankins, D. E.; Homann, S.; Westermark, J. The LLNL CR-39 personnel neutron dosimeter. *Radiat. Prot. Dosim.* 23:195-198; 1988.
- Harvey, J. R. Neutron exposure: sources and radiological significance. *Radiat. Prot. Dosim.* 10:17-22; 1985.

- Horowitz, Y. S. General characteristics of TL materials. In: Horowitz, Y. S., ed. Thermoluminescence and thermoluminescent dosimetry. First Printing. Vol. I, Boca Raton, Florida: CRC Press, Inc.; 1984: 89-125.
- Horowitz, Y. S.; Moscovitch, M.; Wilt, M. Computerized glow curve deconvolution applied to ultralow dose LiF thermoluminescence dosimetry. Nucl. Instrum. and Meth. in Phys. Res. A244:556-564; 1986.
- Hunt, J. B. The calibration of neutron sensitive spherical devices. Radiat. Prot. Dosim. 8:239-251; 1984.
- Ing, H.; Birnboim, H. C. A bubble-damage polymer detector for neutrons. Nucl. Tracks and Radiat. Meas. 8:285-288; 1984.
- Ing, H.; Birnboim, H. C. Bubble-damage polymer detectors for neutron dosimetry. Proceedings of the 5th Symposium on Neutron Dosimetry; 17-21 September 1984; Munich, Neuherberg; Commission of European Communities; EUR-9762; 1985: 883-894.
- Ing, H.; Piesch, E. Status of neutron dosimetry. Radiat. Prot. Dosim. 10:5-15; 1985.
- Ing, H. The status of the bubble-damage polymer detector. Nucl. Tracks and Radiat. Meas. 12:49-54; 1986.
- Ing, H.; Tremblay, K. To develop a set of variable lower-energy threshold bubble neutron detectors for use as a spectrometer. Chalk River, Ontario: Bubble Technology Industries; BTI-88/2-29A; 1988.
- Institute of Nuclear Power Operations. Guidelines for radiological protection at nuclear power stations. Atlanta, GA: INPO; INPO 88-010; 1988.
- International Atomic Energy Agency. Neutron monitoring for radiological protection. Vienna: IAEA; IAEA Technical Report Series No. 252; 1985.

- International Commission on Radiation Units and Measurements. Determination of dose equivalents resulting from external radiation sources. Bethesda, MD: ICRU; ICRU Report 39; 1985.
- International Commission on Radiation Units and Measurements. The quality factor in radiation protection. Bethesda, MD: ICRU; ICRU Report 40; 1986.
- International Commission on Radiological Protection. Data for protection against ionizing radiation for external sources. Oxford: Pergamon Press; ICRP Publication 21; 1973.
- International Commission on Radiological Protection. Statement from the 1985 Paris Meeting of the International Commission on Radiological Protection. *J. Soc. Radiol. Prot.* 5:87-88; 1985.
- International Commission on Radiological Protection. Data for use in protection against external radiation. Oxford: Pergamon Press; ICRP Publication 51; 1987.
- International Organization for Standardization. Exposure meters and dosimeters - general methods for testing. Geneva: ISO; International Standard ISO 4071; 1978.
- International Organization for Standardization. Neutron reference radiations for calibrating neutron measuring devices used for radiation protection purposes and for determining their response as a function of neutron energy. Geneva: ISO; Draft International Standard ISO/DIS 8529; 1986.
- Ipe, N. E.; Busick, D. D. BD-100: The Chalk River Nuclear Laboratories' neutron bubble detector. Stanford, CA: Stanford Linear Accelerator Center, Stanford University; SLAC-PUB-4398; 1987.

- Ipe, N. E.; Busick, D. D.; Pollock, R. W. Factors affecting the response of the bubble detector BD-100 and a comparison of its response to CR-39. *Radiat. Prot. Dosim.* 23:135-138; 1988.
- Jones, K. L.; Roberson, P. L.; Fox, R. A.; Cummings, F. M.; McDonald, J. C. Performance criteria for dosimeter angular response. Richland, WA: Pacific Northwest Laboratories; PNL-6452; 1988.
- Jones, R. Stability, repeatability, and homogeneity of the Chalk River bubble-damage neutron detector. Oak Ridge, TN: Oak Ridge National Laboratory; ORNL-TM-10971 (abstracts); 1988: 53.
- Julius, H. W.; De Planque, G. Influence of annealing and readout procedures on fading and sensitivity changes in LiF for temperatures and humidities typical for environmental and personnel dosimetry. *Radiat. Prot. Dosim.* 6:253-256; 1984.
- Lakshmanan, A. R. A review on the role of thermoluminescent dosimeters in fast-neutron personnel dosimetry. *Nucl. Tracks.* 6:59-78; 1982.
- Lakshmanan, A. R.; Tuyn, J. W. N. Annealing and reusability characteristics of LiF TLD-700 chips. *Radiat. Prot. Dosim.* 18:229-236; 1987.
- Lo, Y.-C. Characterization of a neutron detector based on superheated drops. New Haven, CT: Yale University; Ph.D. Dissertation; 1987.
- Maerker, R. E.; Williams, L. R.; Mynatt, F. R.; Greene, N. M. Response functions for Bonner ball neutron detectors. Oak Ridge, TN: Oak Ridge National Laboratory; ORNL-TM-3451; 1971a.
- Maerker, R. E.; Muckenthaler, F. J.; Manning, J. J.; Hull, J. L.; Money, J. N.; Henry, K. M.; Freestone, R. M. Jr. Calibration of the Bonner ball neutron detectors used at the Tower Shielding Facility. Oak Ridge, TN: Oak Ridge National Laboratory; ORNL-TM-3465; 1971b.

- Majborn, B. Automated counting and analysis of the etched tracks in CR-39 plastic. *Radiat. Prot. Dosim.* 17:153-155; 1986.
- Matiullah, K. J.; Durrani, S. A. A flat dose-equivalent dosimeter for fast neutrons using a CR-39 polymeric track detector with front radiators. *Radiat. Prot. Dosim.* 17:149-152; 1986.
- McDonald, J. C.; Hadley, R. T. Response characteristics of selected personnel neutron dosimeters in use at DOE facilities. *Radiat. Prot. Dosim.* 12:275-283; 1985.
- Menzel, H. G.; Dietze, G.; Schuhmacher, H. Practical determination of dose equivalent using low pressure tissue equivalent proportional counters. Proceedings of the Seventh Congress of the International Radiation Protection Association. 11-15 April 1988; Sydney, Australia; 1988: 308-311.
- Morhart, A.; Burger, G. Specified dose equivalent quantities for neutrons in the ICRU sphere and their applicability. *Radiat. Prot. Dosim.* 12:107-111; 1985.
- Moscovitch, M.; Bruml, W. W.; Velbeck, K. J.; Martis, C. R. The reusability of a new TLD card type. Paper presented at the 32th Health Physics Society Annual Meeting, Salt Lake City, Utah; 5-9 July 1987.
- Nash, A. E.; Johnson, T. L.; Zeman, G. H.; Snyder, G. I.; Riel, G. K.; Woo, K.; Wang, J. C. Y.; Scofield, N. E. The response of an albedo neutron dosimeter to moderated Am-Be and  $^{252}\text{Cf}$  neutron sources. Washington, DC: Naval Research Laboratory; NRL Report 8909; 1985.
- National Council on Radiation Protection and Measurements. Recommendations on limits for exposure to ionizing radiation. Bethesda, MD: NCRP; NCRP Report No. 91; 1987.

- Ogunleye, O. T.; Richmond, R. G.; Cash, B. L.; Jones, K. L. Effects of annealing on the sensitivity of LiF TLD-100 after repeated use for low dose measurements. *Radiat. Prot. Dosim.* 18:101-104; 1987.
- Pacific Northwest Laboratories. Annual report for 1988 to the Assistant Secretary for Environment, Safety, and Health, Part 5: environment, safety, health, and quality assurance. Richland, WA: PNL; PNL-6800 Pt. 5; 1989: 17.
- Perks, C. A.; Harrison, K. G.; Goodenough, R. J.; Hunt, J. B. Neutron dosimetry studies using the new Chalk River Nuclear Laboratories bubble-damage detector. Teddington, Middlesex: National Physical Laboratory; AERE-R-12582; 1987.
- Perks, C. A.; Devine, R. T.; Harrison, K. G.; Goodenough, R. J.; Hunt, J. B.; Johnson, T. L.; Reil, G. L.; Schwartz, R. B. Neutron dosimetry studies using the new Chalk River Nuclear Laboratories bubble-damage detector. *Radiat. Prot. Dosim.* 23:131-134; 1988.
- Piesch, E.; Burgkhardt, B. The role of an analyzer type albedo dosimeter in routine monitoring and the current situation for the calibration technique. Richland, WA: Pacific Northwest Laboratories; PNL-2807; 1978.
- Piesch, E.; Jasiak, J.; Urban, M. Markofol and CR-39 recoil track etch detectors as a supplement of a universal albedo neutron dosimeter. *Nucl. Tracks and Radiat. Meas.* 8:323-326; 1984.
- Piesch, E.; Burgkhardt, B. Albedo neutron dosimetry. *Radiat. Prot. Dosim.* 10:175-188; 1985.
- Plato, P.; Miklos, J. Production of element correction factors for thermoluminescent dosimeters. *Health Phys.* 49:873-881; 1985.

- Portal, G.; Bermann, F.; Buxerolle, M.; Mourgues, M. Neutron and photon radiation fields as encountered in practical radiation protection. *Radiat. Prot. Dosim.* 12:193-201; 1985.
- Pradhan, A. S.; Rassow, J.; Hoffmann, W. Fast neutron responses of  $\text{CaF}_2:\text{Tm}$  Teflon TLD discs of different thicknesses. *Radiat. Prot. Dosim.* 15:233-236; 1986.
- Pradhan, A. S.; Rassow, J. Radiation induced thermoluminescence in  $\text{CaF}_2:\text{Tm}$  detectors. *Nucl. Instrum. and Meth. in Phys. Res. A255:234-237*; 1987.
- Routti, J. T.; Sandberg, J. V. Unfolding activation and multisphere detector data. *Radiat. Prot. Dosim.* 10:103-110; 1985.
- Roy, S. C.; Apfel, R. E.; Lo, Y.-C. Superheated drop detector: a potential tool in neutron research. *Nucl. Instrum. and Meth. in Phys. Res. A255:199-206*; 1987.
- Schwartz, R. B. Calibration and use of filtered beams. Washington, DC: U.S. Department of Commerce, National Institute of Standards and Technology; NBS Special Publication 493; 1977.
- Schwartz, R. B.; Eisenhauer, C. M. Procedures for calibrating neutron personnel dosimeters. Washington, DC: U.S. Department of Commerce, National Institute of Standards and Technology; NBS Special Publication 633; 1982.
- Schwartz, R. B.; Endres, G. W. R.; Cummings, F. M. Neutron dosimeter performance and associated calibrations at nuclear power plants. Washington, DC: U.S. Department of Commerce, National Institute of Standards and Technology; NUREG/CR-2233; 1982.
- Shachar, B. B.; Horowitz, Y. S. Dosimetric characterization of the high temperature peaks of  $\text{LiF:Mg,Ti}$  and  $\text{CaF}_2:\text{Tm}$  using computerized glow curve deconvolution. *Radiat. Prot. Dosim.* 22:87-96; 1988.

- Sims, C. S.; Swaja, R. E.; Weng, P. S. Personnel neutron-gamma and criticality accident dosimetry in perspective. *Nucl. Sci. J.* 24:113-140; 1987.
- Swaja, R. E.; Sims, C. S. Neutron personnel dosimetry intercomparison studies at the Oak Ridge National Laboratory: a summary (1981-1986). *Health Phys.* 55:549-564; 1988.
- Thompson, I. M. G.; Lavender, A. Calibration of the De Pangher long counter. Vienna: International Atomic Energy Agency; IAEA-SM-167/242; 1973: 465-483.
- Thorngate, J. H. Energy spectra of the pneumatically positioned neutron sources at LLNL's Hazards Control Standards and Calibration Facility. Livermore, CA: Lawrence Livermore National Laboratory; UCID-21035; 1987.
- Tommasino, L.; Zapparoli, G.; Spiezia, P.; Griffith, R. V.; Espinosa, G. Different etching processes of damage track detectors for personnel neutron dosimetry. *Nucl. Tracks and Radiat. Meas.* 8:335-339; 1984.
- Turner, T. W.; Henshaw, D. L.; Fews, A. P. A CR-39 neutron spectrometer of sensitivity 1 mrem in the energy range 100 keV - 20 MeV with personal dosimetry applications. *Nucl. Tracks and Radiat. Meas.* 8:341-344; 1984.
- U.S. Department of Energy. Department of Energy standard for the performance testing of personnel dosimetry system. Washington, DC: U.S. Government Printing Office; DOE/EH-0027; 1986.
- U.S. Department of Energy. Department of Energy laboratory accreditation program for personnel dosimetry. Washington, DC: U.S. Government Printing Office; DOE Order 5480.15; 1987.

- U.S. Department of Energy. Radiation protection for occupational workers. Washington, DC: U.S. Government Printing Office; DOE Draft Order 5480.11; 1988.
- U.S. Nuclear Regulatory Commission. Personnel neutron dosimeters. Washington, DC: U.S. Government Printing Office; Regulatory Guide 8.14, Revision 1; August 1977.
- U.S. Nuclear Regulatory Commission. Improved personnel dosimetry processing. Washington, DC: U.S. Government Printing Office; 10CFR.20, Federal Register; 52(30); 1988.
- Uray, I. Dose independent use of LiF detectors in mixed neutron-gamma radiation fields. *Radiat. Prot. Dosim.* 17:127-129; 1986.
- Vasilik, D. G.; Erkkila, B. H.; Waechter, D. A. A portable neutron spectrometer / dosimeter. *Radiat. Prot. Dosim.* 10:121-124; 1985.
- Wagner, S. R. Individual monitoring for neutrons: practical measurements, ICRU recommended quantities and limited quantities. *Radiat. Prot. Dosim.* 23:105-108; 1988.
- Zeman, G. H.; Snyder, G. I. Neutron dose precision using LiF TLD. *Health Phys.* 36:75-76; 1979.

**APPENDIX 1**

**A PRINTOUT OF THE READER CALIBRATION FACTOR**

**REPORT FROM THE HARSHAW 8800 READER**

S-23684.003                      READER CALIBRATION FACTOR REPORT                      Page 1 of 1

Selected Records of Group # 8904035    Reader # 11                      3-Apr-1989    3:54pm  
 TTP 04    TTProfile 4    Nominal Irradiation Value: 500 mR

DATE	TIME	TTP CARD ID	TLD Reading (ECC applied)				UNITS
			(i)	(ii)	(iii)	(iv)	
* 4/03/89	15:43:45	PMT	.0958	.0799	.2614	.0440	nC
* 4/03/89	15:43:58	RL	296.6	281.7	209.0	261.4	nC
4/03/89	15:44:16	04I 900104	261.5	230.5	187.4	197.3	nC
4/03/89	15:44:45	04I 900105	254.9	237.0	185.1	199.3	nC
4/03/89	15:45:14	04I 900106	271.8	232.0	186.8	194.0	nC
4/03/89	15:45:44	04I 900109	281.8	233.8	189.2	198.7	nC
4/03/89	15:46:13	04I 900110	272.4	240.4	186.1	190.1	nC
4/03/89	15:46:42	04I 900111	274.4	233.8	185.8	197.0	nC
4/03/89	15:47:12	04I 900112	265.7	239.4	188.1	204.5	nC
4/03/89	15:47:41	04I 900113	276.0	238.9	186.0	194.0	nC
4/03/89	15:48:10	04I 900114	263.0	237.6	186.1	201.1	nC
4/03/89	15:48:40	04I 900115	271.3	238.3	189.0	196.3	nC
* 4/03/89	15:49:03	PMT	.1019	.0844	.2643	.0542	nC
* 4/03/89	15:49:16	RL	287.1	274.7	204.1	258.3	nC

Reader Summary		Samples	(i)	(ii)	(iii)	(iv)	Units
New Calibration Factor (RCF)			0.5385	0.4723	0.3739	0.3945	nC/mR
Old Calibration Factor (RCF)			0.5242	0.4717	0.3553	0.3976	nC/mR
Mean Reading		10	269.27	236.17	186.97	197.25	nC
% Std. Dev.			2.951	1.437	0.756	2.042	
Ref. Light Mean		2	291.83	278.21	206.53	259.86	nC
Ref. Light % Std. Dev.			2.313	1.783	1.704	0.8322	
PMT Noise Mean		2	0.0988	0.0822	0.2628	0.0491	nC
PMT Noise % Std. Dev.			4.383	3.927	0.7903	14.67	



ORNL-DWG 89M-8739

## APPENDIX 3

## DATA FOR THE PHOTON LINEARITY TESTS OF THE HARSHAW

ALBEDO TLD TO THE  $^{137}\text{Cs}$  SOURCE.

Exposure ( $\mu\text{C kg}^{-1}$ )	TLD Element Signal*			
	I	II	III	IV
5.16	9.6 (3.5)	9.3 (0.7)	6.9 (1.2)	8.1 (3.4)
12.9	24.6 (1.7)	22.8 (0.7)	17.4 (1.0)	20.4 (2.5)
25.8	48.9 (0.9)	45.3 (0.5)	34.6 (1.3)	40.2 (2.2)
129	239.7 (2.3)	229.6 (0.4)	174.4 (0.7)	199.7 (2.7)
516	979.2 (3.3)	938.3 (0.3)	704.1 (0.5)	827.9 (1.6)
2580	4940 (3.0)	4701 (1.2)	3504 (0.8)	4046 (2.9)
Slope	1.915	1.823	1.358	1.568
$r^2$	1.000	1.000	1.000	1.000

\* TL signal is in units of nC. One standard deviation expressed in percent is computed from 4 TLD's per group, and is shown in parentheses.

$r^2$  = Square of correlation coefficient from least squares linear regression analysis.

ORNL-DWG 89M-8738

## APPENDIX 4

**DATA FOR THE NEUTRON LINEARITY TESTS OF THE  
HARSHAW ALBEDO TLD.**

Source	Dose Equivalent (mSv)	Neutron Response*		
		Cd-Covered TLD-600 (A)	TLD-600 (T)	
$^{252}\text{Cf}$ (PE)	0.0480	32.6 (2.7)	65.3 (3.1)	
	0.0900	59.3 (1.7)	122.3 (1.7)	
	0.3010	199.4 (3.0)	402.6 (0.6)	
	0.5230	412.9 (2.5)	815.6 (1.2)	
	3.0060	2038.1 (2.9)	4044.1 (1.3)	
		Slope	677.3	1342.1
	$r^2$	1.000	1.000	
$^{238}\text{Pu-Be}$	0.501	45.3	63.6	
	1.234	111.5	155.5	
	1.998	181.0	248.4	
		Slope	90.7	123.4
		$r^2$	1.000	1.000

\* Neutron response is in units of mR. One standard deviation (in %) is computed from 4 TLD's per group, and is shown in parentheses.

$r^2$  = Square of correlation coefficient from least squares linear regression analysis.

ORNL-DWG 89M-8737

## APPENDIX 5

**DATA FOR THE NEUTRON ANGULAR DEPENDENCE OF THE  
HARSHAW ALBEDO TLD.**

Source	Angle (degrees)	Vertical Irradiation			Horizontal Irradiation		
		A	T	T/A	A	T	T/A
$^{252}\text{Cf}$	85	0.23	0.23	1.286	0.28	0.22	1.009
	60	0.68	0.68	1.278	0.76	0.69	1.157
	30	0.93	0.91	1.253	0.99	0.93	1.202
	0*	1.00	1.00	1.280	1.00	1.00	1.280
	-30	0.96	0.95	1.257	0.92	0.97	1.351
	-60	0.73	0.72	1.271	0.66	0.77	1.495
	-85	0.26	0.27	1.295	0.22	0.29	1.674
$^{252}\text{Cf}(\text{D}_2\text{O})$	85	0.20	0.21	1.275	0.24	0.19	1.006
	60	0.56	0.55	1.243	0.66	0.56	1.064
	30	0.87	0.87	1.253	0.95	0.88	1.171
	0**	1.00	1.00	1.259	1.00	1.00	1.259
	-30	0.94	0.92	1.241	0.87	0.94	1.363
	-60	0.65	0.63	1.226	0.54	0.66	1.540
	-85	0.23	0.24	1.284	0.17	0.24	1.816

\* Normalization point for  $^{252}\text{Cf}$ . The neutron responses A and T are 166.6 mR and 213.2 mR for 2 mSv irradiation.

\*\* Normalization point for  $^{252}\text{Cf}(\text{D}_2\text{O})$ . The responses A and T are 396.9 mR and 499.7 mR for 0.5 mSv irradiation.

ORNL-DWG 89M-8736

## APPENDIX 6

**DATA FOR THE EFFECT OF PHOTON ANGULAR DEPENDENCE  
ON THE RESPONSE OF THE HARSHAW ALBEDO TLD\***

Source	Angle (degrees)	<u>Vertical Irradiation</u>		<u>Horizontal Irradiation</u>	
		A	T	A	T
<sup>137</sup> Cs	85	-2.6 <sup>a</sup>	-7.7 <sup>a</sup>	1.5	2.8
	60	0.7	1.3	1.6	1.4
	30	2.4	1.9	1.7	3.4
	0	1.4	1.3	1.4	1.3
	-30	1.7	2.6	1.6	0.9
	-60	2.5	0.9	1.3	1.4
	-85	+3.8 <sup>a</sup>	+6.5 <sup>a</sup>	2.2	1.6
M150** X-rays	60	-7.8 <sup>a</sup>	2.0	6.3 <sup>b</sup>	2.3
	40	1.4	4.8	3.0	3.2
	20	2.9	1.2	2.6	1.7
	0	1.6	1.5	1.6	1.5
	-20	2.8	1.5	2.1	2.0
	-40	2.0	2.8	3.1	1.9
	-60	+7.6 <sup>a</sup>	2.1	2.7	1.6

\* The values (in %) are the mean of absolute values of the pair response difference (TLD-600 minus TLD-700).

\*\* M150 X-ray: NIST code M150 X-rays (152 kVcp, average energy 74.6 keV).

- a. The difference is due to the angular dependence. The sign of the pair response difference value is also shown.
- b. The difference is due to one outlier in the data group.

ORNL WSM-10131

## APPENDIX 7

## TRU FIELD SURVEY DATA

TRU field survey data prior to the field characterization with multisphere spectrometer.

Site	9" Spherical Remmeter (cpm)	9"/3"	Bare $^{10}\text{BF}_3$ Counter (cpm)	Photon Intensity ( $\mu\text{C kg h}^{-1}$ )
Glove Box	204	0.37	458	1.83
Cave Area A	63	0.27	306	0.10
Control Room	4	0.20	14	0.04
Waste Transfer	110	0.49	111	0.08
Analytical Lab.	89	0.56	63	0.09
Waste Storage	105	0.25	453	0.06
Repair Box	230	0.78	79	0.50
7930 Sample Box	163	0.91	92	0.03

TRU field survey data during the field characterization with multisphere spectrometer.

Site	9" Spherical Remmeter (cpm)	9"/3"	Bare $^{10}\text{BF}_3$ Counter (cpm)
Glove Box	168	0.38	341
Cave Area A	60	0.25	248
Control Room	4.3	0.31	11.5
Waste Transfer	133	0.53	89

ORNL-DWG 89M-7710

**APPENDIX 8**

**RELATIVE DETECTOR RESPONSE OF THE MULTISPHERE  
SPECTROMETER FOR THE NEUTRON FIELDS AT THE  
ORNL TRU FACILITY**

Detector <sup>a</sup> No.	PE Radial Thickness (cm)	Site <sup>b</sup>					
		A	Al	B	C	D	E
2	0	0.045	0.035	0.026	0.033	0.018	0.039
3	1.194	0.425	0.347	0.272	0.404	0.212	0.418
4	1.308	0.458	0.390	0.304	0.463	0.254	0.426
5	2.388	0.792	0.720	0.630	0.738	0.571	0.742
6	2.502	0.814	0.755	0.674	0.784	0.614	0.771
7	3.759	1.000	0.987	0.921	1.000	0.913	1.000
8	4.851	0.939	1.000	0.986	0.930	0.998	0.931
9	5.004	0.925	0.999	1.000	0.886	1.000	0.893
10	7.366	0.673	0.798	0.828	0.624	0.885	0.612
11	9.906	0.408	0.520	0.561	0.369	0.625	0.343
12	12.421	0.248	0.339	0.376	0.218	0.412	0.181
Cd Ratio <sup>c</sup>		18.3	14.6	7.63	12.3	6.14	10.85
No. 12 Response Ratio <sup>d</sup>		11.6	37.1	24.9	1.0	20.6	1.3

a. See Section 5.1.

b. The sites at the Transuranium Processing Plant (TRU) are:

A = Cave area A

Al = Glove box

B = Waste transfer area

C = Control room

D = Analytical laboratory (2nd floor)

E = Corridor 200A (2nd floor)

c. Response ratio of detector no. 1 (bare BF<sub>3</sub> counter) to detector no. 2 (Cd-covered BF<sub>3</sub> counter). An index of the thermal neutron component.

d. An estimate of field intensity, normalized to the field at site C.

ORNL WSM-10132

## APPENDIX 9

**DATA FOR THE 26-ENERGY-GROUP FLUX SPECTRUM EVALUATED  
WITH THE MULTISPHERE SPECTROMETER**

Neutron Energy (MeV)	TRU					<sup>252</sup> Cf(PE) 1 m	RADCAL 2 m
	Glove Box	Cave Area A	Control Room	Waste Transfer	Analytical Laboratory		
2.00E-07	18.83E+00	13.52E+00	0.622E-01	3.93E+00	1.528E-01	14.10E+02	6.09E+02
5.90E-07	9.44E+00	5.39E+00	2.75E-01	4.28E+00	2.07E+00	2.84E+02	1.06E+02
1.20E-06	7.30E+00	4.03E+00	2.52E-01	3.36E+00	1.71E+00	2.17E+02	8.65E+01
2.44E-06	5.15E+00	2.79E+00	2.56E-01	2.19E+00	1.19E+00	1.42E+02	6.56E+01
<u>4.94E-06</u>	<u>4.12E+00</u>	<u>2.22E+00</u>	<u>2.41E-01</u>	<u>1.75E+00</u>	<u>9.80E-01</u>	<u>1.08E+02</u>	<u>5.26E+01</u>
1.00E-05	3.54E+00	1.90E+00	2.32E-01	1.51E+00	8.66E-01	8.89E+01	4.47E+01
2.04E-05	3.22E+00	1.72E+00	2.24E-01	1.39E+00	8.16E-01	7.84E+01	4.00E+01
4.14E-05	3.10E+00	1.65E+00	2.22E-01	1.36E+00	8.15E-01	7.39E+01	3.78E+01
8.41E-05	3.10E+00	1.64E+00	2.23E-01	1.39E+00	8.44E-01	7.26E+01	3.69E+01
<u>1.71E-04</u>	<u>3.04E+00</u>	<u>1.60E+00</u>	<u>2.16E-01</u>	<u>1.39E+00</u>	<u>8.58E-01</u>	<u>7.06E+01</u>	<u>3.55E+01</u>
3.46E-04	3.04E+00	1.59E+00	2.11E-01	1.42E+00	8.95E-01	7.06E+01	3.50E+01
7.03E-04	3.13E+00	1.62E+00	2.10E-01	1.50E+00	9.55E-01	7.24E+01	3.53E+01
1.43E-03	3.14E+00	1.60E+00	2.02E-01	1.54E+00	9.98E-01	7.30E+01	3.48E+01
2.91E-03	3.33E+00	1.67E+00	2.05E-01	1.67E+00	1.10E+00	7.79E+01	3.64E+01
<u>5.90E-03</u>	<u>3.83E+00</u>	<u>1.88E+00</u>	<u>2.24E-01</u>	<u>1.98E+00</u>	<u>1.33E+00</u>	<u>9.08E+01</u>	<u>4.14E+01</u>
1.20E-02	4.64E+00	2.23E+00	2.55E-01	2.47E+00	1.68E+00	1.12E+02	4.99E+01
2.44E-02	5.98E+00	2.79E+00	3.07E-01	3.28E+00	2.29E+00	1.49E+02	6.42E+01
4.94E-02	7.93E+00	3.55E+00	3.73E-01	4.52E+00	3.23E+00	2.06E+02	8.56E+01
1.00E-01	1.05E+01	4.45E+00	4.37E-01	6.27E+00	4.64E+00	2.92E+02	1.16E+02
<u>2.04E-01</u>	<u>1.39E+01</u>	<u>5.42E+00</u>	<u>4.92E-01</u>	<u>8.77E+00</u>	<u>6.81E+00</u>	<u>4.37E+02</u>	<u>1.61E+02</u>
4.14E-01	1.78E+01	6.21E+00	5.25E-01	1.19E+01	9.78E+00	6.84E+02	2.34E+02
8.41E-01	1.99E+01	6.15E+00	4.96E-01	1.37E+01	1.18E+01	1.02E+03	3.23E+02
1.71E+00	1.71E+01	4.81E+00	3.88E-01	1.19E+01	1.03E+01	1.24E+03	3.66E+02
3.46E+00	1.13E+01	3.03E+00	2.46E-01	7.85E+00	6.66E+00	1.09E+03	3.06E+02
<u>7.03E+00</u>	<u>4.96E+00</u>	<u>1.32E+00</u>	<u>1.09E-01</u>	<u>3.46E+00</u>	<u>2.86E+00</u>	<u>5.06E+02</u>	<u>1.42E+02</u>
1.43E+01	2.63E-01	7.01E-02	5.72E-03	1.84E-01	1.49E-01	2.73E+01	7.60E+00

1. Flux per unit logarithmic energy interval ( $\text{cm}^{-2} \text{s}^{-1}$ ).

ORNL-DWG 89M-7708

**APPENDIX 10**

**RELATIVE DETECTOR RESPONSE OF THE MULTI-  
SPHERE SPECTROMETER FOR THE NEUTRON  
SPECTRA AT THE ORNL RADCAL FACILITY**

Detector <sup>a</sup> No.	Spectrum <sup>b</sup>			
	1	2	3	4
2	0.033	0.029	0.024	0.025
3	0.293	0.294	0.238	0.240
4	0.329	0.327	0.272	0.270
5	0.634	0.633	0.555	0.557
6	0.665	0.663	0.589	0.586
7	0.930	0.928	0.882	0.943
8	0.975	0.996	0.984	0.991
9	1.000	1.000	1.000	1.000
10	0.884	0.881	0.945	0.946
11	0.654	0.658	0.751	0.754
12	0.471	0.475	0.533	0.568
Cd Ratio <sup>c</sup>	33.8	37.0	34.1	35.1
No. 12 Response Ratio <sup>d</sup>	1.0	1.01	3.2	3.4

a. See Section 5.1.

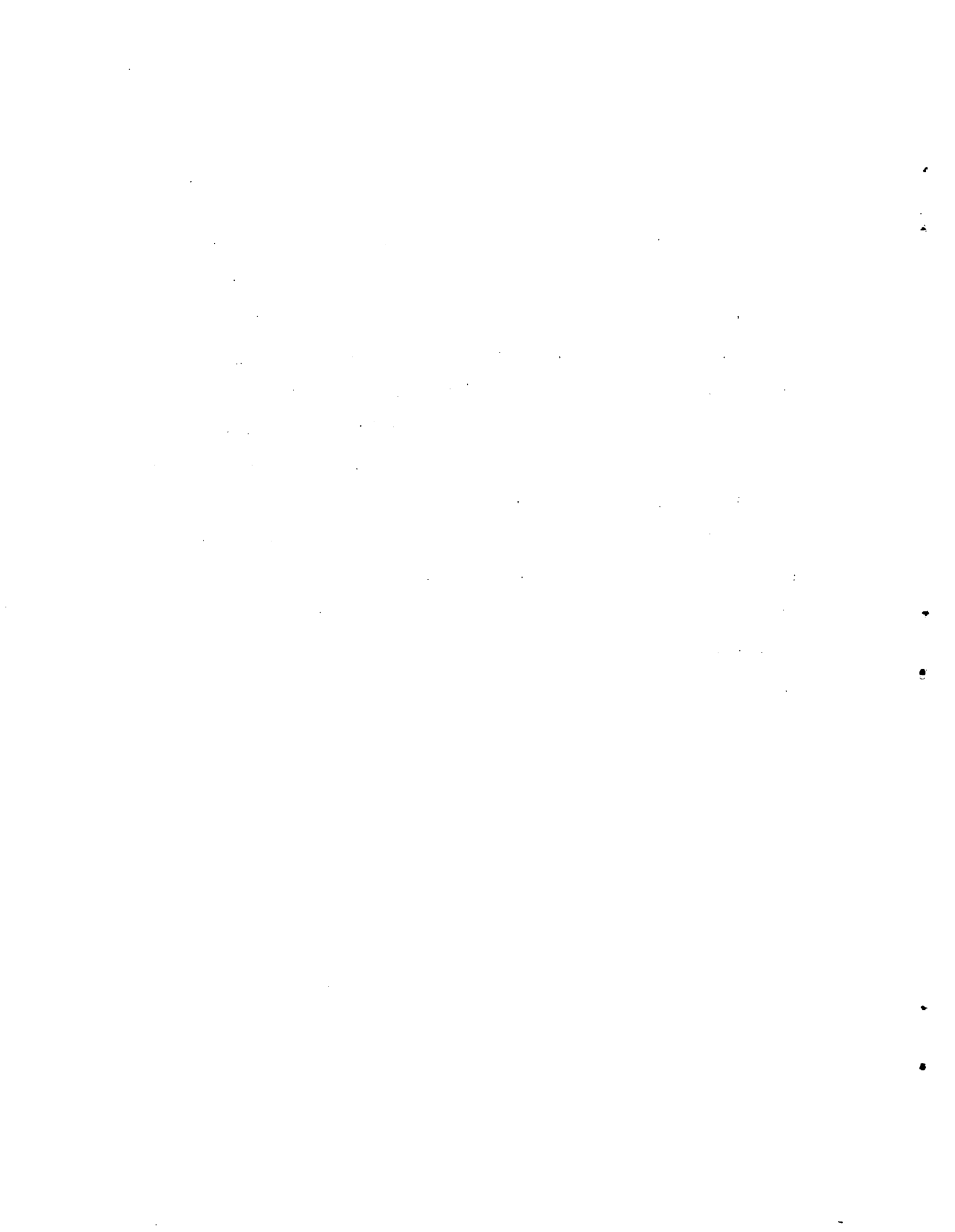
b. The spectra at RADCAL are from the  $^{252}\text{Cf}$  (PE) source. Spectra 1 and 2 are at 2 m with and without the 2 big slab phantoms, respectively. Spectra 3 and 4 are at 1 m with and without the 2 big slab phantoms, respectively.

c. Response ratio of detector no. 1 (bare BF counter) to detector no. 2 (Cd-covered  $\text{BF}_3$  counter). An index of the thermal neutron component.

d. An estimate of field intensity, normalized to the spectrum 1.

**VITA**

The author, Chwei-jeng Liu, was born on January 31, 1956, in Kaoshiung, Taiwan. He is also known as James C. Liu. After attending a six-year elementary school, a three-year junior high school, and a three-year senior high school, he attended the National Tsing-Hua University and earned a B.S. degree in nuclear engineering in 1979. He then served in the Republic of China Army for two years as a lieutenant ordnance officer. He attended the National Tsing-Hua University and earned a M.S. degree in health physics in 1983. He then worked as a staff scientist in the Health Physics Division of the Institute of Nuclear Energy Research in Taiwan for three years. He entered the Texas A&M University Ph.D. program in 1986, and did his dissertation research at the Oak Ridge National Laboratory. His major field is health physics and he expects to earn the degree in 1989. His permanent mailing address is Oak Ridge National Laboratory, Building 7710, P. O. Box 2008, Oak Ridge, TN 37831-6379, U.S.A.



ORNL-6593

## INTERNAL DISTRIBUTION

- |       |                   |        |   |
|-------|-------------------|--------|---|
| 1.    | A. B. Ahmed       | 15.    | H. Murakami   |
| 2.    | E. G. Bailiff     | 16.    | G. R. Patterson   |
| 3.    | B. A. Berven      | 17.    | G. Rao  |
| 4.    | J. S. Bogard      | 18-19. | C. S. Sims  |
| 5.    | M. A. Buckner     | 20.    | R. E. Swaja   |
| 6.    | W. H. Casson      | 21.    | M. Thein  |
| 7.    | K. F. Eckerman    | 22.    | Central Research Library                                  |
| 8.    | J. B. Hunt        | 23.    | Laboratory Records  |
| 9-13. | C. J. (James) Liu | 24.    | Laboratory Records, ORNL-RC                               |
| 14.   | K. L. McMahan     | 25.    | ORNL Patent Section                                       |
|       |                   | 26.    | ORNL Y-12 Technical Library<br>Document Reference Section |

## EXTERNAL DISTRIBUTION

27. Office of Assistant Manager for Energy Research and Development, Department of Energy, Oak Ridge Operations, P. O. Box E, Oak Ridge, TN 37931.
- 28-37. Office of Science and Technical Information, P. O. Box 62, Oak Ridge, TN 37831.
38. G. Akabani, Texas A&M University, Department of Nuclear Engineering, College Station, TX 77843.
39. Robert Apfel, Apfel Enterprises, Inc., 25 Science Park, New Haven, CT 06511.
40. R. D. Carlson, U.S. DOE, 785 DOE Place, Idaho Falls, ID 83402-4149.
41. Wei-Li Chen, Institute of Nuclear Energy Research, Health Physics Division, Lung-Tan, P. O. Box 3-10, Taiwan, REPUBLIC OF CHINA.
42. D. L. Clark, Texas A&M University, IVTE, College Station, TX 77843.
43. D. E. Hankins, Lawrence Livermore National Laboratory, P. O. Box 5505, L-86, Livermore, CA 94550.
44. H. Ing, Bubble Technology Industries, Chalk River, Ontario, CANADA.
45. Donald E. Jones, LLNL, MS L-787, P. O. Box 808, Livermore, CA 94551.

46. H. F. Kerschner, Naval Medical Command, 23rd and E Street, NW, Washington, D.C. 20372-5120.
47. Frank Mangold, Dames & Moore, 1626 Cole Blvd., Golden, CO 80401.
48. T. O. Marshall, NATIONAL RADIOLOGICAL PROTECTION BOARD, Chilton, Didcot, Oxfordshire OX11 ORQ, GREAT BRITAIN.
49. M. E. McLain, Texas A&M University, Department of Nuclear Engineering, College Station, TX 77843.
50. Marko Moskovitch, Harshaw/Filtrol, 29001 Solon Road, Solon, OH 44139.
51. E. Piesch, Kernforschungszentrum Karlsruhe GmbH, Postfach 3640, D7500 Karlsruhe 1, FEDERAL REPUBLIC OF GERMANY.
52. M. A. Parkhurst, Battelle, Pacific Northwest Laboratory, Health Physics Department, P. O. Box PPP, Richland, WA 99352.
- 53-54. John W. Poston, Texas A&M University, Department of Nuclear Engineering, College Station, TX 77843.
55. T. A. Rhea, SAIC, 800 Oak Ridge Turnpike, Oak Ridge, TN 37831.
56. G. A. Schalpper, Texas A&M University, Department of Nuclear Engineering, College Station, TX 77843.
57. Hans O. E. Schraube, GES.F.STRAHLEN-UND UMWELTFORSCHUNG MUNCHEN, Ingolstadter Landstrasse 1, D8042 Neuherberg, FEDERAL REPUBLIC OF GERMANY.
58. R. Schwartz, National Institute of Standards and Technology, A155 Reactor, Gaithersburg, MD 20899.
59. E. A. Schweikert, Texas A&M University, Department of Chemistry, College Station, TX 77843.
60. Rod A. Tawil, Harshaw/Filtrol, 29001 Solon Road, Solon, OH 44139.
61. Pao-Shang Weng, National Tsing-Hua University, Institute of Nuclear Science, Hsing-Chu, Taiwan, REPUBLIC OF CHINA.
62. Leon West, University of Arkansas, Engineering Equipment Station, West 20th Street, Fayetteville, AR 72701.
63. C. F. Wu, Waste Isolation Pilot Plant, Westinghouse Electric Corporation, P. O. Box 2078, Carlsbad, NM 88221.
64. Gary Zeman, AFRRI, Bethesda, MD 20814.